THE UNIVERSITY OF TEXAS AT AUSTIN
CENTER FOR TRANSPORTATION RESEARCH

TECHNICAL REPORT 0-7015-1
TxDOT PROJECT NUMBER 0-7015

Analyze Shear Capacity of Texas Standard Prestressed Beams from Strut-and-Tie Models of Beam Ends: Final Report

Hansol Jang
Zach Webb
Jongkwon Choi
Hwa-Ching Wang
Oguzhan Bayrak

October 2021

Published February 2022

https://library.ctr.utexas.edu/ctr-publications/0-7015-1.pdf

Technical Report Documentation Page

1. Report No. FHWA/TX-21/0-7015-1	2. Government Accession No.	3. Recipient's Catalog No.
4. Title and Subtitle Analyze Shear Capacity of Texas Standard Prestressed Beams from Strut-and-Tie Models of Beam Ends: Final Report		5. Report Date October 2021; Published February 2022
		6. Performing Organization Code
7. Author(s) Hansol Jang, Zach Webb, Jongkwon Choi, Hwa-Ching Wang, and Oguzhan Bayrak		8. Performing Organization Report No. 0-7015-1
9. Performing Organization Name and Address Center for Transportation Research The University of Texas at Austin 3925 W. Braker Lane, 4th Floor Austin, TX 78759		10. Work Unit No. (TRAIS) 11. Contract or Grant No. 0-7015
12. Sponsoring Agency Name and Address Texas Department of Transportation Research and Technology Implementation Division 125 E. 11th Street Austin, TX 78701		13. Type of Report and Period Covered Technical Report July 2019 – October 2021 14. Sponsoring Agency Code
15. Supplementary Notes Project performed in cooperation with the Texas Department of Transportation and the Federal Highway Administration.		

16. Abstract

The shear stress limit in girder end regions as established in the AASHTO LRFD Bridge Design Specifications might be overly conservative for Texas standard prestressed beams. This report confirms that the shear stress limit of Texas standard prestressed beams could be relaxed using STM and anchorage capacity at the end region. Additionally, it confirms that additional expected failures depending on the type of beams, such as nodal failure, horizontal shear failure, and lateral splitting failure, are prevented when the shear stress at the end of the girder is greater than the currently used $0.18f'_c$ shear stress limit. The geometry and strand layout of the girder used by TxDOT is used to calculate the maximum shear stress limit of the girder in this paper. Some but not all Texas standard prestressed beams can relax the shear stress limit, but the relaxed shear stress limit is different according to the type and size of the beams. Therefore, it is more economical to set the shear stress limit of the end region according to each girder's geometry and design manual.

17. Key Words	18. Distribution Statement
Strut-and-Tie Model, Prestressed Beams, End Region, Stress Flow, Shear Stress Limit	No restrictions. This document is available to the public through the National Technical Information Service, Alexandria, Virginia 22312, www.ntis.gov.

19. Security Classif. (of report)	20. Security Classif. (of this page)	21. No. of pages	22. Price
Unclassified	Unclassified	286	

Form DOT F 1700.7 (8-72) Reproduction of completed page authorized

THE UNIVERSITY OF TEXAS AT AUSTIN
CENTER FOR TRANSPORTATION RESEARCH

ANALYZE SHEAR CAPACITY OF TEXAS STANDARD PRESTRESSED BEAMS FROM STRUT-AND-TIE MODELS OF BEAM ENDS

Hansol Jang
Zach Webb
Jongkwon Choi
Hwa-Ching Wang
Oguzhan Bayrak

CTR Technical Report:	0-7015-1
Report Date:	October 2021 | Published February 2022
Project:	0-7015
Project Title:	Analyze Shear Capacity of Texas Standard Prestressed Beams from Strut-and-Tie Models of Beam Ends
Sponsoring Agency:	Texas Department of Transportation
Performing Agency:	Center for Transportation Research at The University of Texas at Austin

Project performed in cooperation with the Texas Department of Transportation and the Federal Highway Administration.

Center for Transportation Research
The University of Texas at Austin
3925 W. Braker Lane, 4th floor
Austin, TX 78759

https://ctr.utexas.edu/

Disclaimers

Author's Disclaimer: The contents of this report reflect the views of the authors, who are responsible for the facts and the accuracy of the data presented herein. The contents do not necessarily reflect the official view or policies of the Federal Highway Administration or the Texas Department of Transportation (TxDOT). This report does not constitute a standard, specification, or regulation.

Patent Disclaimer: There was no invention or discovery conceived or first actually reduced to practice in the course of or under this contract, including any art, method, process, machine manufacture, design or composition of matter, or any new useful improvement thereof, or any variety of plant, which is or may be patentable under the patent laws of the United States of America or any foreign country.

Engineering Disclaimer

NOT INTENDED FOR CONSTRUCTION, BIDDING, OR PERMIT PURPOSES.

Project Engineer: Oguzhan Bayrak
Professional Engineer License State and Number: Texas No. 106598
P.E. Designation: Research Supervisor

Acknowledgments

The authors are grateful to the Texas Department of Transportation (TxDOT) for providing the funds to conduct this research study. The contributions of the Project Monitoring Committee—Laura Garcia, Victoria McCammon, and Addisu Tilahun, all from Bridge Division, and RTI project manager, Joanne Steele—are deeply appreciated.

Table of Contents

List of Tables

List of Figures

Chapter 1. Introduction

1.1. Overview

Texas bridge designers have been facing difficulties, in some instances, due to the $0.18f'_c$ shear stress limit at the end regions of prestressed beams specified in Article 5.7.3.2 of the American Association of State Highway and Transportation Officials Load and Resistance Factor Design (AASHTO LRFD) (2020). AASHTO's $0.18f'_c$ shear stress limit has been established to ensure that the complicated nature of stresses is accounted for as forces are transmitted to the supported ends of pre-tensioned girders. If the $0.18f'_c$ shear stress limit is not satisfied, the effective shear area of members should be increased (e.g., decreasing the beam spacing, providing additional members, or increasing the size of members). Otherwise, the Strut-and-Tie Model (STM) should be employed to justify the load transfer mechanisms at the end regions. In other words, the $0.18f'_c$ shear stress limit can be relaxed if appropriate STMs can justify load transfer onto the supports.

However, the development of STMs can be ambiguous for Texas standard pre-tensioned girders due to harped strands, debonded strands, boundary conditions, specific geometric details (e.g., solid end blocks U-beam, box beam, X-beam, and decked-slab beam), and other characteristics. For example, in Tx-girders with a span near the upper limit, the bottom flange is nearly full of prestressing strands, and the web has harped strands over a significant height. For box beams, U-beams, X-beams, slab beams, and decked-slab beams, there are various lengths of debonded strands in addition to strands bonded over the entire beam length. Also, stress flow changes depending on the number of supports or end blocks. Therefore, the application of the STM to the end region of Texas standard prestressed beams should be studied with particular consideration to geometry and boundary conditions.

According to the NCHRP 579 report (Hawkins and Kuchma 2007), when designing the end regions of a girder, two additional failure modes warrant consideration. First, the longitudinal tensile capacity at the inside face of supports (termed anchorage capacity check in this study) should be considered, as required by AASHTO LRFD (2020). The other mode to account for is the horizontal shear stress at the critical section, located between the bottom flange and the base of the web. The STM can also be used on the cross-section to confirm whether the amount of confining reinforcement used in the beam is sufficient to prevent lateral splitting at the end of the bottom flange (Ross et al. 2013; Shahrooz et al. 2017).

When appropriate strut-and-tie models are developed for the end region of Texas standard prestressed beams and additional expected failure modes of the girder are considered, the feasibility of increasing the $0.18\,f'_c$ shear stress limit without creating issues with respect to structural safety or serviceability of the beams can be studied.

1.2. Project Objectives

Texas Department of Transportation (TxDOT) Research Project 0-7015 is funded by TxDOT. It investigates shear failure mechanisms of the end regions of pre-tensioned girders and develops appropriate strut-and-tie models for Texas standard prestressed beams. Using the STM and considering additional expected failure modes, the shear stress capacity of Texas standard prestressed beam end regions will be estimated. The purpose of this project is to assess whether the end regions of Texas standard prestressed beams can exceed the $0.18\,f'_c$ shear stress limit and to determine the stress limit can be relaxed without issuing serviceability and safety problems.

1.3. Project Scope

To develop STMs, consider additional expected failure mode, and relax the shear stress limit of the beam, the following tasks are addressed:

1. Investigate the geometry and boundary conditions for each type of Texas standard prestressed beam.
2. Investigate the features of prestressed concrete beams that should be considered when developing STMs.
3. Analyze differences between Tx-girders and AASHTO Type I-girders using the database that collected test results of prestressed concrete beam specimens.
4. Develop STMs that consider the features of prestressed concrete beams and Texas beams' geometry and boundary conditions. Also, calculate the shear force of the end region of the beams.
5. Investigate the additional failure modes that should be considered for each type of Texas standard prestressed beam and assess risk from additional failure modes to the end region of the beam.
6. Confirm whether the analytical method used to calculate the shear stress limit of the beam is suitable. Experimental results of Texas standard

prestressed beams that have been tested in the previous research are used in this task.

7. Finally, propose the maximum shear stress limits for each size and type of the beams.

The research performed for these seven tasks is presented in detail in this report. In addition, this report presents not only detailed explanations of these seven tasks but also additional investigations or analyses of analytical results.

1.4. Organization

The background of Texas standard prestressed beams and the STM concepts applied to prestressed beams are provided in Chapter 2. The six main features of the prestressed beam are explained, and strut-and-tie modeling strategies considering each feature are proposed. Also, the results of comparing Tx-girders and AASHTO Type I-girders using the database for prestressed concrete beams are presented. At the end of Chapter 2, the shear force calculation method provided in ACI 318-19 (2019) and AASHTO (2020) provisions are presented. Chapter 3 explains how to calculate the shear stress of end regions using the STM and the method of anchorage capacity. The strategies to develop STMs according to the boundary condition of the end region of the beams are proposed, and the variables used to calculate the shear force are described in detail. Additionally, the effects of strand patterns on calculating the shear stress of the beams using the STM are presented. In Chapter 4, different expected failure modes are proposed according to the geometry of each type of Texas standard prestressed beam; the method for checking additional expected failure modes that can occur at the end of the beam is also explained. Chapter 5 shows the analytical results and analysis for Texas standard prestressed beams. The shear stress capacity of the beam's end is calculated for each girder size and compared with the $0.18 f'_c$ shear stress limit. Also, the beams' capacity and demand for expected failure modes are compared. In Chapter 6, in order to confirm whether the analytical method used in this study is suitable for calculating the shear stress of the Texas standard prestressed beam's end region, the results of the analytical method are compared with the experimental results. Chapter 7 explains the additional investigation, which suggests minor design changes to prevent failure in the strut-to-node interface of the STM in the longitudinal direction. Finally, the research conclusions are summarized in Chapter 8.

Chapter 2. Background

2.1. Introduction

Texas standard prestressed beam consists of six types of beams, and each type has different geometry and boundary conditions. The different features of each beam affect the load transfer mechanisms. Therefore, it is necessary to understand the features of geometry and boundary conditions for each beam type and how those features affect the load transfer mechanisms. The properties for Texas standard prestressed beams—geometry, reinforcement detail, concrete strength, and strand layout—are proposed on the TxDOT's standard design. However, since TxDOT's standard design does not provide the concrete strength and strand layout for some of the Texas standard prestressed beams, a suitable concrete strength and strand layout for each span length were calculated using the PG Super program used to design bridges.

In accordance with the scope of TxDOT Project 0-7015, the comprehensive literature review has been performed to examine previous research related to the structural performance of pre-tensioned girders with various shear failure modes and to identify best design practices with respect to Strut-and-Tie Models (STMs) which are appropriate for use in the end regions of pre-tensioned girders. The summarizations of the difficulties associated with the analysis of pre-tensioned girders and previous studies to address these difficulties are explained in this chapter. Furthermore, the database analysis for the anchorage evaluation of the prestressed beam developed in UT Austin is reviewed. Based on this database, the relationship between the $0.18\,f'_c$ shear stress limit and the shear strength of the prestressed beam is investigated, and the differences between the Tx-girder and AASHTO Type I-girder is compared.

2.2. Texas Standard Prestressed Beams Geometry

Tx-girder is the I-shaped girder, which connects the top and bottom flange with one web. The geometry of the beam is constant over the entire length, so it is not necessary to consider the end block at the end of the Tx-girder. Also, one bearing plate is placed on both supports. In a Tx-girder, harped strands could actively control the stress at the end of the beam, and debonded strands are not used. However, the use of harped strands complicates the stress flow in the end region of Tx-girder. Therefore, the STM of the Tx-girder in which the harped strand is used and the STM of the girder in which the harped is not used should be considered separately.

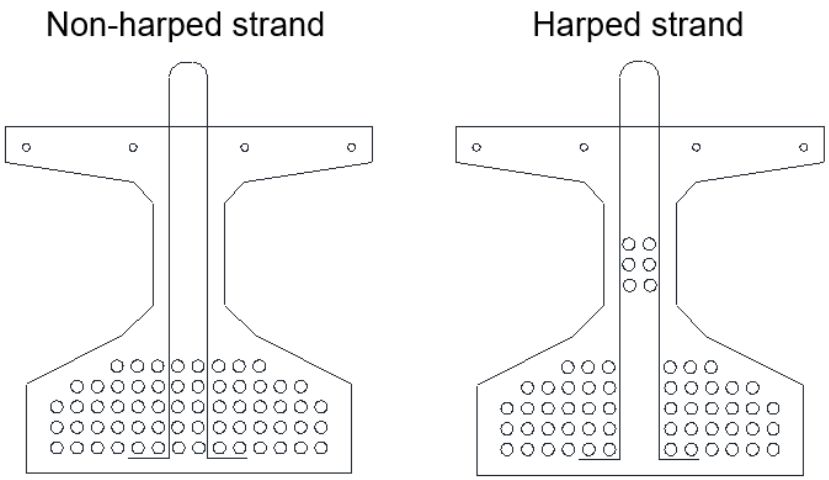

Figure 2-1. Different strand layout between Tx-girder without harped strand and with the harped strand

The box beams have different features compared to Tx-girders, which influence the end support conditions on load transfer mechanisms. The box beam has two webs connected to the top and bottom slabs, and shear should be passed to those two webs. If both webs have the same thickness with no torsion, it can be assumed that they are subjected to the same shear force. Therefore, it is common to use the shear design method, assuming that a box beam containing a two-web thickness of b_w can be designed as an I-girder with a single web thickness of $2b_w$ (refer to Figure 2-2) (Avendano et al. 2013). Therefore, the shear stress of the box beam's end region can be calculated by considering its characteristics.

The box beams contain the end blocks in the end region of the beam; because of the end blocks, stress flow is changed. Also, unlike the Tx-girder, which places one bearing plate on both supports, the box beam has one bearing plate on one support and two bearing plates on the other support. In a Tx-girder, harped strands could actively control the stress at the end of the beam. However, the harped strand is not used in the box beam; only debonded strand is used.

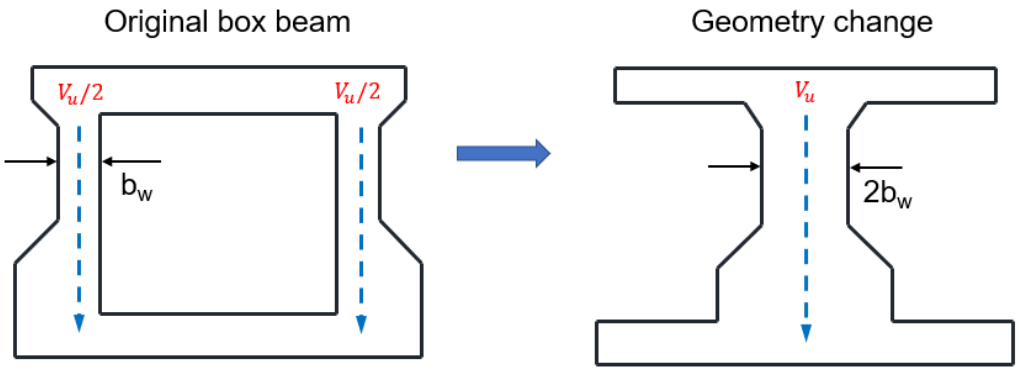

Figure 2-2. Changing cross-section used in box beam for shear design

The X-beam has geometric shapes and boundary conditions similar to those of a box beam. An X-beam has two webs connected to the top and bottom slabs and contains the end block in the beam's end region. Also, the X-beam has one bearing plate on one support and two bearing plates on the other support. There are no harped strands in the X-beam; only debonded strands are used. Since the X-beam characteristics are the same as those of the box beam, the shear stress of the X-beam can be calculated using the same calculation method for the shear stress of the box beam. The two main differences between an X-beam and a box beam are the maximum possible number of strands and the distance from the void of the beam to the edge of the beam. The X-beam can accommodate two rows of bottom strands—double that of a box beam. According to the TxDOT Bridge Design Manual (2020), the web thickness, b_w, and the distance from the bottom to the void, h_b, are greater in the X-beam than in the box beam.

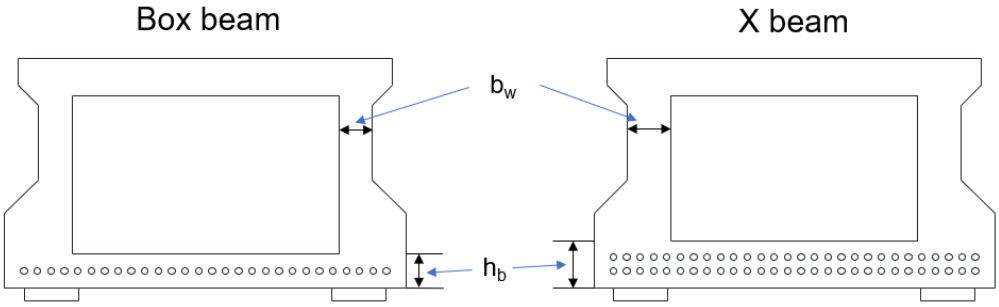

Figure 2-3. Difference between X-beam and box beam

The U-beam has two webs connected to the top and bottom slabs, and there are end blocks at the end of the girder, so the stress flow is similar to the box beam and X-beam. It is common to use the shear design method, assuming that a U-beam containing a two-web thickness of b_w can be designed as the Tx-girder with a single web thickness of $2b_w$ (refer to Figure 2-4) (Hovell et al. 2013). However, the geometry shape and boundary condition of the U-beam is slightly different from

that of the box beam. The web of the U-beam is inclined, and the applied forces acting at the node are affected by the inclined web. Therefore, the shear stress of the U-beam's end region can be calculated by considering its characteristics.

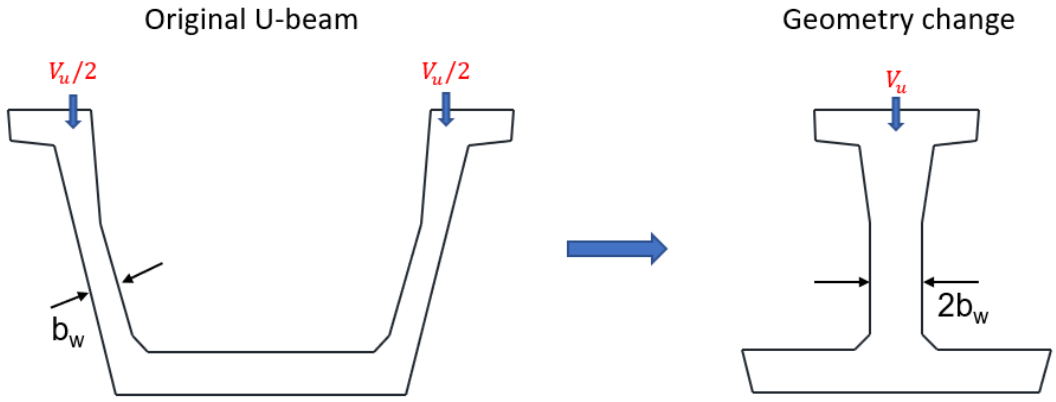

Figure 2-4. Changing cross-section used in box beam for shear design

The slab beam and the decked-slab beam have different geometries, influencing the load transfer mechanisms (refer to Figure 2-5). The slab beam has the same shape as the rectangular beam with a wide web width and includes one web with no end block. The decked-slab beam contains two webs with an end block, and the deck is already included on the top of the beam. The shear stress of the slab beam can be calculated using the same calculation method for that of the Tx-girder. However, unlike the Tx-girder, there is no distinction between the web and the bottom flange for the slab beam. The shear stress of the decked-slab beam can be calculated using the same calculation method used for the shear stress of the box beam and X-beam.

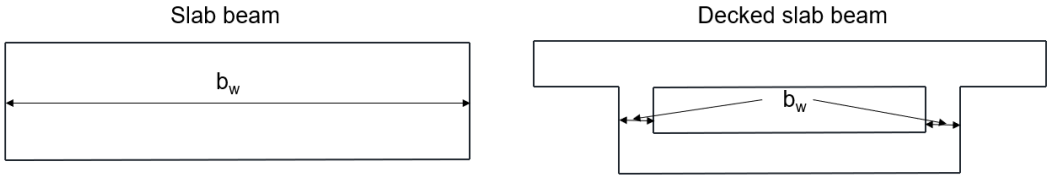

Figure 2-5. The different cross-section between slab beam and decked-slab beam

2.3. Features and Strategies for Strut-and-Tie Modeling of Prestressed Concrete Beams

Based on the literature review, research in STM of reinforced concrete is extensive and readily available; however, applications of STMs with pre-tensioned concrete members are more limited. The difficulty is realized when constructing STMs for pre-tensioned girders due to load transfer mechanisms caused by unique features due to strand development and unique design details of prestressed concrete

members such as the debonded and harped strand. Further, a variety of prestressed concrete girder types are utilized in construction, each with its unique cross-section, end geometry, and support details. Finally, the ends of pre-tensioned girders exhibit splitting and bursting forces at transfer which may influence the stress flow at the support.

Application of STMs for the end region of pre-tensioned beams, in which the unique features of prestressed concrete beams mentioned above are considered, have been investigated by various researchers (Avendano et al. 2013; Avendaño Valderrama 2011; Barton et al. 1991; Bergmeister et al. 1993; Cook and Mitchell 1988; Floyd et al. 2016; Hovell et al. 2013; Klein et al. 2017; Llanos et al. 2009; Martin and Sanders 2007; Mattock 2012; Reineck 2002; Ross et al. 2013; Schlaich et al. 1987; Shahrooz et al. 2017). Based on the literature review performed under Task 2, the potential influence of those unique features of prestressed concrete beams on the disturbed region (D-region) is presented in the following subsections. STM strategies for prestressed concrete members used for the previous research studies have also been identified and briefly summarized. The research team will select the most rational STM strategies and develop those.

2.3.1. Development of strand

Anchorage of the longitudinal reinforcement is typically achieved through bonds in combination with hooked or headed ends in the ends of reinforced concrete members. However, in pre-tensioned girders, the strand is developed by the bond between strand and concrete alone. In the analysis using STM of a simply supported beam, anchorage of the longitudinal reinforcement is achieved through the development of reinforcement(strand). The longitudinal reinforcement should be checked using Equation 2-1 or Equation 2-2 in accordance with Article 5.7.3.5 in AASHTO LRFD (2020) when using STMs. Since the anchorage of the longitudinal reinforcement in pre-tensioned girders typically relies on the bond between prestressing strand and concrete only, the effective stress in prestressing strand should be calculated accurately considering the stress development of prestressing strand as specified in Article 5.9.4.3 in AASHTO LRFD (2020) (refer to Figure 2-6).

General $$A_s f_y + A_{ps} f_{ps} \geq \frac{|M_u|}{d_v \phi_f} + 0.5\frac{N_u}{\phi_c} + \left(\left|\frac{V_u}{\phi_v} - V_p\right| - 0.5V_s\right)\cot\theta$$ Equation 2-1

At end $$A_s f_y + A_{ps} f_{ps} \geq \left(\frac{V_u}{\phi_v} - 0.5V_s - V_p\right)\cot\theta$$ Equation 2-2

Where:

A_{ps} = area of bonded prestressing strands (in^2)

f_{ps} = maximum average stress in prestressing strands at a particular section (ksi)

A_s = area of bonded longitudinal reinforcement (in^2)

f_y = yield stress of reinforcement (ksi)

M_u = moment at the section (kip-in)

N_u = axial force, taken as positive if tensile (kips)

d_v = effective shear depth (in.)

V_u = shear at the section (kips)

$\varnothing_f$, $\varnothing_c$, $\varnothing_v$ = resistance factors

V_p = component in the direction of the applied shear of the effective prestressing force (kips)

V_s = shear resistance provided by the transverse reinforcement found using AASHTO LRFD 2017 General Procedure (kips)

θ = angle of inclination of diagonal compressive stresses found using AASHTO LRFD 2017 General Procedure

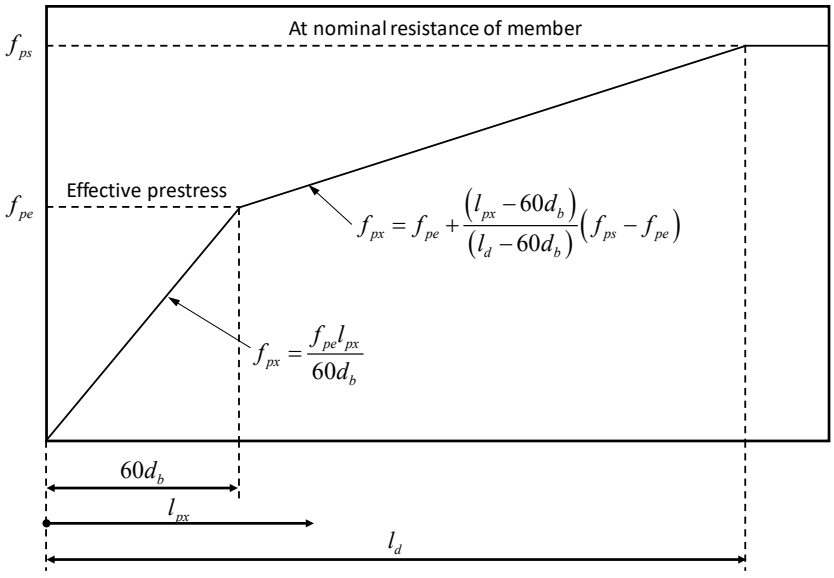

Figure 2-6. Idealized relationship between steel stress and distance from the free end of the strand (from Article 5.9.4.3 in AASHTO LRFD (2020))

STMs for pre-tensioned girders with straight strands only are very similar to those for conventional reinforced concrete girders. However, for pre-tensioned girders, adding extra panels to where STM using one panel typically suffices for the purpose of the load transfer would be necessary due to the development of strands. In this case, it is recommended to check the capacity of the longitudinal tie (i.e., strand) at multiple locations to ensure the proper anchorage of longitudinal reinforcement. STMs for the case of using only one panel and using an additional panel for checking longitudinal tie capacity is exemplified in Figure 2-7.

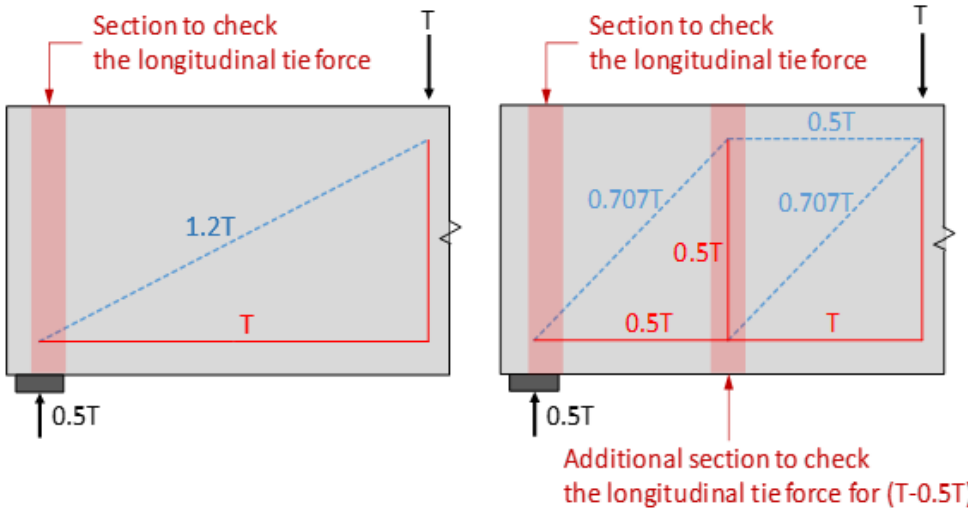

Figure 2-7. Comparison of one panel and two panels to check the longitudinal tie force for anchorage

2.3.2. Debonded strand

Strand debonding is often used in the construction of pre-tensioned concrete girders to relieve the top and bottom fiber stresses at the ends. Debonded strands will change the strand stress distribution and development length along the length of girders. If the development is changed, the maximum average stress in prestressing strands, f_{ps}, which is used for checking the longitudinal tie capacity, is changed. The development length is measured from the point of maximum stress to the point where bonding commences (Buckner 1995)(refer to Figure 2-8). The minimum development length can be calculated following Article 5.9.4.3.2 and 5.9.4.3.3 of AASHTO LRFD (Equation 2-3). The strand capacity should be calculated considering not only the features of the debonded strand mentioned above, the number of debonded strands, and the length of the debonded zone.

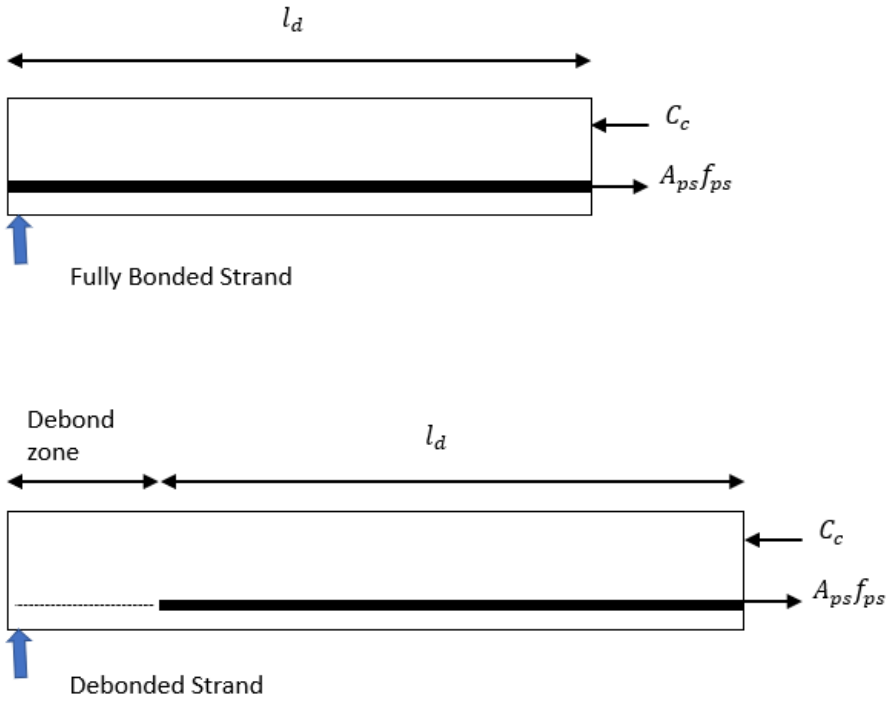

Figure 2-8. Development length of fully bonded and debonded pre-tensioned strand

$$l_d \geq \kappa \left(f_{ps} - \frac{2}{3} f_{pe} \right) d_b \qquad \text{Equation 2-3}$$

Where:

κ = 1.0 for pre-tensioned members with a depth less than or equal to 24-in.

κ = 1.6 for pre-tensioned members with a depth greater than 24-in.

κ = 2.0 for pre-tensioned members with debonded strand

f_{pe} = effective stress in the prestressing steel after losses (ksi)

d_b = nominal strand diameter (in.)

Depending on the length and position of debonded strands, STMs should consider the actual tie force flows expected within the prestressed concrete members. Llanos et al. (2009) proposed models for analyzing pre-tensioned I-girders with fully bonded strands and partially debonded strands under the web. For the I-girder with an excessive number of debonded strands located under the web, two longitudinal ties should be modeled to account for the realistic stress flow within the bottom flange, unlike I-girder with fully bonded strands (refer to Figure 2-9). There are no specific guidelines for locating debonded strands within the TxDOT Bridge Design Manual, so debonded strands can be placed where the designer wants, and both modeling approaches may need to be considered.

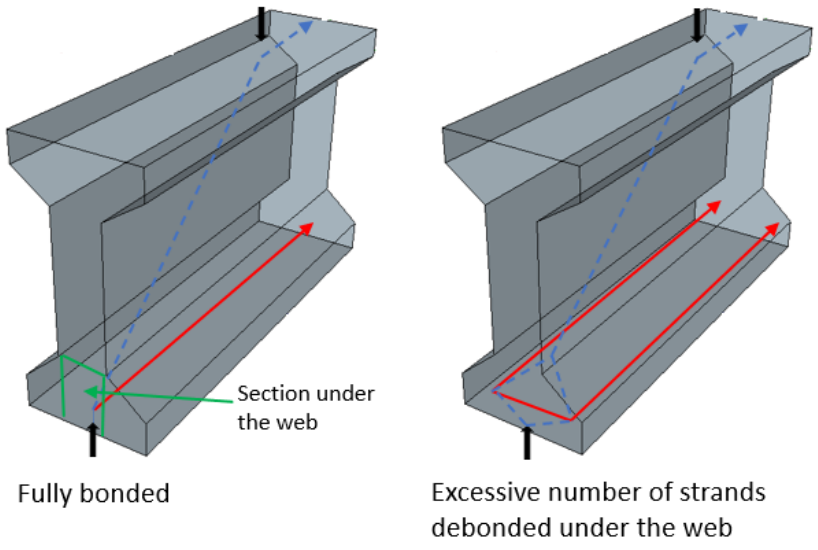

Figure 2-9. A comparison of strut-and-tie modeling approaches for fully bonded (left) versus the excessive number of debonded strands (right)

2.3.3. Harped strand

Despite the use of strand debonding, stresses at the end region may exceed the allowable stress limits, specifically for long-span members. In this case, harped strands could be used to actively control the stress at the end of the beam (refer to Figure 2-10). Furthermore, harped strands are typically the least preferred choice in design and construction due to the additional procedure required (i.e., hold-down strands) and safety concerns during fabrication. However, the application of harped strands still exists in the standard Tx-girder details. Nonetheless, from the perspective of strut-and-tie modeling, if the strands are harped, the force flow within the end region is complicated as such care needs to be taken for constructing STM models. Additionally, checking the tie capacity of the harped strands should be emphasized.

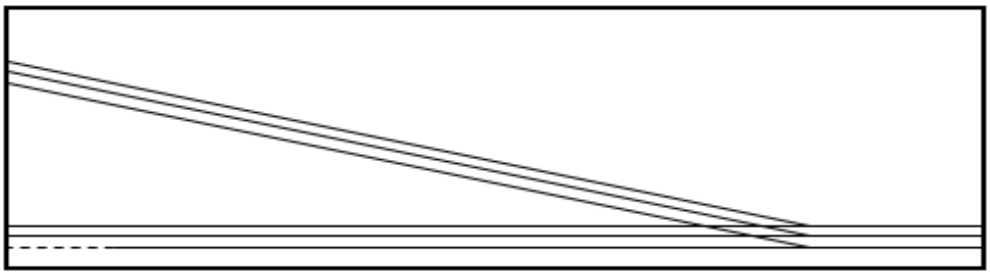

Figure 2-10. Girder with debonded & harped strands

There are limited attempts to generate STM models for prestressed beams with harped strands in the literature. In general, the approaches taken by previous researchers can be classified into two different strategies: (a) considering only one node for the harped strand tie as shown in Figure 2-11, Figure 2-12, and Figure 2-13, and (b) considering intermediate nodes to distribute tie forces as shown in Figure 2-14.

Llanos et al. (2009) calculated the ultimate capacity for prestressed concrete girders containing harped strands using the STM provision of AASHTO LRFD (2007) (Figure 2-11). It was compared with the shear capacities estimated using the simplified MCFT specified in AASHTO LRFD (2007) and the detailed method from ACI (2008). It should be noted that the shear capacity calculated using the STM shows the overly conservative estimation among those predictions. This is because the forces in the ties were limited due to the lack of strand development length and the negligence of mild steel bars detailed in the girder end in the STM model constructed (Llanos et al. 2009). Furthermore, the node on the harped strands was located at one-third of the shear span, and no direct strut from the loading point to the support was considered (refer to Figure 2-11). Therefore, the STM model

cannot completely represent the actual force flow within the member which might cause the overly conservative estimation.

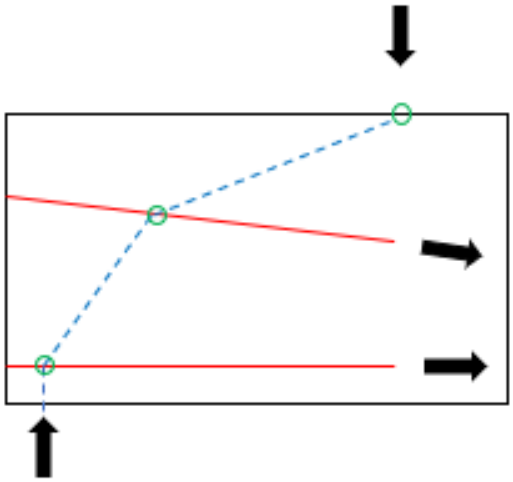

Figure 2-11. Simplified STM model for end of the prestressed beam with a harped strand (Llanos et al. 2009)

Floyd et al. (2016) constructed the STM model as shown in Figure 2-12 in consideration of the actual crack angle above the support, which was measured over the course of the structural test. Based on their STMs, the predicted shear capacity is substantially less than the measured values as observed in Llanos et al. (2009). These studies show that the ultimate capacity prediction using STMs for prestressed concrete beams with harped strands is overly conservative, indicating a lack of understanding of such members. Such rational STM strategies will be investigated and potentially proposed under this research project.

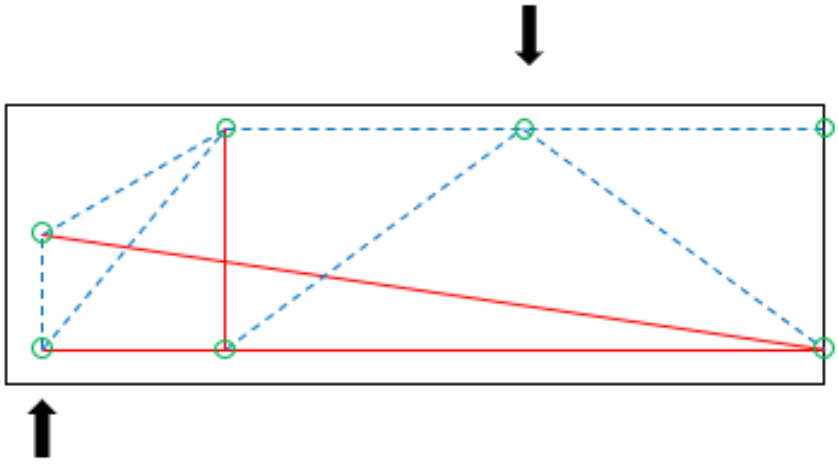

Figure 2-12. STM model for the prestressed beam with harped strand which considers actual crack angle (Floyd et al. 2016)

Figure 2-13 and Figure 2-14 are STM design examples of prestressed concrete members with harped strands subjected to a uniform load which takes into account a design load scenario (Martin and Sanders 2007; Reineck 2002). The STM proposed by Martin and Sanders (2007) is somewhat similar to the previous STM proposed by Floyd et al. (2016) and Llanos et al. (2009). In contrast, the STM proposed by Reineck (2002) has an additional intermediate node on the harped strands. Martin and Sanders (2007) claimed that the use of a single node to consider harped strands at the end region of prestressed concrete members could be a conservative assumption if the transfer length is less than the overall length of the harped prestressing strand. On the other hand, employing an intermediate node along the harped strands used for the STM in Reineck (2002) incorporated the effect of bond stresses on the tie forces and effectively redistributed the strut and tie forces.

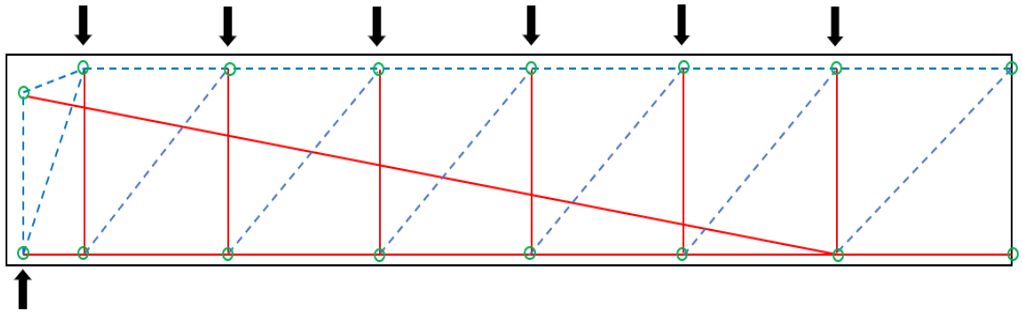

Figure 2-13. STM model for prestressed with harped strand and uniform load (Martin and Sanders 2007)

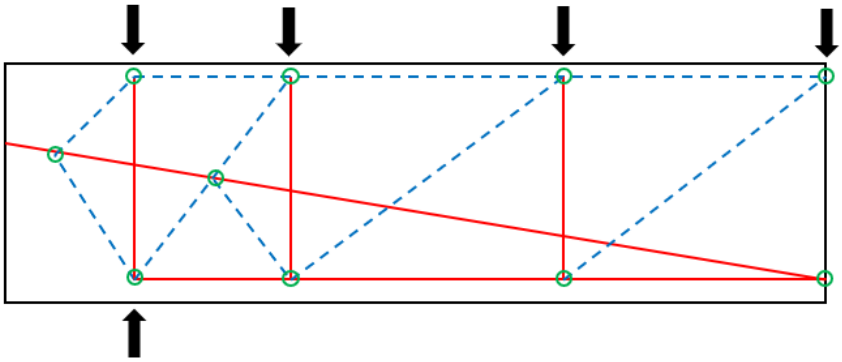

Figure 2-14. STM model for prestressed with harped strand under uniform load (additional node at harped strand) (Reineck 2002)

Since the length of the harped strands for Tx Girder is much longer than the transfer length, it may be conservative to consider a single node at the end of the harped

strand as proposed by (Martin and Sanders 2007). The final and refined STM strategy for prestressed beams will be introduced in the next chapter.

2.3.4. Support condition

To accommodate varying end region geometries and girder shapes, the width of bearing and the number of bearing supports are determined. However, due to the support conditions and the shape of the girders, the end region of girders could be subjected to highly disturbed stress conditions which may lead to premature splitting cracks, as shown in Figure 2-15. When lateral splitting occurs, the bond between the strand and the concrete will weaken, and it can cause strand slip.

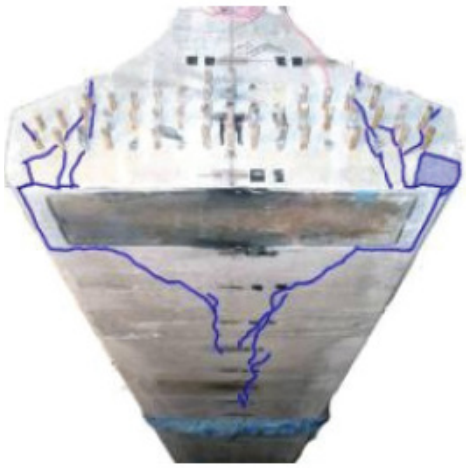

Figure 2-15. Lateral splitting failure (Ross et al. 2013)

The support condition is of importance in the cross-section STM procedure because it affects the force flow in the vicinity of the girder end regions. Figure 2-16 and Figure 2-17 demonstrate the influence of support conditions on the force flow at the end regions of an I-girder and box-girder diaphragm (Ross et al. 2013; Schlaich et al. 1987).

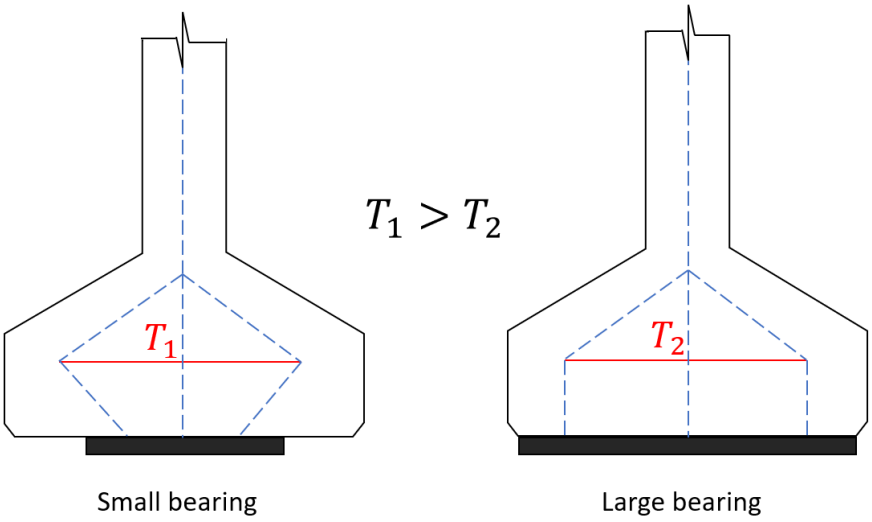

Figure 2-16. Comparison of stress flow and tie force for different sizes of bearing support

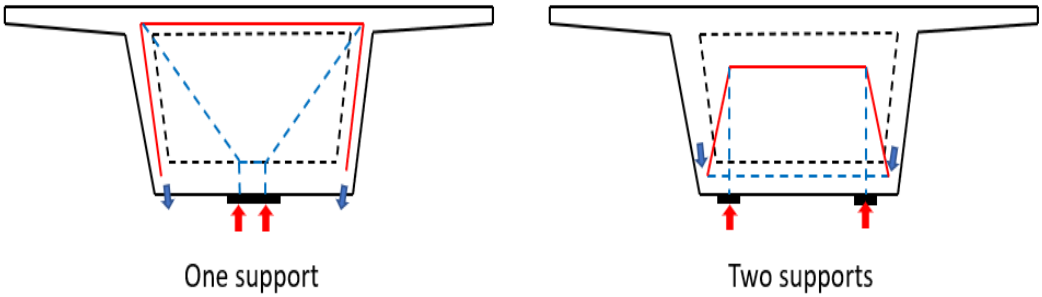

Figure 2-17. Comparison of stress flow in box beam for different number of supports

A review of TxDOT Bridge Standard Drawings reveals that (1) various bearing sizes are used depending on the height of the girder, and the shape of the girder end (i.e., skewed end), and (2) one or two bearing supports can be used for the girder types of U-beams, box-beams, X-beams, slab-beams, and decked-slab beams. Therefore, the STM analysis should carefully consider the influence of the support conditions and the end region geometries.

The appropriate STM approach should be taken at the end region of girders subjected to highly disturbed stress conditions due to the girders' support conditions and shape. Stresses induced by the various support conditions and girder geometries may not cause any adverse effects on the shear stress at the end region because the direction of STM is typically not aligned with the longitudinal direction of the girder. However, it is worthwhile to construct the appropriate STMs to identify other potential defects in the end regions.

2.3.4.1. Support size

To control the lateral splitting forces that may cause longitudinal splitting failure at the bottom flange of I-girder due to the support conditions, several researchers have proposed STM analysis to design confinement reinforcement at the bottom flange of I-girders (Ross et al. 2013; Shahrooz et al. 2017). To calculate the lateral splitting forces required to be carried by confinement reinforcement in the bottom flange (refer to Figure 2-18), STM should take into account the dimensions of the bearing support and the number of debonded strands (Shahrooz et al. 2017). The location of the distributed strut to apply pressure evenly across the bearing plate, c_b, is also determined by the width of the bearing plate and the number of bonded strands, and it can be calculated by Equation 2-4: (Shahrooz et al. 2017)

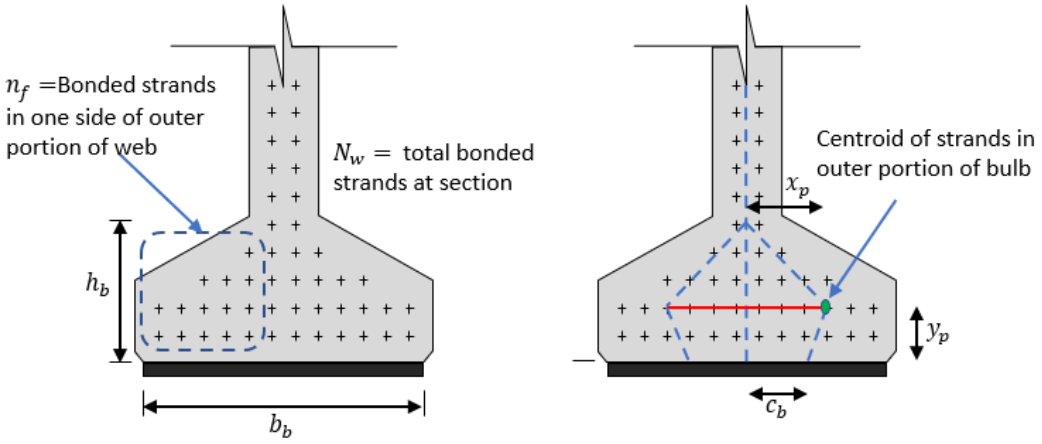

Figure 2-18. STMs for I-girder bulb

$$c_b = \left(\frac{b_b}{2}\right)\left(1 - \frac{n_f}{N_w}\right) \qquad \text{Equation 2-4}$$

Where:

b_b = width of bearing plate (in.)

N_w = total number of bonded strands at the cross-section

n_f = number of bonded strands in one side of the outer portion of the bulb

The horizontal tie force, t, which is the demand to be resisted by the confinement reinforcement, can be calculated by Equation 2-5: (Shahrooz et al. 2017)

$$t = \frac{aV_u}{\phi} = \left(\frac{n_f}{N_W}\right) \cdot \left[\frac{x_p}{h_p - y_p} + \frac{x_p - c_b}{y_p}\right] \cdot \frac{V_u}{\phi}$$ Equation 2-5

Where:

$\emptyset$ = reduction factor for shear (0.9)

V_u = total shear reaction at support (kips)

x_p = horizontal distance to girder centerline to the centroid of n_f strands in the outer portion of the bulb (in.)

y_p = vertical distance to girder soffit of the centroid of n_f strands in the outer portion of the bulb (in.)

A sufficient amount of confinement can control lateral splitting, one of the reasons for strand slip (Ross et al. 2013). In the current research project, TxDOT 0-7015, if the shear stress of the end region of the beam is greater than $0.18 f'_c$ shear stress limit, it may be necessary to check the capacity of typical confinement reinforcement provided in the TxDOT Bridge Standard Design using Equation 2-4 and Equation 2-5.

Also, idealized STMs for beams with double webs can be considered (refer to Figure 2-19) if the two conditions presented below are met. (Shahrooz et al. 2017).

- Bearing is provided under at least the full dimension of each web.
- The strands located in the planes of the webs are fully bonded.

Further, according to TxDOT's bridge design standards, the width of the bearing plate for box beam, U-beam, X-beam, and decked-slab beam is always wider than the web, and the use of debonding is limited to the center portion of the bottom flange. In that case, a simplified STM, such as the one shown in Figure 2-19, might be used for beams with double webs.

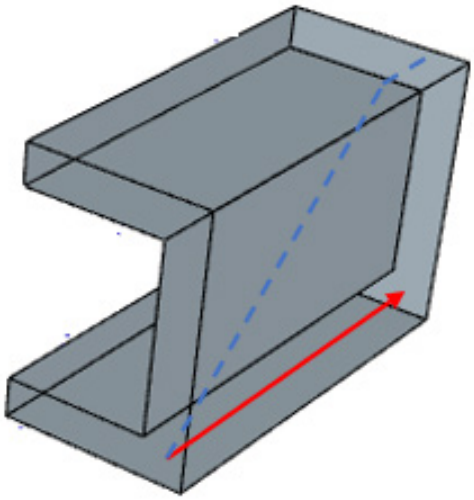

Figure 2-19. Strut-and-tie model for half of a box beam

2.3.4.2. Number of supports

Examples of three-dimensional STMs comparing box beams with different bearing pad supports are shown in Figure 2-20 (Avendano et al. 2013). When two bearing supports are placed under the web regions, as shown in Figure 2-20 (a), the load transfer mechanism is similar to those of a single web girder (i.e., I-girder). However, if one large bearing support is only placed in the center of the girder, the stresses at the end block are disturbed, which complicates the load transfer mechanism, as shown in Figure 2-20 (b). When comparing Figure 2-20 (a) and Figure 2-20 (b), the reaction force at the support and the visual force flow at longitudinal direction remain unchanged regardless of the number of supports. However, if only one bearing plate is used, as shown in Figure 2-20 (b), the stress flow for the cross-section of the end block should be considered in the STM.

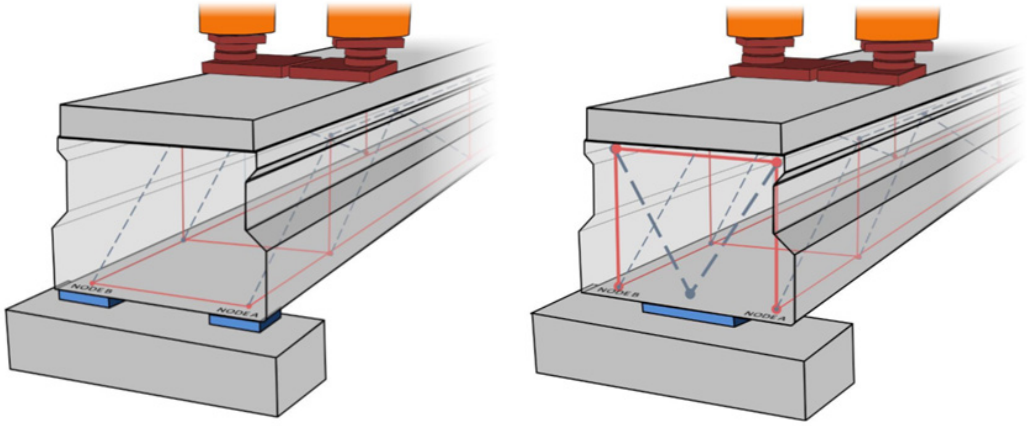

(a) Two bearing plate (b) One bearing plate

Figure 2-20. 3D STM models of box beam for different number of bearing plates (Avendano et al. 2013)

2.3.5. Geometry irregularity

Geometric irregularities (e.g., solid end block, skewed end, dapped end) are frequently introduced at the end regions of the bridge superstructures. Due to geometric irregularities at end regions, an appropriate STM model is critical for the efficient load transfer and the economic design of those regions. If the geometric irregularities are coupled with the aforementioned support conditions (e.g., width and number of bearing support), several in-plane STMs or three-dimensional STMs should be constructed, resulting in extra complexities and cumbersome calculation procedures. The previous TxDOT research projects and other research papers focusing on the behavior of end regions with either skewed or dapped end geometries will be extensively reviewed and utilized within this project to aid in the development and validation of STMs.

Several geometric irregularities that may require consideration when constructing STMs for this project are reviewed below. These irregular geometries are needed to be considered in this study, and the appropriate STMs are suggested.

2.3.5.1. End block

U-beams, box-beams, X-beams, and decked-slab beams have a solid end block at each end region. In those regions, the force transfer mechanisms are disturbed due to the drastic change of the cross-section. Figure 2-21 depicts a horizontal shear stress flow mechanism in the end region of a U-beam (Hovell et al. 2013). As the width of the web changes dimension, the horizontal shear stresses are spread at the end block. Also, the increased concrete area due to the end block will increase the capacity for the horizontal shear. Depending on the length of {Citation}the end

block and the support condition, the force transfer mechanisms should be taken into account for developing the STMs of the end region of such a beam.

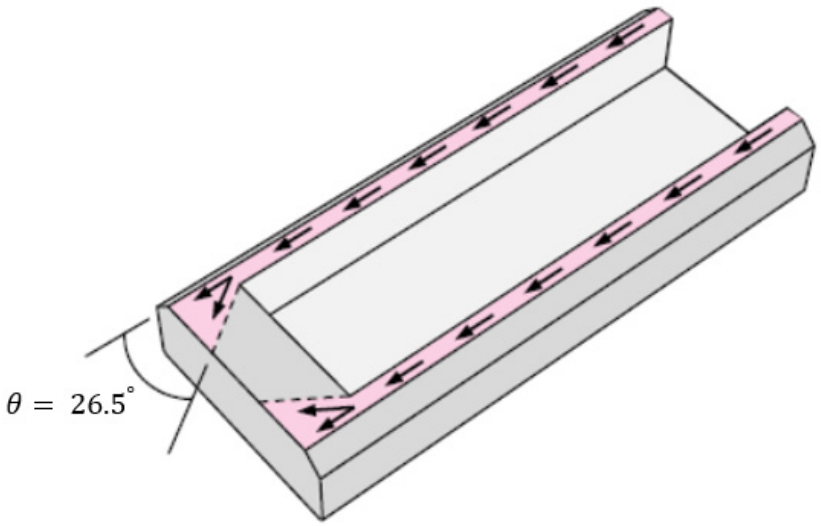

Figure 2-21. Stress spreads at end block (Hovell et al. 2013)

2.3.5.2. Skewed end

If skewed ends are used for prestressed concrete members, the construction of the STM at the end region is complicated. In this case, multiple STM models for the skewed end and longitudinal webs or three-dimensional STM models at the end region might be constructed. In the previous TxDOT research project 0-5831, the structural performances of Texas box beams and U-beams were investigated under shear-critical loads. One of the main variables was the interior void shape which can give an effect to end block geometry at the skewed end, as shown in Figure 2-22. Based on the evaluation of the structural test results, the shape of the interior void in the skewed ends did not influence shear strength (Avendano et al. 2013; Hovell et al. 2013). However, the detailed load transfer mechanism must be influenced by the shape of the skewed end. The end region geometries and experimental data of the TxDOT research project 0-5831 are considered to check the stress at the node, and it is explained in the next chapter.

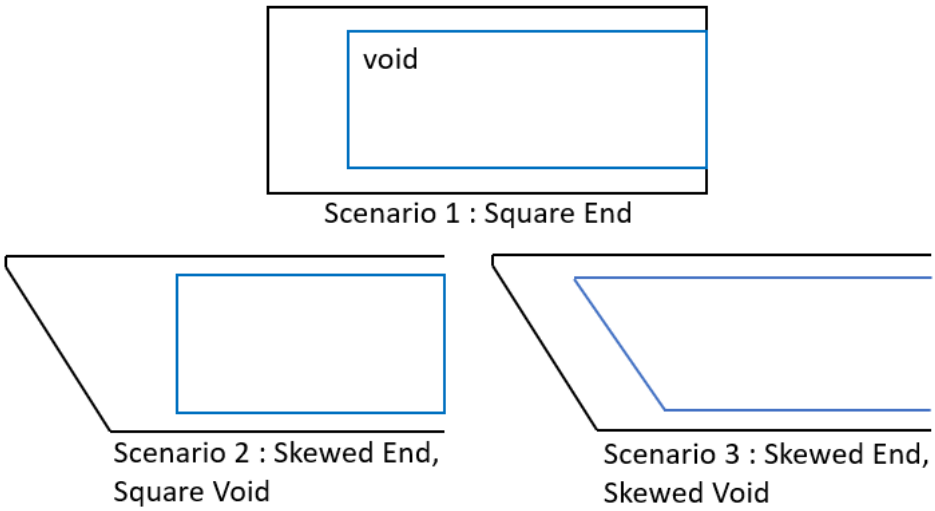

Figure 2-22. Different conditions made by the authors (Avendano et al. 2013; Hovell et al. 2013)

2.3.5.3. Dapped end

The end region of dapped beams is a discontinuity region, so sectional design procedures are unconservative, and the reentrant corner of the dapped end beam is typically subjected to elevated tensile stresses (Cook and Mitchell 1988; Klein et al. 2017; Mattock and Chan 1979). For these reasons, an appropriate STM which can account for the stress flow within the end region of the dapped end beams is typically employed for analysis and design. In the past, STMs were used in many dapped end reinforced concrete beam research studies (Barton et al. 1991; Cook and Mitchell 1988; Larson 2010; Mattock 2012; Schlaich et al. 1987), and STM guidelines are provided in ACI Committee 318-19 (2019) and FIP Commission 3 (1999). Also, there are STM design examples of reinforced concrete members with a dapped end (Bergmeister et al. 1993; Reineck 2002). The STMs for the dapped end used by these researchers are based on the two main STM models shown in Figure 2-23.

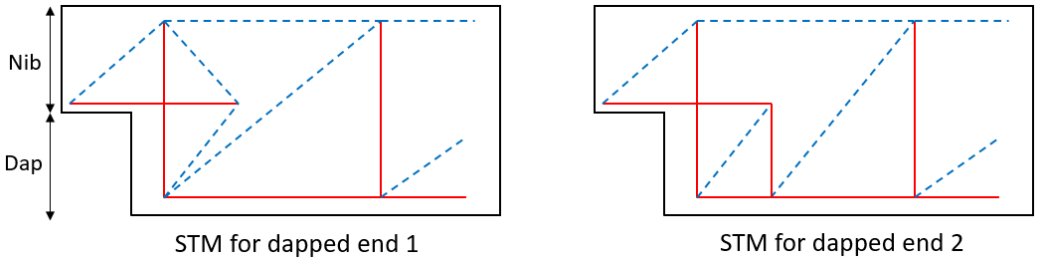

Figure 2-23. STM models for the dapped end (Cook and Mitchell 1988; Schlaich et al. 1987)

In the case of a dapped end beam, cracks can occur well in the reentrant corner due to the concentration of force, so using prestressed strand at the bottom of nib and dap is useful to reduce craking (Botros et al. 2017; Hamoudi and Phang 1975; Klein et al. 2017). The STM of the dapped end prestressed beam will be similar to that of the reinforced beam (refer to Figure 2-23). However, as previously described, the capacity of the longitudinal tie should be checked.

2.3.6. End region behavior at the transfer

End regions of pre-tensioned girders are subjected to transverse tensile stresses that are categorized as bursting, spalling, and splitting stresses (Yousefpour et al. 2017). Spalling stresses can cause horizontal or inclined cracks in the web at an elevation away from the bottom flange strand bundles. Bursting stresses are typically located in the bottom flange of pre-tensioned girders and result in longitudinal cracks. Splitting stress is caused by Hoyer's effect and causes cracks around the strands. The end region cracks owing to bursting, spalling, and splitting stresses are shown in Figure 2-24 (Avendano et al. 2013; FIB Special Activity Group 5 2013).

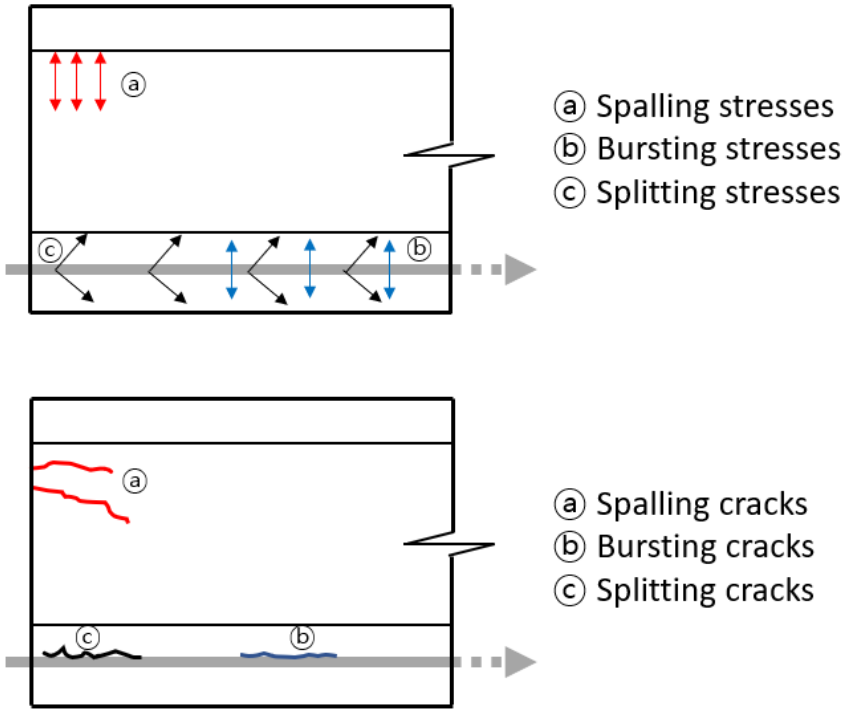

Figure 2-24. Typical end region stresses and cracks in pre-tensioned I-girder

Spalling, bursting, and splitting stresses in the end region are expected not to affect when analyzing beams using strut-and-tie procedures for several reasons. When developing STMs, the struts are formed in a direction that is almost perpendicular to the spalling crack. In addition, bursting cracks and splitting cracks are formed in

the concrete portion of the bottom flange, and these cracks are controlled by confinement reinforcement. The preexisting stresses owing to the pre-tensioning may seemingly influence the shear performance of the girders. However, when the pre-tensioned girders are subjected to design loading conditions, stresses owing to the external loads compensate for those stresses caused by the prestressing (Kim et al. 2018; Yousefpour et al. 2017). In other words, the force flow under the shear loading condition is not aligned with the stresses causing the splitting, bursting, and spalling. Also, the shear force caused by the loading condition even acts as clamping forces for splitting, bursting, and spalling.

2.4. Database Development and Result

Nakamura (2011) developed the latest version of the University of Texas Prestressed Concrete Shear Database (UTPCSDB-2011), containing 1696 tests reported in 99 references from 1954 to 2010. This database included test results published in North America, Japan, and Europe. A list of all references used for the latest version of the UTPCSDB was provided in Nakamura's Thesis (2011). Since the database contains prestressed concrete shear test data from 1954 to 2010, the UT research team will collect additional prestressed concrete shear test data from the literature published between 2010 and 2020 to complement the existing UTPCSDB-2020.

UTPCSDB-2020 expands the original database by including test results from 2011 to 2019 that were published in North America. The following criteria guided the selection of papers, student theses, and dissertations.

- Only the pre-tensioned beam considered in the tests
- Any types of cross-sections
- Both specimens with and without shear reinforcement
- Specimens with fiber-reinforced concrete excluded
- Specimens with fiber-reinforced polymer reinforcement excluded
- Any type of loading conditions and support

The format of the UTPCSDB-2020 is as same as the format of the UTPCSDB-2011. The database was expanded with 69 test results reported in 10 references (Chehab et al. 2018; De Wilder et al. 2015; Garber et al. 2016; Higgs et al. 2015; Katz et al. 2017; Langefeld 2012; Murray et al. 2019; Osborn et al. 2012; Tan et al. 2016; Villamizar et al. 2017), listed in Table 2-1. Several criteria filter the collected database to compare and analyze only the necessary data.

Table 2-1. List of additional references in UTPCSDB-2020

Authors	Year	Number of tests	Journal Sources
Osborn et al.	2012	2	Journal of Bridge Engineering
Langefeld	2012	4	Master's thesis, UT Austin
De wilder et al.	2015	9	Engineering Structures
Higgs et al.	2015	3	Journal of Bridge Engineering
Garber et al.	2016	5	ACI Structural Journal
Tan et al.	2016	28	ACI Structural Journal
Katz et al.	2017	4	ACI Structural Journal
Villamizar et al.	2017	4	ACI Structural Journal
Chehab et al.	2018	6	ACI Structural Journal
Murray et al.	2019	4	PCI Journal

2.4.1. Initial statistical analysis

In an effort to investigate the possibility of relaxing the $0.18 f'_c$ shear stress limit at the end region of TxDOT's standard prestressed concrete girders, an initial evaluation was performed (Figure 2-25 and Figure 2-26).

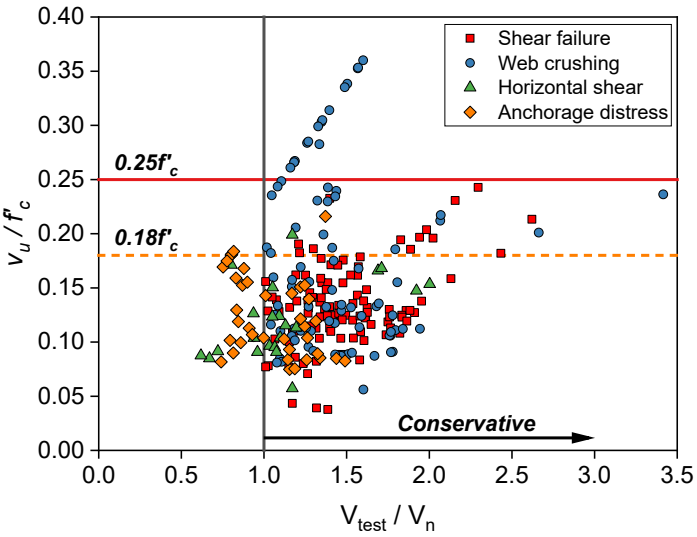

Note: Shear capacity estimations, V_n are calculated based on the AASHTO LRFD General Shear design provisions.

Figure 2-25. Distributions of failure mode for UTPCSDB-2020

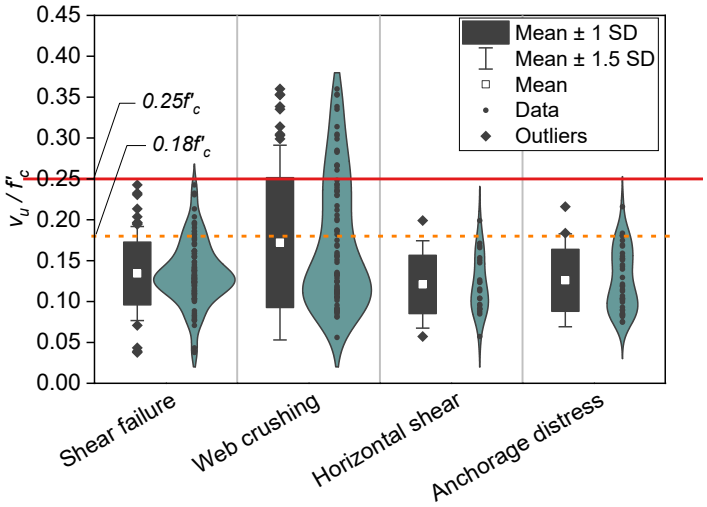

Figure 2-26. Distributions of shear stress to compressive strength ratio for each failure mode

According to the two figures above, there is no direct correlation between the $0.18\ f'_c$ shear stress limit and governing failure mechanisms. The $0.18\ f'_c$ shear stress limit cannot prevent web crushing, horizontal shear, and anchorage distress. Therefore, rather than using the $0.18\ f'_c$ shear stress limit to design the beam end, it might be useful to design the end region of the beam using STM.

2.4.2. Comparison of Tx-girder and AASHTO Type girder

The failure modes of the experimental tests are divided into five categories to compare the difference between the Tx-girder and the AASHTO Type girder in failure mode. The five types of failure modes are flexural failure, traditional shear failure, horizontal shear failure, anchorage zone distress, and no fail. The flexural failure is the failure which top flange concrete crushed or the bottom strands yields. Traditional shear failure is a well-understood shear failure mode, for which the design equations were written and calibrated in general. Traditional shear failure refers to flexure-shear, web-crushing, shear tension, and shear compression. Horizontal shear failure involves sliding at the interface of the web and the bottom flange. Anchorage zone distress includes specimens that failed due to strand slip or breakdown of the concrete-strand bond.

To complement the use of the UTPCSDB-2020 in comparing the two different girder types, the research team constructed the Shear Failure Evaluation Database (SFED), using these six filtering criteria:

1. Consider only the AASHTO Type girder and the Tx-girder
2. 28-day concrete strength is greater than 4 ksi
3. Consider only pre-tensioned girders
4. Effective prestress is greater than or equal to 125 ksi
5. Consider only the concentrated load
6. Consider only the shear failure mode (traditional shear, horizontal shear, and anchorage zone distress)

The SFED contains the results of 106 shear tests, of which 89 were for AASHTO Type girders, and 17 were for Tx-girders. The references used to construct SFED are organized in Table 2-2 (Alshegeir and Ramirez 1992; Avendaño and Bayrak 2008; Chehab et al. 2018; Garber et al. 2016; Hanson and Hulsbos 1964; Higgs et al. 2015; Katz et al. 2017; Kaufman and Ramirez 1988; Langefeld 2012; Laskar et al. 2007; Llanos et al. 2009; Murray et al. 2019; Osborn et al. 2012; Ramirez et al. 2000; Ramirez and Aguilar 2005; Shahawy and Batchelor 1996; Tawfiq 1995; Villamizar et al. 2017). Specific parameters were collected and calculated for SFED. Appendix B summarizes these particular parameters.

Table 2-2. Summary of Shear Failure Evaluation Database

Authors	Year	Tests	Beam Type
Hanson and Hulsbos	1964	3	AASHTO Type II
Kaufman and Ramirez	1988	4	AASHTO Type I & II

Authors	Year	Tests	Beam Type
Alshegeir and Ramirez	1992	3	AASHTO Type I & II
Tawfiq	1995	12	AASHTO Type II
Shahawy and Batchelor	1996	24	AASHTO Type II
Ramirez et al.	2000	4	AASHTO Type I
Labonte and Hamilton	2005	5	AASHTO Type II
Ramirez and Aguilar	2005	2	AASHTO Type I
Laskar et al.	2007	5	AASHTO Type I
Llanos et al.	2009	10	AASHTO Type III
Osborn et al.	2012	2	AASHTO Type II
Higgs et al.	2012	3	AASHTO Type II
Villamizar et al.	2017	3	AASHTO Type I
Chehab et al	2018	6	AASHTO Type II
Murray et al.	2019	3	AASHTO Type II
Avendano and Bayrak	2008	4	Tx-28
Langefeld	2012	4	Tx-46
Garber et al.	2016	5	Tx-46
Katz et al.	2017	4	Tx-46 & Tx-70

The difference in the ratio of bottom flange width to web width is a suitable basis for comparing the Tx-girder and AASHTO Type girder (Langefeld 2012). Therefore, the rate of shear stress-to-concrete strength, v_u/f'_c, is plotted versus the ratio of flange width-to-web width, b_f/b_w (refer to Figure 2-27) to compare the two girders. Figure 2-27 illustrates this comparison, in which AASHTO LRFD (2020) and SFED's data (refer to Equation 2-6) are used to calculate v_u/f'_c. The distribution

of the ratio of bottom flange width-to-web width of the AASHTO Type girder is between 2.5 and 3.5, but the ratio of bottom flange width-to-web width, b_f/b_w, of a Tx-girder is 4.6.

$$\frac{v_u}{f_c'} = \frac{\left|V_u - \phi V_p\right|}{\phi \times b_v \times d_v \times f_c'} \qquad \text{Equation 2-6}$$

Where :

b_v = effective web width (in.)

d_v = effective shear depth (in.)

$\emptyset$ = resistance factor for shear, 0.9

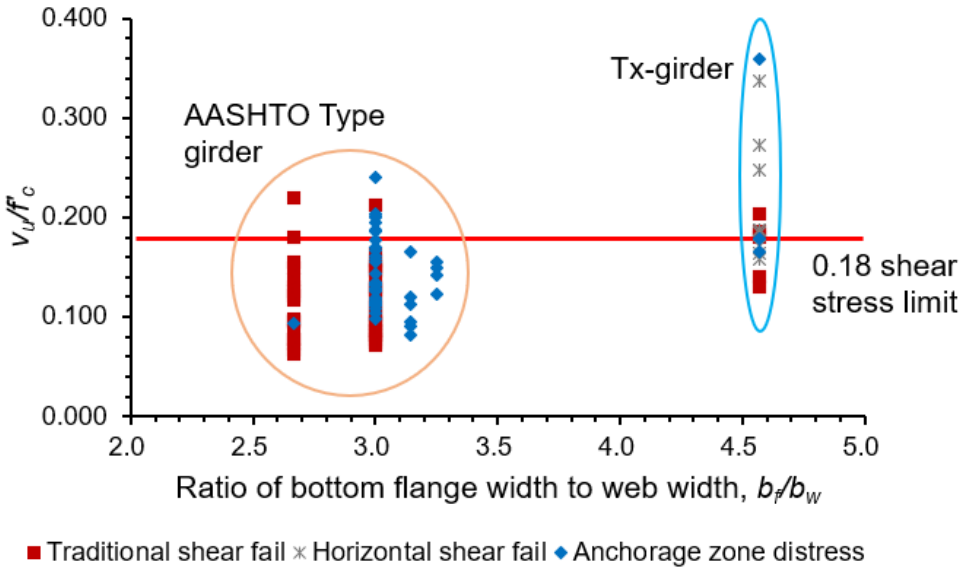

Figure 2-27. Compare the v_u/f'_c versus the b_f/b_w for AASHTO Type I-girder and Tx-girder

Figure 2-27 reveals two significant differences between AASHTO Type girders and Tx-girder. First, the average v_u/f'_c of the Tx-girders is larger than that of the AASHTO Type girders. In the AASHTO Type girders, the v_u/f'_c for 79 out of 89 test results is lower than the $0.18\,f'_c$ shear stress limit. However, in the Tx-girders, v_u/f'_c was lower than the $0.18\,f'_c$ shear stress limit for 4 out of 17 test results. Table 2-3 summarizes these differences.

Table 2-3. The difference for v_u/f'_c between Tx-girder and AASHTO Type girder

v_u/f'_c	Tx- girder	AASHTO Type girder
≥ 0.18	13 (76.5%)	10 (11.2%)
< 0.18	4 (23.5%)	79 (88.8%)

Also, the AASHTO Type girder and Tx-girder show a significant difference in failure mode. Among 89 failure results for AASHTO Type girders, traditional failure governed 46 times, anchorage zone distress governed 43 times, and horizontal shear failure did not occur. However, among the 17 failure results for Tx-girders, horizontal shear failure governed most often (nine times), and traditional shear failure and anchorage zone distress occurred five and three times, respectively (refer to Table 2-4). Therefore, horizontal shear failure is less likely to occur in the AASHTO Type girder but more likely in the Tx-girder. Despite their similar I-shape, a significant difference in failure mode as well as in v_u/f'_c was identified between the two girders.

Table 2-4. The difference for failure mode between Tx-girder and AASHTO Type girder

	Tx- girder	AASHTO Type girder
Traditional shear fail	5 (29.4%)	46 (51.7%)
Anchorage zone distress	3 (17.6%)	43 (48.3%)
Horizontal shear fail	9 (53%)	0 (0%)

AASHTO Type girder and Tx-girder show different behavior in experimental results due to the difference in geometry. A comparison of the two types of a similar height (refer to Figure 2-28) reveals that the Tx-girder has a broader bottom flange than the AASHTO Type girder, and more strands can be placed on the bottom flange. In actual experiments, the AASHTO Type girder has an average of 14 strands placed on the bottom flange, whereas the Tx-girder has an average of 37 strands (refer to Table 2-5).

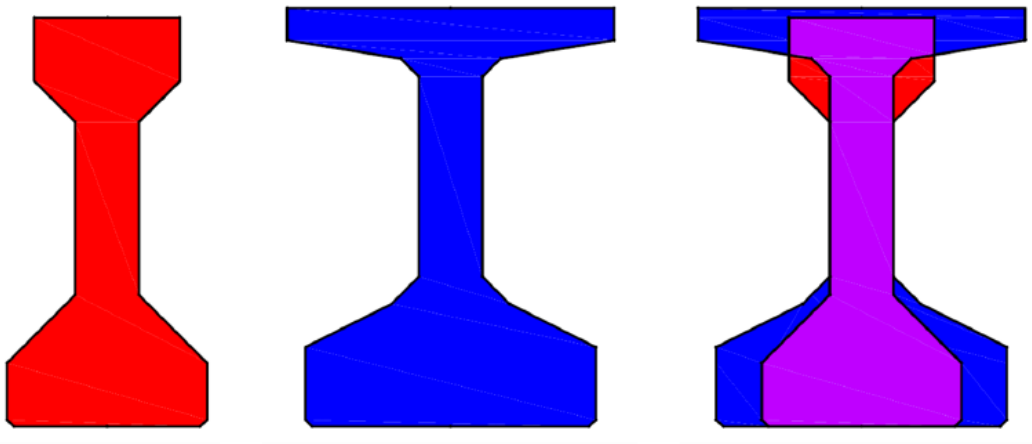

Figure 2-28. Comparison between AASHTO Type Ⅲ and Tx-46 cross-section (Langefeld 2012)

Table 2-5. The difference in the number of strands between Tx-girder and AASHTO Type girder

Number of strands	Tx-girder	AASHTO Type girder
0~10	0	23
11~20	0	57
21~30	5	9
31~40	6	0
41~50	1	0
51~60	5	0

The $0.18 f'_c$ shear stress limit might be too conservative for the Tx-girder because it can contain a greater number of strands, and thus a greater shear capacity than the AASHTO Type girder. For this reason, it is essential to study whether beams with relatively large bottom flange, such as Tx-girders, can relax $0.18 f'_c$ shear stress limits by using STM. When more strands are used in the bottom flange, the difference in stress between the bottom flange and the web due to prestress increases. So, the risk of horizontal shear failure in the interface between the web and bottom flange increases in the Tx-girder. Therefore, checking for horizontal

shear failure should be considered for girders that use many strands on the bottom flange. Depending on the geometry of the beam or the number of strands, the possibility of releasing the shear stress limit might be different. Therefore, this research will check whether the $0.18f'_c$ shear stress limit can be relaxed using STM not only for Tx-girder but also for other types of Texas beams.

2.5. Shear Strength Calculation Method in Provisions

This research tried to figure out how to calculate the shear strength capacity suggested in the bridge design provisions. Two bridge design provisions are investigated, one is AASHTO LRFD bridge design specification 9th edition, and the other is ACI building code 318-19. The processes of calculating shear strength through each method are briefly described in the following subsections. The more detailed descriptions are given in each design code provision.

2.5.1. AASHTO LRFD bridge design specification 9th edition

The 9th edition of the AASHTO LRFD bridge design specification was published in 2020, and the general procedure for calculating shear strength is used. This document will be referred to from here on as AASHTO LRFD (2020). The general procedure for shear calculations proposed in AASHTO LRFD (2020) is based on the Modified Compression Field Theory (MCFT). The MCFT is the method based on the response of cracked concrete to shear and normal load (Vecchio and Collins 1986). From the AASHTO LRFD (2020), the shear strength of the beam can be calculated by combining the contributions from concrete and steel. The nominal shear resistance, V_n, of the beam is given by Equation 2-7, shown below.

$$V_n = V_c + V_s + V_p \le 0.25 f'_c b_v d_v + V_p \qquad \text{Equation 2-7}$$

Where :

V_c = nominal shear resistance of the concrete (kip)

V_s = shear resistance provided by transverse reinforcement (kip)

V_p = component of prestressing force in the direction of the shear force (kip)

f'_c = compressive strength of concrete for use in design (ksi)

b_v = effective web width (in.)

d_v = effective shear depth (in.)

The nominal shear resistance of the beam's upper limit exists to prevent the web concrete from being crushed before the transverse reinforcement yields. The nominal shear resistance of the concrete can be calculated by Equation 2-8.

$$V_c = 0.0316\beta\sqrt{f_c'}b_v d_v \qquad \text{Equation 2-8}$$

Where :

β = factor indicating the ability of diagonally cracked concrete to transmit tension and shear

The parameter β is determined based on the amount of shear reinforcement. When the sections containing at least the minimum amount of transverse reinforcement specified in Article 5.7.2.5 in AASHTO LRFD (2020), the parameter β may be determined by Equation 2-9.

$$\beta = \frac{4.8}{\left(1 + 750\varepsilon_s\right)} \qquad \text{Equation 2-9}$$

However, when the sections contain the transverse reinforcement less than the required minimum amount of transverse reinforcement, the parameter β may be as specified in Equation 2-10.

$$\beta = \frac{4.8}{\left(1 + 750\varepsilon_s\right)} \frac{51}{\left(39 + s_{xe}\right)} \qquad \text{Equation 2-10}$$

In Equation 2-10, s_{xe} is the crack spacing parameter as influenced by the aggregate size, and it can be calculated as:

$$s_{xe} = s_x \frac{1.38}{a_g + 0.63} \qquad \text{Equation 2-11}$$

Where :

s_x = crack spacing parameter (in.)

a_g = maximum aggregate size (in.)

The parameter ε_s used in Equation 2-10 is the net longitudinal tensile strain in the section at the centroid of the tension reinforcement. This parameter may be determined by Equation 2-12.

$$\varepsilon_s = \frac{\left(\frac{|M_u|}{d_v} + 0.5N_u + |V_u - V_p| - A_{ps}f_{po}\right)}{E_s A_s + E_p A_{ps}} \qquad \text{Equation 2-12}$$

Where :

$|M_u|$ = absolute value of the factored moment, not less than $|V_u - V_p|d_v$ (kip-in.)

V_u = factored shear force (kip)

N_u = factored axial force (kip)

A_{ps} = area of prestressing steel on the flexural tension side of the member (in^2)

f_{po}= a value of 0.7 f_{pu} will be appropriate for prestressing members (ksi)

E_s = modulus of elasticity of longitudinal reinforcing bars (ksi)

A_s = area of non-prestressed steel on the flexural tension side of the member (in^2)

E_p = modulus of elasticity of prestressing tendons (ksi)

When the calculation for parameter ε_s is negative, the denominator of Equation 2-12 should be replaced by $(E_s A_s + E_p A_{ps} + E_c A_{ct})$, where E_c is the modulus of elasticity of concrete and A_{ct} is the area of concrete in tension. However, the calculated result of the parameter ε_s should not be taken as less than -0.4×10^{-3}. The shear resistance provided by transverse reinforcement can be calculated by Equation 2-13.

$$V_s = \frac{A_v f_y d_v \cot\theta}{s} \qquad \text{Equation 2-13}$$

Where :

A_v = area of transverse reinforcement within a distance s (in^2)

f_y = yield strength of reinforcing bars (ksi)

s = spacing of transverse reinforcement (in.)

In Equation 2-13, the angle of inclination of diagonal compressive stress, θ, is determined by following equation:

$$\theta = 29 + 3500\varepsilon_s \qquad \text{Equation 2-14}$$

2.5.2. ACI building code 318-19

The detailed method on ACI building code 318-19 is considered to calculate the shear strength in this research and referred to from this point on as ACI 318-19 (2019). The calculation for nominal shear strength of the beam, V_n, is consists of the nominal shear strength provided by concrete, V_c, and the nominal shear strength provided by shear reinforcement, V_s, and it can be calculated by Equation 2-15.

$$V_n = V_c + V_s \qquad \text{Equation 2-15}$$

The nominal shear strength provided by concrete is taken as the lesser of two shear strengths: the nominal shear strength provided by concrete when diagonal cracking results from combined shear and moment, V_{ci}, and the nominal shear strength provided by concrete when diagonal cracking results from high principal tensile stress in the web, V_{cw}. When normal-weight concrete is used, the equation for the parameter V_{ci} is as follows:

$$V_{ci} = 0.6\sqrt{f_c'}b_w d_p + V_d + \frac{V_i M_{cre}}{M_{\max}} \geq 1.7\sqrt{f_c'}b_w d \qquad \text{Equation 2-16}$$

Where :

f'_c = specified compressive strength of concrete (psi)

b_w = web width (in.)

d_p = distance from extreme compression fiber to centroid of prestressing steel (in.)

V_d = shear force at section due to unfactored dead load (lb)

V_i = factored shear force at section due to externally applied loads occurring simultaneously with M_{max} (lb)

M_{max} = maximum factored moment at section due to externally applied loads (lb-in.)

M_{cre} = moment causing flexural cracking at section due to externally applied loads (lb-in.)

$$M_{cre} = \frac{I}{y_t}\left(6\sqrt{f_c'} + f_{pe} - f_d\right) \qquad \text{Equation 2-17}$$

I = moment of inertia of section resisting externally applied loads (in^4)

y_t = distance from the centroidal axis of section resisting externally applied loads to tension face (in.)

f_{pe} = compressive stress in concrete due to effective prestress force only at the extreme fiber of section where tensile stress is caused by externally applied load (psi)

f_d = stress due to unfactored dead load at the extreme fiber of section where tensile stress is caused by externally applied load (psi)

Also, the nominal shear strength provided by shear reinforcement, V_s, is given by Equation 2-18.

$$V_{cw} = \left(3.5\sqrt{f_c'} + 0.3f_{pc}\right)b_w d_p + V_p \qquad \text{Equation 2-18}$$

Where :

f_{pc} = compressive strength of concrete at the centroid of cross-section resisting externally applied load (psi)

V_p = vertical component of effective prestress force at section (lb)

The nominal shear strength provided by shear reinforcement, V_s, is based on a 45-degree truss model representing the crack angle with respect to the longitudinal axis. It may be determined by Equation 2-19.

$$V_s = \frac{A_v f_{yt} d}{s} \qquad \text{Equation 2-19}$$

Where :

A_v = area of vertical shear reinforcement at spacing s (in^2)

f_{yt} = specified yield strength of transverse reinforcement (psi)

d = distance from extreme compression fiber to centroid of longitudianl tension reinforcement (in.)

s = center-to-center spacing of reinforcement (in.)

2.6. Chapter Summary

Before calculating the shear stress limit of Texas standard prestressed beam using STM, background knowledge for this study is investigated. First, the geometry features and differences of six typed beams in Texas standard prestressed beam are analyzed. Since the stress flow changes with and without the distinction between web and flange, this difference in geometry should be considered when calculating shear strength.

Next, the characteristics to be considered in order to use STM for prestressed girder are investigated, and strategies to consider these characteristics in STM are prepared. Through the design codes (AASHTO LRFD, ACI building code, fib) and various researches performed previously (Avendano et al. 2013; Avendaño Valderrama 2011; Barton et al. 1991; Bergmeister et al. 1993; Cook and Mitchell 1988; Floyd et al. 2016; Hovell et al. 2013; Klein et al. 2017; Llanos et al. 2009; Martin and Sanders 2007; Mattock 2012; Reineck 2002; Ross et al. 2013; Schlaich et al. 1987; Shahrooz et al. 2017), features and strategies for STM of the prestressed concrete beam are prepared. There are a total of six main characteristics of the prestressed beam, and these features should be considered when calculating the shear stress limit of the end region of Texas standard prestressed beam using STM.

Furthermore, the correlation between the $0.18\,f'_c$ shear stress limit and governing failure mechanisms is analyzed using the University of Texas Prestressed Concrete Shear Database (UTPCSD), and as a result, there is no significant correlation between the $0.18\,f'_c$ shear stress limit and governing failure mechanisms. In addition, Tx-girder and AASHTO Type I-girder are compared using the database. It is found that the $0.18\,f'_c$ shear stress limit may be too conservative for the Tx-girder because the Tx-girder can have a larger shear stress capacity than the AASHTO Type I-girder. This is because the Tx-girder has a larger area of the bottom flange, and a larger amount of strand can be placed in the bottom flange. Plus, in order to compare the shear strength calculated by the method presented in the bridge design provisions with the shear strength calculated by the analytical method proposed in this study, two different bridge design provisions are investigated. One is the general procedure in AASHTO LRFD (2020), and the other is the detailed method on ACI 318-19 (2019).

Chapter 3. Calculation of Shear Stress for Prestressed Beams

3.1. Introduction

According to AASHTO LRFD (2020), shear design stresses can exceed $0.18 f'_c$, provided that the end region is appropriately detailed using Strut-and-Tie Model (STM) procedures. The purpose of this chapter is to propose an analytical method to calculate the shear stress at the end region of Texas beams using STM and other factors and explore the possibility of increasing the shear stress limit. When calculating the shear force using STM, consideration must be given to whether the beam does or does not contain harped strands and debonded strands. In addition, the shear strength related to anchorage capacity is calculated by the longitudinal tension capacity equation presented in Article 5.7.3.5 of AASHTO LRFD (2020). Finally, the shear stress of the end region of the beam should be calculated using the smaller of the shear forces calculated by STM and anchorage capacity.

In this research, the geometries and strand layouts provided in the TxDOT's standard design are considered to develop the STM. Also, for girders which properties are not suggested in TxDOT's standard design, the properties should be calculated using PG Super which is the commercial software that can design and analyze precast-prestressed girders and evaluate the load. PG Super can design, check, and load rate of precast, prestressed girders based on AASHTO LRFD Bridge Design Specification and TxDOT Bridge Design Criteria. The flexural design function calculates the required number and layout of prestressing strands and the minimum required concrete strength. Also, the number, size, spacing of transverse reinforcement for vertical shear, horizontal shear, bursting, and strand construction are determined when using the shear design function. Thus, for girders which properties (strand and rebar layout and concrete strength) are not suggested in TxDOT's standard design, the properties can be calculated using PG Super. Detailed explanation for using the PG Super is described in BridgeLink-PGSuper Design Guide(TxDOT 2020b) and Precast, Prestress Bridge girder Design Example (Brice 2020).

The girder in which the strands are arranged sequentially at the bottom row is the standard strand pattern girder. However, there are cases where the strands are not arranged sequentially from the lowest row, and this case is the non-standard strand pattern. When calculating the shear stress capacity of the beam's end region using the developed STM, the differences between the standard and non-standard strand patterns will be compared. To calculate the shear stress capacity of a texas beam using STM, the total prestress loss of the strand must be assumed.

3.2. Basic Concept of Analytical Method to Calculate Shear Stress

In this study, the value of the total prestress loss is determined using the experimental results of measuring the total prestress loss. Garber (2014) studied the total prestress loss of the prestressing strand. He collected experimental results measuring total prestress loss from various studies found in the literature. The total prestress losses of the experimental results he collected are shown in Figure 3-1. As shown in Figure 3-1, an analysis of the 140 test results revealed that the overwhelming majority reported a prestress loss of 19%, and the average prestress loss was 19.9%. Therefore, in this research, the shear stress is calculated by assuming a total prestress loss of 20%. In addition, about 70% of the measured value of the total prestress loss is distributed between 15% and 25%. Therefore, the calculated shear stress of the Texas standard prestressed beam when the total prestress loss is 15%, 20%, and 25%, respectively, is compared, and the results are explained in Chapter 5.

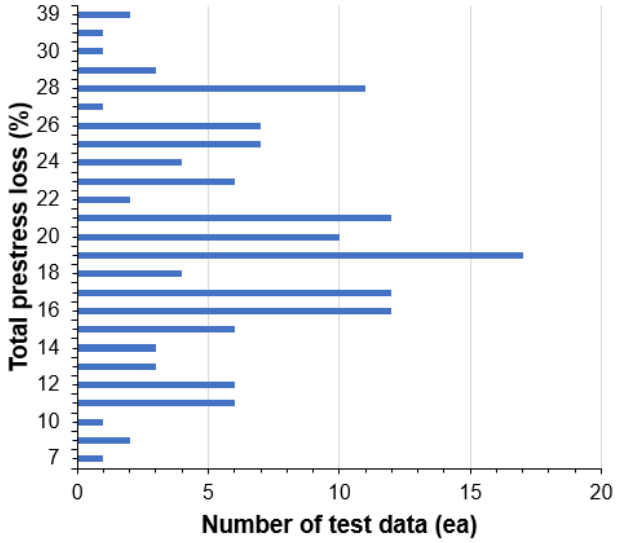

Figure 3-1. Total prestress losses (140 test)

This study uses two different methods to calculate shear force, V_u. First, the shear force is calculated based on the STM, and the anchorage capacity of the girder end is used to calculate the shear force again. After calculation, the smaller of the two computed shear forces are used to calculate v_u/f'_c. Before calculating the shear force, the girder's geometric properties and material properties need to be confirmed. Girder geometry, strand layout, and reinforcement layout comprise the geometric properties. The yield strength of the prestressing strand and reinforcement, as well as the concrete strength, are some of the material properties.

The flowchart for calculating the maximum shear stress of the Texas beam is shown in Figure 3-2, and each component is explained in the following subsections.

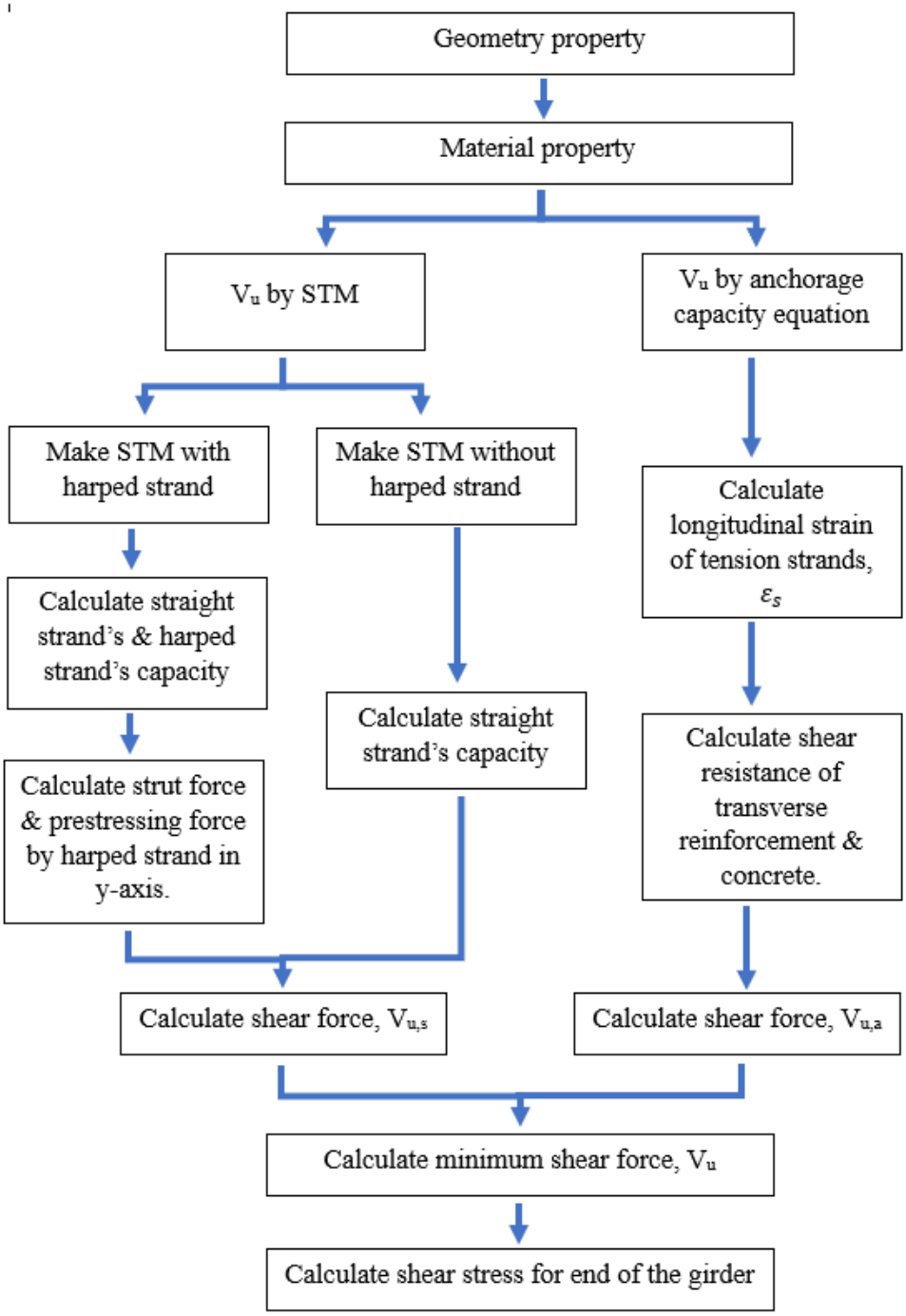

Figure 3-2. Flow chart for shear stress calculation

The average stress in prestressing steel, f_{ps}, effective prestress, f_{pe}, and effective shear depth, d_v, for the girder should be calculated by geometric properties and material properties. The average stress in prestressing steel, f_{ps}, and effective

prestress, f_{pe}, are calculated using the equation given by AASHTO LRFD (2020). The equation for calculating the average stress in prestressing steel, f_{ps}, is provided in Article 5.6.3.1.1 of AASHTO LRFD (2020) and is provided here as Equation 3-1.

$$f_{ps} = f_{pu}\left(1 - k\frac{c}{d_p}\right) \qquad \text{Equation 3-1}$$

Where :

f_{pu} = ultimate strength of prestressing steel (ksi)

d_p = distance from extreme compression fiber to the centroid of the prestressing force (in.)

In which :

$$k = 2\left(1.04 - \frac{f_{py}}{f_{pu}}\right) \qquad \text{Equation 3-2}$$

Where :

f_{py} = yield strength of prestressing steel, 90% of f_{pu} (ksi)

The calculation formula for distance from the extreme compression fiber to the neutral axis, *c*, can be changed according to the shape of section and length of the depth of equivalent rectangular stress block, *a*, which can be calculated by Equation 3-3.

$$a = \beta_1 \times c \qquad \text{Equation 3-3}$$

Where :

β_1 = stress block factor for deck

The stress block factor, α_1, shall be taken as 0.85 and the other stress block factor, β_1, shall be considered 0.85 for compressive strengths of concrete not exceeding 4.0 ksi. For compressive strengths of concrete exceeding 4.0 ksi, β_1 shall be reduced at a rate of 0.05 for each 1.0 ksi of strength over 4.0 ksi, except that β_1 shall not be taken to be less than 0.65. Suppose the length of the depth of equivalent rectangular stress block, a, is smaller than the deck thickness. In that case, the top section of the beam is assumed to be a rectangular section and using Equation 3-4 to calculate the distance from the extreme compression fiber to the neutral axis, *c*.

When the top part for calculating the distance from the extreme compression fiber to the neutral axis, *c*, is a rectangular section, the design concrete strength of the deck, $f'_{c,deck}$, should be used in Equation 3-4.

$$c = \frac{A_{ps}f_{pu} + A_s f_s + A_s' f_s' - A_s'' f_s''}{\alpha_1 f_{c,deck}' \beta_1 b_{deck} + kA_{ps}\frac{f_{pu}}{d_{ps}}} \qquad \text{Equation 3-4}$$

Where :

A_{ps} = area of prestressing steel (in.^{2})

A_s = area of non-prestressed tension reinforcement (in.^{2})

A_s' = area of compression reinforcement in girder (in.^{2})

A_s'' = area of compression reinforcement in the deck (in.^{2})

f_s = stress in the non-prestressed tension reinforcement at nominal flexural resistance (ksi)

f_s' = stress in the non-prestressed compression reinforcement at nominal flexural resistance in girder (ksi)

f_s'' = stress in the non-prestressed compression reinforcement at nominal flexural resistance in the deck (ksi)

b_{deck} = the effective width of the deck (in.)

When the rectangular stress block, *a*, is larger than the deck thickness, the top section of the beam is assumed to be a T-section, and Equation 3-5 is used to calculate the extreme compression fiber to the neutral axis, *c*. Because the rectangular stress block, *a*, for the Texas beam is typically either smaller or slightly larger than the deck thickness, the concrete strength of the deck is only considered to calculate the extreme compression fiber to the neutral axis, *c*, even if the rectangular stress block, *a*, is greater than the thickness of the deck.

$$c = \frac{A_{ps}f_{pu} + A_s f_s + A_s' f_s' - A_s'' f_s'' - \alpha_1 f_{c,deck}'(b_{deck} - b_w)h_{deck}}{\alpha_1 f_{c,deck}' \beta_1 b_{deck} + kA_{ps}\frac{f_{pu}}{d_{ps}}} \qquad \text{Equation 3-5}$$

Where :

b_w = web width (in.)

h_{deck} = deck depth (in.)

The calculated variables from Equation 3-2 to Equation 3-5 are used to calculate the average stress in prestressing steel. In order to calculate the capacity of the prestressing strand, not only the average stress in prestressing steel, f_{ps}, but also the effective prestress, f_{pe}, should be calculated. The final prestress loss is assumed to be 20% (refer to Figure 3-1), so the effective prestress is calculated by Equation 3-6. In Equation 3-6, the stress in prestressing steel immediately before the transfer, f_{po}, is assumed to be 75% of the ultimate strength of prestressing steel, f_{pu}, in the case of low relaxation strand according to Table 5.9.2.2-1 of AASHTO LRFD (2020). Since Texas standard prestressed beam uses low relaxation strand for all types of beams, 75% of ultimate strength of prestressing steel, f_{pu}, is suitable for stress in prestressing steel immediately before the transfer, f_{po}.

$$f_{pe} = 0.80 f_{po} \qquad \text{Equation 3-6}$$

After calculating the average stress and effective stress of the prestressing strand, the effective depth, d_v, can be calculated. According to the AASHTO LRFD (2020), the effective shear depth can be calculated using the nominal flexural resistance, M_n. When the depth of the equivalent rectangular stress block, a, is smaller than the deck thickness, Equation 3-7 is used to calculate the nominal flexural resistance, M_n. However, if the equivalent rectangular stress block, a, is larger than the deck thickness, the nominal flexural resistance, M_n, is calculated using Equation 3-8.

$$M_n = A_{ps} f_{ps}\left(d_p - \frac{a}{2}\right) + A_s f_s\left(d_s - \frac{a}{2}\right) + A_s' f_s'\left(d_s' - \frac{a}{2}\right) - A_s'' f_s''\left(d_s'' - \frac{a}{2}\right) \qquad \text{Equation 3-7}$$

$$M_n = A_{ps} f_{ps}\left(d_p - \frac{a}{2}\right) + A_s f_s\left(d_s - \frac{a}{2}\right) + A_s' f_s'\left(d_s' - \frac{a}{2}\right) - A_s'' f_s''\left(d_s'' - \frac{a}{2}\right) + \alpha_1 f_{c,deck}'\left(b_{deck} - b_w\right) h_{deck}\left(\frac{a}{2} - \frac{h_{deck}}{2}\right) \qquad \text{Equation 3-8}$$

The effective shear depth, d_v, is the distance between the resultants of the tensile and compressive forces due to flexure, and it can be determined as Equation 3-9. Also, the effective shear depth, d_v, should not be less than the greater of $0.9d_p$ or $0.72h$ (in.).

$$d_v = \frac{M_n}{A_s f_y + A_{ps} f_{ps}} \qquad \text{Equation 3-9}$$

3.3. Calculate Shear Strength by STM

The tie capacity of strands should be calculated at first to calculate the shear stress using STM. After calculating the tie capacity of the strand, the shear strength, V_u, of the end region of the beam can be computed using STM. The basic concept for calculating the shear strength, V_u, using STM with tie capacity according to the number of strands, is shown in Figure 3-3. Also, the STM of the end region of the beam will differ depending on whether it does or does not contain the harped strand; those differences are described in the following subsections.

- Calculate tie force (T) from the number of strands
- Calculate diagonal strut force (S) from the tie force
- Calculate reaction force (R_u)
- Calculate shear stress (v_u) when the concentrated load acts on d_v from the support.

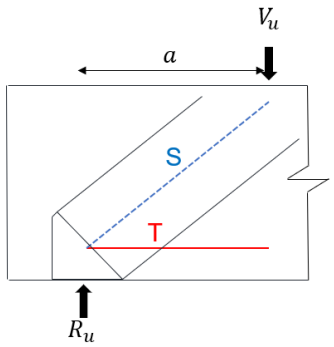

Figure 3-3. Basic concept of calculating shear strength using STM

3.3.1. STM consider the straight strand only

If the prestressing strands are present only on the bottom flange, one tie and strut need to be considered in the STM at the end of the beam. Before using the STM at the end of the beam, the shear span and height of the STM model, h_{stm}, should be calculated. For the convenience of calculation, the height of the STM model, h_{stm}, used the same value as the effective shear depth, d_v, calculated through Equation 3-9. According to the 2010 fib model code for concrete structures (FIB Special Activity Group 5 2013), the limit of the compressive stress field inclination, θ, relative to the longitudinal axis of the prestress member (Figure 3-4), is larger than 25 degrees but smaller than 45 degrees.

When the angle between the strut and tie increases, the maximum shear force acting at the shear span will increase. It is an extreme case to calculate shear stress when the compressive stress field inclination, θ, is 45 degrees. Therefore, a shear span with the compressive stress field inclination, θ, for 45 degrees is used to compute the shear stress of the end region of the beam. The tie's location is the same as the distance from the bottom to the centroid of the straight strands, y_b. The STM model for the end of the beam is shown in Figure 3-4.

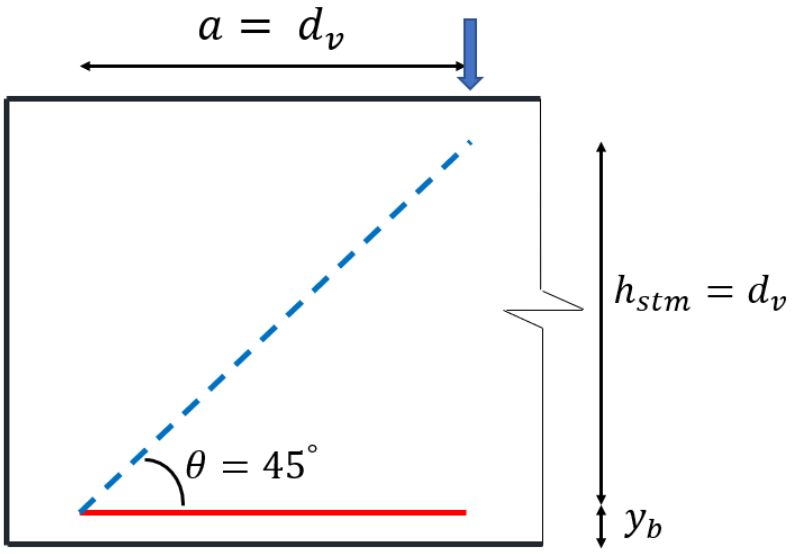

Figure 3-4. STM model for the end of the beam

The tie force of the STM model should be calculated first to calculate the shear stress in the end region of the beam using STM. The strand stress at the beam's end region increases along with the distance from the free end of strands. Therefore, the tie force of the critical section for the development of the tie (refer to Figure 3-5) is more significant and has a more realistic tie capacity than the tie force at the central point of support.

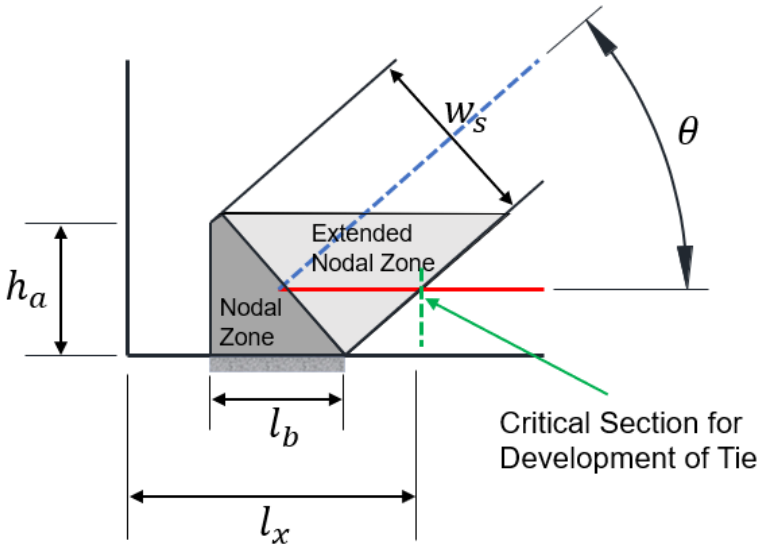

Figure 3-5. Calculate tie force at extended nodal zone

In Figure 3-5, the length of the back face of the node, h_a, is twice the width of the tie that represents the straight strands in the beam, y_b. The length of the bearing

plate, l_b, for each girder can be found in TxDOT's standard design. The strut-to-node interface is the face where the diagonal strut enters the node, and this face is perpendicular to the axis of the diagonal strut. The point where the extended nodal zone meets the tie for the straight strand is the critical section of the strand, and the available length for the straight strand is the distance from the end of the beam to the critical section. The length of the strut-to-node interface, w_s, and available length for strand, l_x, can be calculated through Equation 3-10 and Equation 3-11 (Williams et al. 2012).

$$w_s = h_a \times \cos\theta + l_b \times \sin\theta \qquad \text{Equation 3-10}$$

$$l_x = \frac{w_s / 2}{\sin\theta} + oh \qquad \text{Equation 3-11}$$

Where :

oh = distance from the end of the girder to the central point of support (in.)

The tie force at the critical section is calculated by available length for strand, transfer length, l_t, and the total area of bonded straight strands, A_{bp} (as expressed in Equation 3-12). Per the AASHTO LRFD (2020), the transfer length, l_t, is 60 times the strand diameter, and available length, l_x, for strand should be less than transfer length, l_t.

$$T = A_{bp} \times f_{pe} \times \frac{l_x}{l_t} \qquad \text{Equation 3-12}$$

When there are no harped strands, the reaction force, R_u, can be calculated from the straight strand's tie force and the compressive stress field inclination, θ. In this study, $V_{u,s}$ is the shear force calculated by STM and is equal to the reaction force, R_u. Therefore, the equation for calculating the shear force of the end region of the beam without harped strands is as follows:

$$V_{u,s} = R_u = T \times \tan\theta \qquad \text{Equation 3-13}$$

3.3.2. STM consider the harped strand

Only Tx-girder uses harped strands among Texas beams, and other texas beams do not use harped strands. Therefore, the STM with the harped strand is only used for the Tx-girder. In the beam where the harped strand is used, the location of the hold-down point of the harped strand should be considered. In the case of Tx-girders, the length from the hold-down point to the center of the beam, L_{hp}, is set to 0.05 times the span length, L, and should not exceed 5 ft. The angle between the tie for the

harped strand and the tie for the straight strand, θ_1, can be calculated as the distance from beam end to a hold-down point, L_h, and the length from the centroid of the harped strand to the centroid of the straight strand, H_h .

$$\theta_1 = \tan^{-1}\left(\frac{H_h}{L_h}\right) \qquad \text{Equation 3-14}$$

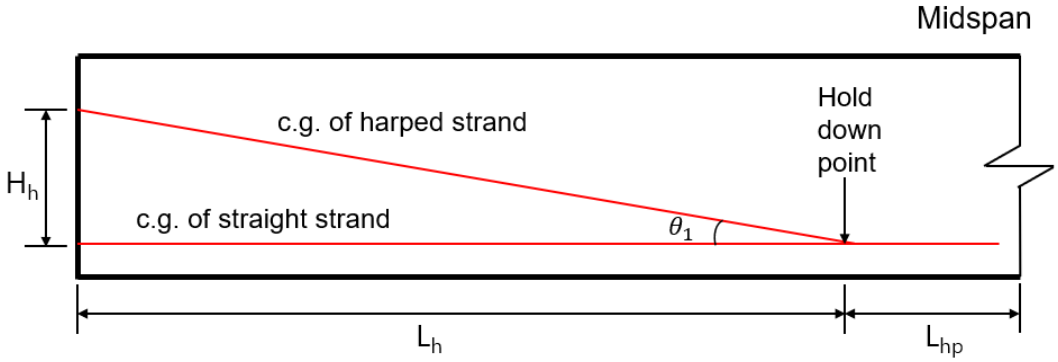

Figure 3-6. Harping configuration

The STM for the end of the beam with the harped strands contains two ties and three struts, as shown in Figure 3-7. From the STM for the beam's end region, which includes harped strands, the location of the node for the harped strand should be calculated. The angle between the upper strut (S_1) and harped strands' tie (T_3) should be more than 25 degrees. In this study, the angle between the lower strut (S_2) and straight strands' tie (T_1) is assumed not to exceed 90 degrees. The angle between the strut connecting the straight strand's tie and concentrated load (S_3) and the straight strands' tie (T_1) is set to 45 degrees, the same as for the beam without harped strands.

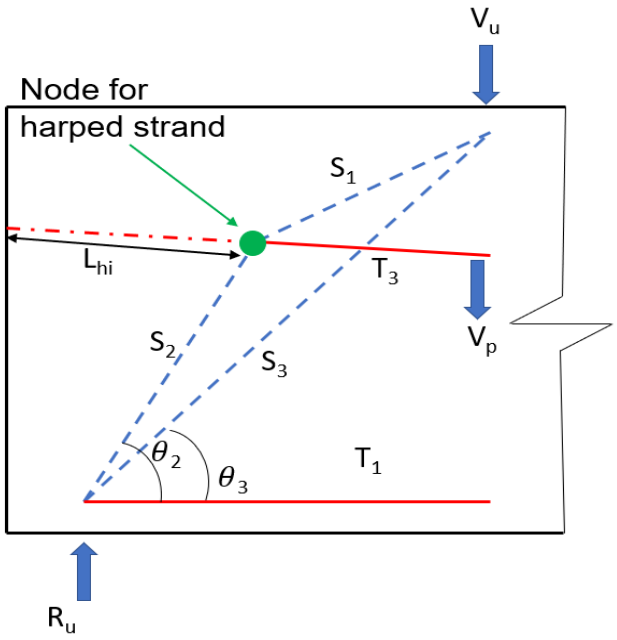

Figure 3-7. STM model at the end of the beam with the harped strand

The tie force should be calculated according to the node's location at the end region, and Equation 3-12 is used to calculate the tie force by the straight strands. On the other hand, the tie force by the harped strands should be calculated using the length from the end of the beam to the node for the harped strand, L_{hi}, using Equation 3-15. The length from the end of the beam to the node for the harped strand, L_{hi}, should not be greater than the transfer length, l_t.

$$T_3 = A_{hbp} \times f_{pe} \times \frac{L_{hi}}{l_t} \qquad \text{Equation 3-15}$$

Where :

A_{hbp} = total area of bonded harped strand at the end (in.)

The tie force for harped strands, T_3, and the equation of equilibrium is used to calculate the upper strut force, S_1, and lower strut force, S_2, that gather at the node of the harped strand. Similarly, the strut force for connecting the straight strand's tie and concentrated load, S_3, is calculated through the simultaneous equations using tie force for straight strand, T_1, and lower strut force, S_2. Equation 3-16 is the equation used for calculating the component of prestressing force by harped strand in the direction of the shear force, V_p.

$$V_p = A_{hbp} \times f_{pe} \times \sin(\theta_1) \qquad \text{Equation 3-16}$$

When using harped strands, the reaction force, R_u, can be calculated from strut forces (S_2, S_3) and angles for each strut (θ_2, θ_3). Also, the shear force calculated by STM is obtained by subtracting the component of prestressing force by harped strand from the reaction force.

$$R_u = S_2 \times \sin(\theta_2) + S_3 \times \sin(\theta_3) \quad \text{Equation 3-17}$$

$$V_{u,s} = R_u - V_p \quad \text{Equation 3-18}$$

Therefore, the maximum shear force of the end region of the Texas beam can be calculated by either Equation 3-13 or Equation 3-18, depending on whether it contains the harped strands.

3.4. Calculate Shear Strength by Anchorage Capacity

In this study, $V_{u,a}$ is the shear force at the end of the beam calculated by anchorage capacity, which is explained in Article 5.7.3.5 of AASHTO LRFD (2020). The texas standard prestressed beams are simply supported beams, including bearing plate, so Equation 3-19 is adequate to consider anchorage capacity.

$$A_s f_y + A_{ps} f_{px} \geq \left(\frac{V_{u,a}}{\phi_v} - 0.5V_s - V_p \right) \cot\theta' \quad \text{Equation 3-19}$$

Therefore, the shear force at the end of the beam calculated by anchorage capacity, $V_{u,a}$, is calculated using Equation 3-20, which comes from Equation 3-19. In the case of the beam without harped strands, the component of prestressing force by harped strand, V_p, is zero. Also, the reinforcement area on the flexural tension side is only considered for A_s and A_{ps} (refer to Figure 3-8).

$$V_{u,a} = \phi_v \left(\frac{A_s f_y + A_{ps} f_{px}}{\cot\theta'} + 0.5V_s + V_p \right) \quad \text{Equation 3-20}$$

Where :

f_y = yield stress in the non-prestressed tension reinforcement at nominal flexural resistance (ksi)

f_{px} = prestress at the critical section for the development of tie (ksi)

$\emptyset_v$ = resistance factor for shear, 0.9

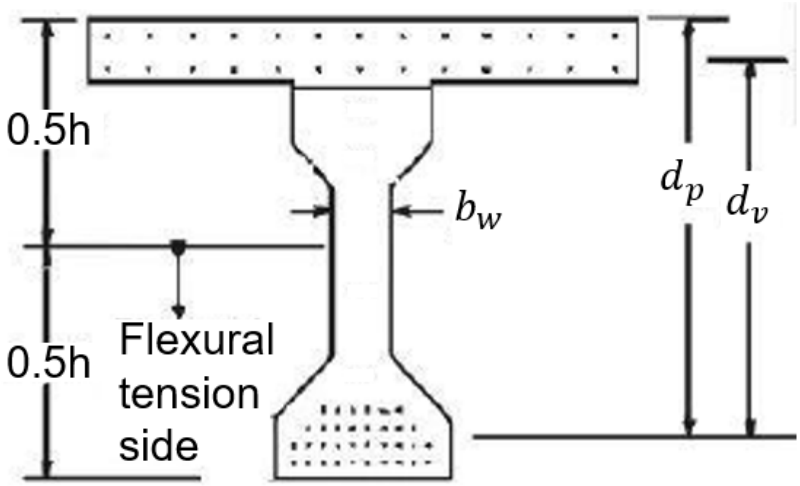

Figure 3-8. Flexural tension side for the beam (AASHTO 2020)

The shear resistance provided by transverse reinforcement, V_s, is calculated by Equation 3-21, which is based on the AASHTO LRFD (2020).

$$V_s = \frac{A_v \times f_y \times d_v \times \cot\theta'}{S} \leq 0.25 \times f_c' \times b_w \times d_v - V_c \qquad \text{Equation 3-21}$$

Where :

A_v = area of transverse reinforcement within distance S (in.^{2})

f_c' = design concrete strength (ksi)

S = spacing of transverse reinforcement measured in a direction parallel to the longitudinal reinforcement (in.)

A minimum amount of transverse reinforcement, $A_{v,min}$, can be calculated by Equation 3-22 to restrain the growth of diagonal cracking.

$$A_{v,\min} = 0.0316 \times \sqrt{f_c'} \times \frac{b_v \times S}{f_y} \qquad \text{Equation 3-22}$$

The angle of inclination of diagonal compressive stresses, θ', and nominal shear resistance of the concrete, V_c, can be specified in Equation 3-23 and Equation 3-24, respectively.

$$\theta' = 29 + 3500 \times \varepsilon_s \qquad \text{Equation 3-23}$$

$$V_c = 0.0316 \times \beta \times \sqrt{f_c'} \times b_w \times d_v \qquad \text{Equation 3-24}$$

When the end of the beam contains at least the minimum amount of transverse reinforcement as calculated by Equation 3-22, the value of the factor indicating the

ability of diagonally cracked concrete to transmit tension and shear, β, is as determined by Equation 3-25.

$$\beta = \frac{4.8}{(1+750\times\varepsilon_s)} \qquad \text{Equation 3-25}$$

However, if the end of the beam does not contain at least the minimum amount of shear reinforcement, the value of the factor, β, can be specified in Equation 3-26.

$$\beta = \frac{4.8}{(1+750\times\varepsilon_s)} \times \frac{51}{(39+S_{xe})} \qquad \text{Equation 3-26}$$

Where :

S_{xe} = crack spacing parameter as influenced by aggregate size (in.)

The longitudinal tensile strain in the section at the centroid of the tension reinforcement, ε_s, is calculated by Equation 3-27. The shear strength, V_u, used in Equation 3-27 is the shear force calculated by STM, $V_{u,s}$, in Equation 3-13 or Equation 3-18.

$$\varepsilon_s = \frac{\left(\frac{|M_u|}{d_v} + 0.5N_u + |V_u - V_p| - A_{ps}f_{po}\right)}{E_sA_s + E_pA_{ps}} \qquad \text{Equation 3-27}$$

Where :

M_u = factored moment at the end of the beam (kip-in.)

N_u = factored axial force (kip)

E_s = modulus of elasticity of steel reinforcement (ksi)

E_p = modulus of elasticity of prestressing steel (ksi)

However, if the longitudinal tensile strain, ε_s, calculated from Equation 3-27 is negative, the longitudinal tensile strain, ε_s, in the section at the centroid of the tension reinforcement should be recalculated with Equation 3-28, and it should not be less than -0.40×10^{-3}.

$$\varepsilon_s = \frac{\left(\frac{|M_u|}{d_v} + 0.5N_u + |V_u - V_p| - A_{ps}f_{po}\right)}{E_sA_s + E_pA_{ps} + E_cA_{ct}} \qquad \text{Equation 3-28}$$

Where :

E_c = modulus of elasticity of concrete (ksi)

A_{ct} = area of concrete on the flexural tension side of the member (in.^{2})

According to the anchorage capacity, the shear forces are calculated through Equation 3-20, which uses the variables calculated by Equation 3-21 to Equation 3-28.

3.5. Calculate Shear Stress

To prevent anchorage zone distress that may occur in the end region of the Texas beam, this study uses STM and the anchorage capacity proposed by AASHTO LRFD (2020) to calculate shear force. The smaller of the two calculated shear forces are used to calculate the maximum shear stress of the Texas beams' end region according to the number of strands. Therefore, shear stress, v_u, can be calculated using Equation 3-29 and Equation 3-30. In the case of a Texas beam without harped strands, the component of prestressing force by harped strand in the direction of the shear force, V_p, of Equation 3-30 is zero.

$$V_u = Min(V_{u,s}, V_{u,a}) \quad \text{Equation 3-29}$$

$$v_u = \frac{\left|V_u - V_p\right|}{\phi \times b_v \times d_v} \quad \text{Equation 3-30}$$

When the shear stress, v_u, (as determined in Equation 3-30) divided by design concrete strength, v_u/f'_c, is higher than *0.18* shear stress limit ratio, the shear stress in the end region of the beam can exceed the $0.18\,f'_c$ shear stress limit. Appendix E suggests examples of using STM and anchorage capacity to calculate the shear stress of the Tx-girder's end. Appendix E.1 is an example for Tx-46 that does not contain harped strands. Appendix E.2 is an example of Tx-46 that contains harped strands.

3.6. Debonded Strand

According to the TxDOT standard design, Tx-girder uses harped strands to control the stress of the beam end, but other Texas beams use debonded strands to control it. The minimum debonded length is limited to a minimum of 3 feet (36-in.). Therefore, it is necessary to consider how the debonded strand affects the shear capacity of the beam's end region. As described above, the beam end's shear

capacity is calculated using the strand capacity in the critical section for the development of ties (refer to Figure 3-5). Since the length from the end of the box-beam to the critical section, l_x is always smaller than the minimum debonded length (36-in.) of the strand, so the debonded strand does not affect the shear capacity of the end region. Therefore, only the full bonded strands are considered when calculating the shear capacity of the Texas beams at the end.

3.7. Comparison Between Standard Strand Patterns and Non-Standard Strand Patterns

The standard strand pattern of standard prestressed Texas beams places the strands sequentially from the lowest row of the beam. For example, when setting 20 strands in Tx-46, place 14 strands in the lowest row and then six strands in the second row. This is because the maximum number of strands that can be placed in one row in Tx-46 is 14. However, if a non-standard strand pattern is used, the arrangement of the strands becomes diverse, and the arrangement of the strands affects the tie location and shear capacity of the STM. To investigate the influence of the strand pattern, this research considers Figure 3-9, which compares Tx-46 when the strand pattern is standard and non-standard. It is assumed that a total of 14 strands are used. In the case of the standard strand pattern, every strand is placed in the lowest row, whereas in the case of the non-standard strand pattern, the strands are arranged in three layers.

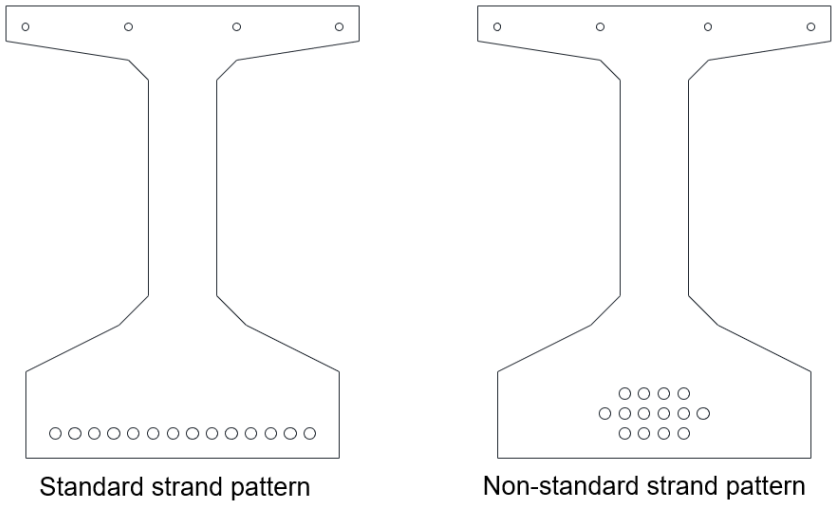

Figure 3-9. Standard strand pattern versus non-standard strand pattern

If the non-standard strand pattern is used, the centroid of the strand from the soffit increases when compared to the standard strand pattern—the centroid of the strand influences not only the location of the tie but also the node geometry. In the case of a non-standard strand pattern, as the length of the back face of the node increases,

the length from the end of the beam to the critical section for the development of the tie increases (refer to Figure 3-10). Therefore, the tie force and the strut force that can act at the strut-to-node interface increase. However, as the length of the back face of the node increases, the node's geometry also increases, and the node capacity increases. The detailed method to calculate the capacity of the node is explained in the following chapter. The node capacity at the strut-to-node interface is 73% higher than strut force when a standard strand pattern is used, but the node capacity is 101.9% higher when a non-standard strand pattern is used. It means that the difference between capacity and demand is lower when a standard strand pattern is used, so using a standard strand pattern is more extreme case than using a non-standard strand pattern. Table 3-1 compares the result between using standard strand pattern and non-standard strand pattern.

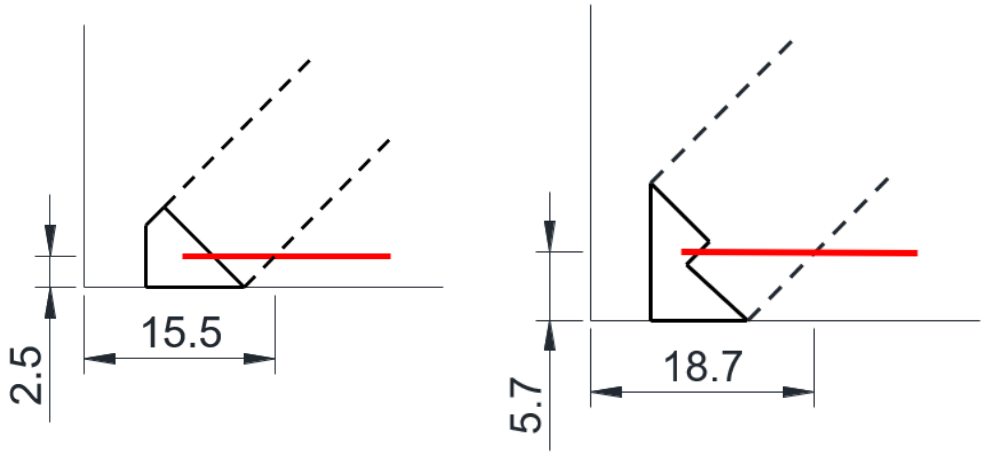

Standard strand pattern Non-standard strand pattern

Figure 3-10. Different node geometry between standard and non-standard strand pattern

Table 3-1. Comparison between standard and non-standard strand pattern

	Standard strand pattern	Non-standard strand pattern
No. of strand (ea)	14	14
Tie force (ksi)	225	254
Strut force (kips)	319	359
Node capacity (kips)	554	725
Differences (%)	73.6	101.9

In conclusion, if all variables except strand pattern remain unchanged (e.g., the total number of strands, concrete strength, beam's cross-section, etc.), then the calculated shear stress capacity of the standard prestressed beam based on a standard strand pattern is the most conservative. This is the basis for suggesting the shear stress limit of each Texas beam based on the standard strand pattern

3.8. Chapter Summary

Based on the result of measuring the total prestress loss of the strands used in the prestressed beam, the prestressed beam's total prestress loss is about 20% on average (refer to Garber 2014). Therefore, it is suitable to assume that total prestress loss is 20% when developing the STM. The shear strength of the end region of the Texas standard prestressed beam can be calculated using the developed STM and anchorage capacity equation. However, before calculating the shear strength, the effective depth, d_v, and the effective prestress, f_{pe}, must be calculated first. That is, the effective prestress, f_{pe}, is assumed to be 80% of the stress in prestressing steel immediately before the transfer, f_{po}. The effective depth of the beam is calculated based on AASHTO LRFD (2020), and it should be calculated considering the size of the rectangular stress block and the deck thickness.

The STM for calculating the shear strength of the beam's end should differ depending on whether it does or does not contain the harped strand. In addition, unlike previous studies where the tie force is calculated at the center of the bearing plate (the node where the strut and tie overlap), the tie force is calculated from the critical section using the extended nodal zone in this study. Also, the debonded strand does not affect the shear capacity of the end region, so only the full bonded strands are considered when calculating the shear capacity of the Texas beams at the end.

After calculating the shear strength using STM, the shear strength is calculated once again using the anchorage capacity equation. The anchorage capacity equation is the modified expression of the longitudinal tension equation presented in Article 5.7.3.5 of AASHTO LRFD (2020). Finally, the shear strength of the end region of the Texas standard prestressed beam is the smaller of the shear strength calculated using the STM and the anchorage capacity equation. The shear stress capacity at the beam's end can be calculated using the calculated shear strength.

As a result of comparing the standard strand pattern and the non-standard strand pattern, the calculated shear stress capacity of the standard prestressed beam based on a standard strand pattern is the most conservative when using the analytical

method proposed in this research. Therefore, the shear stress limit calculated using the standard strand pattern can be applied to the beam of the non-standard strand pattern. In conclusion, it is appropriate to calculate the shear stress limit of Texas standard prestressed beam using a standard strand pattern.

Chapter 4. Failure Mode Prediction

4.1. Introduction

If the shear stress of the Texas beam's end region is calculated by the method described in Chapter 3, the anchorage zone distress does not occur when the calculated shear force acts on the Texas beam. However, it is necessary to consider other failure modes in addition to the anchorage zone distress. A nodal failure check is performed on the anchorage portion of the bottom flange; the horizontal shear failure mode that can occur between the bottom flange and the base of the web is also checked. Additionally, the Strut-and-Tie Model (STM) on the cross-section is used to confirm that sufficient confinements are used in the Tx-girder to prevent lateral splitting failure, and cross-section STM is used to check the nodal strength at the end block for Texas beams except Tx-girder.

4.2. Nodal Strength Check for Beams

Since the node of the anchorage of the bottom flange has the most significant strut and tie force, as compared to the nodes at the harped strand, the nodal strength needs to be checked in the anchorage node. The node of the anchorage portion of the bottom flange is a CCT node because it contains only one tie, which contains straight strands. Also, the geometry of the anchorage node can be determined using the bearing plate in the beam support and centroids of straight strands (refer to Figure 3-5). The design strength of the bearing plate and strut-to-node interface is calculated based on a node's geometry. Then, design strengths are compared to the applied force for each face. When calculating the design strengths for the node, the methods used are based on the AASHTO LRFD (2020).

4.2.1. Factors for checking nodal strength

The confinement modification factor, m, should be calculated to check the nodal strength. If the node abuts a bearing plate that is narrower than the beam, an increased concrete strength can be assumed for the node because of triaxial confinement. The confinement modification factor is determined from Equation 4-1.

$$m = \sqrt{\frac{A_2}{A_1}} \leq 2.0 \qquad \text{Equation 4-1}$$

Where A_1 is the bearing plate area, and A_2 is measured on the plane (illustrated in Figure 4-1) defined by the location at which a line with a 2-to-1 slope extending from the bearing plate area meets the end of the beam.

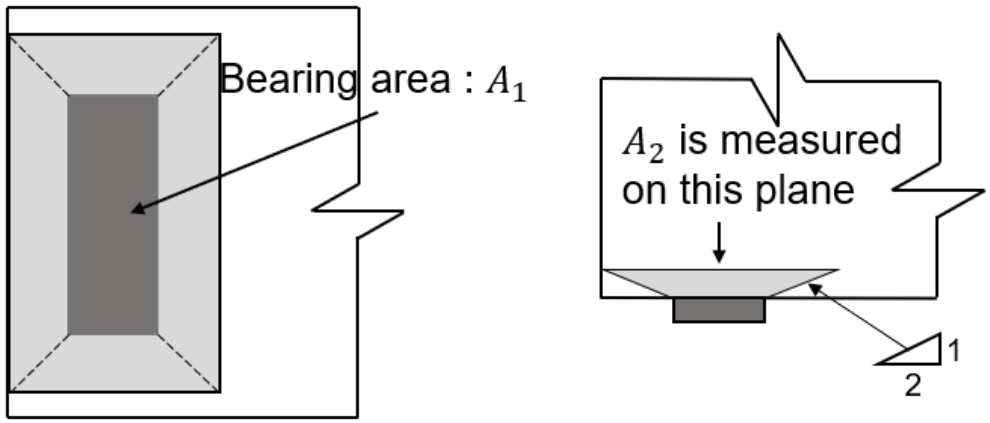

Plan Elevation

Figure 4-1. Determination of A_2 for the support

The concrete efficiency factor, v, needs to be considered for the nodal face specifically. This factor, v, varies according to the type of node and face. In Article 5.8.2.5.3 of AASHTO LRFD (2020), different concrete efficiency factors are given depending on the type of node and face, and the values are shown in Table 4-1. When the beam does not contain crack control reinforcement as specified in AASHTO LRFD Article 5.8.2.6, the concrete efficiency factor, v, for the strut-to-node interface is 0.45.

Table 4-1. Concrete efficiency factors, v

	CCC	CCT	CTT
Bearing Face	0.85	0.7	0.85 - f_c'/20 ksi $0.45 \leq v \leq 0.65$
Back Face			
Strut-to-Node Interface	0.85 - f_c'/20 ksi $0.45 \leq v \leq 0.65$	0.85 - f_c'/20 ksi $0.45 \leq v \leq 0.65$	

As the Texas beam does not satisfy the requirements of AASHTO LRFD Article 5.8.2.6 because there is no crack control reinforcement in the horizontal direction, the v of the strut-to-node interface is 0.45. The concrete efficiency factor for each face of the anchorage node of the bottom flange, CCT node, is illustrated in Figure 4-2.

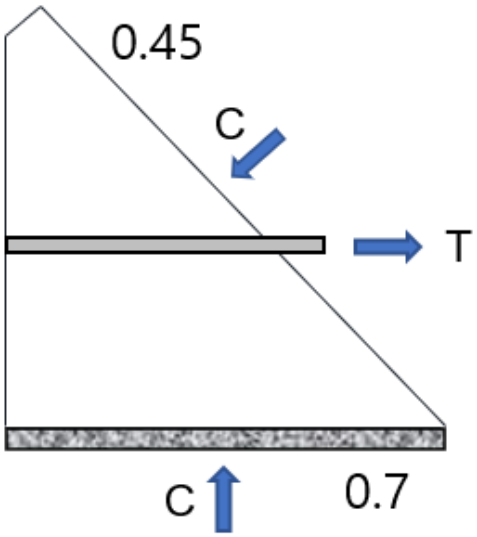

Figure 4-2. Concrete efficiency factors, v (anchorage node illustration)

4.2.2. Check maximum bearing stress

The design strength of the bearing face is calculated and compared to the corresponding applied reaction force. The maximum compressive stress at the bearing plate, f_{cu1}, is calculated by Equation 4-2.

$$f_{cu1} = m \times v \times f_c' \qquad \text{Equation 4-2}$$

Where f'_c is the designed compressive strength of the concrete, v is 0.7, and m is the result from Equation 4-1. The design strength of the bearing face, P_{n1}, is then calculated as Equation 4-3, and it should be larger than the reaction force, R_u, which is the load applied to the bearing plate.

$$P_{n1} = \phi_c \times f_{cu1} \times l_b \times w_p \qquad \text{Equation 4-3}$$

Where :

$\emptyset_c$ = resistance factor for compression in STM, 0.7.

b_p = length of the bearing plate (in.)

w_p = width of the bearing plate (in.)

4.2.3. Check strut-to-node interface

The design strength of the strut-to-node interface is calculated and compared to the corresponding applied strut force. The limited compressive stress at the strut-to-

node interface, f_{cu2}, is calculated by Equation 4-4, which is as same as Equation 4-2, but v is 0.45 for the Equation 4-4.

$$f_{cu2} = m \times v \times f_c^{'} \qquad \text{Equation 4-4}$$

The design strength of the strut-to-node interface, P_{n2}, is then calculated as Equation 4-5, where the length of the strut-to-node interface, w_s, is calculated by Equation 3-10, and the geometry of the anchorage node for the bottom flange is shown in Figure 4-3. Also, the calculated design strength of the strut-to-node interface, P_{n2}, must be greater than the strut force, S, actually applied to the strut-to-node interface.

$$P_{n2} = \phi_c \times f_{cu2} \times w_s \times w_p \qquad \text{Equation 4-5}$$

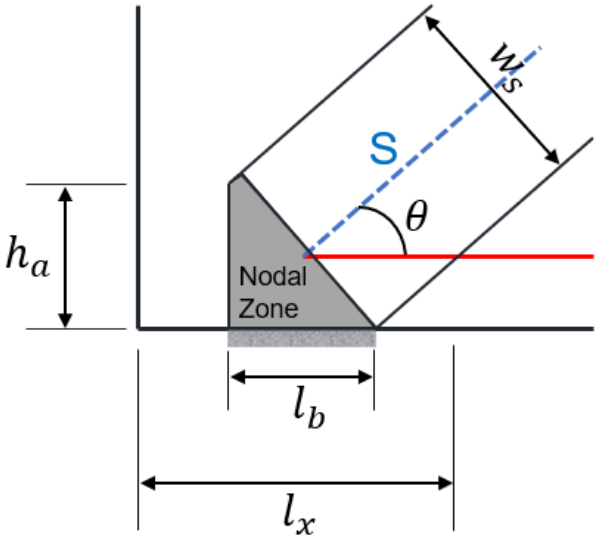

Figure 4-3. The geometry of the anchorage node for the bottom flange

If harped strands are used in the beam, two struts are in contact with the bottom flange's anchorage node, as shown in Figure 3-7. Therefore, as illustrated in Figure 4-4, the strut-to-node interface should be checked after transforming two struts into one strut. Moreover, the length of the strut-to-node interface should be calculated using the revised compressive stress field inclination, θ_r, instead of the compressive stress field inclination, θ, in Equation 3-10, and the final calculated design strength of the strut-to-node interface, P_{n2}, must be greater than the revised strut force, S_r.

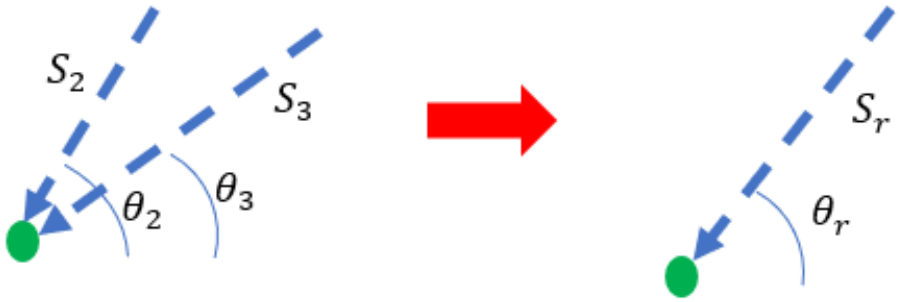

Figure 4-4. Combine the stress flows for strut

When the nodal strength of the bearing face and strut-to-node interface is greater than the demands placed on it, the anchorage capacity is sufficient even if the shear stress exceeds the $0.18 f'_c$ shear stress limit.

4.3. Additional Consideration when Checking Nodal Strength for Beams with Two Webs

The geometry for the Texas beams with two webs, which is different from that of the Texas beams with one web, affects the beam's stress flow. Moreover, the end blocks or the increase in the number of bearing plates should be further considered when checking the nodal strength. Also, the inclined web will change the strut force applied at the node, so it should be considered when checking the failure modes.

4.3.1. Box beam & X-beam

Texas beam with one web places one bearing plate on each support, while the box-beam and X beam place one bearing plate on one support and two bearing plates on the other support. Depending on the number of bearing plates, the stress flow of the end region of the box beam and X-beam changes, as shown in Figure 4-5. If the geometry of the box beam and X-beam includes a skewed end and two bearing plates, different shear stresses are acting on each bearing plate. Also, the nodal strength should be checked using cross-section STM at the end of the box beam and X-beam, where only one bearing plate is placed on the support.

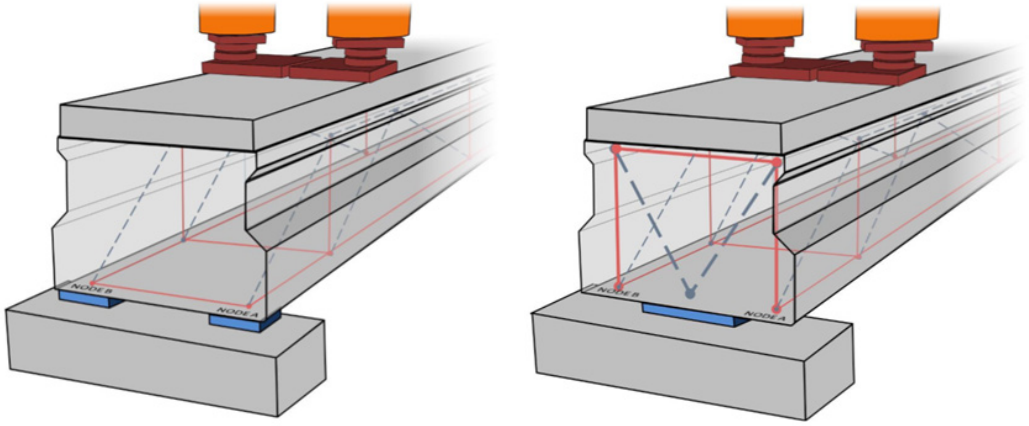

(a) Two bearing plate (b) One bearing plate

Figure 4-5. Stress flow differences between different numbers of bearing plates (Avendano et al. 2013)

4.3.1.1. Two bearing plates at the end

In a previous TxDOT project (0-5831), Avendano et al. (2013) tested and compared the shear capacity of the box beam and X-beam with a square end and a 30° skewed end. The findings from that project indicate that the shear capacity of the box beam and X-beam were the same regardless of whether the end was square or skewed. However, if the end shape is a skewed end and two bearing plates are used, the bearing plate at the obtuse angle is subjected to greater shear stress than the bearing plate at the acute angle. The bearing plate at the obtuse angle can receive shear force up to 60% of the total shear force (Avendano et al. 2013; Hovell et al. 2013). On the other hand, if the end shape of the box beam and X-beam with two bearing plates is a square end, the two bearing plates receive the same shear force (refer to Figure 4-6). According to the TxDOT Bridge Design Manual (2020), the maximum angle of the skewed end of the box beam and X-beam is 30°. Therefore, this study confirmed that nodal failure does not occur even if 60% of the total shear force is applied to the nodes at the obtuse angle of the box beam and X-beam with a 30° skewed end.

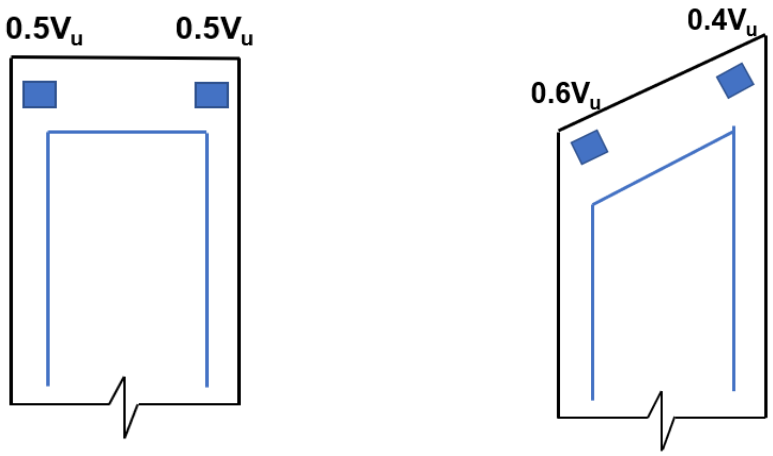

Figure 4-6. Applied shear force differences between square end and skewed end at bearing plate for box beam & X-beam

4.3.1.2. One bearing plate at the end

When the box beam uses two bearing plates, the nodal strength can be checked in the same method described above using STM in the longitudinal direction. However, if the box beam places one bearing plate on the support, the stress flow in the end block is changed, as shown in Figure 4-5-(b). Therefore, it is necessary to check the nodal strength of the node directly above the support using the cross-section STM (refer to Figure 4-7). For the convenience of calculation, the length from the top of the beam to the top horizontal tie, y_t, is assumed to be equal to the length from the bottom of the beam to the centroid of the strand, y_b.

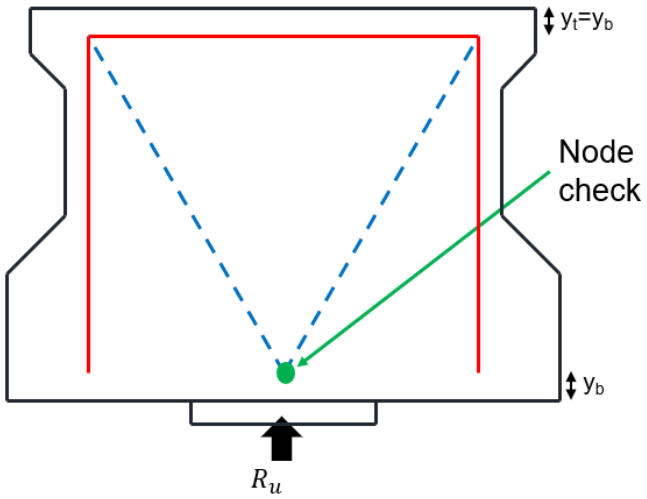

Figure 4-7. Cross-section STM model at the end block

When two struts meet at one nodal point, the nodal strength should be checked by changing the stress flow as shown in Figure 4-8 after considering the node's geometry (Williams et al., 2012). If the end of the beam is the square end, the node's width is half the width of the bearing plate. Since the node geometry and stress on the left and right are symmetrical, the nodal strength is checked for only one node. Also, the ratio of the nodal capacity to demand is constant in both the square end and the skewed end of the beam, so only the square end shape is considered. If the right strut force is greater than the left strut force, the node geometry for the right half is also increased.

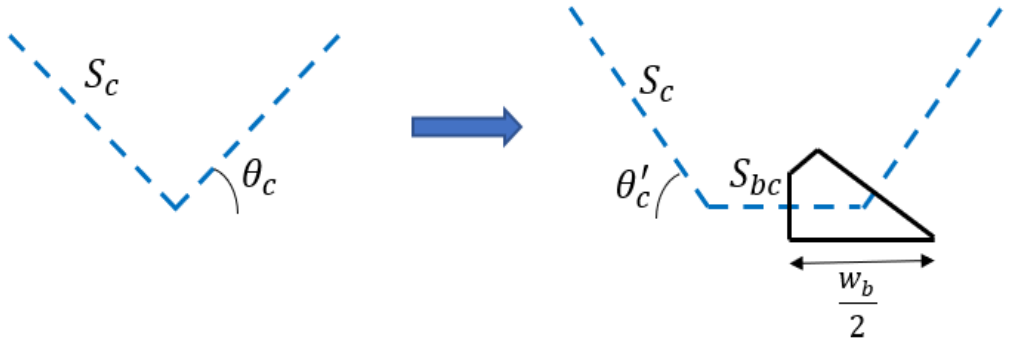

Figure 4-8. Stress flow changed

4.3.2. U-beam

The U-beam's geometry is different from that of the box beam or X-beam, so the difference affects the shear stress calculation at the beam end. The U-beam places one bearing plate on one support and two bearing plates on the other, same as box beam or X-beam. If the geometry of the U-beam includes a skewed end and two bearing plates, different shear forces are acting on each bearing plate. In addition, at the end of the U-beam, where only one bearing plate is placed on the support, the nodal strength should be checked using cross-section STM. Therefore, it can be seen that the stress flow of the U-beam is similar to that of the box beam or X-beam. However, the inclined web affects the strut force applied to the strut-to-node interface when using STM in the longitudinal direction. In addition, the stress flow in the end block can be expressed using two different shapes of cross-section STMs when one bearing plate is used at the end of the U-beam (refer to Figure 4-9).

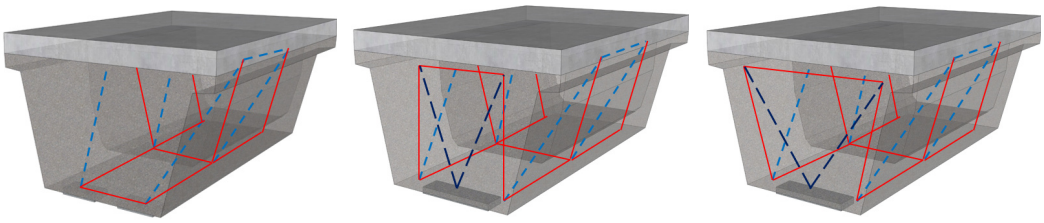

Two bearings One bearing

Figure 4-9. Stress flow differences between different numbers of bearing plates

4.3.2.1. Two bearing plates at the end

In a previous TxDOT project (0-5831), (Hovell et al. 2013) tested and compared the shear capacity of the U-beam with a square end and a 45° skewed end. The findings from that project indicate that the U-beam's shear capacity was the same regardless of whether the end was square or skewed. However, if the end shape is a skewed end and two bearing plates are used, the bearing plate at the obtuse angle is subjected to greater shear stress than the bearing plate at the acute angle. The bearing plate at the obtuse angle can receive shear force up to 60% of the total shear force (Avendano et al. 2013; Hovell et al. 2013). According to the TxDOT Bridge Design Manual (2020), the maximum angle of the skewed end of the U-beam is 45°. Therefore, this study confirmed that nodal failure does not occur even if 60% of the total shear force is applied to the nodes at the obtuse angle of the U-beam with a 45° skewed end.

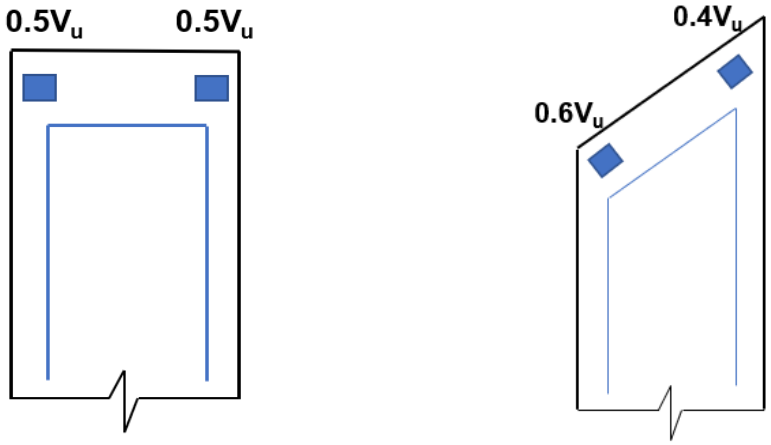

Square end 45° skewed end

Figure 4-10. Applied shear force differences between square end and skewed end at bearing plate for U-beam

When two bearing plates are used, STM in the longitudinal direction is used to check the nodal failure. The method to calculate the strut force is different for the U-beam compared with other beams. For other beams, the applied strut force at the

node, V_2, can be calculated only using the shear force, V_1, and strut angle because the web is not inclined. However, since a U-beam includes the inclined web, the applied strut force at the node of the U-beam, V_3, must be calculated considering the inclined angle of the web (as shown in Figure 4-11). The equation for calculating the strut force applied at the node around the bearing plate of the U-beam is as follows.

$$V_3 = \left(\frac{\sqrt{a^2 + {h_{stm}}^2 + x^2}}{\sqrt{a^2 + {h_{stm}}^2}} \right) \times V_2 \qquad \text{Equation 4-6}$$

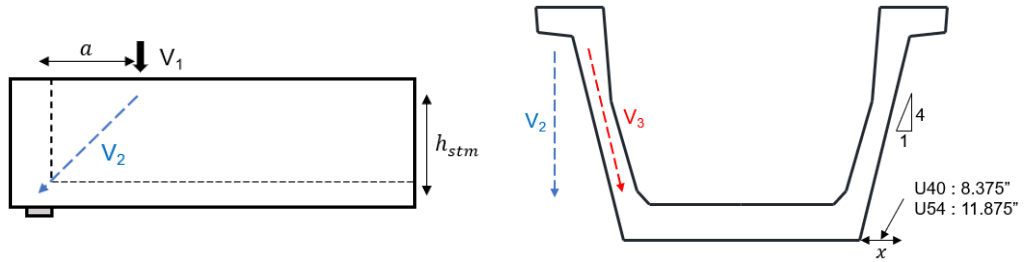

Other beams U-beam

Figure 4-11. Applied strut force for U-beam and other beams

4.3.2.2. One bearing plate at the end

The stress flow of the end block with one bearing plate can be expressed using two different cross-sections STMs. In the first method, the tie is arranged vertically, and in the second method, the tie is inclined by the same angle as the web (refer to Figure 4-12). The tie in the STM model is positioned vertically in general, so the tie in the cross-section STM of the box beam's end block was arranged vertically. However, a U-beam does not have the same stress flow in the end block as in the box beam due to the inclined web. Therefore, this study compared the tie force and strut force when the tie of the cross-section STM is vertical and inclined to determine which cross-section STM is more appropriate for the U-beam.

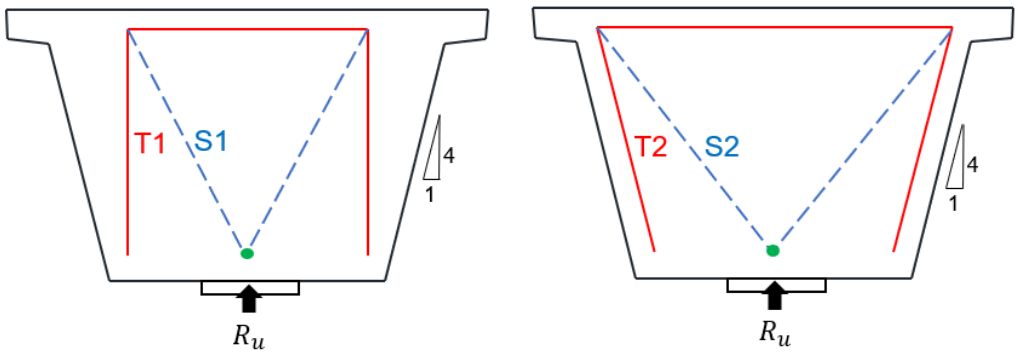

Vertical tie Inclined tie

Figure 4-12. Different cross-section STM models for U-beam's end block

4.3.3. Decked-slab beam

The geometry of the decked-slab beam is similar to that of the box beam, but the height of the beam is significantly lower than that of the box beam. The decked-slab beam contains the end block at the end of the beam, and one bearing plate is used at one end, and two bearing plates are used at another end, same as box beam and X-beam. The method which is used to check the nodal strength of the box beam and X-beam is used for the decked-slab beam when checking the nodal strength because of the similar geometry and boundary conditions. No previous study tested and compared the shear stress of the decked-slab beam according to the different shapes of the end block. However, the maximum angle of the skewed end of the decked-slab beam suggested in the TxDOT Bridge Design Manual (2020) is 30 degrees, which is the same as the maximum angle of the box beam. Therefore, the same assumption which is used for box beam and X-beam is used to check the nodal strength at the obtuse angle for the decked-slab beam. It is assumed that 60% of the shear force acts on the obtuse angle when there is a skewed end with two bearing plates.

4.4. Horizontal Shear Check

Texas beams, except for the slab beam, have a relatively thin web compared to the bottom flange, so the Texas beams have a risk of horizontal shear failures at the interface of the web and the bottom flange. Hovell et al. (2013) proposed the method for calculating the horizontal shear capacity and demand of Texas beams. And this study will use this method to check whether the beam is safe from horizontal shear failure. Horizontal shear failure happens when a diagonal crack oriented at 45 degrees occurs from the load point to the interface of the web and bottom flange, and a horizontal crack extends to the end of the beam. Then, the intersection point of the diagonal crack and the interface of the web and the bottom flange is called the ultimate evaluation point (UEP). The length from the beam end to the UEP, l_{UEP}, can be calculated from Equation 4-7, and the location of the UEP is shown in Figure 4-13.

$$l_{UEP} = a + oh - \frac{l_{LP}}{2} - h + y_{crit} \qquad \text{Equation 4-7}$$

Where :

a = shear span (in.)

l_{LP} = length of the load plate (in.)

h = total depth of the composite section (in.)

y_{crit} = height of critical interface, measured from the bottom (in.)

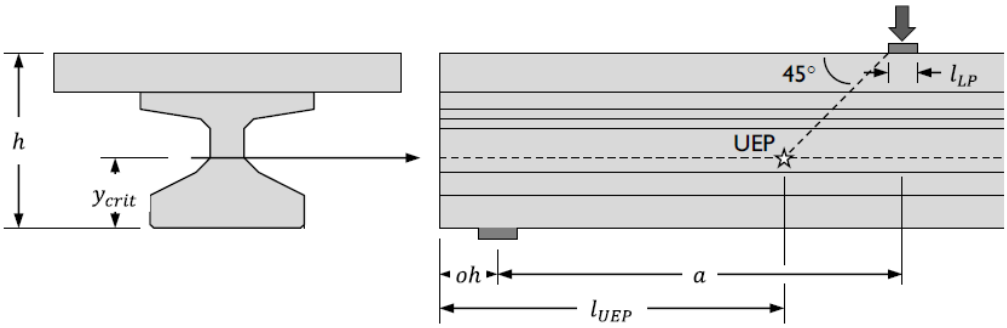

Figure 4-13. Location of ultimate evaluation point (Hovell et al. 2013)

Horizontal shear capacity, V_{ni}, can be calculated based on the shear friction concept, which is typically used for the interface between the deck and the top flange of the girder (Hovell et al. 2013). The equation for horizontal shear capacity recommended by Hovell is slightly different from the equation for shear friction. First, the bursting stress is considered, which reduces the ability of the reinforcement to resist horizontal shear stress. This bursting stress is almost 4% of the prestressing force within the transfer length. Also, depending on the shape of the beam, another factor is additionally considered. For example, in an I-beam, the beam shape factor is 1.0, and Hovell's equation for horizontal shear capacity is as shown in Equation 4-8.

$$V_{ni} = K_d \left[c \times A_{cv} + \mu \left(A_{vf} \times f_y - 0.04 P_{ps} \right) \right] \qquad \text{Equation 4-8}$$

Where :

k_d = beam shape factor, equal to 1.0 for I-beams (Tx-girder), Box beams (Box beam, X-beam, Decked-slab beam), and 0.8 for U-beam

c = cohesion coefficient, equal to 0.4 (ksi)

A_{cv} = area of concrete considered to be engaged in interface shear transfer (in^2)

μ = friction coefficient, equal to 1.4

A_{vf} = area of interface shear reinforcement crossing the shear plane within the area A_{cv} (in^2)

f_y = specified yield strength of reinforcement, limited to 60 (ksi)

P_{ps} = force of prestressing transferred to the beam within the region of interest (kips)

Two different equations can calculate the limit of horizontal shear capacity based on the AASHTO LRFD (2020), and each equation is shown below. Equation 4-9 limits horizontal shear force to a percentage of the concrete compressive strength, and Equation 4-10 places an absolute limit on the horizontal shear force.

$$V_{ni} \le K_1 \times f_c^{'} \times A_{cv} \qquad \text{Equation 4-9}$$

$$V_{ni} \le K_2 \times A_{cv} \qquad \text{Equation 4-10}$$

Where :

K_1 = For normal-weight monolithic concrete, 0.25

K_2 = For normal-weight monolithic concrete, 1.5 (ksi)

The horizontal shear capacity for the Texas beam can be calculated using Hovell's horizontal shear capacity equation and the limits of horizontal shear capacity. The horizontal shear capacity of the entire beam is equal to the sum of the horizontal shear capacity of each divided region. To calculate the horizontal shear capacity of each region, these beam properties should be used: the point at which the strand begins to bond, the transfer length of the strand, the change of spacing of the vertical reinforcement, and the change in the geometry of the beam.

For the Tx-girder, the geometry of the beam is constant over the entire length, so it is not necessary to consider the change in geometry when dividing the region to calculate the horizontal shear capacity. Since the TxDOT's standard design for the Tx-girder does not use debonded strands, the spacing changes of the vertical reinforcement and the transfer length are the only parts to be considered. The vertical reinforcement spacing of the Tx-girder is constant until the transfer length (3 ft from the end of the beam) is reached and then increases. Therefore, the horizontal shear capacity of the Tx-girder can be calculated by dividing regions before and after transfer length.

However, other Texas beams with two webs such as box beam, X-beam, U-beam, and Decked-slab beam contain end block at the end of the beam. These beams' web width increases rapidly at the end block, and the horizontal stress flow changes at the end block (refer to Figure 4-14). The shear stress spreads in a ratio of 2:1 (26.5 degrees) in the end block (Hovell et al. 2013). Because of the end block, more concrete area at the end resists horizontal shear stress compared to the web in the

center of the beam with two webs. That is, the area of concrete considered to be engaged in interface shear transfer, A_{cv}, increases, and the horizontal shear capacity, V_{ni}, of the end region of the beam with two webs also increases (refer to Equation 4-8). Also, the spacing of the transverse reinforcement of the Texas beams with two webs is constant until the transfer length is reached as same as Tx-girder. Therefore, in order to calculate the horizontal shear capacity of Texas beams with two webs, the beam should consider the horizontal shear capacity separately at the end block and the void region.

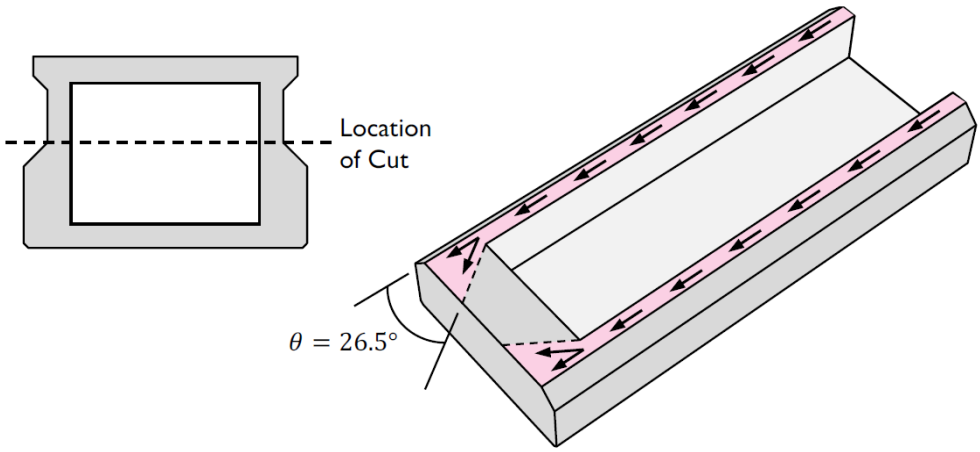

Figure 4-14. Horizontal shear stress flow in end block (Hovell et al. 2013)

When the calculated horizontal shear capacity of the entire beam is equal to the horizontal shear demand, the maximum applied shear force for the end region of the beam, $V_{applied}$, can be calculated.

$$V_{applied} = v_{hs} \times b_w \times d_p \qquad \text{Equation 4-11}$$

Where :

b_w = width of the web (in.)

d_p = distance from extreme compression fiber to the centroid of the prestressing strands (in.)

v_{hs} = average horizontal shear stress (ksi)

From Equation 4-11, the average horizontal shear stress, v_{hs}, is calculated by using calculated horizontal shear capacity, V_{ni}, web width, b_w, and the length of demand, l_{crit}. The length of demand, l_{crit}, considers the overhang beyond the bearing plate. The average horizontal shear stress, v_{hs}, and the length of demand, l_{crit}, can be calculated using Equation 4-12 and Equation 4-13, respectively.

$$v_{hs} = \frac{V_{ni}}{b_w \times l_{crit}} \quad \text{Equation 4-12}$$

$$l_{crit} = l_{UEP} - oh \quad \text{Equation 4-13}$$

The maximum shear force that might be applied to the end region of the beam can be calculated by the variables through Equation 4-12 and Equation 4-13. Suppose the maximum shear strength calculated through the horizontal shear capacity is greater than the shear strength calculated using the STM and anchorage capacity. In that case, the horizontal shear failure does not occur at the beam. However, when the maximum shear strength calculated through the horizontal shear capacity is less than the shear strength calculated using the STM and anchorage capacity, horizontal shear failure governs the beam. Under this situation, the maximum shear force for the beam is the shear force based on the horizontal capacity instead of the shear force using STM and anchorage capacity from Equation 3-29.

4.5. Confinement Check for Tx-girder

Lateral splitting failure occurs due to the outward movement of the edge of the bottom flange. It occurs when the edge of the bottom flange has more strands than does the area under the web. The Tx-girder has a relatively large bottom flange as compared to the AASHTO Type girder, and more strands can be used at the edge, so the risk of lateral splitting failure is higher. Therefore, to prevent lateral splitting failure, determining whether enough confinement reinforcement is used in the bottom flange of the end region of the Tx-girder is a necessary area of inquiry.

The cross-section STM for an I-girder proposed by (Ross et al. 2013; Shahrooz et al. 2017) is used to calculate the quantity of confinement reinforcement required to prevent lateral splitting failure at ultimate load. To calculate the lateral splitting force in the bottom flange, which is carried by confinement reinforcement (refer to Figure 4-15), STM should take into account the dimensions of the bearing support and the number of bonded strands in the bottom flange. For Tx-girders with harped strands, the harped strands are not considered when calculating the lateral splitting force because the harped strands in the end region of the beam are in the web area.

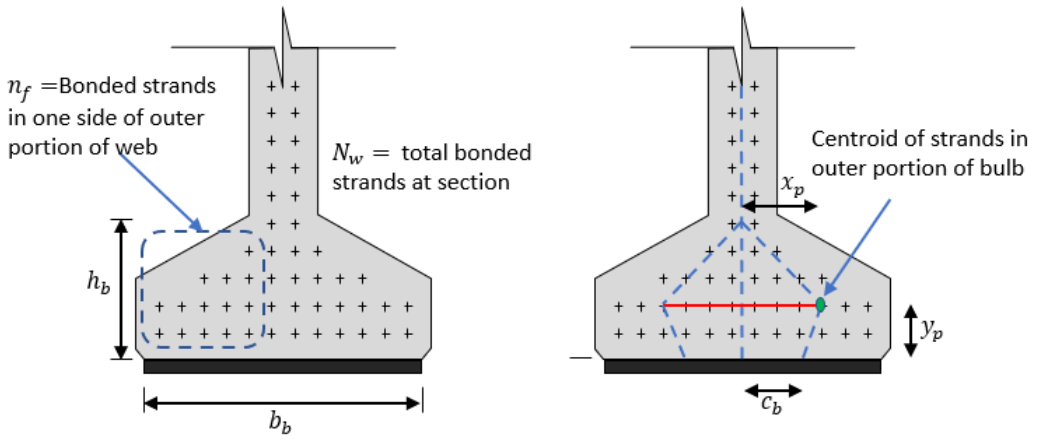

Figure 4-15. Cross-section STM for I-girder bulb

(Shahrooz et al. 2017) calculated the variables shown in Figure 4-15 using strand pattern and girder geometry. From Figure 4-15, the location of a distributed strut to apply pressure evenly across the bearing plate, c_b, is determined by the width of the bearing plate and the number of bonded strands, and it can be calculated by Equation 4-14.

$$c_b = \left(\frac{b_b}{2}\right)\left(1 - \frac{n_f}{N_w}\right) \qquad \text{Equation 4-14}$$

Where :

b_b = width of bearing plate (in.)

N_w = total number of bonded strands at the cross-section

n_f = number of bonded strands in one side of the outer portion of the bulb

The horizontal tie force, t, which is the demand provided by the shear reaction at support, can be calculated by Shahrooz's equation shown in Equation 4-15.

$$t = \frac{aV_u}{\phi} = \left(\frac{n_f}{N_W}\right) \cdot \left[\frac{x_p}{h_p - y_p} + \frac{x_p - c_b}{y_p}\right] \cdot \frac{V_u}{\phi} \qquad \text{Equation 4-15}$$

Where :

$\emptyset$ = reduction factor for shear (0.9)

V_u = total shear reaction at support (kips)

x_p = horizontal distance to girder centerline to the centroid of n_f strands in the outer portion of the bulb (in.)

y_p = horizontal distance to girder centerline to the centroid of n_f strands in the outer portion of the bulb (in.)

The quantity of confinement required at ultimate load, A_{cr}, is calculated from the horizontal tie force, t, divided by the yield stress of the confinement reinforcement, f_y. When steel bearing plates are used for beam supports, up to 50% of the required amount of confinement can be replaced (Ross et al. 2013). Therefore, the quantity of confinement reinforcement that prevents lateral splitting failure is calculated through Equation 4-16.

$$A_{cr} = \frac{t / 0.9}{a \times f_y} \qquad \text{Equation 4-16}$$

Where :

When steel bearing plates are in place, a = 2, no bearing plate, a = 1

When the quantity of confinement required at ultimate load, A_{cr}, calculated from Equation 4-16, is less than the total area of the confinement reinforcement used from the end of the Tx-girder to the location of effective depth, d_v, the lateral splitting failure at the end of the beam is prevented.

4.6. Chapter Summary

When the shear strength of the beam's end is calculated using the STM and the anchorage capacity equation, the beam is safe from anchorage zone distress up to the calculated shear force. However, additional failure modes also needed to be considered for the end region of the Texas standard prestressed beam when a calculated shear force is acted at the end of the beam. Texas standard prestressed beam consists of a total of 6 types of beams, and each type has different geometry and boundary conditions. Geometry and boundary conditions affect the stress flow of the beam, so consideration should be given when calculating the capacity of the expected failure modes.

For the beams that do not contain void regions, such as Tx-girder and slab beam, it is unnecessary to consider the stress flow that may occur in the cross-section direction in the end block. Since only the stress flow in the longitudinal direction needs to be considered, the nodal failure that may occur in the anchorage node for the longitudinal STM needs to be checked. When calculating the design strengths

for the node, the methods used are based on the AASHTO LRFD (2020). However, beams with end blocks due to a void region, such as box beam, X-beam, U-beam, and decked-slab beam, should consider the stress flow in the cross-section direction that may occur in the end block (refer to Figure 4-5). When two bearing plates are used at the end of the beams with two webs, the node of longitudinal STM needs to be checked like Tx-girder or slab beam. On the other hand, if only one bearing plate is used, the stress flow changes in the end block of the beam, so the cross-section STM should be used to check the nodal failure. Additionally, when the web is inclined like U-beam, the strut force applied to the strut-to-node interface of the node changes according to the angle of the web.

Texas standard prestressed beams except for the slab beam have a relatively thin web compared to the bottom flange, so there is a distinction between the web and the bottom flange. Because of this distinction, Texas beams have a risk of horizontal shear failures at the interface of the web and the bottom flange. Therefore, when a calculated shear force is applied to the Texas beam, it should be checked to ensure that the beam is safe from horizontal shear failure. In addition, there is a risk of lateral splitting failures at the bottom flange due to the stress difference caused by the strands in Tx-girder using harped strand. Due to this risk of occurrence, it is also necessary to verify that the amount of confinement reinforcement used in Tx-girder is sufficient to prevent lateral splitting failure.

Chapter 5. Analysis and Results

5.1. Introduction

Using the method described in Chapter 3 to calculate the shear stress at the end of the beam, the shear stress capacity at the Texas beams' end region can be calculated. This method can also be used to determine whether the design is controlled by other failure modes (nodal failure, horizontal shear failure, and lateral splitting failure) that may arise when the calculated shear force acts on the end of the beam. In the case of Tx-girder and slab beam, the end block is not included at the end, so only Strut-and-Tie Model (STM) in the longitudinal direction is used to check the nodal strength. However, since the box beam, X-beam, U-beam, and decked-slab beam contains the end block at the end region, it is necessary to check the nodal strength using not only longitudinal STM but also cross-section STM. All types of the Texas standard prestressed beams, except the slab beam, have a risk of horizontal shear fail because the width of the bottom flange is larger than the width of the web, so a horizontal shear check should be performed. Also, in the case of Tx-girders, lateral splitting failure may occur at the bottom flange, so additional checks should be made to ensure that the amount of confinement reinforcement used is sufficient (Ross et al. 2013).

This chapter assesses the shear stresses for six different geometries of Texas beams according to the number of strands and establishes both the demands for failure mode and the capacity of the six different types of Texas beams. The properties required for calculation—geometry, reinforcement detail, and strand layout—are based on the TxDOT's standard design. However, since TxDOT's standard design does not provide the strand layout for some of the Texas beams, a suitable strand layout for each span length was calculated using the PG Super program, which is used to design bridges. The Texas beams for which the strand layout is calculated using PG Super are as follows; Tx-70, 4B40, 5B40, 4XB20, 4XB28, 4XB34, 4XB40, U-40, and U-54. The strand layout and concrete strength for Texas standard prestressed beams are summarized in Appendix A. Then, the analysis results for each Texas beam are used to characterize changes in v_u/f'_c for Texas standard prestress beam according to the geometry type, size of the beam, and the number of strands.

Texas standard prestressed beams consist of a total of six types of beams, and if the sizes of each type are considered, a total of 35 beams are composed. Each girder type has a similar trend result, so it is unnecessary to explain all the results of 35 beams in the main body. Therefore, the analysis results of the girder with the largest

calculated v_u/f'_c among girders of each type are described in Chapter 5, and the analysis results of other girders are arranged in Appendix C.

5.2. Tx-girder

The number of strands and the height and angle of the harped strands are essential factors to calculate the shear stress of the Tx-girder's end region when using STM and anchorage capacity. In this study, the shear stress calculation is based on the strand layout for the Tx-girders used in a 24-ft roadway (6.8-ft beam spacing). Straight strands are placed at 2-in. intervals from the bottom row. When there are no harped strands, 14 strands are set in one row, and if there are harped strands, 12 strands are placed in one row. Harped strands are placed in a downward direction at 2-in. intervals from the height of a harped strand, as shown in Figure 5-1. The diameter of the prestressing strand used for Tx-girder is 0.6-in.; the ultimate strength of prestressing steel, f_{pu}, is 270 ksi; and the web width is 7-in. for all Tx-girders. The geometry and strand layout differences for each Tx-girder are summarized in the following subsections, Appendix A and Appendix C. When calculating v_u/f'_c for the number of strands of each girder, concrete strength, f'_c, is one of the essential variables. Therefore, this study compared v_u/f'_c when using the f'_c based on TxDOT's standard design (depending on the number of strands) and the v_u/f'_c obtained when using the maximum f'_c (8.5 ksi), as suggested in the TxDOT Bridge Design Manual (2020).

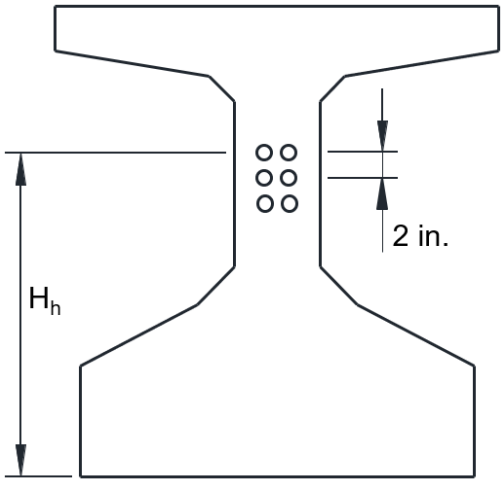

Figure 5-1. Location for harped strands

5.2.1. Analysis for Tx-46

Geometry and reinforcement details for Tx-46 and deck used to calculate shear stress are shown in Figure 5-2. The cross-section areas of the R bar and S bar, which

are shear reinforcements, are 0.2 in^2 and 0.44 in^2, respectively. The R bar is spaced at 3-in. intervals for 3 ft from the end of the beam and thereafter increases to 6-in. intervals. The S bar is also spaced at 3-in. intervals for 3 ft from the end of the beam (combined with R bar) but is not placed beyond that 3-ft span. The cross-section area for longitudinal reinforcement of the top flange and girder deck is 0.2 in^2. Confinement reinforcement consists of the rebars which cross-section area is 0.2 in^2, and they are spaced at 6-in. intervals out to 69-in. from the end of the beam. All lengths of the figure below are in inches.

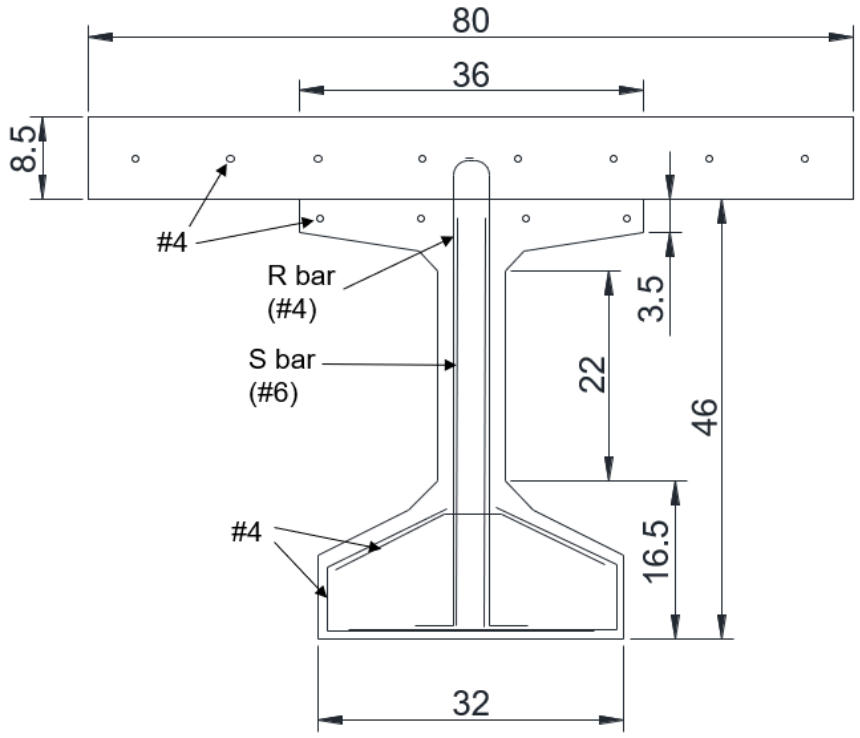

Figure 5-2. The cross-section geometry and reinforcement detail for Tx-46 and 8.5-in. height deck

The span length of Tx-46 ranges from 40 ft to 115 ft., and the number of strands increases as the span length increases. Harped strands are used to control the release stresses, which increase as the number of strands increases. The total number of strands for Tx-46 proposed by TxDOT's standard design is at least ten and at most 42, of which the number of harped strands is zero to six. The design concrete strength, f'_c, increases from 5.0 ksi to 7.0 ksi depending on the number of strands and span length. Strand layout and design concrete strength for the various span lengths of Tx-46 are given in Appendix A.

The calculated ratio of shear stress-to-concrete strength, v_u/f'_c, for Tx-46 can be plotted versus the total number of strands (refer to Figure 5-3). In Figure 5-3, the blue circles represent the v_u/f'_c obtained when using the design concrete strength suggested in the TxDOT's standard design. The orange triangles represent the v_u/f'_c

obtained when using maximum design concrete strength presented in the TxDOT Bridge Design Manual (2020). The v_u/f'_c for Tx-46's end region of the TxDOT's standard design (blue line) is governed by the shear strength calculated through STM when the strands number fewer than 22. However, when more than 22 strands are used, v_u/f'_c is governed by the shear strength calculated using anchorage capacity. As the total number of strands increases, the shear force, V_u, calculated from STM or anchorage capacity increases, and thus v_u/f'_c increases. Also, the graph by the blue circle converges to a constant value due to the increase in the number of harped strands and the increase in the concrete strength. Figure 5-3 shows that the calculated v_u/f'_c for Tx-46 exceeds the *0.18* shear stress limit ratio when the total number of strands is 22 or more, and the maximum v_u/f'_c is 0.236.

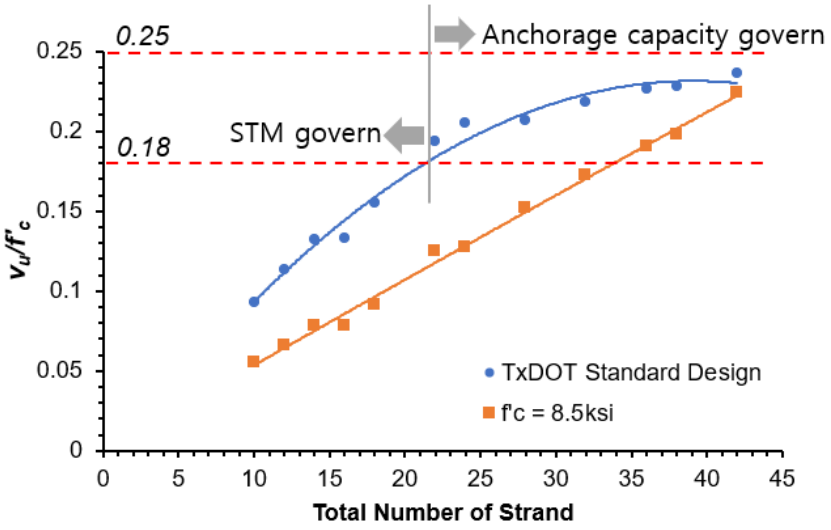

Figure 5-3. v_u/f'_c for Tx-46 by STM and anchorage capacity

As shown in Figure 5-3, if the maximum concrete strength is used (orange triangle), v_u/f'_c is below the *0.18* shear stress limit ratio when the number of strands is 32 or fewer. In addition, if high-strength concrete is used when all other boundary conditions and geometries are the same, the v_u/f'_c can be lowered. However, above the certain number of strands, the effect of using high-strength concrete is reduced. Figure 5-4 compares the demand for strut and horizontal shear for the calculated shear force and the capacity of Tx-46. Since the Tx-girder does not have the end block and always uses only one bearing plate, check the nodal strength using only the longitudinal STM. When the nodal failure and horizontal shear failure are checked, Tx-46 does not reach failure at every level of strand quantity. Tx-46 shows that the capacity for nodes and horizontal shear in all strands is always greater than the demand.

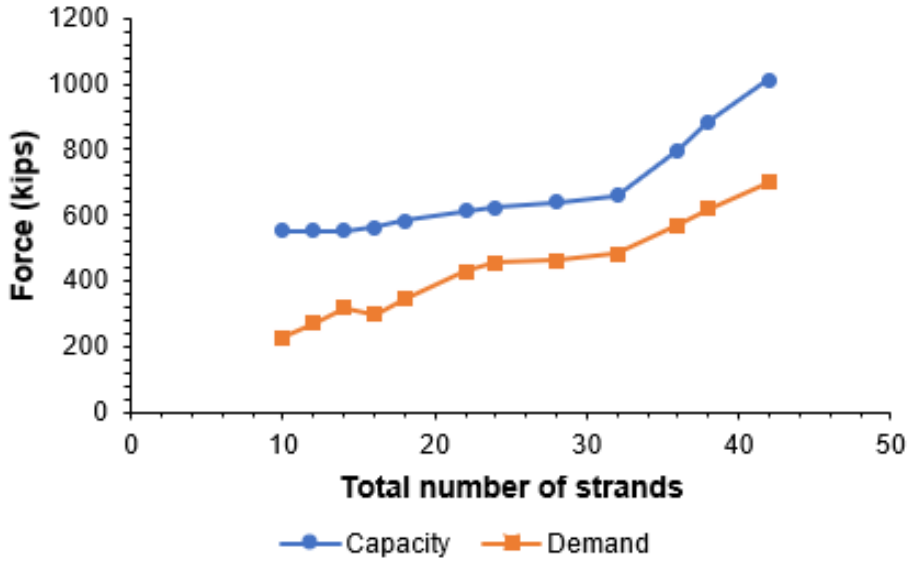

(a) Strut-to-node interface

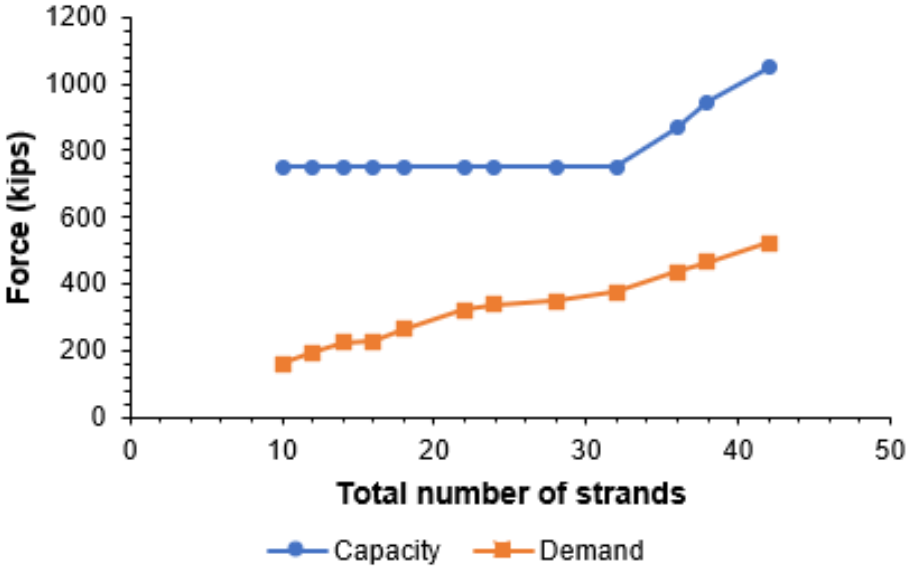

(b) Bearing

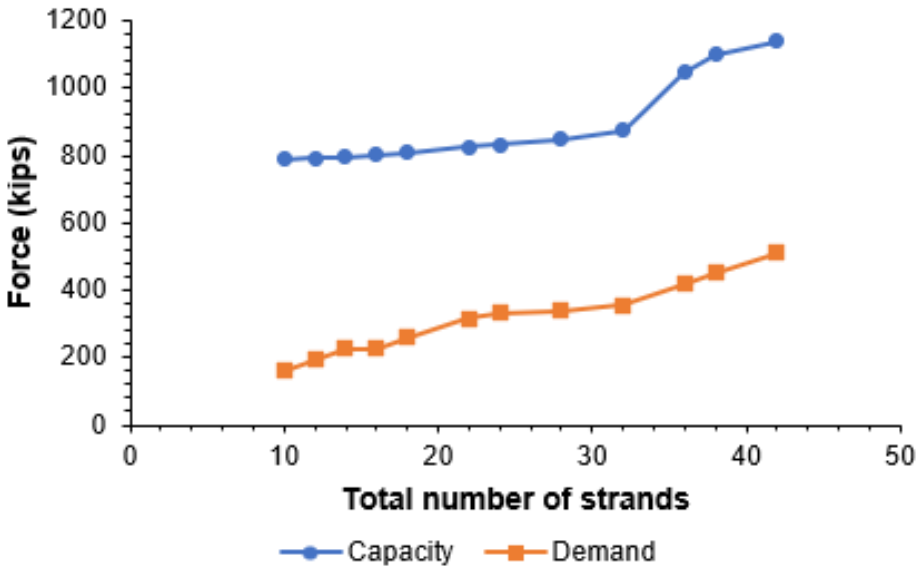

(c) Horizontal shear

Figure 5-4. Difference between capacity and demand for Tx-46

Tx-46 shows that the capacity for nodes and horizontal shear in all strands is always greater than the demand. Therefore, in Tx-46, nodal failure and horizontal shear failure do not occur in the end region even if the shear stress is greater than the $0.18 f'_c$ shear stress limit. Additionally, for Tx-46 with 42 strands, the tie force in the cross-section STM is 291.40 kips (refer to Figure 4-15). The quantity of confinement required at the calculated applied load, A_{cr}, is 2.7 in^2. Still, the actual quantity of confinement is 4.2 in^2, so Tx-46 does not experience lateral splitting failure even if the shear stress is greater than the $0.18 f'_c$ shear stress limit. The check of the additional failure modes indicates that failure did not occur even when the v_u/f'_c of the end region of Tx-46 exceeded the 0.18 shear stress limit ratio when calculated according to the TxDOT's standard design (blue circle). Therefore, the shear stress by STM or anchorage capacity governs the shear capacity for Tx-46.

Analysis results for other sizes of Tx-girders are shown in Appendix C. According to the analytical results for Tx-girders, the difference between capacity and demand of node (especially strut-to-node interface) decreases as the size of the Tx-girder increases. Even though the difference between demand and capacity is the smallest in Tx-70 (as compared to other girders), the expected failure in the end region of the beam did not occur. Finally, the shear stress of every Tx-girder can be greater than the $0.18 f'_c$ shear stress limit, and the nodal failure, horizontal shear failure, and lateral splitting failure will not occur. Therefore, the shear stress limit of Tx-girders can be relaxed up to the maximum v_u/f'_c of each girder.

5.2.2. Extension of v_u/f'_c in Tx-girders

The extension of v_u/f'_c in Tx-girders is investigated by placing more strands in the girder than the maximum suggested by TxDOT's standard design. The concrete stresses limit the possible maximum number of strands for the girder. The concrete stresses at pre-tensioning release for the top and bottom of the beam are calculated by Equation 5-1 and Equation 5-2. Concrete stress is calculated at the transfer point, harped point, and midspan, and the moment of the girder considered only the self-weight of the girder. Effective strand stress ($0.75f_{pu}$-Δf_{pES}) suggested by TxDOT Bridge Design Manual (TxDOT 2020a) is used to calculate the total effective strand force, P_t, in Equation 5-1 and Equation 5-2.

$$f_t = -\frac{P_t}{A_g} + \frac{P_s \times e_s + P_h \times e_h}{S_{top}} - \frac{M_{sw}}{S_{top}} \qquad \text{Equation 5-1}$$

$$f_b = -\frac{P_t}{A_g} - \frac{P_s \times e_s + P_h \times e_h}{S_{bot}} + \frac{M_{sw}}{S_{bot}} \qquad \text{Equation 5-2}$$

Where :

f_t = concrete stress at pre-tensioning release for the top of the beam (ksi)

f_b = concrete stress at pre-tensioning release for the bottom of the beam (ksi)

P_t = total effective strand force (kip)

A_g = area for girder's cross-section (in^2)

P_s = effective prestress force for straight strand (kip)

P_h = effective prestress force for harped strand (kip)

e_s = eccentricity for straight strand (in.)

e_h = eccentricity for harped strand (in.)

M_{sw} = moment for self-weight (kip-in.)

S_{top} = section modulus for the extreme fiber of the top section (in^3)

S_{bot} = section modulus for the extreme fiber of the bottom section (in^3)

The concrete stress limits for "Temporary Stresses before Losses," Equation 5-3 and Equation 5-4, as specified in Article 5.9.2.3 in AASHTO LRFD (2020), are used to check the concrete stresses at the extreme fibers. The concrete strength at release, f'_{ci}, which is suggested by TxDOT's standard design or calculated by PG Super (shown in Appendix A), is used to calculate the concrete stress limits. If the concrete stress calculated by Equation 5-1 and Equation 5-2 is positive, it should be less than the tensile stress limit, and if the concrete stress is negative, the absolute value of concrete stress should be less than the absolute value of the compressive stress limit.

$$\text{Compressive stress limit: } -0.65 f'_{ci} \qquad \text{Equation 5-3}$$

$$\text{Tensile stress limit: } 0.24\sqrt{f'_{ci}} \qquad \text{Equation 5-4}$$

Three sizes of Tx-girders (Tx-28, Tx-46, and Tx-70) are used to check the changes in v_u/f'_c. The maximum possible number of strands that can be arranged for each girder is calculated using concrete strength at release, which is suggested by TxDOT's standard design or calculated by PG Super (shown in Appendix A). Then, concrete strength, f'_c, suggested by TxDOT's standard design (refer to Table 5-1), is used to calculate the v_u/f'_c when increasing the number of strands. The straight strands are increased until the concrete stresses at the top and bottom of the beam for all three points (transfer point, harped point, and midspan) almost reach the concrete stress limits. After obtaining the maximum number of straight strands, the number of harped strands is increased until the concrete stress exceeds the limit. Based on this rationale, the maximum number of strands that can be incorporated without exceeding the stress limit for the three girders checked (Tx-28, Tx-46, and Tx-70) are shown in Table 5-1.

Table 5-1. Maximum number of strands until the stress limit is exceeded

	Tx-28 at 75 ft		**Tx-46 at 115 ft**		**Tx-70 at 150 ft**	
	SD no. of strands	**Increased no. of strands**	**SD no. of strands**	**Increased no. of strands**	**SD no. of strands**	**Increased no. of strands**
f'_c (ksi)	7.8	7.8	7	7	6.3	6.3
f'_{ci} (ksi)	5.6	5.6	6	6	5.3	5.3
Total strands (ea)	28	30	42	48	46	50
Harped strands (ea)	4	6	6	12	8	12

Maximum v_u/f'_c	0.229	0.229	0.236	0.236	0.208	0.209

Note: SD refers to TxDOT's standard design

According to Table 5-1, Tx-28 can increase two strands in total—two harped strands. Tx-46 can increase six strands in total—six harped strands; Tx-70 can increase four strands in total—four harped strands. When using the stress limit to calculate an increase in the number of strands, the maximum number of strands is limited to 54 due to the handling constraints, and three girders keep the number of strands limit. The plot for v_u/f'_c development when increasing the strands is shown in Figure 5-5.

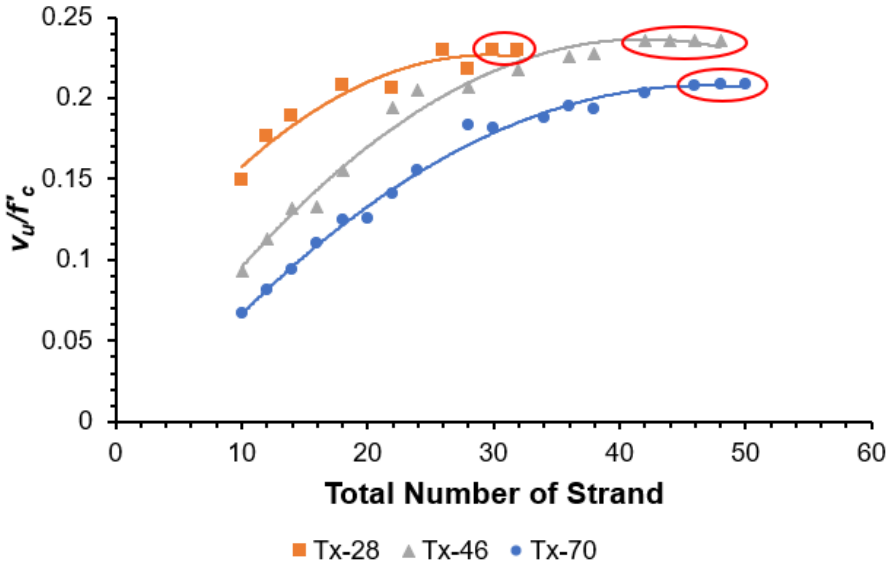

Figure 5-5. v_u/f'_c for three different girders when increasing the number of strands

As Figure 5-5 illustrates, all three girders show a trend in which v_u/f'_c does not increase when it reaches a specific value. That is, even if the number of strands increases until the concrete stress of the beam reaches the limit, v_u/f'_c converges to a constant value. Since the maximum v_u/f'_c does not significantly increase when setting additional strands, the maximum v_u/f'_c calculated by the standard number of strands can be determined as the shear stress limit of the girder.

5.2.3. Compare the shear stress depending on different total prestress loss

In this research, the shear stress is calculated by assuming a total prestress loss of 20%. However, about 70% of the measured value of the total prestress loss is

distributed between 15% and 25%. Therefore, the sensitivity study is performed to investigate the influence of the total prestress loss on the STMs. Results for three different assumed losses are tabulated in Table 1 thru Table 3. Based on this analysis, long-term losses have a clear impact on the shear stress limits; however, the impact is not profound. Even if the total prestresses loss changes to 15% or 25%, the calculated shear stress ratio, v_u/f'_c, using the analytical method shows the difference of less than 5%. As a result, it is appropriate to use the STM assuming that the total prestress loss is 20%.

Table 5-2. Compare the shear stress ratio with different prestress loss

Shear stress ratio, v_u/f'_c			
	15% loss	**20% loss**	**25% loss**
Tx-28	0.238 (+4.3%)	0.229	0.218 (-4.8%)
Tx-34	0.230 (+4.3%)	0.220	0.210 (-4.5%)
Tx-40	0.241 (+4.6%)	0.230	0.219 (-4.8%)
Tx-46	0.247 (+4.5%)	0.236	0.225 (-4.7%)
Tx-54	0.232 (+4.3%)	0.222	0.212 (-4.7%)
Tx-62	0.224 (+4.5%)	0.214	0.205 (-4.4%)
Tx-70	0.217 (+4.1%)	0.208	0.199 (-4.5%)

Table 5-3. Compare shear force with different prestress loss

Shear force, kips			
	15% loss	**20% loss**	**25% loss**
Tx-28	294.89	282.11	269.36
Tx-34	325.78	311.52	297.52
Tx-40	418.97	400.25	381.56
Tx-46	512.44	489.61	466.83
Tx-54	531.9	508.83	485.80

Tx-62	562.48	538.67	514.89
Tx-70	613.54	587.7	561.89

Table 5-4. Compare strut force with different prestress loss

	Strut force, kips		
	15% loss	**20% loss**	**25% loss**
Tx-28	406	388.52	370.97
Tx-34	447.8	428.2	407.57
Tx-40	571.07	545.56	520.08
Tx-46	701.78	670.51	639.31
Tx-54	725.18	693.72	662.33
Tx-62	767.12	734.63	702.21
Tx-70	829.13	794.21	759.33

5.2.4. Summary for Tx-girder

The maximum shear stress of the end regions of Tx-girders can be calculated without anchorage zone distress when using the STM and anchorage capacity. When the calculated shear stress exceeded the $0.18\,f'_c$ shear stress limit, three additional design checks are performed: nodal failure, horizontal shear failure, and lateral splitting failure. The results indicated that the shear stress of the end region of all Tx-girders conforming to the TxDOT's standard design could exceed the $0.18\,f'_c$ shear stress limit. Moreover, when the calculated shear stress exceeds $0.18\,f'_c$, the anchorage capacity mainly governs the calculated shear stress of the Tx-girder's end. Even if the computed shear stress is greater than the $0.18\,f'_c$ shear stress limit, the demands of nodes, horizontal shear, and lateral splitting do not exceed the beam capacity. Furthermore, since the shear stresses of Tx-girders converge to the maximum shear stress for each girder, the shear stress limit can be relaxed up to the calculated maximum shear stress. However, as the maximum v_u/f'_c varies depending on the size of the Tx-girder, a different shear stress limit should be considered for each Tx-girder (refer to Figure 5-6).

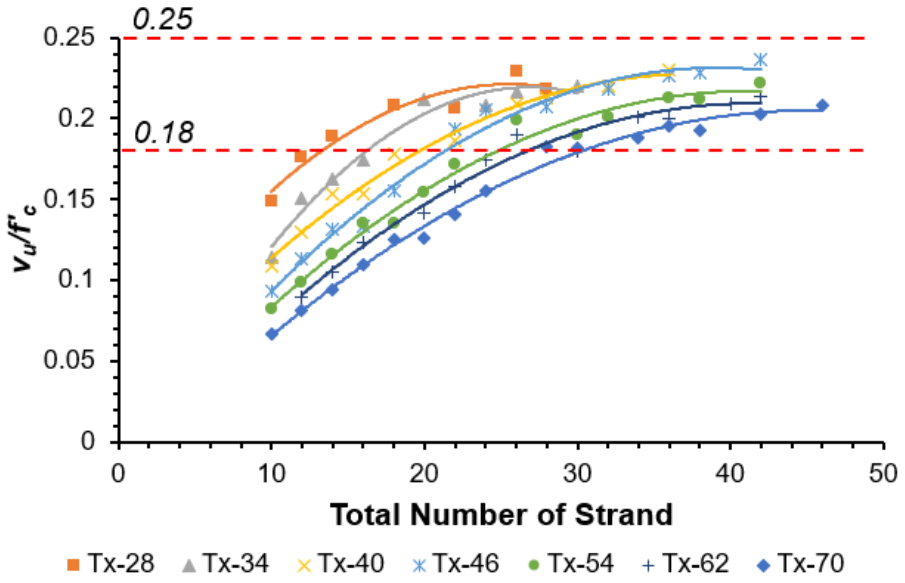

Figure 5-6. v_u/f'_c for different sizes of Tx-girders

As the size of the Tx-girder increases, the v_u/f'_c decreases even if the same number of strands is used (refer to Figure 5-6). The maximum v_u/f'_c of each girder is shown in Table 5-5. Finally, the Tx-girder can relax a shear stress limit from 0.208 to 0.236 and does not exceed the 0.25 shear stress limit based on the Modified Compression Field Theory (MCFT).

Table 5-5. Analytical results of different Tx-girders

	Tx-28	Tx-34	Tx-40	Tx-46	Tx-54	Tx-62	Tx-70
Maximum v_u/f'_c	0.229	0.220	0.230	0.236	0.222	0.214	0.208

5.3. Box Beam

Unlike in the Tx-girder, for the box beam, the horizontal shear should be checked in consideration of the end block's geometry, and the nodal strength should be checked using STM in different directions according to the number of bearing plates. At the end of the beam using one bearing plate, nodal failure is checked using the cross-section STM. At the end of the beam using two bearing plates, the nodal failure of the obtuse angle of the beam of the 30° skewed end, which is the most extreme case, is checked. The remaining beams from the box beam did not take into account the maximum f'_c (8.5 ksi), as suggested in the TxDOT Bridge Design Manual (2020). This is because if the number of strands is increased, the calculated v_u/f'_c is less affected by the strength of concrete (refer to Figure 5-3). In addition, the main purpose of this study is to confirm whether the shear stress limit

of the end region of the Texas standard prestressed beam can be relaxed without increasing the concrete strength.

The number of fully bonded strands is essential in calculating the shear stress of the box-beam's end region when using STM and anchorage capacity. In this study, the shear stress calculation is based on the strand layout for the box beams used in a 24-ft roadway. Straight strands are placed at 2-in. intervals from the bottom row. Twenty-two strands are set in the first row for type 4B, and 28 strands are set in the first row for type 5B. From the second row, the number of strands that can be placed is sharply reduced due to the void of the box beam. The number of strands from the second row varies according to the size of the box beam. The prestressing strand's diameter is 0.6-in.; the ultimate strength of prestressing steel, f_{pu}, is 270 ksi; and the web width is 10-in. for all box beams. The concrete strength, f'_c, used for each box beam is based on TxDOT's standard design (depending on the number of strands).

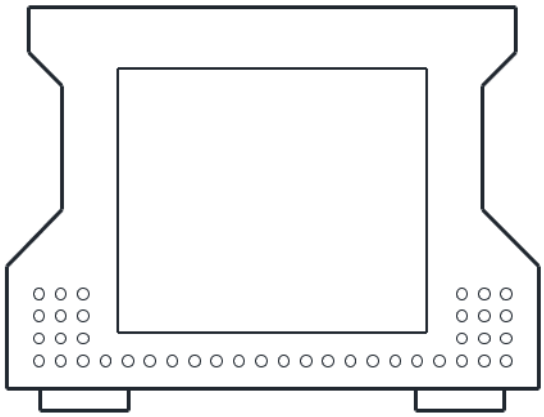

Figure 5-7. Strand pattern for box beam

5.3.1. Analysis for 5B20

Geometry and reinforcement details for 5B20 and the deck used to calculate shear stress are shown in Figure 5-8. The shear reinforcement is spaced at 3-in. intervals at the end of the beam, and the cross-section areas of the shear reinforcements are 0.2 in^2 (#4). The cross-section area for each longitudinal reinforcement of the top flange is 0.31 in^2 (#5) and of the deck is 0.2 in^2 (#4). All lengths of the figure below are in inches.

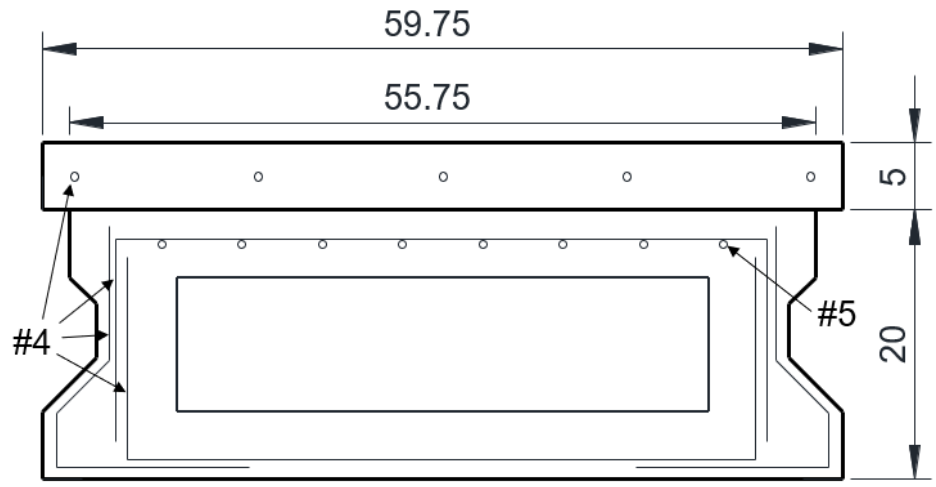

Figure 5-8. The cross-section geometry and reinforcement detail for 5B20 and 5-in. height deck

The span length of 5B20 ranges from 30 ft to 65 ft, and the number of strands increases as the span length increases. Debonded strands are used to control the relaxed stresses, which increase as the number of strands increases. The total number of strands for 5B20 proposed by TxDOT's standard design is at least eight and at most 24, of which the number of the debonded strands is zero to six. The design concrete strength is 5.0 ksi for overall span length.

The calculated ratio of shear stress-to-concrete strength, v_u/f'_c, for 5B20 using STM and anchorage capacity can be plotted versus the total number of strands (refer to Figure 5-9). The v_u/f'_c for 5B20's end region, per TxDOT's standard design, is governed by the shear strength calculated through STM when the strands number fewer than 16. However, when more than 16 strands are used, v_u/f'_c is governed by the shear strength calculated using anchorage capacity. As the total number of strands increases, the shear force, V_u, calculated from STM or anchorage capacity increases, and thus v_u/f'_c increases. Figure 5-9 shows that the calculated v_u/f'_c for 5B20 slightly exceeds the *0.18* shear stress limit ratio when the total number of strands is 16 or more, and the maximum v_u/f'_c is 0.197.

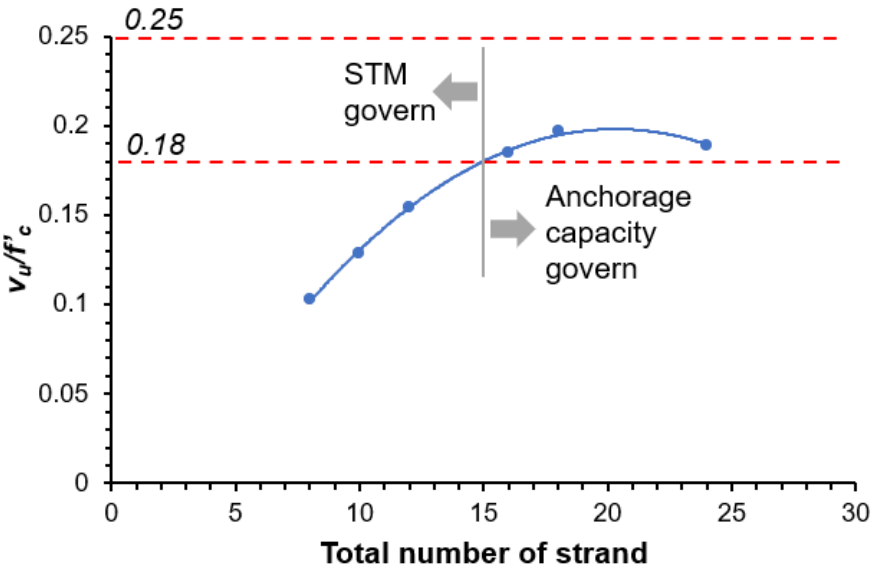

Figure 5-9. v_u/f'_c for 5B20 by STM and anchorage capacity

Figure 5-10 compares graphs of the demand of nodes and horizontal shear for the calculated shear force and the capacity of 5B20. Unlike the Tx-girder, the box beam has an end block, and the number of bearing plates is one at the end but two at another end. Therefore, when two bearing plates are used, the nodal strength can be checked using longitudinal STM like Tx-girder, but the nodal strength must be checked using cross-section STM when one bearing plate is used. Also, when two bearing plates are used, the nodal capacity at the obtuse angle becomes larger than the nodal capacity at the acute angle. Therefore, Figure 5-10 is the result of comparing the demand and capacity of nodes above the bearing plate at the obtuse angle when using two bearing plates.

When the maximum shear strength calculated by STM or anchorage capacity acts on the end of the 5B20, the strut-to-node interface for the beam end using two bearing plates with a skewed end fails. Therefore, nodal strength governs the shear capacity for the end of the 5B20 and the maximum v_u/f'_c for 5B20 decreases. When nodal strength governs the shear capacity for the end of the box beam, applied maximum shear force should be decreased until nodal failure is prevented. If the shear strength decreased, the v_u/f'_c would also be decreased, so the v_u/f'_c for 5B20 without nodal failure is 0.190.

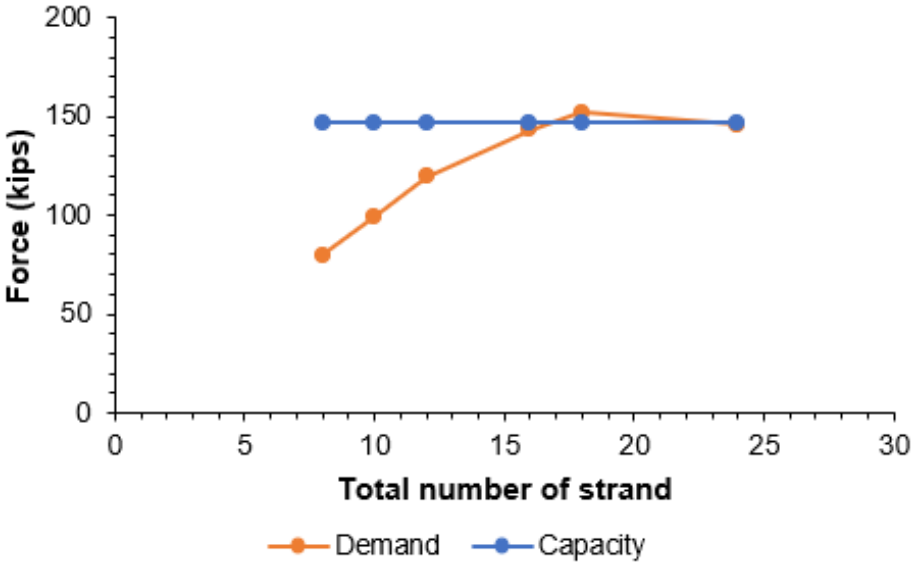

(a) Strut-to-node interface (two plates, 30° skewed)

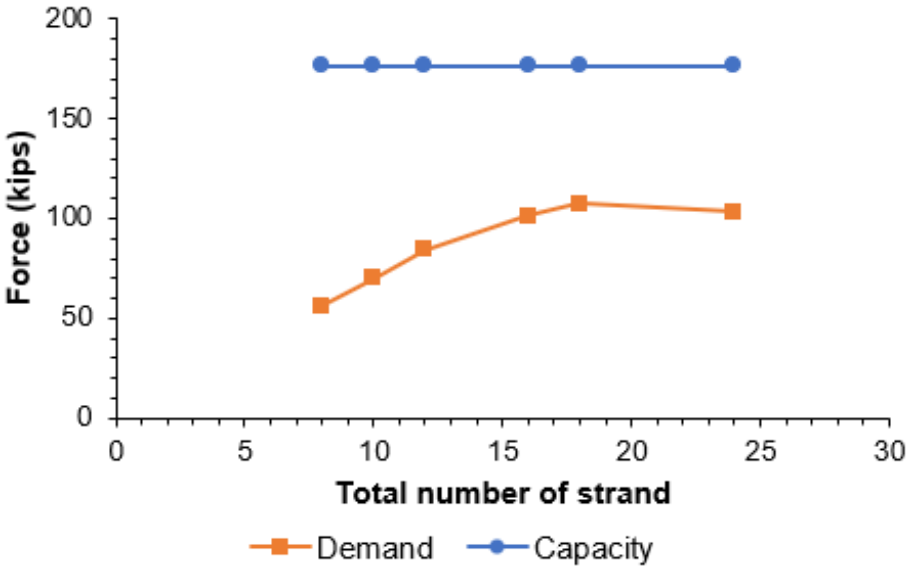

(b) Bearing (two plates, 30° skewed)

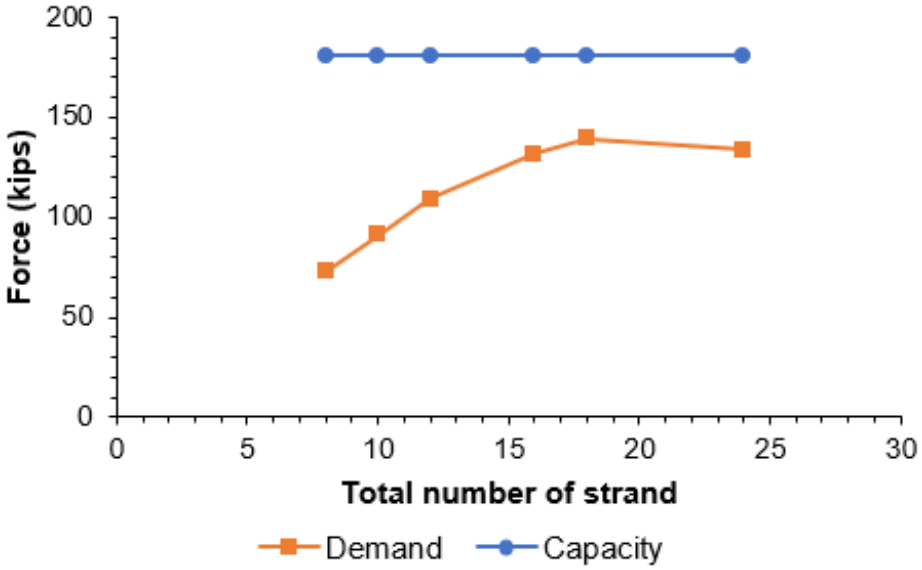

(c) Strut-to-node interface (one plate)

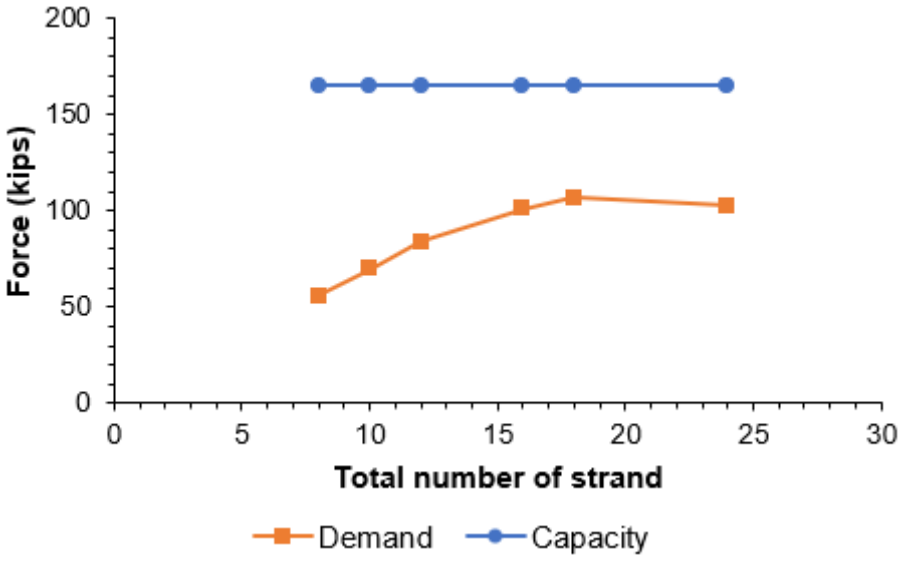

(d) Back face (one plate)

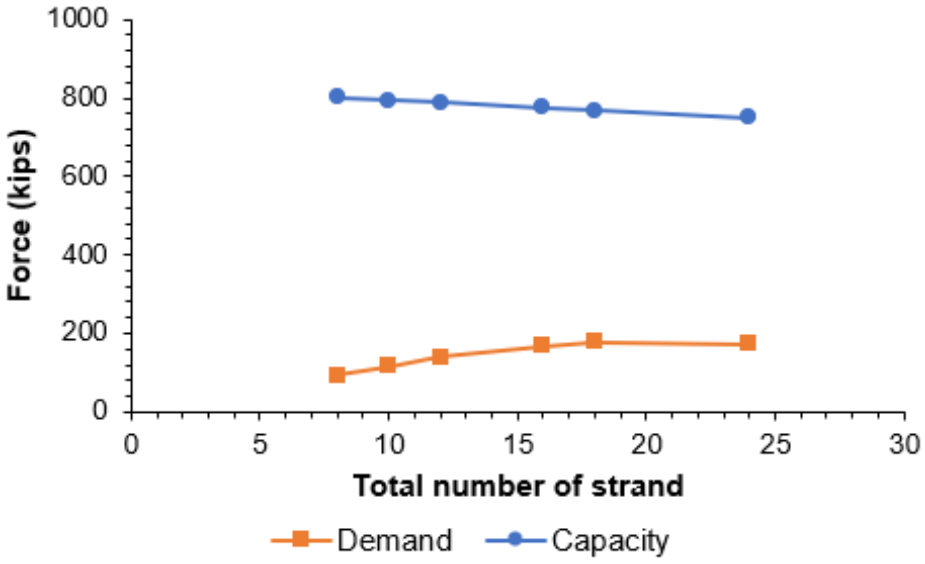

(e) Horizontal shear

Figure 5-10. Difference between capacity and demand for 5B20

Analysis results for other sizes of box beams are shown in Appendix C. According to the analytical results for box beams, the maximum shear capacity of four beams (4B20, 4B34, 4B40, 5B40) is governed by anchorage capacity, but the other four beams (4B28, 5B20, 5B28, 5B34) are governed by nodal strength. Also, maximum v_u/f'_c for almost all the box beams cannot exceed the *0.18* shear stress limit ratio, with the exception of 5B20. Only 5B20, of all the box beams, can relax the $0.18\,f'_c$ shear stress limit of the beam end (0.18 → 0.19). However, the value that can relax the shear stress limit of 5B20 is quite small compared to the Tx-girder.

5.3.2. Summary for box beam

The findings indicate that the maximum shear stress of the end regions of the box beam can be calculated without anchorage zone distress when using the STM and anchorage capacity. Further, the research team performed two additional design checks: nodal failure and horizontal shear failure. The results indicated that the shear stress of the end region of only one box beam (5B20) conforming to TxDOT's standard design could exceed the $0.18\,f'_c$ shear stress limit. Moreover, when the calculated shear stress of 5B20 exceeds $0.18\,f'_c$, the anchorage capacity governs the calculated shear stress of the 5B20's end. The same as the Tx-girder, the maximum v_u/f'_c of the box beam displays a trend in which the value decreases as the beam's height increases. However, when the width of the beam is increased, the maximum v_u/f'_c of the box beam increases. The graphs of v_u/f'_c from STM and anchorage capacity versus the total number of strands for type 4B and type 5B are shown in Figure 5-11.

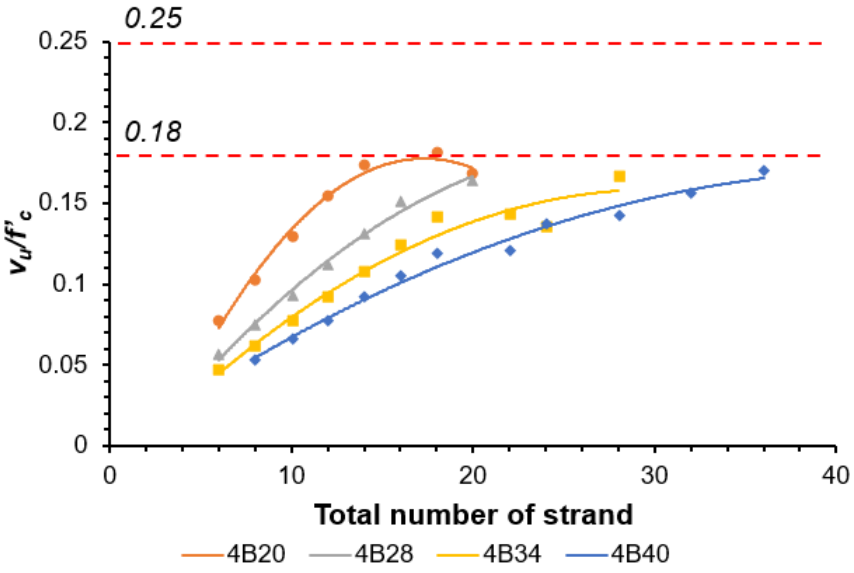

Type 4B

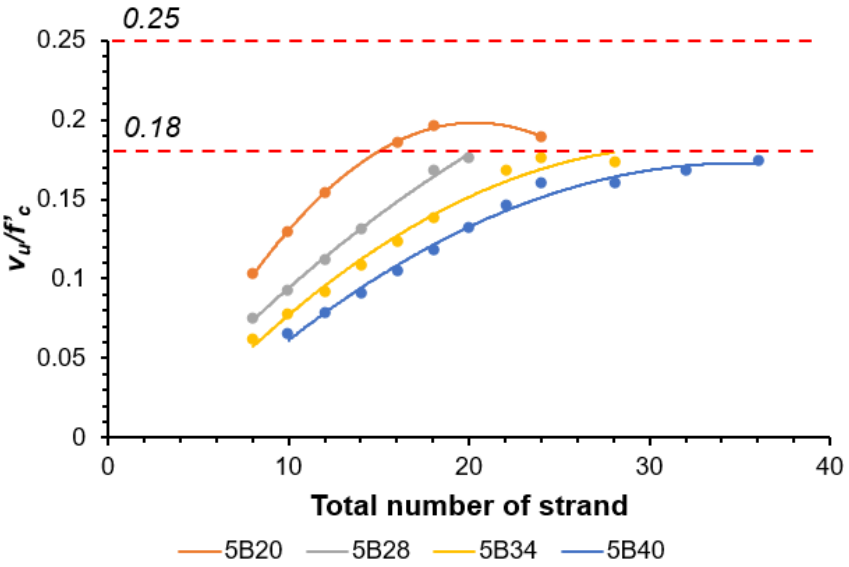

Type 5B

Figure 5-11. Different v_u/f'_c calculated by STM and anchorage capacity depending on the size of box beams

For the four box beams (4B28, 5B20, 5B28, and 5B34), nodal failure will occur when the maximum shear strength calculated by STM and anchorage capacity is applied to the end of the beam. Since these four beams' nodal capacity governs the beam's shear capacity, the maximum v_u/f'_c becomes smaller than the value calculated by STM and anchorage capacity (refer to Table 5-6). However, the box beam's nodal failure can be prevented by slightly modifying the standard design, which is explained in Chapter 7 (increasing the size of the bearing plate, adding additional horizontal reinforcement). The analytical results of box beams following the TxDOT Standard design are shown in Table 5-6.

Table 5-6. Analytical results of different box beams

	4B20	4B28	4B34	4B40	5B20	5B28	5B34	5B40
Maximum v_u/f'_c	0.180	0.163	0.166	0.170	0.190	0.163	0.155	0.174

The research team adds more strands than the standard design for Tx-girder until the girder reaches the stress limit and check shear capacity. However, for the box beams, no more fully bonded strands can be added at the end because of the stress limit. Also, two debonded strands can be added, but debonded strands cannot affect shear strength at the end of the beam.

5.4. X-beam

The boundary condition of the X-beam is the same as that of the box beam, and the geometry is almost the same. Also, the X-beam has one bearing plate on one support and two bearing plates on the other support. According to the TxDOT Bridge Design Manual (2020), the X-beam's skewed end's maximum angle is 30° same as the box beam. Since the X-beam characteristics are the same as those of the box beam, v_u/f'_c of the X-beam can be calculated using the same calculation method for v_u/f'_c of the box beam. Furthermore, the horizontal shear failure and nodal failure can be checked using the same method used for the box beam.

The number of fully bonded strands is an essential factor in calculating the shear stress of the X-beam's end region using STM and anchorage capacity. In this study, the shear stress calculation is based on the strand layout for the X-beams used in a 32-ft roadway. Straight strands are placed at 2-in. intervals from the bottom row. Twenty-two strands are set in one row for type 4XB, and twenty-eight strands are set in one row for type 5XB. For the third row, the number of strands that can be placed is sharply reduced due to the void of the X-beam. The number of strands in the third row varies according to the size of the X-beam. The prestressing strand's diameter is 0.6-in.; the ultimate strength of prestressing steel, f_{pu}, is 270 ksi; and the web width is 13-in. for all X-beams. The concrete strength, f'_c, used for type 5XB is suggested in TxDOT's standard design; the PG Super program suggests the concrete strength used for type 4XB. The concrete strengths for each span length of type 4XB are shown in Appendix A. Figure 5-12 illustrates the X-beam strand pattern.

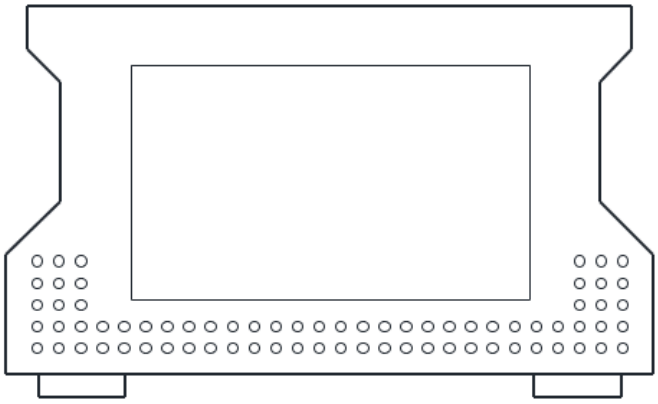

Figure 5-12. Strand pattern for X-beam

5.4.1. Analysis for 5XB28

Geometry and reinforcement details for 5XB28 and the deck used to calculate shear stress are shown in Figure 5-13. The shear reinforcement is spaced at 4-in. intervals at the end of the beam, and the cross-section areas of the shear reinforcements are 0.2 in^2 (#4). The cross-section area for each longitudinal reinforcement of the top flange is 0.31 in^2 (#5) and of the deck is 0.2 in^2 (#4). All lengths of the figure below are in inches.

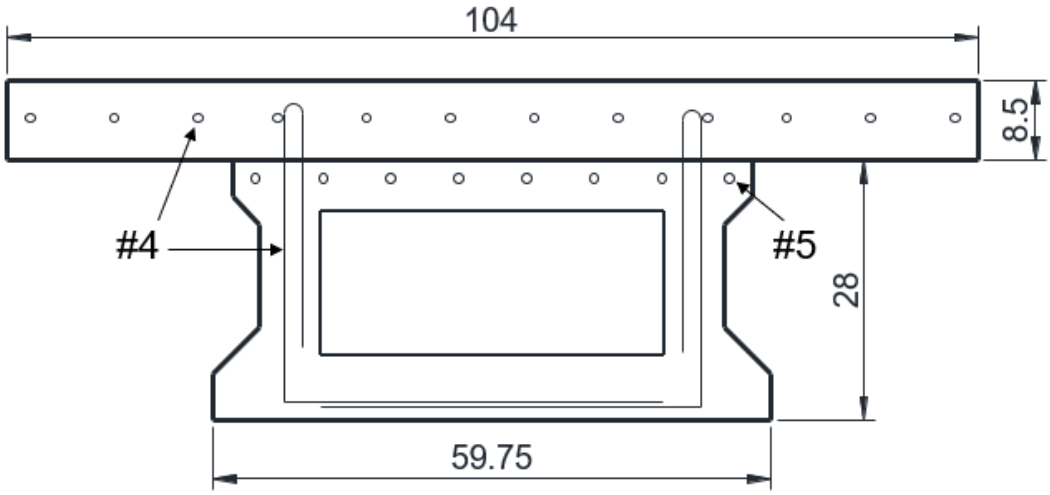

Figure 5-13. The cross-section geometry and reinforcement detail for 5XB28 and 8.5-in. height deck

The span length of 5XB28 ranges from 40 ft to 80 ft, and the number of strands increases as the span length increases. Debonded strands are used to control the release stresses, which increase as the number of strands increases. The total number of strands for 5XB28 proposed by TxDOT's standard design is at least 12

and at most 36, of which the number of the debonded strands is zero to six. The design concrete strength is 5.0 ksi for overall span length.

The calculated ratio of shear stress-to-concrete strength, v_u/f'_c, for 5XB28 using STM and anchorage capacity can be plotted versus the total number of strands (refer to Figure 5-14). The v_u/f'_c for 5XB28's end region, per TxDOT's standard design, is governed by the shear strength calculated through STM when the number of strands is fewer than 22. However, when more than 22 strands are used, v_u/f'_c is governed by the shear strength calculated using anchorage capacity. As the total number of strands increases, the shear strength, V_u, calculated from STM or anchorage capacity increases, and thus v_u/f'_c increases. Figure 5-14 shows that the calculated v_u/f'_c for 5XB28 exceeds the *0.18* shear stress limit ratio when the total number of strands is 26 or more, and the maximum v_u/f'_c is 0.209.

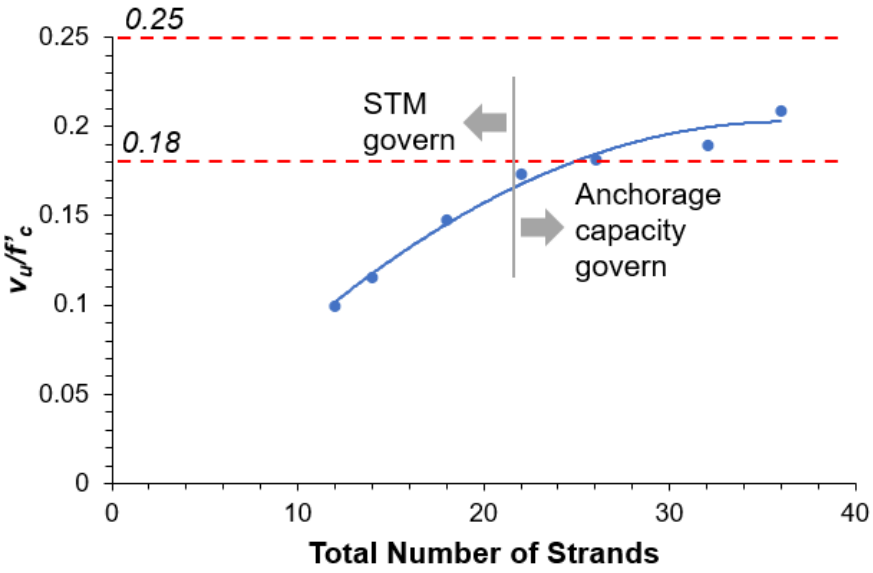

Figure 5-14. v_u/f'_c for 5XB28 by STM and anchorage capacity

Figure 5-15 compares the demand for nodes and horizontal shear for the calculated shear force and the capacity of 5XB28. When maximum shear strength calculated by STM or anchorage capacity acts on the end of the 5XB28, the strut-to-node interface for the beam end using two bearing plates with a skewed end fails. Therefore, nodal strength governs the shear capacity for the end of the 5XB28, and the maximum v_u/f'_c for the beam is decreased. When nodal strength governs the shear capacity for the end of the X-beam, applied maximum shear force should be decreased until nodal failure is prevented. If the shear strength decreased, the v_u/f'_c would also be decreased, so the v_u/f'_c for 5XB28 without nodal failure is 0.205.

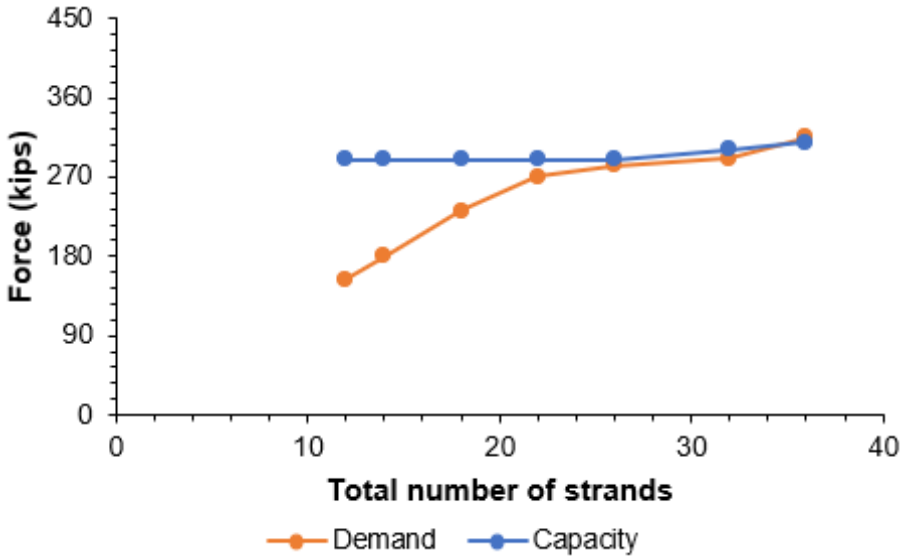

(a) Strut-to-node interface (two plates, 30° skewed)

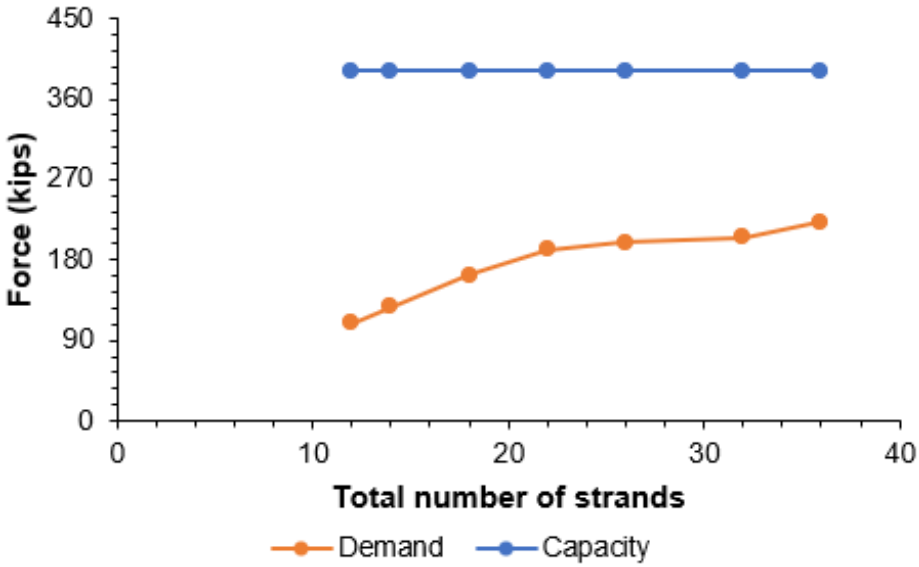

(b) Bearing (two plates, 30° skewed)

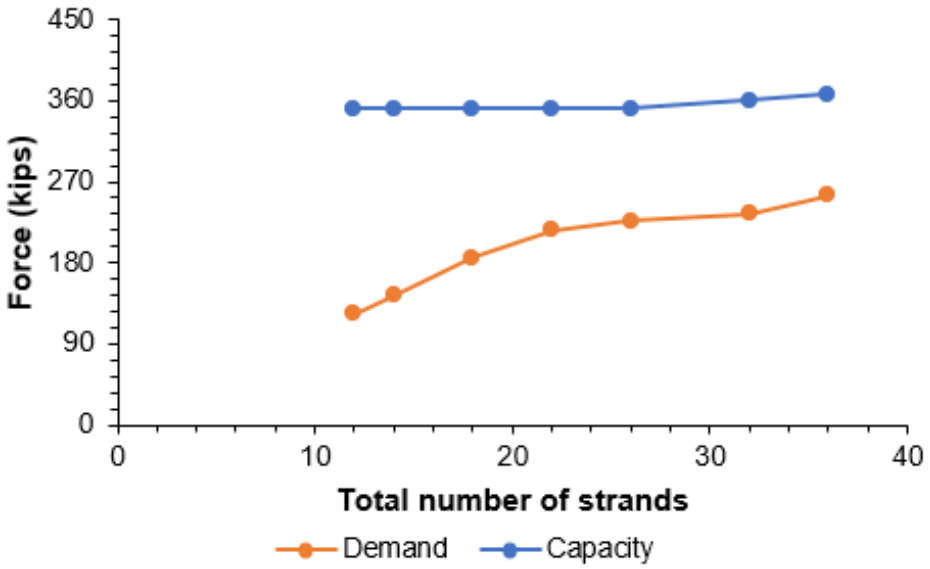

(c) Strut-to-node interface (one plate)

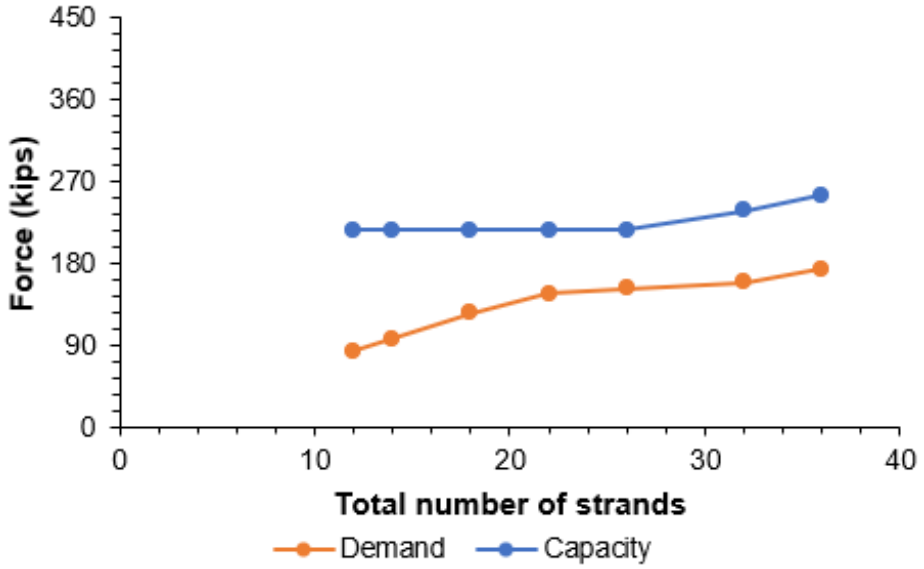

(d) Back face (one plate)

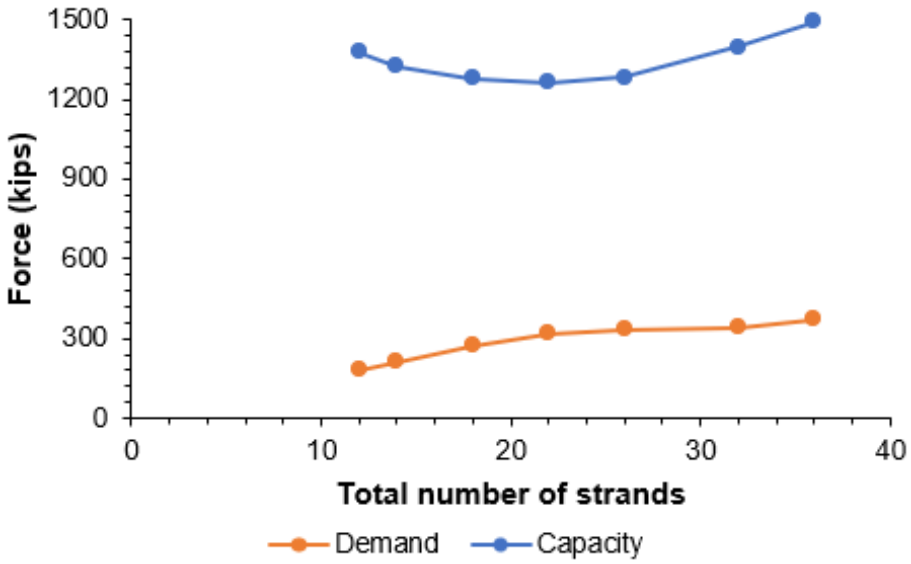

(e) Horizontal shear

Figure 5-15. Difference between capacity and demand for 5XB28

Analysis results for other sizes of X-beams are shown in Appendix C. According to the analytical results for X-beams, the maximum shear stress capacities of X-beams are governed by anchorage capacity except for 5XB28, which is governed by nodal strength. Also, the maximum v_u/f'_c for four X-beams (4XB28, 5XB20, 5XB28, 5XB34) can exceed the *0.18* shear stress limit ratio, but others cannot. This finding indicates that only four X-beams, with a maximum v_u/f'_c larger than *0.18* shear stress limit ratio, can relax the $0.18\,f'_c$ shear stress limit of the beam end.

5.4.2. Summary for X-beam

The findings indicate that the maximum shear stress of the X-beam's end regions can be calculated without anchorage zone distress when using the STM and anchorage capacity. Further, the research team performed two additional design checks: nodal failure and horizontal shear failure. The results indicated that the shear stress of the end region of four X-beams conforming to TxDOT's standard design (4XB28, 5XB20, 5XB28, 5XB34) could exceed the $0.18\,f'_c$ shear stress limit. Although the shear stress limit is exceeded, STM or anchorage capacity analysis tells us the beam is still safe, which confirms that $0.18\,f'_c$ is too strict, and the result in Table 5-7 can be used. Moreover, when X-beams' calculated shear stress exceeds $0.18\,f'_c$, the anchorage capacity governs the calculated shear stress of the end of X-beams. Just as in the box-girder, the maximum v_u/f'_c of the X-beam displays a trend in which the value decreases as the beam's height increases. However, when the width of the beam is increased, the maximum v_u/f'_c of the X-beam increases. The graphs of v_u/f'_c from STM and anchorage capacity versus the total number of strands for type 4XB and type 5XB are shown in Figure 5-16.

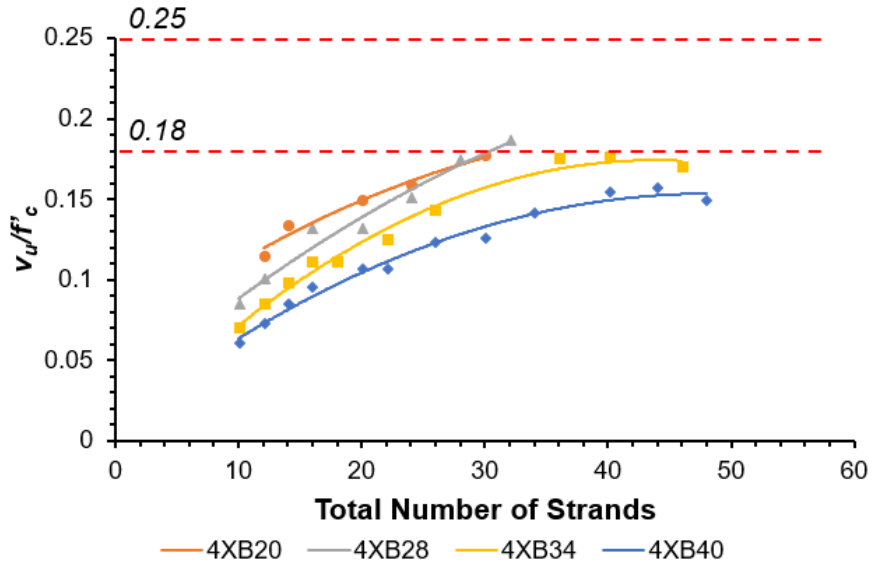

Type 4XB

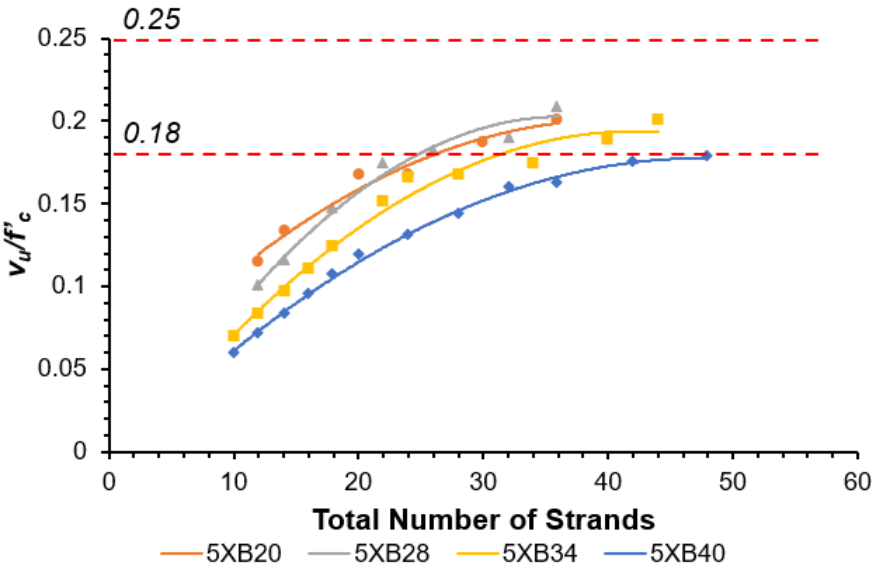

Type 5XB

Figure 5-16. Different v_u/f'_c calculated by STM and anchorage capacity depending on the size of X-beams

For the one X-beam (5XB28), nodal failure will occur when the maximum shear strength calculated by STM and anchorage capacity is applied to the beam's end. Since these X-beams' nodal capacity governs the beam's shear capacity, the maximum v_u/f'_c becomes smaller than the value calculated by STM and anchorage capacity (refer to Table 5-7). However, the X-beam's nodal failure can be prevented by slightly modifying the standard design, which is explained in Chapter 7 (increasing the bearing plate's size, adding additional horizontal reinforcement). The analytical results of X-beams following the TxDOT Standard design are shown in Table 5-7.

Table 5-7. Analytical results of different X-beams

	4XB20	4XB28	4XB34	4XB40	5XB20	5XB28	5XB34	5XB40
Maximum v_u/f'_c	0.177	0.186	0.176	0.157	0.201	0.205	0.201	0.179

For Tx-girder, the results of adding more strands than specified in the standard design until the girder reaches the concrete stress limit are reported, and then the shear capacity is checked. However, no more fully bonded strands can be added at the end for the X-beams because of the concrete stress limit. While two debonded strands can be added, debonded strands cannot affect shear strength at the end of the beam.

5.5. U-beam

Calculating shear capacity and checking additional failure mode for the end of the decked-slab beam can be performed using the similar methodology applied for the box beam because both beams have the same boundary condition and similar features for geometry. However, two different cross-section STMs are used to calculate the applied force acting at the node for U-beams when one bearing plate is used at the end, and the results are compared. At the end of the beam using two bearing plates, the nodal failure of the obtuse angle of the beam's 45° skewed end, which is the most extreme case, is also checked. Since TxDOT's standard design does not provide the strand layout and concrete strength for every U-beam, a suitable strand layout and concrete strength for each span length was calculated using the PG Super program. When using the PG Super program to calculate strand layout and concrete strength, the default value of PG Super for the U-beam's girder spacing is used (9.25 in. for U-40 & 10.25 in. for U-40), and span length is increased until concrete design strength reaches the 8.5-ksi limit suggested in the TxDOT Bridge Design Manual (2020).

The number of fully bonded strands is an essential factor in calculating the shear stress of the U-beam's end region using STM and anchorage capacity. Straight strands are placed at 1.97-in. intervals from the bottom row. Twenty-seven strands are set in one row for the U-beam. For the fourth row, the number of strands that can be placed is sharply reduced due to the void of the U-beam. The prestressing strand's diameter is 0.6 in.; the ultimate strength of prestressing steel, f_{pu}, is 270 ksi; and the web width is 10 in. for all U-beams. The PG Super program suggests the concrete strength, f'_c, used for the U-beam. The strand layouts and concrete strengths for each span length of the U-beam are shown in Appendix A. Figure 5-17 illustrates the U-beam strand pattern.

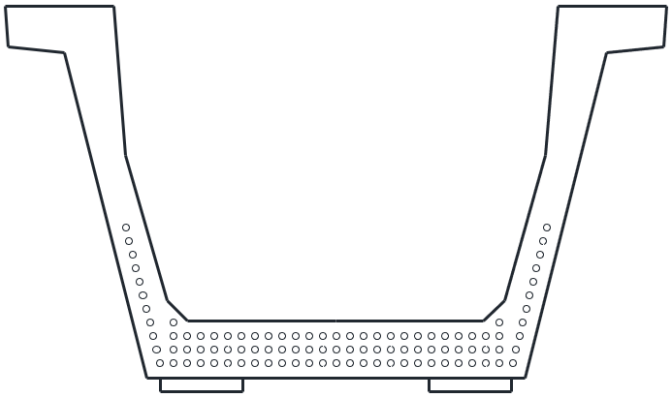

Figure 5-17. Strand pattern for U-beams

5.5.1. Analysis for U-40

Geometry and reinforcement details for U-40 and the deck used to calculate shear stress are shown in Figure 5-18. The shear reinforcement is spaced at 4-in. intervals at the end of the beam. The cross-section area for each longitudinal reinforcement of the top flange is 0.31 in^2 (#5); that area for the deck and the stirrup is 0.2 in^2 (#4). All lengths of the figure below are in inches.

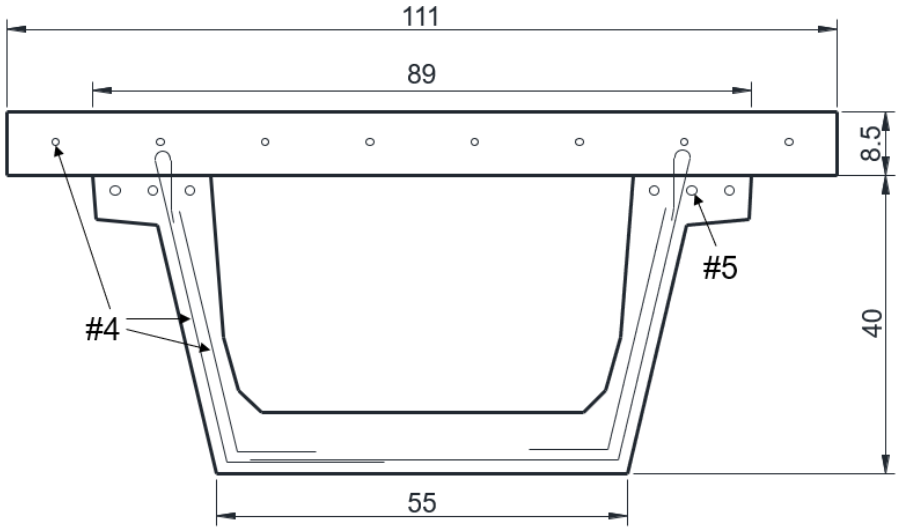

Figure 5-18. The cross-section geometry and reinforcement detail for U-40 and 8.5-in. height deck

The strand layout and design concrete strength for the U-40 are not provided in TxDOT's standard design. Therefore, in this study, the strand layout and concrete strength for the U-40 with 9.25-in. girder spacing are calculated using the bridge design program PG Super. The span length of U-40 ranges from 40 ft to 110 ft. As the span length increases, the total number of strands and the number of debonded strands increase. The total number of strands for U-40 proposed by PG Super is at

least ten and at most 49, of which the number of the debonded strands is zero to 19. The design concrete strength, f'_c, increases from 5.0 ksi to 8.0 ksi depending on the number of strands and span length. Strand layout and concrete strength for the various span lengths of U-40 are given in Appendix A.

The calculated ratio of shear stress-to-concrete strength, v_u/f'_c, for U-40 using STM and anchorage capacity can be plotted versus the total number of strands (refer to Figure 5-19). The v_u/f'_c for U-40's end region, per TxDOT's standard design, is governed by the shear strength calculated through STM for every quantity of strands are used. As the total number of strands increases, the shear force, V_u, calculated from STM increases, and thus v_u/f'_c increases. Figure 5-19 shows that the calculated v_u/f'_c for U-40 using STM cannot exceed the *0.18* shear stress limit ratio, and the maximum v_u/f'_c is 0.170.

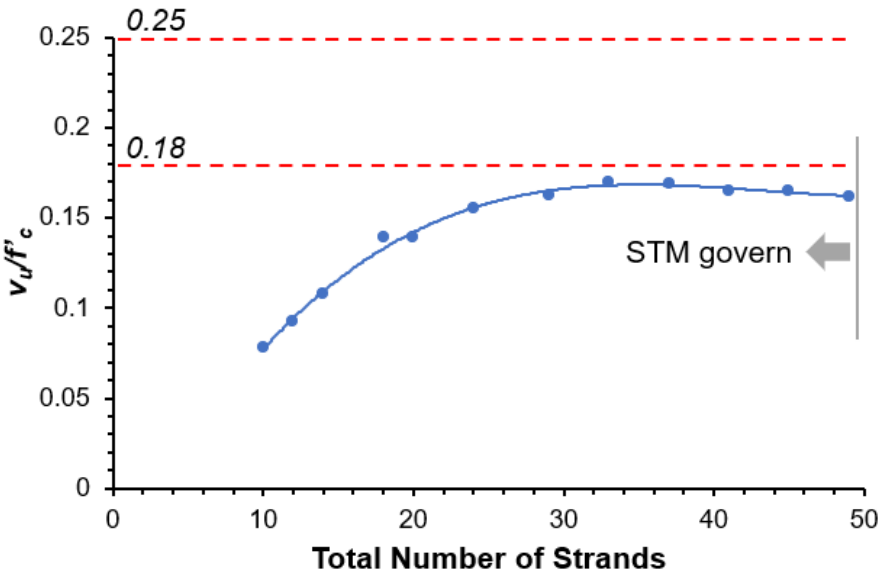

Figure 5-19. v_u/f'_c for U-40 by STM and anchorage capacity

Figure 5-20 compares the demand for nodes and horizontal shear with the calculated shear force and the capacity of U-40. The cross-section STM with the vertical tie is used to check the strut-to-node interface when one bearing plate is placed at the end. The reason for using a vertical tie instead of the inclined tie is explained in the following chapter. U-40 does not reach failure at every level of strand quantity when the nodal failure and horizontal shear failure are checked. U-40 shows that the capacity for nodes and horizontal shear in all strands is always greater than the demand. Therefore, the shear strength by STM governs the shear capacity for U-40.

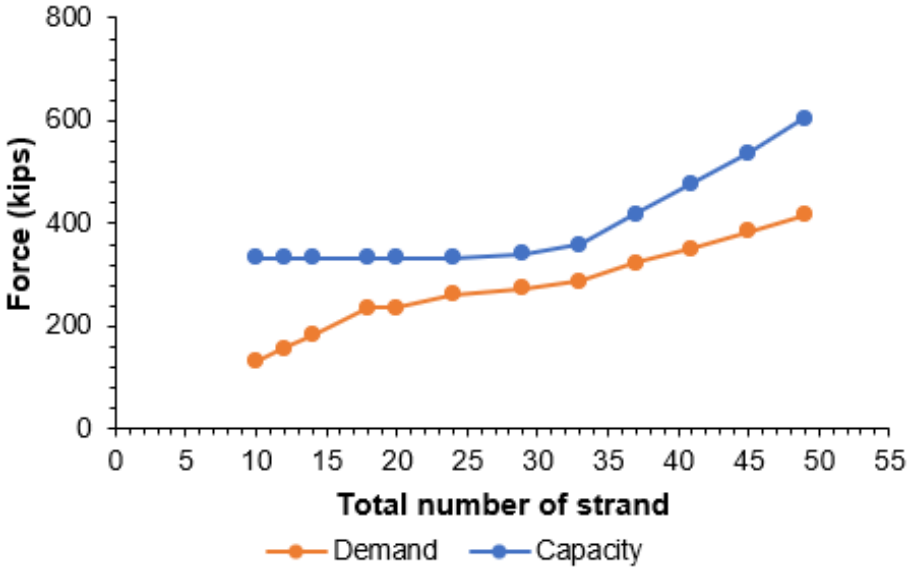

(a) Strut-to-node interface (two plates, 45° skewed)

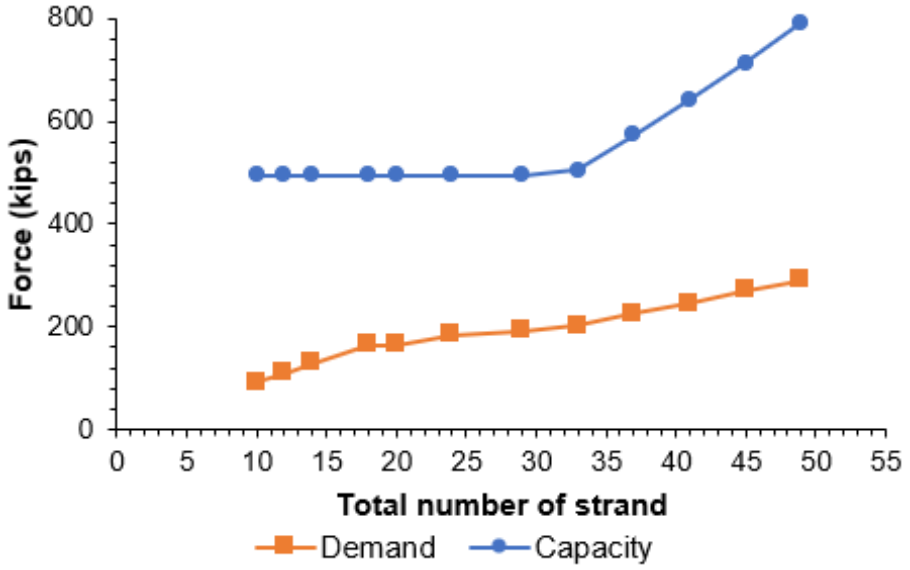

(b) Bearing (two plates, 45° skewed)

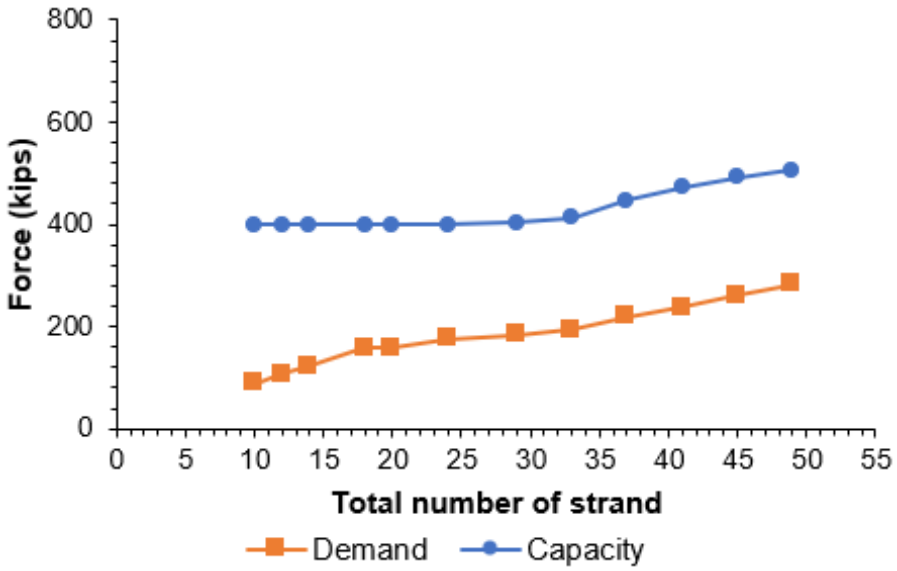

(c) Strut-to-node interface (one plate)

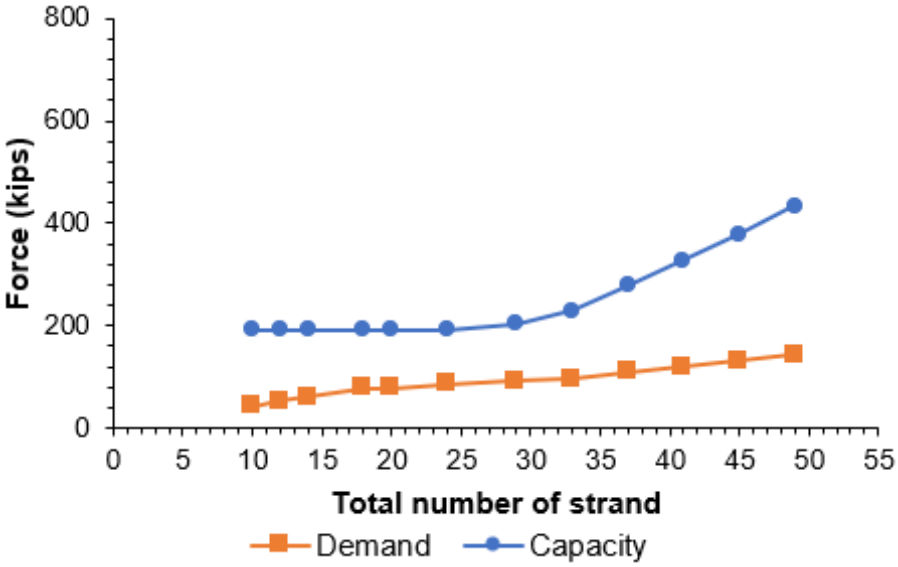

(d) Back face (one plate)

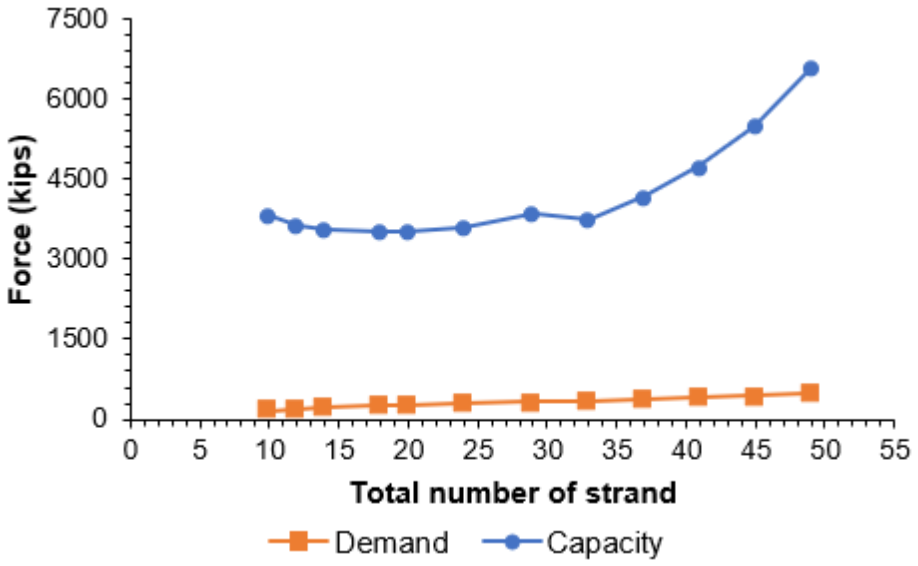

(e) Horizontal shear

Figure 5-20. Difference between capacity and demand for U-40

Analysis results for other sizes of U-beams are shown in Appendix C. According to the analytical results for U-beams, nodal failure, and horizontal shear failure will not occur for every size of the U-beams when the maximum shear force that does not cause anchorage zone distress is applied to the end region of the beam. Therefore, the maximum shear capacities of two U-beams (U-40 & U-54) are governed by tie capacity and STM. However, the maximum v_u/f'_c for every U-beam cannot exceed the *0.18* shear stress limit ratio.

5.5.2. The difference in the forces of cross-section STM

Two different cross-section STM models can be considered for the end block of the U-beam: one STM model uses a vertical tie, and another uses an inclined tie (refer to Figure 5-21).

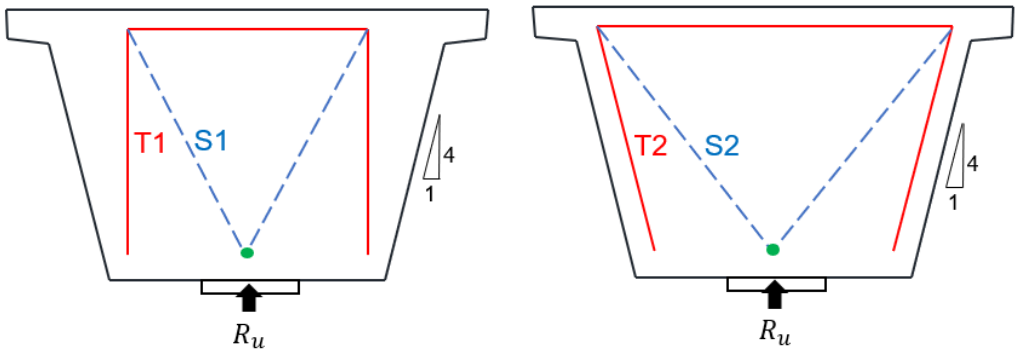

Figure 5-21. Different cross-section STMs for U-beam's end block

When considering the inclined tie, the tie force and strut force of the cross-section STM are affected by the angle of inclination of the web. The ratio of the inclination of the web of the U-beam is 1:4, and the tie force when the tie is inclined is always 3% greater than the tie force using the vertical tie, as shown in Equation 5-5.

$$T_2 = \left(\sqrt{17}/4\right) \times T_1 = 1.03T_1 \qquad \text{Equation 5-5}$$

The strut force of the STM using the inclined tie, S1, has a larger value than the strut force of the STM using the vertical tie, S2, and the difference between the two values increases as the total number of strands increases (refer to Figure 5-22).

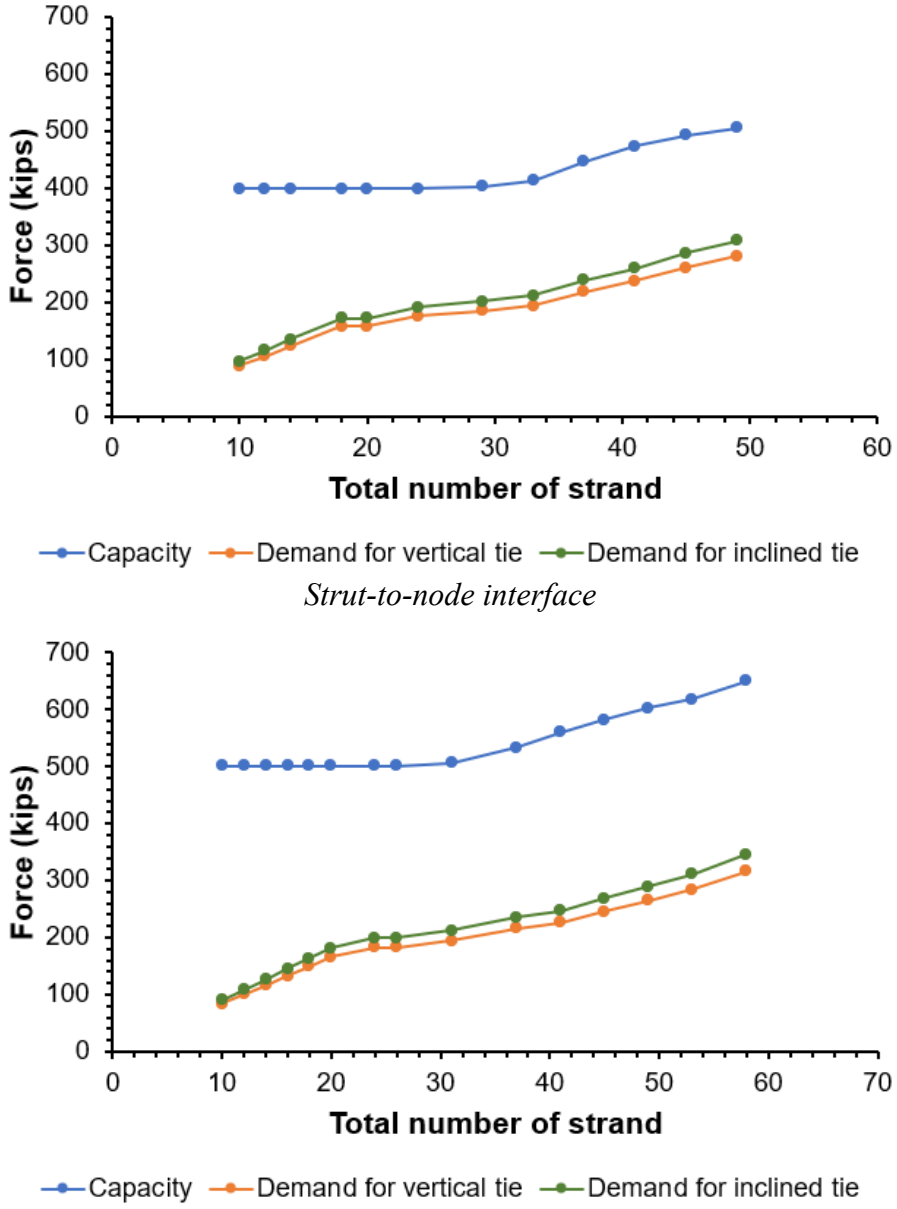

Figure 5-22. Applied force differences between the vertical tie and inclined tie for cross-section STMs

In a U-beam with the inclined tie, the applied strut force of the strut-to-node interface is up to 9% greater than the vertical tie is considered. In other words, the tie force increased 3%, and the strut force increased up to 9% when checking the nodal failure of the U-beam with one bearing plate using cross-section STM, which is considered the inclined tie. However, in both cases, the demand value is always smaller than the node capacity value. The difference in the value that occurs when the inclined tie is used also does not significantly affect the result. Therefore, in the U-beam, it is appropriate to check the nodal strength using the cross-section STM with the vertical tie when one bearing plate is used, which allows for a simpler calculation.

5.5.3. Summary for U-beam

The findings indicate that the maximum shear stress of the end regions of the U-beam can be calculated without anchorage zone distress when using the STMs. Further, the research team performed two additional design checks: nodal failure and horizontal shear failure. The results indicated that the shear stress of the end region of every U-beam conforming to TxDOT's standard design (5B20) could not exceed the $0.18\ f'_c$ shear stress limit. The graphs of v_u/f'_c from STM versus the total number of strands for U-beam are shown in Figure 5-23.

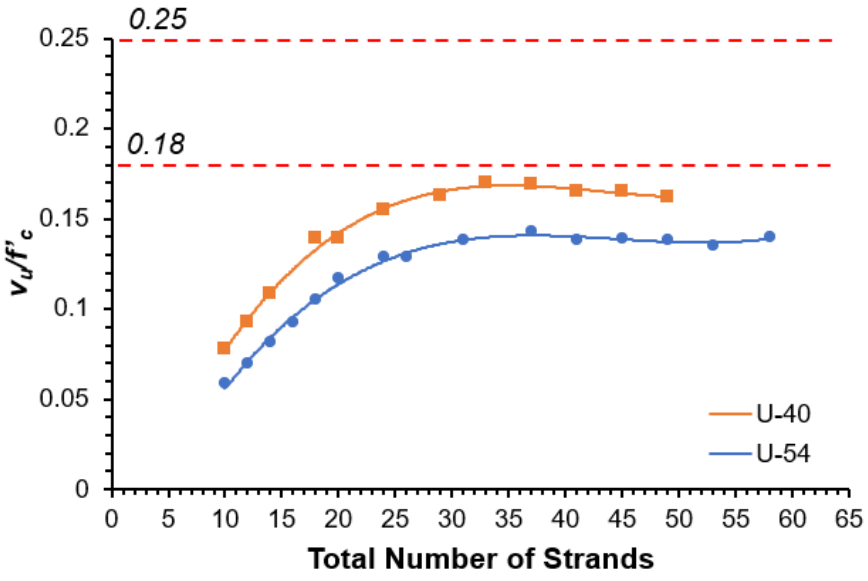

Figure 5-23. Different v_u/f'_c calculated by STM depending on the size of U-beams

The same as the other beams, the maximum v_u/f'_c of the U-beam displays a trend in which the value decreases as the beam's height increases. The analytical results of the investigation of U-beams following the TxDOT Standard design are shown in Table 5-8.

Table 5-8. Analytical results of different U-beams

	U-40	U-54
Maximum v_u/f'_c	0.170	0.143

The research team adds more strands than specified in the standard design for Tx-girders until the girder reaches the stress limit, and the team can check shear capacity. However, no more fully bonded strands can be added for the U-beams at the end because of the stress limit.

5.6. Decked-slab Beam

Calculating shear capacity and checking additional failure mode for the end of the decked-slab beam can be performed using the same methodology applied for the box beam because both beams have the same boundary condition and similar geometry. Also, the decked-slab beam's geometry is similar to the box beam, so three different failure modes (anchorage failure, nodal failure, and horizontal failure) can be checked in this project as same as box beams. There are no test results to compare the shear capacity of the decked-slab beam with a square and a skewed end. However, the maximum degree for the skewed end of the decked-slab beam is 30°, which is the same as the maximum degree of the box beam. Therefore, the research team assumed that the bearing plate at the obtuse angle could receive shear force up to 60% of the total shear force, the same as the box beam.

During construction, the width of the roadway determines the size of decked-slab beams to incorporate. For example, a bridge crew may use a decked-slab beam for type 6DS when the width of the roadway is 24 ft, type 7DS when it is 28 ft, and type 8DS when it is 30 ft. The number of fully bonded strands is an essential factor in calculating the shear stress of the box beam's end region when using STM and anchorage capacity. Straight strands are placed at 2-in. intervals from the bottom row (as illustrated in Figure 5-24). Twenty-eight strands can be set in both the first and second row for every type of decked-slab beam. The prestressing strand's diameter is 0.6-in.; the ultimate strength of prestressing steel, f_{pu}, is 270 ksi; and the web width is 12-in. for all decked-slab beams. The concrete strength, f'_c, used for each decked-slab beam is suggested in TxDOT's standard design (depending

on the number of strands). For the decked-slab beam, the longitudinal direction STM is used to check the nodal failure when there are two bearing plates, and the cross-section STM is used to check the nodal failure when there is one bearing plate as same as box beam. Also, horizontal shear failure needs to be checked because the web width is shorter than the width of the bottom flange. Even though the geometry and boundary condition for the decked-slab beam and box beam is similar, the shear stress capacity at the end is quite different.

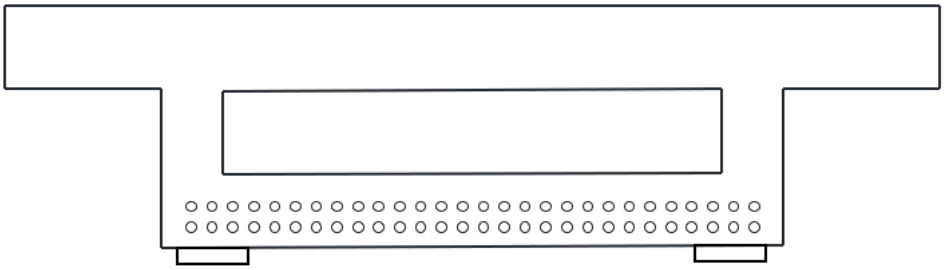

Figure 5-24. Stand pattern for decked-slab beam

5.6.1. Analysis for 7DS23

Geometry and reinforcement details for 7DS23 used to calculate shear stress are shown in Figure 5-25. The shear reinforcement is spaced at 4.5-in. intervals at the end of the beam, and the cross-section areas of the shear reinforcements are 0.2 in^2 (#4). The cross-section area for longitudinal reinforcement of the top flange is 0.44 in^2 (#6). All lengths of the figure below are in inches.

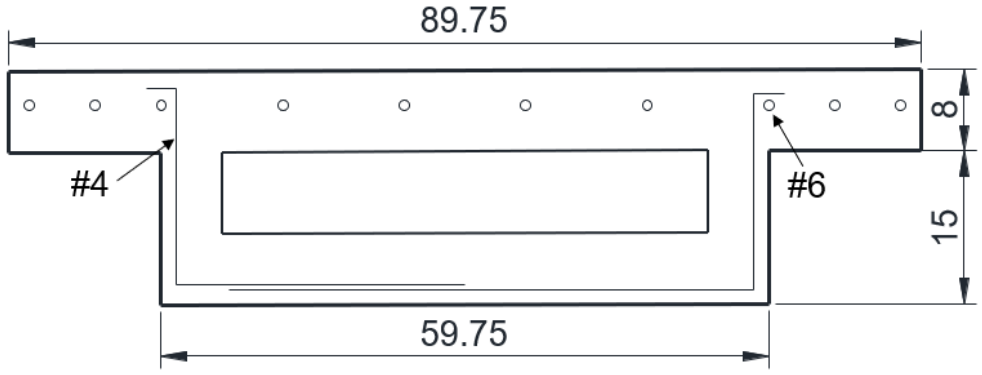

Figure 5-25. The cross-section geometry and reinforcement detail for 7DS23

The span length of 7DS23 ranges from 30 ft to 60 ft, and the number of strands increases as the span length increases. Debonded strands are used to control the release stresses, which increase as the number of strands increases. The total number of strands for 7DS23 proposed by TxDOT's standard design is at least ten

and at most 30, of which the number of the debonded strands is zero to six. The design concrete strength is 5.0 ksi for overall span length.

The calculated ratio of shear stress-to-concrete strength, v_u/f'_c, for 7DS23 using STM and anchorage capacity can be plotted versus the total number of strands (refer to Figure 5-26). The v_u/f'_c for 7DS23's end region, per TxDOT's standard design, is governed by the shear strength calculated through STM when the number of strands is fewer than 14. However, when more than 14 strands are used, v_u/f'_c is governed by the shear strength calculated using anchorage capacity. As the total number of strands increases, the shear force, V_u, calculated from STM or anchorage capacity increases, and thus v_u/f'_c increases. Figure 5-26 shows that the calculated v_u/f'_c for 7DS23 exceeds the 0.18 shear stress limit ratio when the total number of strands is 16 or more, and the maximum v_u/f'_c is 0.237.

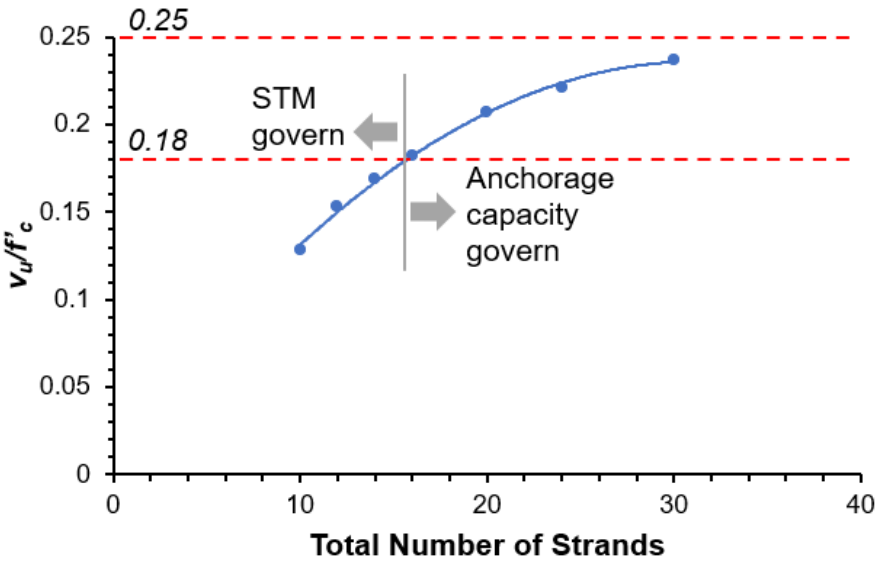

Figure 5-26. v_u/f'_c for 7DS23 by STM and anchorage capacity

Decked-slab beam has similar geometry and same boundary conditions to box beam. Therefore, the decked-slab beam should check the same additional failure mode as the box beam. This study confirmed that nodal failure does not occur even if 60% of the total shear force is applied to the nodes at the decked-slab beams' obtuse angle with a 30° skewed end. Figure 5-27 compares the demand for nodes and horizontal shear for the calculated shear force and the capacity of 7DS23. When the nodal failure and horizontal shear failure are checked, 7DS23 does not reach failure at every level of strand quantity. 7DS23 shows that the capacity for nodes and horizontal shear for all amounts strands is always greater than the demand. Therefore, the shear stress by STM or anchorage capacity governs the shear capacity for 7DS23.

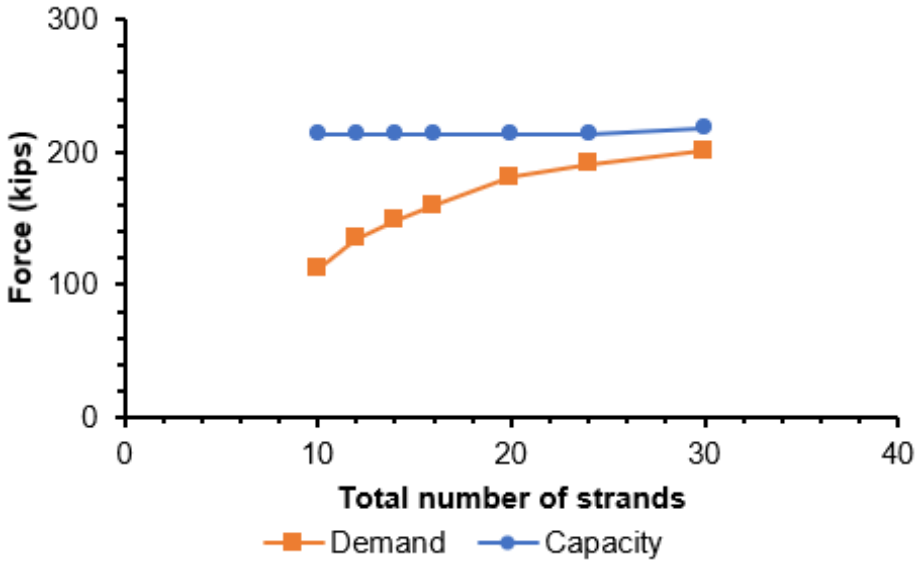

Strut-to-node interface (two plates, 30° skewed)

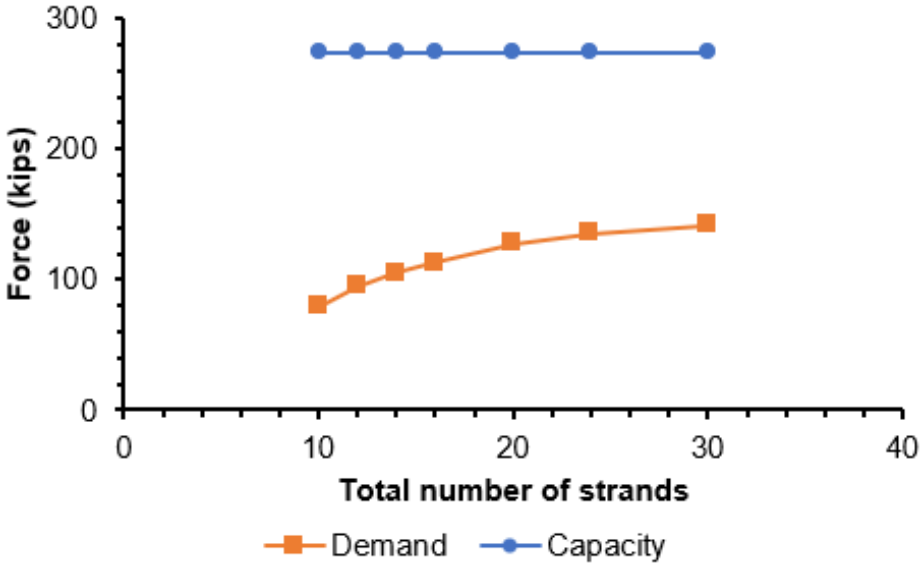

Bearing (two plates, 30° skewed)

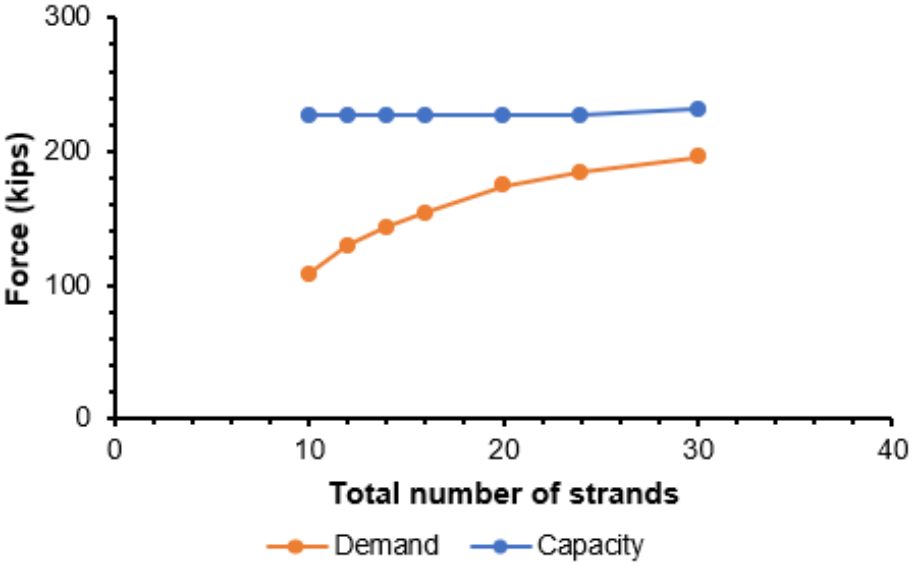

Strut-to-node interface (one plate)

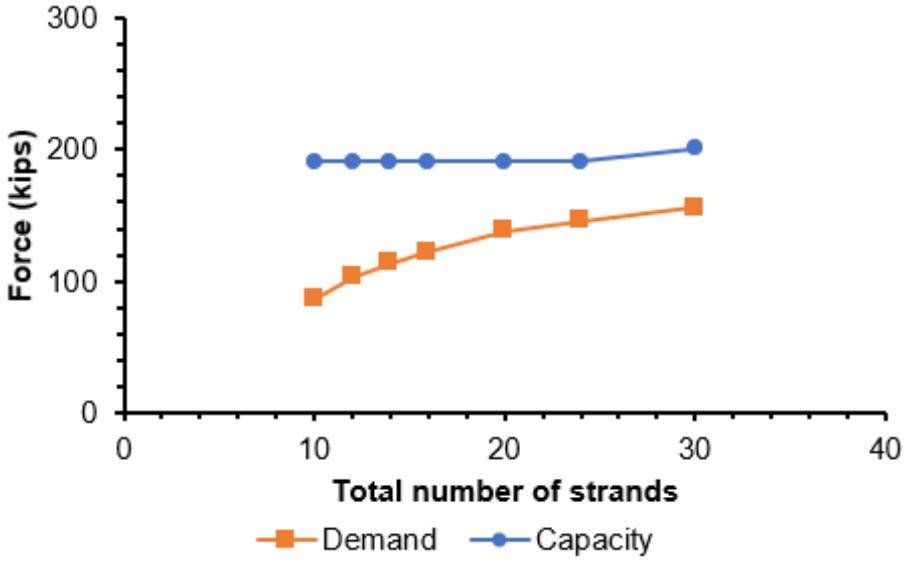

Backface (one plate)

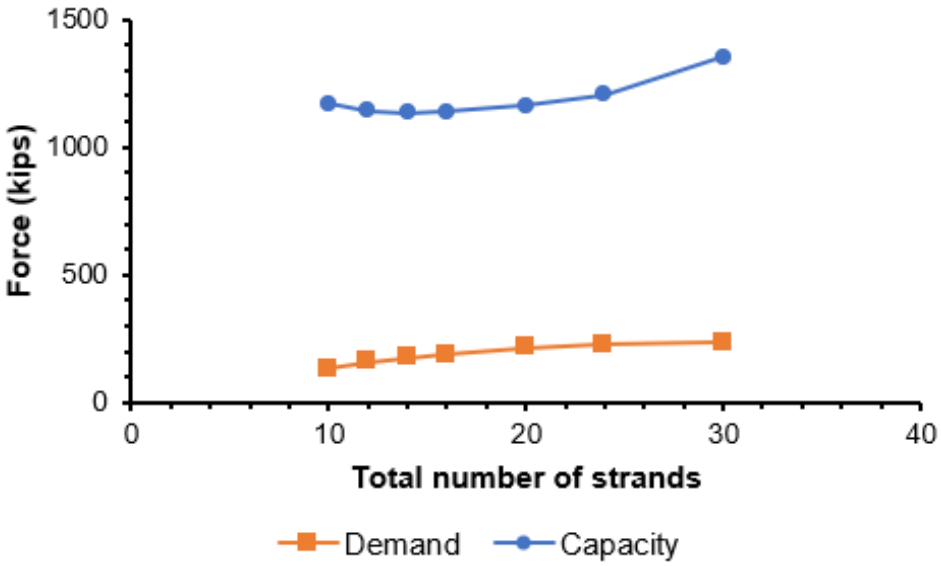

Horizontal shear

Figure 5-27. Difference between capacity and demand for 7DS23

Analysis results for other sizes of decked-slab beams are shown in Appendix C. According to the analytical results for decked-slab beams, nodal failure or horizontal shear failure will not occur for every size of the decked-slab beams when the maximum shear force that does not cause anchorage zone distress is applied to the end region of the beam. The anchorage capacity determines the maximum shear capacity of decked-slab beams of all sizes. Finally, the shear stress of every decked-slab beam can exceed the $0.18f'_c$ shear stress limit without resulting in the expected failures (nodal failure and horizontal shear failure). Therefore, the shear stress limit of the decked-slab beam can be relaxed up to the maximum v_u/f'_c of each size of the beam.

5.6.2. Decked-slab beam versus box beam

Decked-slab beams and box beams have similar shapes, so the expected failure mode to be considered is the same. Also, the maximum number of strands used for both beams is similar. However, the maximum v_u/f'_c shows different patterns according to beam type. Only one box beam's maximum v_u/f'_c was greater than the $0.18f'_c$ shear stress limit of the eight different sizes of box beams. However, in the decked-slab beam, the maximum v_u/f'_c is for every decked-slab beam always greater than the $0.18f'_c$ shear stress limit in all six different sizes. Therefore, the research team compared two beams with the most similar boundary conditions to determine why the decked-slab beam has a larger maximum v_u/f'_c than the box beam. 7DS23 is selected for the decked-slab beam, and 5B34 is selected for the box beam. Both beams have the same number of fully bonded strands, and the concrete

strength is also the same. Other geometries and rebar conditions are shown in Table 5-9.

Table 5-9. Compare the geometry and rebar condition between 7DS23 and 5B34

	7DS23	5B34
No. of fully bonded strands (ea)	24	24
Concrete strength, f'_c (ksi)	5.0	5.0
Web width, b_w (in.)	12	10
Area of stirrup, A_v (in^2)	0.4	0.4
Stirrup spacing (in.)	4.5	4
Effective depth, d_v (in.)	18.33	32.85
Shear force, V_u (kips)	236	255
$d_v \times b_w$ (in^2)	220	329
Shear stress capacity, v_u	1.192	0.863
v_u/f'_c	0.238	0.173

When using 24 fully bonded strands, 7DS23 and 5B34 can endure similar shear forces, V_u. However, the capacity of shear stress for 7DS23 is 43% larger than that of 5B34. This is because the effective depth of 5B34 is about twice the effective depth of 7DS23. The shear stress is calculated using Equation 5-6, and the shear stress is inversely proportional to the value of $d_v \times b_w$.

$$v_u = \frac{V_u}{0.9 \times d_v \times b_w} \qquad \text{Equation 5-6}$$

Therefore, as the effective depth increases, the shear stress capacity of the beam decreases, and the value of v_u/f'_c of 5B34 becomes smaller than that of 7DS23. As a result, even though the decked-slab beam has a similar shear strength compared to the box beam, the maximum v_u/f'_c is larger because the effective depth for the decked-slab beam is smaller than that of the box beam.

5.6.3. Summary for decked-slab beam

The findings indicate that the maximum shear stress of the end regions of the decked-slab beam can be calculated without anchorage zone distress when using the STM and anchorage capacity. Further, the research team performed two additional design checks for decked-slab beams: nodal and horizontal shear failures. The results indicated that the shear stress of the end region of all decked-slab beams conforming to TxDOT's standard design could exceed the $0.18f'_c$ shear stress limit. STM or anchorage capacity analysis indicates that the decked-slab

beam is still safe despite exceeding that limit, confirming that the $0.18\,f'_c$ shear stress limit is too strict, and the result in Table 5-10 can be used. Moreover, when decked-slab beams' calculated shear stress exceeds $0.18\,f'_c$, the anchorage capacity governs the calculated shear stress of the end of the beam. Just as in other types of beams, the maximum v_u/f'_c of the decked-slab beam displays a trend in which the value decreases as the beam's height increases. The graphs of v_u/f'_c from STM and anchorage capacity versus the total number of strands are shown in Figure 5-28 for decked-slab beams.

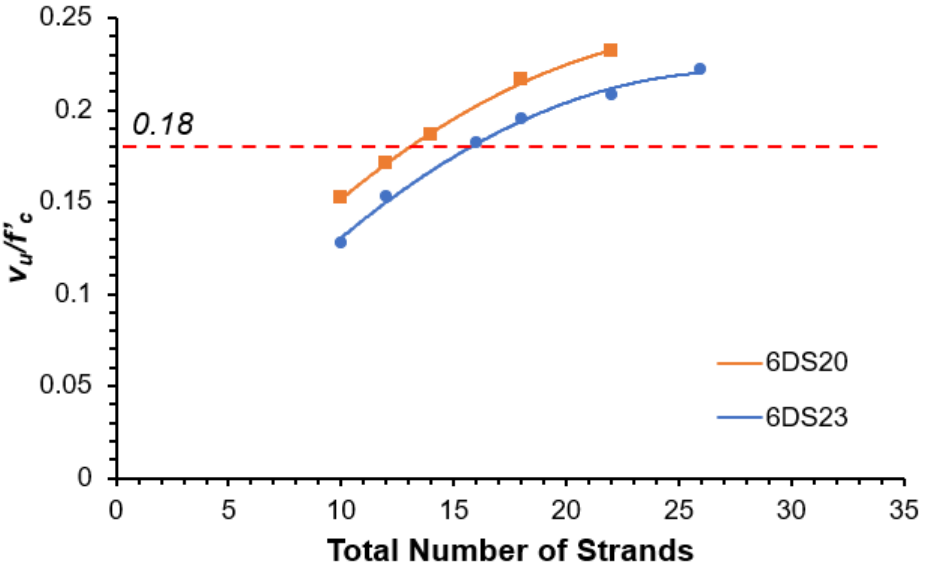

Type 6DS

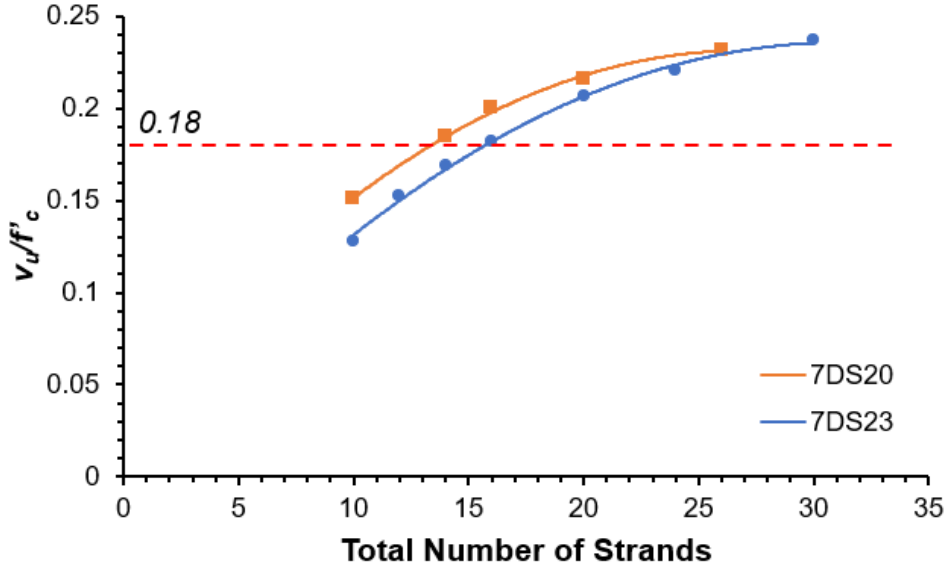

Type 7DS

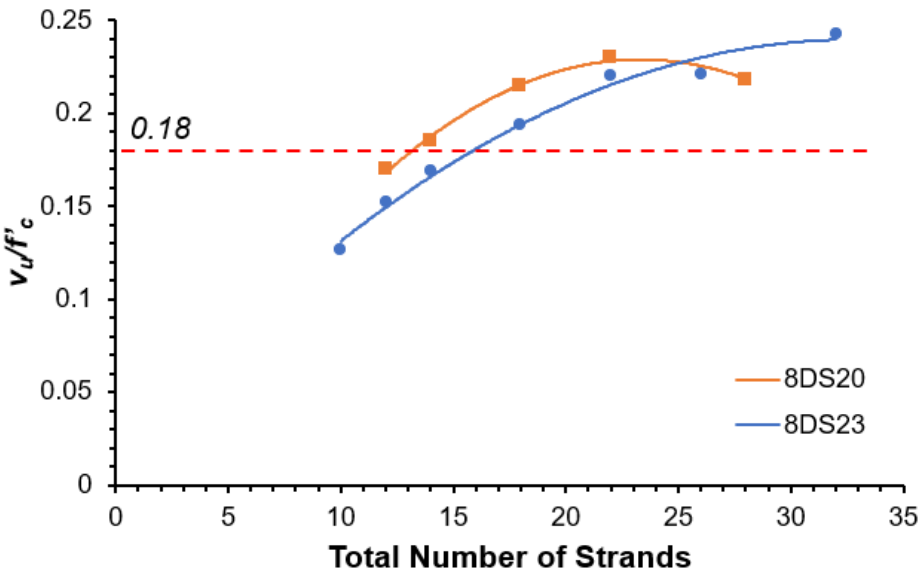

Type 8DS

Figure 5-28. Different v_u/f'_c calculated by STM and anchorage capacity depending on the size of decked-slab beams

Decked-slab beams and box beams have similar shapes, so the expected failure mode to be considered is the same. Therefore, it can be expected that the maximum v_u/f'_c of the two beams will have a similar trend. However, the maximum v_u/f'_c shows different patterns according to beam type. Even if the same number of strands are used, the maximum v_u/f'_c of the decked-slab beam is larger than that of the box beam. Also, the maximum v_u/f'_c of the decked-slab beam is greater than the 0.18 shear stress limit ratio in all sizes. The analytical results of the decked-slab beam following the TxDOT standard design are shown in Table 5-10.

Table 5-10. Analytical results of different decked-slab beams

	6DS20	6DS23	7DS20	7DS23	8DS20	8DS23
Maximum v_u/f'_c	0.232	0.222	0.232	0.237	0.230	0.243

The research team adds more strands than specified in the standard design for Tx-girders until the girder reaches the stress limit, and the team can check shear capacity. However, for the decked-slab beam, no more fully bonded strands can be added at the end because of the stress limit, such as the box beam, X-beam, and U-beam.

5.7. Slab Beam

Both decked-slab and slab beams have a lower height than other Texas beams, but the geometry is quite different. Calculating shear capacity for the end of the slab beam can be performed using the same methodology applied for the Tx-girder because there are no end blocks for both beams. Also, unlike other Texas prestressed beams, there is no distinction between bottom flange and web. Therefore, the slab beam does not have to consider horizontal shear failure

As same as the decked-slab beam, different sizes of slab beams are used according to the width of the roadway. When incorporating slab beams into a bridge, type 5SB is used when the roadway width is 24 ft, and type 4SB is used when the roadway width is 30 ft. The number of fully bonded strands is an essential factor in calculating the shear stress of the slab beam's end region when using STM and anchorage capacity. Straight strands are placed at 2-in. intervals from the bottom row (as illustrated in Figure 5-29). Twenty-two strands can be set in each row for type 4SB, and 28 strands can be set in each row for type 5SB. The prestressing strand's diameter is 0.6-in.; the ultimate strength of prestressing steel, f_{pu}, is 270 ksi. The web width is 47.75-in. for type 4SB and 59.75-in. for type 5SB. The concrete strength, f'_c, used for each slab beam is suggested in TxDOT's standard design (depending on the number of strands). Even though both decked-slab beam and slab beam have a lower height than other types of beams, the shear stress capacity at the end is quite different.

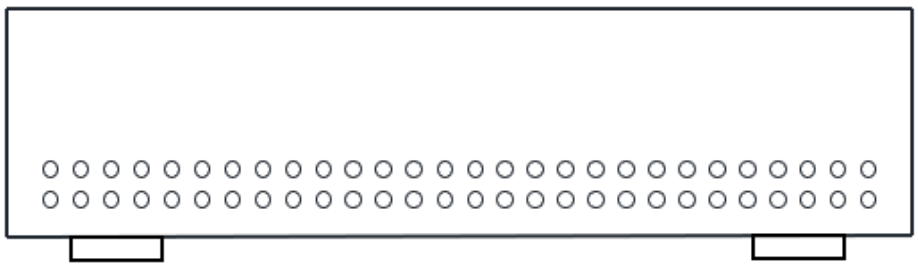

Figure 5-29. Stand pattern for slab beam

5.7.1. Analysis for 4SB12

The geometry and reinforcement details for 4SB12 and its deck used to calculate shear stress are shown in Figure 5-30. The shear reinforcement is spaced at 4-in. intervals at the end of the beam, and the cross-section areas of the shear reinforcements are 0.2 in^2 (#4). The cross-section area for each longitudinal reinforcement of the top flange is 0.44 in^2 (#6); that area for the deck is 0.2 in^2 (#4). All lengths of the figure below are in inches.

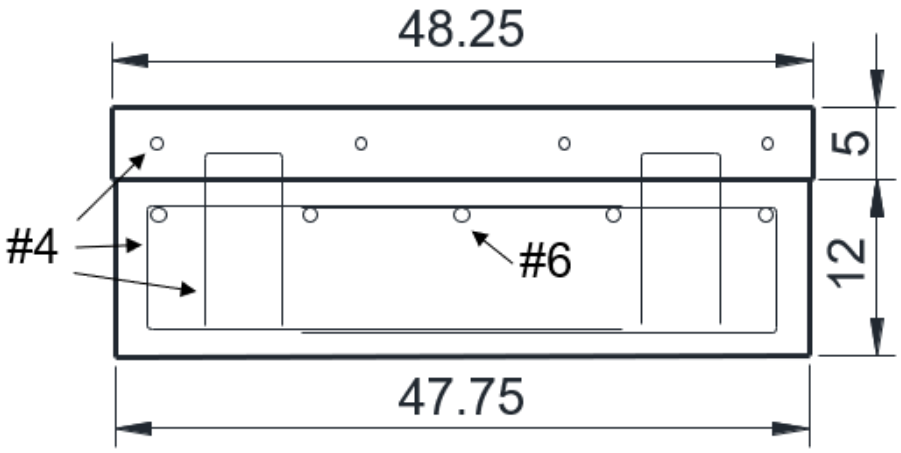

Figure 5-30. The cross-section geometry and reinforcement detail for 4SB12 and 5-in. deck

The span length of 4SB12 ranges from 25 ft to 40 ft, and the number of strands increases as the span length increases. Debonded strands are used to control the release stresses, which increase as the number of strands increases. The total number of strands for 4SB12 proposed by TxDOT's standard design is at least six and at most 14, of which the number of the debonded strands is zero for all span lengths. The design concrete strength is 5.0 ksi for overall span length.

The calculated ratio of shear stress-to-concrete strength, v_u/f'_c, for 4SB12 using STM and anchorage capacity can be plotted versus the total number of strands (refer to Figure 5-31). The v_u/f'_c for 4SB12's end region, per TxDOT's standard design, is governed by the shear strength calculated through STM when the number of strands is fewer than ten. However, when more than ten strands are used, v_u/f'_c is governed by the shear strength calculated using anchorage capacity. As the total number of strands increases, the shear force, V_u, calculated from STM or anchorage capacity increases, and thus v_u/f'_c increases. Figure 5-31 shows that the calculated v_u/f'_c for 4SB12 using STM and anchorage capacity cannot exceed the 0.18 shear stress limit ratio, and the maximum v_u/f'_c is 0.058.

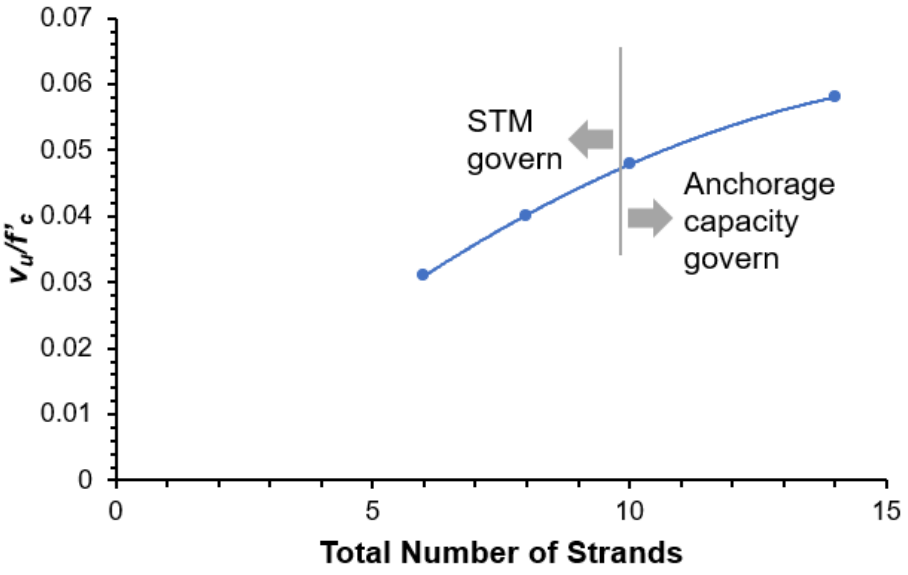

Figure 5-31. v_u/f'_c for 4SB12 by STM and anchorage capacity

There is no end block for the slab beam, so the longitudinal direction STM is only used to check the nodal failure, same as Tx-girder. However, there is no separation between the bottom flange and web for the slab beam, so horizontal shear failure is not needed to be checked for the slab beam. Only the nodal failure at longitudinal STM is needed to be checked for slab beam. Figure 5-32 compares the demand for nodes and horizontal shear for the calculated shear force and the capacity of 4SB12. When the nodal failure is checked, 4SB12 does not reach failure at every level of strand quantity. 4SB12 shows that the capacity for nodes in all strands is always greater than the demand. Therefore, the shear stress by STM or anchorage capacity governs the shear capacity for 4SB12 instead of nodal capacity.

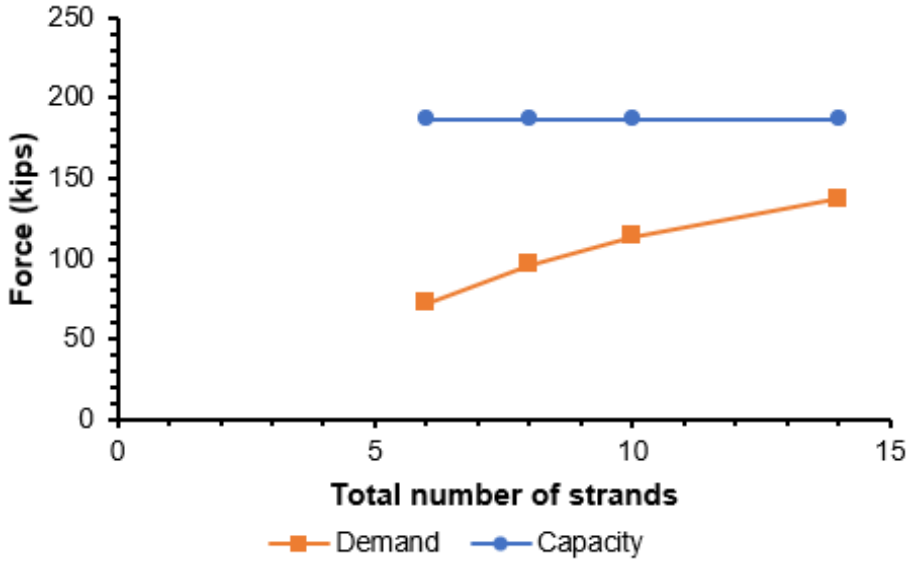

Strut-to-node interface

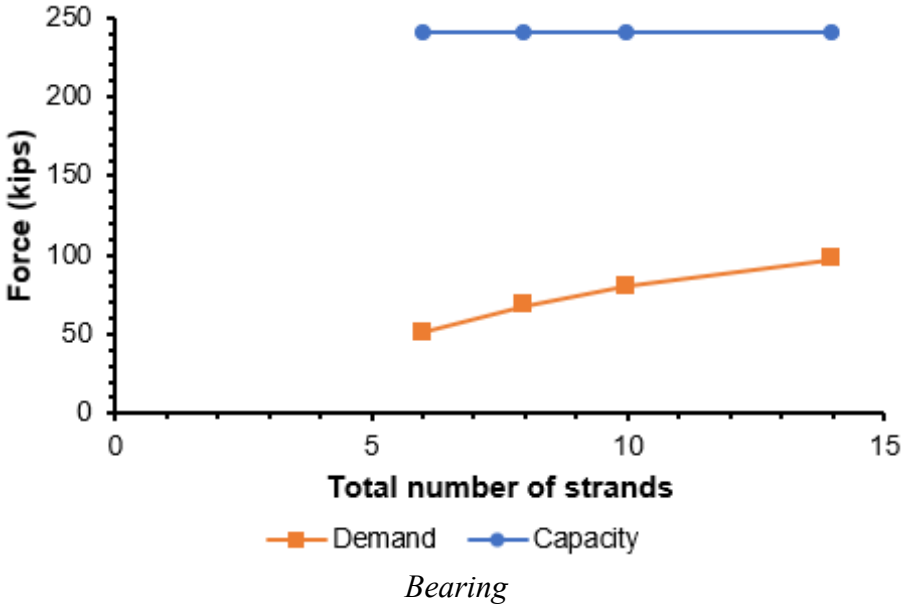

Figure 5-32. Difference between node capacity and demand for 4SB12

Analysis results for other sizes of slab beams are shown in Appendix C. According to the analytical results for slab beams, nodal failure will not occur for every size of the slab beams when the maximum shear force that does not cause anchorage zone distress is applied to the end region of the beam. Therefore, the maximum shear capacity of slab beams of all sizes is determined by the anchorage capacity. However, the shear stress of every slab beam cannot be greater than the $0.18\,f'_c$ shear stress limit because of the wide web width.

5.7.2. Slab beam versus decked-slab beam

Decked-slab beams and slab beams share the characteristic of having a greater width than height, but otherwise, the geometry of the two beams is quite different (refer to Figure 5-24 and Figure 5-29). Thus, the maximum v_u/f'_c is quite different even if the two beams have similar shear capacities. Table 5-11 compares the geometry and rebar conditions of slab beams (5SB12) and decked-slab beams (6DS20) with the same number of fully bonded strands. When 18 strands are used, the two beams have similar shear strengths because the anchor capacity of the strand governs the shear strengths of the two beams. However, since the web width, b_w, of the 5SB12 is about five times greater than that of 6DS20, the v_u/f'_c of 5SB12 calculated using the analytical method becomes much smaller. As a result, the maximum v_u/f'_c of the slab beam, calculated using the analytical method, has a smaller value than the decked-slab beam due to the greater width of the slab beam.

Table 5-11. Compare the geometry and rebar condition between 5SB12 and 6DS20

	5SB12	6DS20
No. of fully bonded strands (ea)	18	18
Concrete strength, f'_c (ksi)	5.0	5.0
Web width, b_w (in.)	59.75	12
Area of stirrup, A_v (in^2)	0.4	0.4
Stirrup spacing (in.)	4	4.5
Effective depth, d_v (in.)	13.05	16.01
Shear force, V_u (kips)	255	237
$d_v \times b_w$ (in^2)	780	192
Shear stress capacity, v_u	0.27	1.08
v_u/f'_c	0.054	0.216

5.7.3. Summary for slab beam

The findings indicate that the maximum shear stress of the end regions of the slab beam can be calculated without anchorage zone distress when using the STM and anchorage capacity. Further, one additional design check—for nodal failure—was performed for the slab beam. The results indicated that the $0.18f'_c$ shear stress limit in all slab beams could not be relaxed. Just as in the other type of beams, the maximum v_u/f'_c of the slab beam displays a trend in which the value decreases as the beam's height increases. The graphs of v_u/f'_c from STM and anchorage capacity versus the total number of strands for slab beams are shown in Figure 5-33.

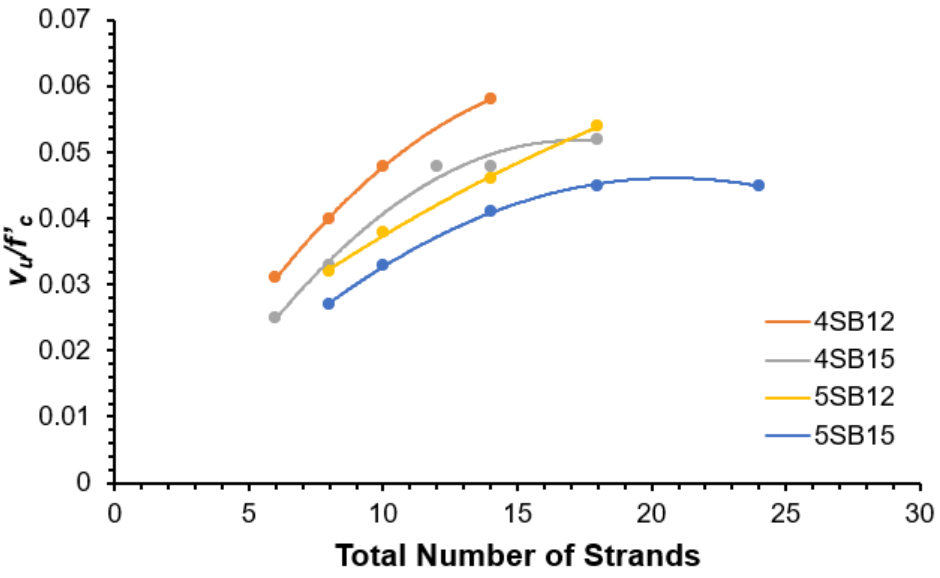

Figure 5-33. Different v_u/f'_c calculated by STM and anchorage capacity depending on the size of slab beams

Both the decked-slab beam and the slab beam have a considerably smaller beam height than other girders. Therefore, it can be expected that the maximum v_u/f'_c of the two beams will have a similar trend. Still, the maximum values of the two beams show very different patterns. The maximum v_u/f'_c of the decked-slab beam is greater than the *0.18* shear stress limit ratio in all sizes, but the maximum value of the slab beam is always less than the *0.18* ratio. The analytical results of the slab beam following the TxDOT standard design are shown in Table 5-12.

Table 5-12. Analytical results of different slab beams

	4SB12	4SB15	5SB12	5SB15
Maximum v_u/f'_c	0.058	0.052	0.054	0.045

The research team adds more strands than specified in the standard design for Tx-girders until the girder reaches the stress limit, and the team can check shear capacity. However, for the slab beam, no more fully bonded strands can be added at the end because of the stress limit, such as the box beam, X-beam, U-beam, and decked-slab beam.

5.8. Chapter Summary

Using the STM and anchorage capacity equation, the shear strength of Texas standard prestressed beam without anchorage zone distress is calculated. When the

calculated shear force is applied to the end region of the beam, the beams' demand and the capacity of the expected failure modes for the beam are compared. Since geometry is different for each type of beam and geometry affects stress flow, the expected failure mode varies from each type of beam. For all Texas standard prestressed beams, node capacity and demand according to longitudinal STM are compared. Tx-girder uses one bearing plate for both ends, but all other types of beams can use two bearing plates. For beams using two bearing plates at the end, the case where the end of the beam is skewed should be considered. The reason is that when the beam ends are skewed, the node at the obtuse angle receives greater shear force than the node at the acute angle, which is the most extreme case. Therefore, beams other than Tx-girder should consider the maximum skewed angle when comparing node capacity and demand of longitudinal STM. Also, all types of beams except for the slab beam perform horizontal shear check because there is a distinction between the web and the bottom flange. Additionally, box beam, X-beam, and U-beam also compare node capacity and demand for cross-section STM. The reason is that these beams contain end blocks, and when one bearing plate is used at the end, the stress flow in the end block is different from when two bearing plates are used at the end. Finally, Tx-girders are examined to ensure that sufficient amounts of confinement reinforcements are used to prevent lateral splitting failure that may occur due to using harped strands.

When the shear stress capacity of beams is calculated using the analytical method, the trend of v_u/f'_c varies for each girder type. In addition, the v_u/f'_c is different for each size of the girder, even for the same type of girder. The analytical results indicated that the shear stress of the end region of every size of Tx-girder and decked-slab beam conforming to TxDOT's standard design could exceed the $0.18\ f'_c$ shear stress limit without expected failure. Therefore, the $0.18\ f'_c$ shear stress limit is too strict for the end region of the Tx-girder and decked-slab beam, and the limit can be relaxed. The end region of the Tx-girder can relax a shear stress limit from 0.20 to 0.23 depending on the size of the girder. Also, the end region of the decked-slab beam can relax a shear stress limit from 0.22 to 0.24 depending on the size of the girder. Box beams and X-beams contain some of the beams with a calculated maximum v_u/f'_c greater than 0.18 shear stress limit ratio, but also with a calculated maximum v_u/f'_c smaller than 0.18 shear stress limit ratio. Among every size of box beam and X-beam, only beams that the maximum v_u/f'_c calculated using the analytical method is greater than 0.18 shear stress limit and expected failure modes are not occurring can relax the shear stress limit of the end region. The end region of the box beam and X-beam can relax a shear stress limit from 0.19 to 0.20 depending on the size of the girder. The calculated maximum v_u/f'_c of all size beams for U-beam and slab beams is less than 0.18 shear stress limit ratio.

Consequently, the shear stress limit cannot be relaxed in the end region of these two beams.

Expected failure will not occur for almost all the Texas standard prestressed beams when the maximum shear force calculated by STM and anchorage capacity is applied to the beam's end. However, nodal failure will occur for the four box-beams (4B28, 5B20, 5B28, and 5B34) and the one X-beam (5XB28), so the nodal capacity will occur governs the beam's shear capacity, and maximum v_u/f'_c becomes smaller than the value calculated by STM and anchorage capacity. Also, the extension of v_u/f'_c in Tx-girders is investigated by placing more strands in the girder than the maximum suggested by TxDOT's standard design. The number of strands is increased until the concrete stress at release reaches the concrete stress limit. As a result, even if the number of strands increases, v_u/f'_c converges to a constant value. Since the converged v_u/f'_c of Tx-girder is similar to the maximum of v_u/f'_c calculated using TxDOT standard design, the calculated maximum v_u/f'_c using TxDOT standard design can be determined as the shear stress limit of the girder. However, no more fully bonded strands can be added at the end for other types of beams because of the stress limit. Debonded strands can be added for other types of beams, but debonded strands cannot affect shear strength at the end of the beam.

In this research, the effect of the difference in total prestresses loss on the calculated shear stress is checked. Even if the total prestresses loss changes to 15%, 20%, or 25%, the calculated shear stress ratio, v_u/f'_c, using the analytical method shows the difference of less than 5%. As a result, it is appropriate to use the STM calculation assuming that the total prestress loss is 20%. Finally, the shear strength and shear stress of beams with similar boundary conditions are compared. As a result, even with similar shear strength, the shear stress capacity can vary significantly depending on the geometry of the beam.

Chapter 6. Comparison of 0-7015 Analysis and Experimental Studies

6.1. Introduction

In this chapter, the shear stresses of Texas standard prestressed beams calculated by the analytical method described in Chapter 3 and Chapter 4 are compared with the shear stresses of Texas standard prestressed beam measured through previous experimental work conducted in literature. Experimental studies on Texas standard prestressed beams have been conducted in the past. The experimental studies for Tx-girder, box beam, X-beam, and U-beam are conducted at The University of Texas at Austin in several years, and study for slab beam is conducted at University of Houston. However, there is no previous experimental study for deck-slab beams. Therefore, in this project, the analytical and experimental shear capacities are compared for many different types of beams except the decked-slab beam. By comparing the shear capacities, it is possible to determine whether the analytical method suggests the conservative calculation result for the shear strength of each type of girder.

The shear span-to-depth ratios of most test specimens are larger than 2.0 to prevent deep beam behavior in the tests. When the shear span-to-depth ratios are larger than 2.0, the shear stress of the end region of the beam cannot be calculated using the Strut-and-Tie Model (STM) using a single-panel. Therefore, the shear strength of most of the test specimens should be calculated using STMs using two-panels. Before comparing the shear stresses of specimens calculated by the analytical method and measured through previous experimental work, it will explain how to calculate the shear strength using STM using two panels.

Since each specimen has a different strand or reinforcement layout and other boundary conditions, the properties of the specimens are described in each subsection. Also, the expected failure modes when using the analytical method and the actual failure modes are compared to check whether the governing failure mode predicted when using the analytical method presented in this study is appropriate.

6.2. STM using Two Panels

When the shear span-effective depth ratio of experiments is 2.0 or more, the angle between strut and tie is smaller than 25 degrees when using only one panel for STM. Therefore, shear stress is calculated using STM containing two panels (refer to Figure 6-1).

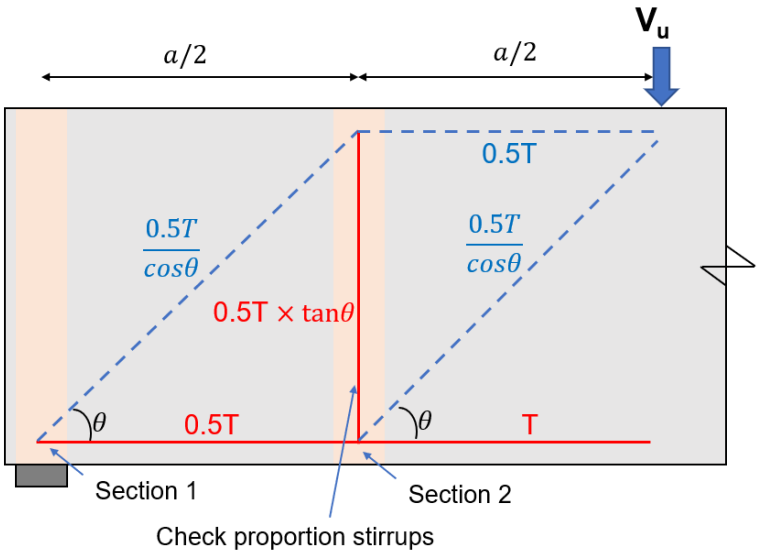

Figure 6-1. STM model with two panels

When using two panels, basic theory and calculation are as same as using one panel (as shown in Chapter 3), but two more elements must be considered. First, anchorage capacity should be regarded as both section 1 and section 2 in Figure 6-1. When there is only one panel for STM, only the anchorage capacity around the support needs to be considered. When there are two panels, the anchorage capacity should be considered not only around the support but also in the vertical tie section (section 2 in Figure 6-1). The anchorage capacity in section 2 in Figure 6-1 should consider factored moment at section, M_u, which satisfies Equation 6-1.

$$A_s f_y + A_{ps} f_{px} \geq \frac{M_u}{d_v \phi_f} + \left(\frac{V_{u,a}}{\phi_v} - 0.5V_s - V_p \right) \cot\theta' \qquad \text{Equation 6-1}$$

The shear force at the end of the beam calculated by anchorage capacity, $V_{u,a}$, for section 2 should be calculated by Equation 6-2, and in the case of the beam without harped strands, the component of prestressing force by harped strand in the direction of the shear force, V_p, is zero. Also, the area of the reinforcement on the flexural tension side is considered only for the area of non-prestressed tension reinforcement, A_s, and the area of prestressing steel, A_{ps} (refer to Figure 3-8).

$$V_{u,a} = \phi_v \left(\left(A_s f_y + A_{ps} f_{px} - \frac{M_u}{d_v \phi_f} \right) \times \frac{1}{\cot\theta'} + 0.5V_s + V_p \right) \qquad \text{Equation 6-2}$$

Where :

$\emptyset_f$ = resistance factor for a moment, 0.9

Therefore, when there are two panels, the shear stress of the beam should be calculated using the minimum value among the shear force at the end of the beam calculated by anchorage capacity, $V_{u,a}$, using Equation 6-2 and the shear force at the end of the beam calculated by STM, $V_{u,s}$. In addition to the anchorage capacity in section 2, the researcher has to consider the vertical tie force of the STM when using two panels. If one panel is used for STM, only the anchorage node (CCT node) of the bottom flange is considered, but when there are two panels, the node where the vertical tie and longitudinal tie meet (CTT node) should also be counted. CTT node can be classified as a smeared node, and it does not have a geometry that can be clearly defined by a bearing plate. Therefore, the calculations must ensure that the stirrup reinforcements can carry the force in a vertical tie extending from a smeared CTT node (Williams et al. 2012). The available length, l_a, over which the stirrups are considered to carry the force in the tie can be spread is indicated in Figure 6-2, as recommended by Wight and Parra-Montesinos (2003). The cross-section area of the entire stirrup placed in the available length multiplied by the yield stress of the stirrup should be greater than the vertical tie force of the STM.

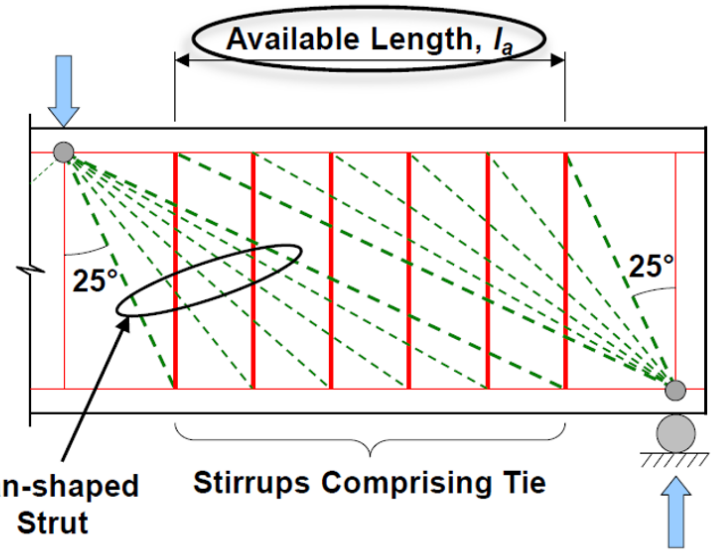

Figure 6-2. Determination of available length of the vertical tie (Wight and Parra-montesinos 2003)

Shear stress is calculated using STM using two panels in consideration of the factors mentioned above. The analytical results for each type of the Texas standard prestressed beam are computed using the analytical method proposed in this research, and the experimental results are compared in the following subsections.

6.3. Tx-girder Comparison

The shear stresses of Tx-girders calculated by the analytical method are compared with the shear stresses of Tx-girders measured through previous experimental work conducted at UT Austin. This chapter compares the expected failure modes when using the analytical method and the actual failure modes. A total of nine experiment results are used, of which five girders tested contain harped strands, and four do not. Avendaño and Bayrak (2008) tested four times for Tx-girder, which were not contain harped strands; Garber et al. (2016) tested five different Tx-girders that contained harped strands. Since the shear span-effective depth ratio of all experiments is three or more, shear stress is calculated using STM using two panels.

6.3.1. Tx-28 without the harped strand

For the Avendaño and Bayrak (2008) research report, two Tx-28 (Tx-28-1 and Tx-28-2) girders with different lengths for shear span, concrete strengths for girder and deck, and types of shear reinforcement were tested; the span length for both was 28 ft. The shear reinforcement for the live-end (right-end) and dead-end (left-end) of each specimen were spaced differently, and each beam was tested twice, one test at each end. Every specimen used low relaxation prestressing steel, and the ultimate strength of prestressing steel, f_{pu}, was 285 ksi. The tested specimens did not contain the harped strands, had 36 straight strands on the bottom flange, and used four straight strands on the top flange (refer to Figure 6-3). The properties for test specimens are shown in Table 6-1, and the geometry or overhang length of the girder (other than shown in Table 6-1) is the same as the TxDOT's standard design.

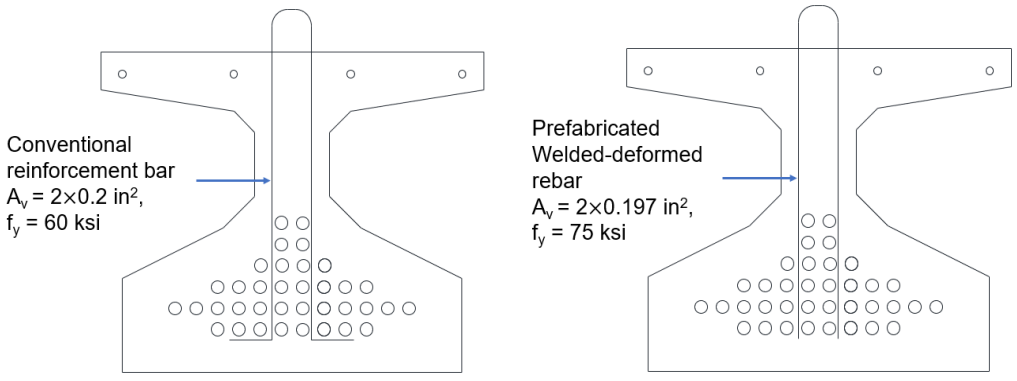

Tx-28-1-L & Tx-28-1-D *Tx-28-2-L & Tx-28-2-D*

Figure 6-3. Reinforcement detail and strand layout for the specimens (Tx-28)

Table 6-1. Test specimen properties (Tx-28)

		Tx-28-1-L	Tx-28-1-D	Tx-28-2-L	Tx-28-2-D
Shear reinforcement	Area (in^2)	0.4	0.4	0.394	0.394
	f_y (ksi)	60	60	75	75
	Spacing (in.)	4@3”, 8@4”	12@4”	4@3”, 8@4”	12@4”
Prestressing steel	Effective stress (bottom) (ksi)	188.53	188.53	195.73	195.73
	Effective stress (top) (ksi)	21.33	21.33	20.82	20.82
Concrete	Girder f'_c (psi)	13825	13825	11375	11375
	Deck f'_c (psi)	5050	5050	6550	6550
Loading	a (ft)	7	7	9	9

Figure 6-4 illustrates the spacing and size of reinforcement for the composite deck, which used conventional Grade 60 reinforcing bars for longitudinal reinforcement.

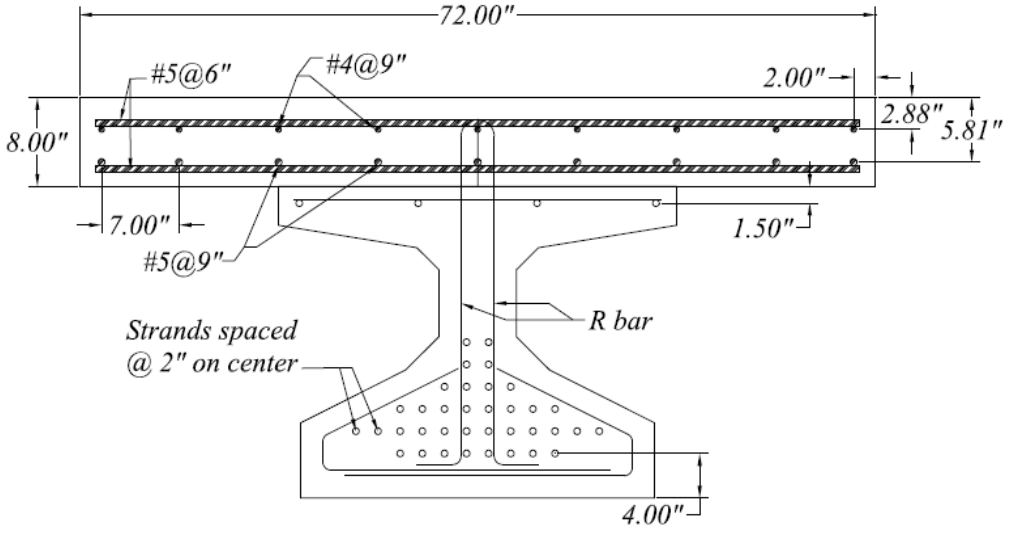

Figure 6-4. Composite deck detail (Avendaño and Bayrak 2008)

The shear stress of Avendaño’s specimen is calculated by STM and anchorage capacity using the parameters presented above, and nodal strength, stirrup, horizontal shear, and confinement are checked additionally. The results of the

calculated shear strengths for each test specimen and the shear strengths obtained by the experiment are compared in Table 6-2.

Table 6-2. Compare the shear strength between analytical and experimental (Tx-28)

Specimens	Experimental Results		Analytical Predictions		
	V_{test}	$v_u/f_c^{'}$	$V_{n,AASHTO}$	$V_{n,ACI}$	V_{calc}
Tx-28-1-L	400	0.18	265	231	241
Tx-28-1-D	417	0.19	265	231	264
Tx-28-2-L	371	0.20	265	222	259
Tx-28-2-D	375	0.20	265	222	257

In Table 6-2, V_{calc} is the maximum shear strength calculated with the analytical method developed in this research project. V_{test} is the actual capacity of shear for the beam as a result of the experiment. $V_{n,AASHTO}$ and $V_{n,ACI}$ are shear strengths calculated by the sectional shear stress calculation method proposed by AASHTO LRFD (2020) and ACI 318-19 (2019), respectively. As shown in Table 6-2, the shear strengths of Avendaño's specimens calculated by the analytical method used in this study are conservative compared to the experimental result and similar to the shear strength according to AASHTO LRFD (2020) and ACI 318-19 (2019).

Table 6-3. Compare the failure mode between analytical and experimental (Tx-28)

Specimens	Analytical failure mode	Experimental failure mode
Tx-28-1-L	Traditional shear failure	Horizontal shear, web crushing
Tx-28-1-D	Traditional shear failure	Horizontal shear, anchorage zone distress, web crushing
Tx-28-2-L	Horizontal shear	Horizontal shear
Tx-28-2-D	Horizontal shear	Horizontal shear

According to the analytical method, all four specimens from Tx-28-1-L to Tx-28-2-D are governed by horizontal shear. Table 6-3 shows the expected failure mode due to the analytical method of each specimen and the failure mode observed through the actual experiment. Table 6-3 indicates that horizontal shear cracks were found in all four specimens throughout the experiment. Therefore, the expected failure mode due to the analytical method and the failure mode observed through actual experiments are similar in all four specimens.

6.3.2. Tx-46 with the harped strand

From the Garber et al. (2016) paper, five Tx-46 girders (Q-8, Q-10, Q-20A, Q-20B, Q-46) with different lengths for overhang and without deck were tested; the span length for every specimen was 45 ft. For all five specimens, 52 straight strands (at bottom flange) and six harped strands were used (refer to Figure 6-5). In addition, the strand layout, the shear reinforcement type, and spacing were the same for all beams. The prestressing strands for every specimen used were Grade 270, low relaxation, and 0.5-in. diameter, and the effective stress for all strands was 172 ksi. In the shear reinforcement, the R bar and S bar are spaced at 3-in. intervals for 3 ft from the end of the beam; after that 3-ft span, the R bar continues at 6-in. intervals. The yield strength of the reinforcing bars is found to be 63 ksi for the R bars and 61 ksi for the S bars. The properties for test specimens are shown in Table 6-4, and the geometry of the girder and properties for reinforcement (other than shown in Table 6-4) are the same as the TxDOT's standard design.

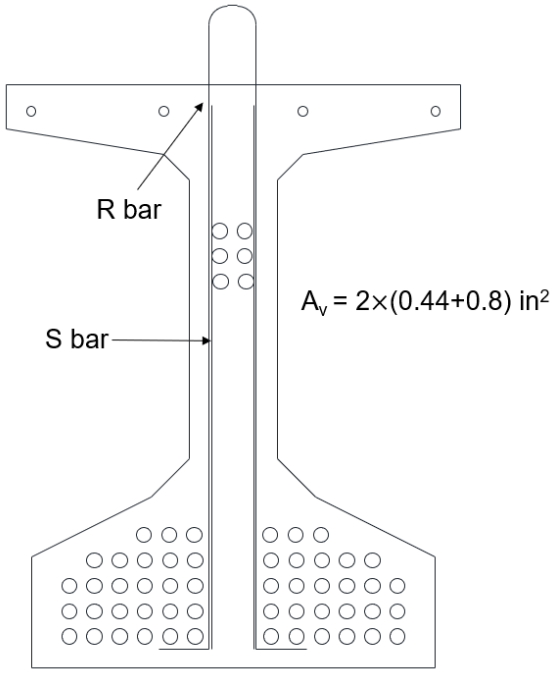

Figure 6-5. Reinforcement detail and strand layout for the specimens (Tx-46)

Table 6-4. Test specimen properties (Tx-46)

Specimens	Concrete strength, ksi	Overhang length, in.
Q-8	11.8	8
Q-10	11.8	10
Q-20A	11.8	20
Q-20B	11.8	20
Q-46	11.8	46

The shear stress of Garber's specimen is calculated by STM and anchorage capacity using the parameters presented above, and nodal strength, stirrup, horizontal shear, and confinement are checked additionally. The results of the calculated shear strengths for each test specimen and the shear strengths obtained by the experiment are compared in Table 6-5.

Table 6-5. Compare the shear strength between analytical and experimental (Tx-46)

Specimens	Experimental Results		Analytical Predictions		
	V_{test}	$v_u/f_c^{'}$	$V_{n,AASHTO}$	$V_{n,ACI}$	V_{calc}
Q-8	543	0.21	419	400	406
Q-10	570	0.22	419	400	406
Q-20A	566	0.21	419	400	337
Q-20B	555	0.21	419	400	337
Q-46	549	0.21	419	400	336

As shown in Table 6-5, the shear forces of Garber's specimens calculated by the analytical method used in this study are conservative compared to the experimental result and similar to the shear strength according to AASHTO LRFD (2020) and ACI 318-19 (2019), respectively.

Table 6-6. Compare the failure mode between analytical and experimental (Tx-46)

Specimens	Analytical failure mode	Experimental failure mode
Q-8	Anchorage zone distress	Anchorage zone distress
Q-10	Anchorage zone distress	Horizontal shear
Q-20A	Traditional shear failure	Flexural shear
Q-20B	Traditional shear failure	Web crushing
Q-46	Traditional shear failure	Flexural shear

According to the analytical method, all five specimens from Q-8 to Q-46 are governed by anchorage zone distress. Table 6-6 shows the expected failure mode due to the analytical method of each specimen and the failure mode observed through the actual experiment. As shown in Table 6-6, traditional shear failure (flexural shear, web crushing) governs the specimens with relatively long overhang

lengths (Q-20A, Q-20B, and Q-46). However, non-traditional shear failure (anchorage zone distress, horizontal shear) governs the specimens with relatively short overhang lengths (Q-8 and Q-10). Q-8, with the shortest overhang length, is governed by the anchorage zone distress, which is the same failure mode predicted through the analytical method. For Q-10, which has the second shortest overhang, the anchorage zone distress is expected to govern according to the analytical method. Still, in the test result, the horizontal shear failure governs the specimen. However, the horizontal shear capacity of Q-10 (461 kips) calculated through the analytical method is almost the same as the calculated shear strength using the analytical method, V_{calc}, and it is smaller than the experimental shear capacity, V_{test} of Q-10. Therefore, the analytical method almost predicts the risk of horizontal shear failure for Q-10.

The comparison of the experimental results of the Avendaño and Garber, and the results of the analytical method used in this study, indicate that the shear strength calculated by the analytical method is always conservative and similar to the result of AASHTO or ACI's shear calculation method. Moreover, the prediction of the non-traditional shear failure mode is entirely accurate. Therefore, the shear stress of the end region of the Tx-girder can be calculated using the analytical method described in Chapter 3 and Chapter 4, and the shear stress limit can be relaxed when the shear stress calculated exceeds the $0.18f'_c$ shear stress limit.

However, the shear span-to-depth ratios of Avendaño and Garber's test specimens are larger than 3.0 to prevent deep beam behavior in the tests. Since the purpose of this study is to calculate the shear capacity for the end region of the Tx-girder, it is better to tailor the experiment for a beam with a smaller shear span-to-depth ratio to compare the shear stress and governing failure mode more accurately.

6.4. Box beam & X-beam Comparison

The shear stresses of box beams and X-beams calculated by the analytical method are compared with the shear stresses of both types of beams measured through previous experimental work conducted at UT Austin. The expected failure modes when using the analytical method and the actual failure modes are compared. A total of 30 experiment results are described: 20 using girders of size 4B28, eight using 5B40, and two using 5XB40 specimens. Since all experiments' shear span-effective depth ratio is 2.5 or more, shear stress is calculated using STM using two panels.

6.4.1. 4B28

For the Avendano et al. (2013) research, the shear stress of ten 4B28 (from BB-01 to BB-10) box-beams with different concrete strengths, f'_c, and numbers of bearing plates were tested. All the specimens had different end shapes on both sides, and each beam was tested twice—one test at each end. One end shape was the square end, and the other end shape was a 30° skewed end. The prestressing strands for every specimen used were Grade 270, low relaxation, and 0.5-in. diameter, and the effective stress for all strands was 166 ksi. Also, every specimen used Grade 60 reinforcing bars for stirrups with 20-in. spacing. Eight strands were debonded for every specimen: four are debonded through 4-ft length, and the other four are debonded through 10-ft length, as shown in Figure 6-6. The properties for test specimens are shown in Table 6-7, and the geometry or overhang length of the girder is the same as in TxDOT's standard design.

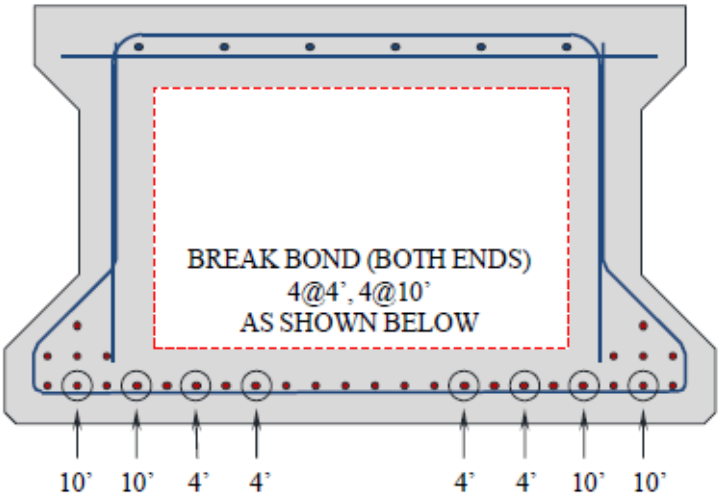

Figure 6-6. Reinforcement detail and debonding pattern for the specimens (4B28)(Avendano et al. 2013)

Table 6-7. Test specimen properties (4B28)

Specimens	End shape	Concrete strength, ksi	NO. of bearing, ea
BB-01	Square	11.30	1
	30° skewed	11.30	2
BB-02	Square	11.30	1
	30° skewed	11.30	1

BB-03	Square	11.16	2
	30° skewed	11.16	2
BB-04	Square	10.67	2
	30° skewed	10.67	1
BB-05	Square	10.90	2
	30° skewed	10.90	2
BB-06	Square	9.53	2
	30° skewed	9.53	1
BB-07	Square	9.58	1
	30° skewed	9.58	1
BB-08	Square	8.73	1
	30° skewed	8.73	1
BB-09	Square	8.90	2
	30° skewed	8.90	2
BB-10	Square	9.73	1
	30° skewed	9.73	1

The shear stresses of Avendaño's 4B28 specimen are calculated by the analytical method using STM and anchorage capacity; also, the shear capacity for nodes, stirrup, and the horizontal shear are checked. The results of the calculated shear strengths for each test specimen and the shear strengths obtained by the experiment are compared in Table 6-8.

Table 6-8. Compare the shear strength between analytical and experimental (4B28)

Specimens		Experimental Results		Analytical Predictions		
		V_{test}	$v_u/f_c^{'}$	$V_{n,AASHTO}$	$V_{n,ACI}$	V_{calc}
BB-01	Square	225	0.097	188	177	144
	30° skewed	230	0.099	181	177	151.5
BB-02	Square	240	0.104	188	177	144
	30° skewed	242	0.105	181	177	151.5
BB-03	Square	246	0.108	187	176	144
	30° skewed	251	0.110	181	176	151.4
BB-04	Square	260	0.119	185	174	144
	30° skewed	245	0.112	178	174	150.8
BB-05	Square	261	0.117	186	175	144
	30° skewed	248	0.111	179	175	151.1
BB-06	Square	212	0.110	179	170	144
	30° skewed	221	0.115	172	170	149.3
BB-07	Square	211	0.109	179	170	144
	30° skewed	203	0.105	172	170	149.4
BB-08	Square	216	0.123	174	167	144
	30° skewed	215	0.122	168	167	146.3
BB-09	Square	219	0.122	175	167	144
	30° skewed	221	0.123	168	167	148.7
BB-10	Square	213	0.108	173	171	149.6

Specimens	Experimental Results		Analytical Predictions		
	V_{test}	$v_u/f_c^{'}$	$V_{n,AASHTO}$	$V_{n,ACI}$	V_{calc}
30° skewed	232	0.118	173	171	149.6

As shown in Table 6-8, the shear strengths of specimens for 4B28 calculated by this study's analytical method are very conservative. The error of the analytical method is similar to the shear strength calculation method proposed by AASHTO LRFD (2020) and ACI 318-19 (2019), respectively.

Table 6-9. Compare the failure mode between analytical and experimental (4B28)

Specimens		Analytical failure mode	Experimental failure mode
BB-01	Square	Traditional shear failure	Strand slip, Traditional shear failure
	30° skewed	Anchorage zone distress	Strand slip, Traditional shear failure
BB-02	Square	Traditional shear failure	Strand slip, Traditional shear failure
	30° skewed	Anchorage zone distress	Strand slip, Traditional shear failure
BB-03	Square	Traditional shear failure	Strand slip, Traditional shear failure
	30° skewed	Anchorage zone distress	Flexure failure
BB-04	Square	Traditional shear failure	Strand slip, Traditional shear failure
	30° skewed	Anchorage zone distress	Flexure failure
BB-05	Square	Traditional shear failure	Strand slip, Traditional shear failure
	30° skewed	Anchorage zone distress	Strand slip, Traditional shear failure
BB-06	Square	Traditional shear failure	Strand slip, Traditional shear failure
	30° skewed	Anchorage zone distress	Strand slip, Traditional shear failure
BB-07	Square	Traditional shear failure	Strand slip, Traditional shear failure

Specimens		Analytical failure mode	Experimental failure mode
	30° skewed	Anchorage zone distress	Strand slip, Traditional shear failure
BB-08	Square	Traditional shear failure	Strand slip, Traditional shear failure
	30° skewed	Anchorage zone distress	Strand slip, Traditional shear failure
BB-09	Square	Traditional shear failure	Strand slip, Traditional shear failure
	30° skewed	Anchorage zone distress	Strand slip, Traditional shear failure
BB-10	Square	Anchorage zone distress	Strand slip, Traditional shear failure
	30° skewed	Anchorage zone distress	Strand slip, Traditional shear failure

According to the analytical method, of the 20 test specimens, 11 are governed by the anchorage zone distress, and nine are governed by strut-to-node interface failure in longitudinal STM. However, the shear capacities calculated based on traditional shear failure and anchorage zone distress are almost equal for every specimen. Also, Table 6-9 indicates that strand slip and traditional shear failure were both found in every specimen throughout the experiment except BB-03 and BB-04 with a skewed end. Table 6-9 shows the expected failure mode due to the analytical method of each specimen and the failure mode observed through the actual experiment. Therefore, the expected failure mode due to the analytical method and the failure mode observed through actual experiments are similar in every specimen.

6.4.2. 5B40 & 5XB40

Avendano et al. (2013) also tested the shear stress of four box beams (5B40-1, 5B40-2, 5B40-3, and 5B40-3) and one X-beam (5XB40) in TxDOT project 0-5831. The only difference between the four box beams was concrete strength, f'_c. All the specimens for the box beam had different end shapes on both sides, and each beam was tested twice—one test at each end. One end shape was the square end, and the other end shape was a 30° skewed end. In total 76 strands were used for every specimen, and every strand was fully bonded, as shown in Figure 6-7 (a). The Avendano et al. (2013) research indicates that reinforcement detail at the end block is almost the same as in TxDOT's standard design. However, Bar E is added to address problems observed at the fabrication stages in heavily prestressed beams.

Therefore, added bars at the end block are considered in the analytical method when using cross-section STM to check the nodal strength (refer to Figure 6-7 (b)).

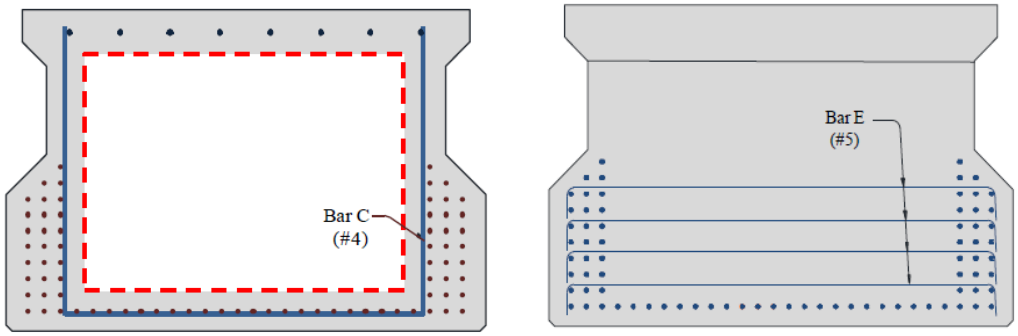

(a) After the end block (b) End block

Figure 6-7. Reinforcement detail and debonding pattern for the specimens (5B40)(Avendano et al. 2013)

The specimens for X-beam had a different number of bearing plates on both sides, and each beam was tested twice—one test at each end. In total 66 strands were used for the specimen, and every strand was fully bonded, as shown in Figure 6-8. Bar E is also added at the X-beams' end block. Therefore, added bars at the end block are considered in the analytical method when using cross-section STM same as box beam.

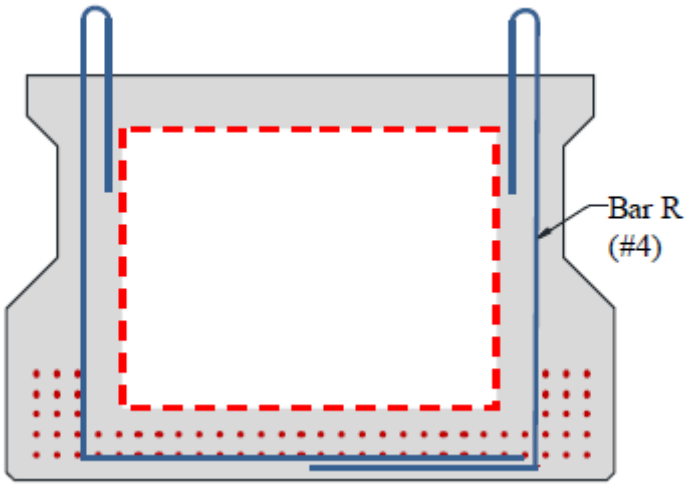

Figure 6-8. Reinforcement detail and debonding pattern for the specimens (5XB40)(Avendano et al. 2013)

The prestressing strands for every specimen used were Grade 270, low relaxation, and 0.5-in. diameter. The effective stress for strands was 163.5 ksi for box beams and 167.5 ksi for X-beams. Also, every specimen used Grade 60 reinforcing bars

for stirrups with 6-in. spacing. The properties for test specimens are shown in Table 6-10, and the geometry or overhang length of both girders are the same as in TxDOT's standard design.

Table 6-10. Test specimen properties (5B40 and 5XB40)

Specimens	End shape	Concrete strength, ksi	No. of bearing, ea
5B40-1	Square	11.8	1
	30° skewed	11.8	1
5B40-2	Square	9.4	1
	30° skewed	9.4	1
5B40-3	Square	11.2	1
	30° skewed	11.2	1
5B40-4	Square	10.0	1
	30° skewed	10.0	1
5XB40	Square	10.5	1
	Square	10.5	2

The shear stresses of Avendaño's specimens are calculated by the analytical method using STM and anchorage capacity; also, the shear capacity for nodes, stirrup, and horizontal shear are checked. The results of the calculated shear strengths for each test and the shear strengths obtained by the experiment are compared in Table 6-11. There are no results for 5B40-2 with the skewed end because the test fails to obtain the result.

Table 6-11. Compare the shear strength between analytical and experimental (5B40 and 5XB40)

Specimens		Experimental Results		Analytical Predictions		
		V_{test}	$v_u/f_c^{'}$	$V_{n,AASHTO}$	$V_{n,ACI}$	V_{calc}
5B40-1	Square	438	0.143	443	433	437

Specimens		Experimental Results		Analytical Predictions		
		V_{test}	$v_u/f_c^{'}$	$V_{n,AASHTO}$	$V_{n,ACI}$	V_{calc}
	30° skewed	585	0.191	443	433	437
5B40-2	Square	543	0.223	421	421	437
5B40-3	Square	623	0.215	439	429	437
	30° skewed	664	0.229	439	429	437
5B40-4	Square	590	0.228	434	425	437
	30° skewed	601	0.232	434	425	437
5XB40	One bearing	675	0.130	603	527	565
	Two bearing	710	0.136	603	527	565

As Table 6-11 indicates, the shear strengths of specimens for 5XB40 calculated by the analytical method used in this study are very conservative compared to the test result and similar compared to the calculation results using AASHTO LRFD (2020) and ACI 318-19 (2019).

Table 6-12. Comparison of the analytical and experimental failure mode (5B40 and 5XB40)

Specimens		Analytical failure mode	Experimental failure mode
5B40-1	Square	Horizontal shear failure	Spalling of cover at end, Horizontal shear failure
	30° skewed	Horizontal shear failure	Spalling of cover at end, Horizontal shear failure, Traditional shear failure
5B40-2	Square	Horizontal shear failure	Spalling of cover at end, Horizontal shear failure, Traditional shear failure
5B40-3	Square	Horizontal shear failure	Spalling of cover at end, Horizontal shear failure, Traditional shear failure
	30° skewed	Horizontal shear failure	Spalling of cover at end, Traditional shear failure

5B40-4	Square	Horizontal shear failure	Spalling of cover at end, Horizontal shear failure, Traditional shear failure
	30° skewed	Horizontal shear failure	Spalling of cover at end, Traditional shear failure
5XB40	One bearing	Anchorage zone distress	Traditional shear failure, Anchorage zone distress
	Two bearing	Anchorage zone distress	No fail

According to the analytical method, all specimens for 5B40 are governed by horizontal shear failure, and all specimens for 5SB40 are governed by anchorage zone distress. Table 6-12 shows the expected failure mode due to the analytical method of each specimen and the failure mode observed through the actual experiment. Table 6-12 indicates that horizontal shear failure was found in almost all the box beam specimens throughout the experiment. However, traditional shear failure and anchorage zone distress were found in one of the X-beam specimens throughout the experiment, but another specimen for X-beam did not fail. Therefore, the expected failure mode due to the analytical method and the failure mode observed through actual experiments are similar in almost every specimen.

6.5. U-beam Comparison

In this chapter, the shear stresses of U-beams calculated by the analytical method described in the previous chapters are compared with those measured through previous experimental work conducted at UT Austin. This chapter also compares the expected failure modes when using the analytical method and the actual failure modes for U-beam. The results of ten experiments using U-54 girders are described. Since all experiments' shear span-effective depth ratio is more than 2.5, shear stress is calculated using STM using two panels.

6.5.1. U-54

For the Hovell et al. (2013) research, the shear stress of ten U-54 (from U54-1-N to U54-7-N) girders with different concrete strengths, stirrup areas, end block lengths, and bearing plate quantities were tested. The prestressing strands for every specimen used were Grade 270, low relaxation and 0.5 in. diameter, and the effective stress for all strands is 167.8 ksi. Each specimen had a different stirrup spacing and number of strands, and no debonded strands were used. The reinforcement details and sections of the U-beam for beams 1 through 3 and for beams 4 through 7 are shown in Figure 6-9. The properties for test specimens are

shown in Table 6-13 and Table 6-14, the overhang length of the girder is 6 in., and the geometry of the girder is the same as in TxDOT's standard design.

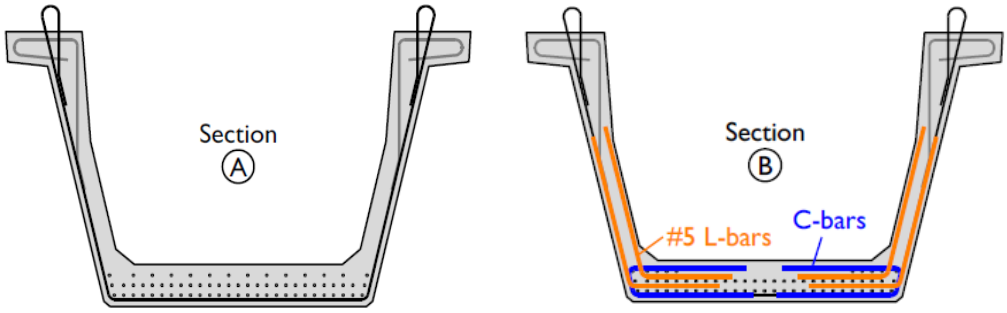

Figure 6-9. Reinforcement detail for the U-beam specimens

Table 6-13. Test specimen properties 1 (U-54)

Specimen ID	End block, in.	Concrete strength, ksi	No. of bearing, ea
U54-1-N	18	11.96	1
U54-1-S (skewed)	24	11.96	2
U54-2-N	18	11.48	1
U54-3-N	18	11.31	1
U54-3-S	18	14.10	2
U54-4-N	18	11.44	1
U54-4-S	18	11.44	1
U54-5-N	18	13.23	1
U54-6-S	30	12.02	1
U54-7-N (skewed)	36	12.45	1

Table 6-14. Test specimen properties 2 (U-54)

Specimen ID	Stirrup area, in^2	Stirrup spacing, in.	No. of strand, ea
U54-1-N	0.4	4	78
U54-1-S (skewed)	0.4	4	78
U54-2-N	0.4	4	78
U54-3-N	0.4	4	78
U54-3-S	0.4	4	78
U54-4-N	0.4	3	84
U54-4-S	2.26	3	84
U54-5-N	2.12	4	66
U54-6-S	1.6	4	64
U54-7-N (skewed)	1.6	4	52

The shear stresses of Hovell's U-54 specimen are calculated by the analytical method using STM and anchorage capacity; also, the capacities for nodal strength, stirrup, and horizontal shear are checked. The results of the calculated shear strengths for each test specimen and the shear strengths obtained by the experiment are compared in Table 6-15.

Table 6-15. Compare the shear strength between analytical and experimental (U-54)

Specimens	Experimental Results		Analytical Predictions		
	V_{test}	$v_u/f_c^{'}$	$V_{n,AASHTO}$	$V_{n,ACI}$	V_{cal}
U54-1-N	659	0.12	699	555	447
U54-1-S (skewed)	612	0.11	699	555	374
U54-2-N	610	0.11	776	648	552

Specimens	Experimental Results		Analytical Predictions		
	V_{test}	$v_u/f_c^{'}$	$V_{n,AASHTO}$	$V_{n,ACI}$	V_{cal}
U54-3-N	655	0.12	508	485	382
U54-3-S	663	0.10	510	487	383
U54-4-N	973	0.12	685	535	530
U54-4-S	1191	0.14	672	513	527
U54-5-N	1031	0.16	761	705	597
U54-6-S	1054	0.18	704	624	575
U54-7-N (skewed)	1210	0.20	689	572	529

As shown in Table 6-15, the shear strengths of specimens for U-54 calculated by the analytical method used in this study are very conservative compared to the test result. According to the analytical method, six of the ten test specimens are governed by the anchorage zone distress. The other four are governed by traditional shear fail or horizontal fail.

Table 6-16. Compare the failure mode between analytical and experimental (U-54)

Specimens	Analytical failure mode	Experimental failure mode
U54-1-N	Horizontal failure	Horizontal failure
U54-1-S (skewed)	Horizontal failure	Horizontal failure
U54-2-N	Horizontal failure	Horizontal failure, Strand slip
U54-3-N	Anchorage zone distress	Horizontal failure, Strand slip
U54-3-S	Anchorage zone distress	Horizontal failure, Strand slip
U54-4-N	Traditional shear failure	Horizontal failure, Web crushing
U54-4-S	Anchorage zone distress	No fail

Specimens	Analytical failure mode	Experimental failure mode
U54-5-N	Anchorage zone distress	Flexure-shear failure
U54-6-S	Anchorage zone distress	Flexure-shear failure
U54-7-N (skewed)	Anchorage zone distress	Web crushing

Table 6-16 shows the expected failure mode due to the analytical method of each specimen and the failure mode observed through the actual experiment. Table 6-16 indicates that horizontal fail was found in all specimens until the amount of stirrup was increased (from U54-1-S to U54-4-N). However, horizontal failure did not occur after the amount of stirrup was increased, and flexure-shear failure or web crushing occurred (from U54-4-S to U54-7-N). When using the analytical method, the governing failure modes can be accurately predicted when horizontal shear failure or anchorage zone distress governs the capacity of the beam. In addition, it is possible to calculate the conservative shear strength for U-beam.

6.6. Slab beam Comparison

The shear stresses of slab beams calculated by the analytical method are compared with the shear stresses of slab beams measured through previous experimental work at University of Houston. This chapter compares the expected failure modes when using the analytical method and the actual failure modes for slab beam. Ten test results are described based on the use of the 5SB12 and 5SB15 specimens. Since all experiments' shear span-effective depth ratio is almost between one and two, the shear stresses are calculated using an STM using one panel.

6.6.1. 5SB12 & 5SB15

This study builds on the findings of the Tan et al. (2016) research, in which 28 slab beam specimens of various heights were tested. This study used ten tested specimens, eliminating some specimens as unsuitable. The specimen height of 8-in. is excluded because a slab beam with that height is no longer included in the TxDOT standard design. Also excluded are the specimens that do not use stirrups or use only the minimum number of stirrups suggested by AASHTO LRFD.

The testing conducted in this task considered only specimens with an angle between 25° and 45° from the centerline of the bearing plate to the loading point. In all, six 5SB12 and four 5SB15 slab beams with different concrete strengths, shear span-

effective depth ratio, number of strands, and numbers of bearing plates were compared. Six specimens contain the deck on the top; the remaining four have no deck. The prestressing strands used for every specimen were Grade 270, low relaxation, and 0.5-in. diameter; the effective stress for all strands was 162 ksi. The study team used Grade 60 reinforcing bars for stirrups with 4-in. spacing on all specimens. Debonded strands are not used, and the total number of strands used varies from 8 to 14 for each specimen (Figure 6-10). The properties for test specimens are shown in Table 6-17, and the geometry or overhang length of the girder is the same as in TxDOT's standard design.

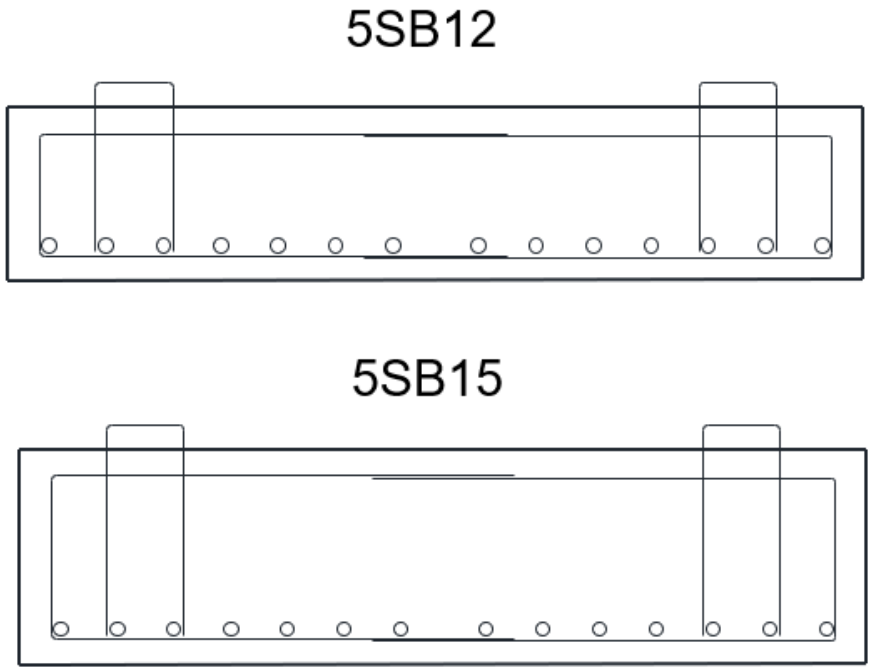

Figure 6-10. Reinforcement detail and strand layout for the specimens (5SB12 and 5SB15)

Table 6-17. Test specimen properties (5SB12 and 5SB15)

Specimen ID	a/d_v	Concrete strength, ksi	No. of bearings, ea	No. of strands, ea	Deck
5SB12-1	1.23	10.7	1	10	Y
5SB12-2	1.94	10.7	2	10	Y
5SB12-3	1.25	9.6	1	10	N
5SB12-4	1.62	9.6	1	10	N
5SB12-5	1.23	9.6	2	14	Y

Specimen ID	a/d_v	Concrete strength, ksi	No. of bearings, ea	No. of strands, ea	Deck
5SB12-6	2.0	9.6	2	14	Y
5SB15-1	1.15	9.7	2	8	Y
5SB15-2	1.23	8.5	1	8	N
5SB15-3	2.02	8.5	2	8	N
5SB15-4	1.21	9.1	2	14	Y

The shear stresses of Tan's type 5SB specimens were calculated by the analytical method using STM and anchorage capacity; also, the shear capacity for nodes is checked. The results of the calculated shear strengths for each test specimen and the shear strengths obtained by the experiment are compared in Table 6-18.

Table 6-18. Compare the shear strength between analytical and experimental (5SB12 and 5SB15)

Specimens	Experimental Results		Analytical Predictions		
	V_{test}	$v_u/f_c^{'}$	$V_{n,AASHTO}$	$V_{n,ACI}$	V_{calc}
5SB12-1	266	0.032	208	195	96
5SB12-2	249	0.030	198	195	70
5SB12-3	175	0.035	181	170	95
5SB12-4	187	0.038	181	151	79
5SB12-5	275	0.037	260	189	135
5SB12-6	319	0.043	243	189	96
5SB15-1	298	0.033	195	223	81
5SB15-2	185	0.032	171	192	77
5SB15-3	172	0.030	161	161	55

Specimens	Experimental Results		Analytical Predictions		
	V_{test}	$v_u/f_c^{'}$	$V_{n,AASHTO}$	$V_{n,ACI}$	V_{calc}
5SB15-4	347	0.041	276	221	136

As shown in Table 6-18, if the shear strengths of the slab beams are calculated using the design provision (ACI 318-19, AASHTO LRFD), the result might be greater than the shear strength measured through the experimental test. However, the shear strengths of specimens for type 5SB calculated using this study's analytical method are always overly conservative compared to the test results.

Table 6-19. Compare the failure mode between analytical and experimental (5SB12 and 5SB15)

Specimens	Analytical failure mode	Experimental failure mode
5SB12-1	Anchorage zone distress	Anchorage zone distress
5SB12-2	Anchorage zone distress	Anchorage zone distress
5SB12-3	Anchorage zone distress	Anchorage zone distress
5SB12-4	Anchorage zone distress	Anchorage zone distress
5SB12-5	Anchorage zone distress	Anchorage zone distress
5SB12-6	Anchorage zone distress	Anchorage zone distress
5SB15-1	Anchorage zone distress	Anchorage zone distress
5SB15-2	Anchorage zone distress	Flexure failure
5SB15-3	Anchorage zone distress	Anchorage zone distress
5SB15-4	Anchorage zone distress	Flexure failure

Table 6-19 shows the expected failure mode derived from the analytical method of each specimen and the failure mode observed through the actual experiment. According to the analytical method, all the test specimens are governed by the anchorage zone distress. Table 6-19 indicates that anchorage zone distress was

found throughout the experiment in all but two specimens. Therefore, the expected failure mode due to the analytical method and the failure mode observed through actual experiments are similar.

6.7. Chapter Summary

The shear strength of different types of Texas standard prestressed beams calculated by the analytical method are compared with the shear strength measured through previous experimental works. Shear strength is compared for all types of Texas standard prestressed beams except for decked-slab beams. The maximum shear strength calculated with the analytical method developed in this research project, V_{calc}, and the actual capacity of shear strength capacity for the beam as a result of the experiment, V_{test}, are compared for a total of 57 specimens. Also, the shear strength calculated by the analytical method, V_{calc}, is compared with the shear strengths calculated by the sectional shear stress calculation method proposed by AASHTO LRFD (2020) and ACI 318-19 (2019). As a result, the shear strengths of every specimen calculated by the analytical method used in this study are very conservative compared to the test result. In addition, the result of the analytical method is similar or more conservative compared to the shear strength based on AASHTO LRFD (2020) and ACI 318-19 (2019).

When using the analytical method, it is possible to calculate the conservative shear strength of the beam. The experimental studies on decked-slab beams have not been conducted in the past, so comparing the shear strength based on analytical method and test result is not performed. However, the shape of the decked-slab beam is very similar to the box beam, and the same analytical method is used, so the research team assumed that the shear stress of the decked-slab beam is calculated using the analytical method is conservative such as box beam. Therefore, it is appropriate to determine whether the shear stress limit of the end region of the beam can be relaxed using the analytical method. Also, the failure modes of the beams predicted using the analytical method coincided with the failure mode found through the experiment for 48 specimens out of 57 specimens. Therefore, the governing failure mode of the Texas standard prestressed beam may be predicted using the analytical method. The shear span-to-depth ratios, a/d_v, of test specimens for Texas standard prestressed beam in literature except slab beam are mostly larger than 2.0 to exclude deep beam behavior in the tests. Since the purpose of this study is to calculate the shear capacity for the beam's end region, which has a value of a/d_v less than 2.0, it is needed to tailor the experiment for beams with a smaller shear span-to-depth ratio. The experimental program can be more representative to relax the shear stress limit and more accurately capture failure modes.

Chapter 7. Additional Investigation

7.1. Introduction

When there is a skewed end with two bearing plates, the strut-to-node interface in longitudinal STM can fail for box beams or X-beams. When the failure of the strut-to-node interface in longitudinal STM (one of the nodal failures) governs the box-beam of X-beam's shear capacity, the maximum v_u/f'_c of both beams becomes smaller than when the anchorage zone distress governs (refer to Table 7-1). However, nodal failure can be prevented by slightly changing the geometry and boundary conditions of the beam. This section presents two methods that can prevent nodal failure. Changing the bearing plate's size or placing additional longitudinal reinforcement on the web is useful to prevent nodal failure. Also, the anchorage capacity governs the shear capacity of the beam if nodal failure is prevented. Therefore, the maximum shear capacity of the beam increases when nodal failure governs it.

Table 7-1. Different maximum v_u/f'_c and governing failure mode depending on the geometry of beam end for box beams and X-beams

	Two bearing plates				One bearing plate	
	Square end		30° skewed end		Square, skewed end	
	v_u/f'_c	Governing failure mode	v_u/f'_c	Governing failure mode	v_u/f'_c	Governing failure mode
4B20	0.181	Anchorage	0.181	Anchorage	0.181	Anchorage
4B28	0.164	Anchorage	0.163	Nodal	0.164	Anchorage
4B34	0.166	Anchorage	0.166	Anchorage	0.166	Anchorage
4B40	0.170	Anchorage	0.170	Anchorage	0.170	Anchorage
5B20	0.197	Anchorage	0.190	Nodal	0.197	Anchorage
5B28	0.176	Anchorage	0.163	Nodal	0.176	Anchorage
5B34	0.176	Anchorage	0.155	Nodal	0.176	Anchorage
5B40	0.174	Anchorage	0.174	Anchorage	0.174	Anchorage

4XB20	0.177	Anchorage	0.177	Anchorage	0.177	Anchorage
4XB28	0.186	Anchorage	0.186	Anchorage	0.186	Anchorage
4XB34	0.176	Anchorage	0.176	Anchorage	0.176	Anchorage
4XB40	0.157	Anchorage	0.157	Anchorage	0.157	Anchorage
5XB20	0.201	Anchorage	0.201	Anchorage	0.201	Anchorage
5XB28	0.209	Anchorage	0.205	Nodal	0.209	Anchorage
5XB34	0.201	Anchorage	0.201	Anchorage	0.201	Anchorage
5XB40	0.179	Anchorage	0.179	Anchorage	0.179	Anchorage

7.2. Change the Size of the Bearing Plate

The bearing plate at the obtuse angle receives a larger load than the bearing plate at the acute angle when the beam's end shape is skewed with two bearing plates. Therefore, the strut-to-node interface in longitudinal STM can fail at the node of the obtuse angle. A bigger bearing plate at the support can prevent this failure mode. As the bearing plate's size increases, the node's geometry also increases, so the capacity of the strut-to-node interface increases. It is evaluated whether increasing the bearing plate size of the obtuse angle from a minimum of 1-in. to a maximum of 2-in. for a beam with failure of the strut-to-node interface in longitudinal STM. The bearing plate's width, which affects only the capacity of the strut-to-node interface, is changed in this study because increasing the length of the bearing plate changes many variables that can affect the total capacity of the beam, such as the critical section of the tie and the degree of the strut. The capacity for the strut-to-node interface and maximum v_u/f'_c after increasing the bearing plate size are shown in Table 7-2. As shown in Table 7-2, nodal failure can be prevented, and the maximum v_u/f'_c of the beams can be increased by slightly increasing the size of the bearing plate at the obtuse angle.

Table 7-2. Comparison for the capacity of strut-to-node interface and maximum v_u/f'_c for box beams and X-beam (Increase bearing plate size)

Demand (kips)	Original design			Increase bearing plate's size		
	Bearing size (in.)	Capacity (kips)	v_u/f'_c	Bearing size	Capacity (kips)	v_u/f'_c

4B28	172.4	6×7	171.5	0.163	6×8	196.0	0.164
5B20	152.2	6×6	147.0	0.190	6×7	171.5	0.197
5B28	185.4	6×7	171.5	0.163	6×8	196.0	0.176
5B34	222.4	6×8	196.0	0.155	6×10	235.1	0.176
5XB28	315.36	8×10	309.36	0.205	8×11	340.30	0.209

7.3. Add Longitudinal Crack Control Reinforcement

The horizontal crack control reinforcement in the box beam does not exist on the web. According to article 5.8.2.5.3 in AASHTO LRFD (2020), the crack control reinforcement in the horizontal direction should satisfy Equation 7-1. If the crack control reinforcement ratio does not satisfy Equation 7-1, the concrete efficiency factor, v, is always 0.45 regardless of the concrete strength, f'_c.

$$\frac{A_h}{b_w s_h} \geq 0.003 \qquad \text{Equation 7-1}$$

Where :

A_h = total area of horizontal crack control reinforcement within the spacing s_h (in.^{2})

b_w = width of member's web (in.)

s_h = spacing of horizontal crack control reinforcement (in.)

However, the concrete efficiency factor, v, can be calculated through Equation 7-2 when the amount of horizontal crack control reinforcement satisfying Equation 7-1 is used in the beam's web. The box beam or X-beam's concrete strength is always less than 8.0 ksi, so the concrete efficiency factor is always greater than 0.45. If the concrete efficiency factor increases, the strut-to-node interface's capacity in longitudinal STM increases, and nodal failure can be prevented. Therefore, anchorage zone distress governs the beam's shear capacity when an appropriate amount of longitudinal crack control reinforcement is placed on the web, and the maximum v_u/f'_c can be increased. Table 7-3 shows the concrete efficiency factor, the strut-to-node interface's capacity, and maximum v_u/f'_c when the horizontal reinforcement is added to the web.

$$v = 0.85 - f_c^{'} / 20 \leq 0.65 \qquad \text{Equation 7-2}$$

Table 7-3. Comparison for the capacity of strut-to-node interface and maximum v_u/f'_c for box beams and X-beam (Add longitudinal reinforcement)

	Demand (kips)	Original design			Add longitudinal crack control reinforcement		
		v	Capacity (kips)	v_u/f'_c	v	Capacity (kips)	v_u/f'_c
4B28	172.4	0.45	171.5	0.163	0.6	228.7	0.164
5B20	152.2	0.45	147.0	0.190	0.6	196.0	0.197
5B28	185.4	0.45	171.5	0.163	0.6	228.7	0.176
5B34	222.4	0.45	196.0	0.155	0.6	261.3	0.176
5XB28	315.36	0.45	309.36	0.205	0.6	412.48	0.209

7.4. Chapter Summary

As shown in Table 7-2 and Table 7-3, the failure of the strut-to-node interface in longitudinal STM can be prevented when the bearing plate's size increases or an appropriate number of longitudinal crack control reinforcement added in the web to refine the calculation for the capacity of the nodes. The method of adding longitudinal reinforcement increases the capacity of the strut-to-node interface more than the method of increasing the size of the bearing plate. However, increasing the bearing plate's size is easier to change than the reinforcement layout of the beam. If nodal failure is prevented, anchorage zone distress starts to govern the shear capacity of the beam's end. Therefore, the maximum v_u/f'_c of each beam is the same as the maximum value in Figure 5-11 and Figure 5-16 (refer to Table 7-4). According to Table 7-4, even modifying the box beam or X-beam according to the recommended design does not significantly increase the maximum v_u/f'_c.

Table 7-4. Different maximum v_u/f'_c depending on the design

	Maximum v_u/f'_c (Standard design)	Maximum v_u/f'_c (After modification*)
4B28	0.163	0.164
5B20	0.190	0.197
5B28	0.163	0.178

	Maximum v_u/f'_c (Standard design)	Maximum v_u/f'_c (After modification*)
5B34	0.155	0.176
5XB28	0.205	0.209

Note: *Increasing the size of the bearing plate. Adding additional horizontal reinforcement.

Chapter 8. Summary and Conclusions

8.1. Summary

Since the $0.18\ f'_c$ shear stress limit was incorporated into the 4th edition of AASHTO LRFD (2007), the end region design has been more conservative. If the $0.18\ f'_c$ shear stress limit is not satisfied when designing the end regions of bridge beams, the effective shear area of the members should be increased unless the Strut-and-Tie Model (STM) is used for the end regions. In other words, the $0.18\ f'_c$ shear stress limit can be relaxed at the end regions of prestressed beams if appropriate STMs can justify load transfer into the supports. In addition, when evaluating Tx-girders and AASHTO Type I-girders using the SFED, it was observed that the $0.18\ f'_c$ shear stress limit might be overly conservative for Tx-girders because they contain a greater number of strands and thus possess a greater shear capacity than AASHTO Type I-girders. Also, AASHTO Type I-girders and Tx-girders demonstrate different governing failure modes in experimental results, which can be attributed to the difference in their geometry. Therefore, it is appropriate to evaluate the current $0.18\ f'_c$ shear stress limit for the end regions of Texas standard prestressed beams.

To accomplish the objective, shear failure mechanisms of the end regions of Texas standard prestressed beams were investigated, and appropriate STMs were developed for prestressed beams. This project's final purpose is to check whether the end region of the Texas standard prestressed beams can exceed the $0.18\ f'_c$ shear stress limit and assess the extent to which the stress limit can be relaxed. However, the shear stress of all parts of the girder cannot exceed the $0.25\ f'_c$ shear stress limit derived from the Modified Compression Field Theory (MCFT)_ (Vecchio and Collins 1986). Therefore, in this study, the $0.25\ f'_c$ shear stress limit is the upper limit of the shear stress of the girder's end.

Shear stress was calculated by assuming a total prestress loss of 20 percent, based on the evaluation database. Two different methods, STM and anchorage capacity, were used to calculate the shear strength of prestressed beam end regions. After calculation, the smaller of the two calculated shear strengths were used to determine the maximum shear stress capacity. The geometries, boundary conditions, and strand layouts provided in the TxDOT's standard design or PG Super were considered to calculate the maximum shear stress of Texas standard prestressed beams. The calculated shear stress limit of Texas standard prestressed beams with standard strand pattern was used in this research because the calculated shear stress capacity of the standard prestressed beam based on a standard strand pattern was the most representative when using the analytical method proposed in this research.

The shear strength of the Texas beam end region was calculated by the STM and anchorage capacity proposed in this research. Anchorage zone distress did not occur when the calculated shear force was applied as the shear force on the end of the Texas beams. However, it is necessary to consider other failure modes in addition to anchorage zone distress. A nodal strength check was performed on the anchorage portion of the bottom flange; the horizontal shear failure mode that could occur between the bottom flange and the base of the web was also checked. Additionally, the STM was used on the cross-section to confirm that sufficient confinement was used in Tx-girders to prevent lateral splitting failure, and the cross-sectional STM was also used to check the nodal strength at the end block for Texas standard prestressed beams.

8.2. Conclusions

The purpose of the 0-7015 project is to determine whether the shear stress in the end region of the Texas standard prestressed beams can exceed the $0.18 f'_c$ shear stress limit when using the STM and anchorage capacity as suggested in NCHRP 579 (Hawkins and Kuchma 2007)—and this outcome was achieved for every size of Tx-girder and decked-slab beam. This research also sought to confirm that additional expected failure mode will not occur when the shear strength calculated using the STM and anchorage capacity acts as the shear force on the end of the beam. Furthermore, the analytical results were compared with existing experimental results to determine whether the analytical method used in this study is conservative in calculating shear stress. The results and conclusions for each type of Texas standard prestressed beams were yielded as explained in the subchapters. In addition, the shear stress limits for each type and size of Texas standard prestressed beam ends are proposed.

8.2.1. Tx-girder

The maximum shear stress of every size of the Tx-girder's end region can exceed the $0.18 f'_c$ shear stress limit through the analytical method. Even when the shear stress exceeds the $0.18 f'_c$ shear stress limit, horizontal shear failure, nodal failure, and lateral splitting failure do not limit the capacity. Since the maximum shear stress varies depending on the size of the Tx-girder, different shear stress limits recommended by this project should be specified according to the sizes of the Tx-girders. Also, the analytical method used for this study is conservative in calculating the shear stress of Tx-girder. However, the shear span-to-depth ratios of test specimens are larger than 2.5 to prevent deep beam behavior in the tests. Since the purpose of this study is to calculate the shear capacity for the end region of the Tx-girder, it is better to tailor the experiment for a beam with a smaller shear

span-to-depth ratio (less than 2.0) to compare the shear stress and governing failure mode more accurately. In conclusion, it is justifiable to relax the shear stress limit of the Tx-girder, allowing for a more economical design of bridges as the shear stress limit of the girder increases.

8.2.2. Box beam

The Findings obtained through the analytical method indicate that the maximum shear stress of only one box-beam's end region—the 5B20—can exceed the $0.18 f'_c$ shear stress limit. Since the nodes' capacity governs the shear capacity of the 5B20 according to the TxDOT standard design, the shear stress limit can be relaxed up to $0.19 f'_c$. However, if nodal failure is prevented, the shear stress limit can be relaxed up to $0.197 f'_c$ because anchorage capacity governs the beam's shear capacity instead of the nodes' capacity. The strut-to-node failure in longitudinal STM can occur when the shear strength is calculated using STM and anchorage capacity acts as the force on the end of the box beams. This kind of nodal failure can be prevented by increasing the bearing plate's size or adding longitudinal crack control reinforcement on the web to refine the calculation for the capacity of the nodes. However, even if nodal failure is prevented, there is only a slight increase in the box beam's maximum shear capacity. This study's analytical method is conservative in calculating the shear stress of the box beam. However, the shear span-to-depth ratios of test specimens for box beam are larger than 2.5 to prevent deep beam behavior in the tests. Since the purpose of this study is to calculate the shear capacity for the end region of the box beams, it is better to tailor the experiment for a beam with a smaller shear span-to-depth ratio (less than 2.0) to compare the shear stress and governing failure mode more accurately. To sum up, the shear stress limit of the box beam cannot be relaxed based on the analytical method, with the exception of 5B20.

8.2.3. X-beam

The analytical result indicates that the maximum shear stress of the end regions of three X-beams—the 5XB20, 5XB28, 5XB34—can exceed the $0.18 f'_c$ shear stress limit. Also, the node capacity governs the shear capacity of the 5XB28 according to the TxDOT standard design, and the shear stress limit can be relaxed up to $0.205 f'_c$. However, if nodal failure is prevented, the shear stress limit can be relaxed up to $0.209 f'_c$ because anchorage capacity governs the beam's shear capacity. The strut-to-node failure in longitudinal STM can occur when the shear stress calculated using STM and anchorage capacity acts on the end of the X-beams. This kind of nodal failure can be prevented by increasing the bearing plate size or adding horizontal crack control reinforcement on the web to refine the node's capacity

calculation. However, even if nodal failure is prevented, there is only a slight increase in the X-beam's maximum shear capacity. Also, this study's analytical method is conservative in calculating the shear stress of the X-beam. However, the shear span-to-depth ratios of test specimens for X-beam are larger than 2.5 to prevent deep beam behavior in the tests. Since the purpose of this study is to calculate the shear capacity for the end region of the X-beams, it is better to tailor the experiment for a beam with a smaller shear span-to-depth ratio (less than 2.0) in order to compare the shear stress and governing failure mode more accurately. In summary, the shear stress limit of the four different sizes of X-beams (4XB28, 5XB20, 5XB28, 5XB34) can be relaxed based on the analytical method.

8.2.4. U-beam

The findings obtained through appropriate STMs indicate that the maximum shear stresses of every size of the U-beam's end region are always lower than the $0.18f'_c$ shear stress limit. Also, this study's analytical method is conservative in calculating the shear stress of the U-beam. However, the shear span-to-depth ratios of test specimens are greater than 2.5 to prevent deep beam behavior in the tests. Since the purpose of this study is to calculate the shear capacity for the end region of the U-beams, it is better to tailor the experiment for a beam with a smaller shear span-to-depth ratio (less than 2.0) to compare the shear stress and governing failure mode more accurately. According to the results of the analysis, the shear stress limit of the U-beam cannot be relaxed.

8.2.5. Decked-slab beam

The maximum shear stress of every size of decked-slab beam's end region can exceed the $0.18f'_c$ shear stress limit through the analytical method. Even when the shear stress exceeds the $0.18f'_c$ shear stress limit, horizontal shear failure and nodal failure do not limit the capacity. In addition, the maximum shear stress of the beam is greatly influenced by the geometry of the beam. Therefore, even if the shear strength of the decked-slab beam is similar to that of the box beam, the maximum shear stress is greater due to the small effective depth. The results of the analytical method for the decked-slab beam are not compared to the experimental result because there are no experimental results in previous research. Since the shape of the decked-slab beam is very similar to the box beam and the same analytical method is used, the study team predicts that the shear stress of the decked-slab beam calculated using the analytical method is conservative (such as box beam). However, since the possibility of unexpected variables cannot be ruled out, it is better to tailor a future experiment for the decked-slab beam. In the end, it is

justifiable to relax the shear stress limit of the decked-slab beam, allowing for a more economical design of bridges as the shear stress limit of the girder increases.

8.2.6. Slab beam

Through the analytical method, the maximum shear stress of the slab beam's end region always cannot exceed the $0.18 f'_c$ shear stress limit. This study's analytical method is conservative in calculating the shear stress of the slab beam. The shear span-to-depth ratios of test specimens for slab beam are between one and two, so it is appropriate to compare the results of the analytical method in this study with the experimental result. Also, the maximum shear stress of the beam is greatly influenced by its geometry. Even though the shear strength of the slab beam is similar to that of the decked-slab beam, the maximum shear stress becomes very low because the web width is much larger. Therefore, the shear stress limit of the slab beam cannot be relaxed based on the analytical method.

8.2.7. Shear stress limit of Texas standard prestressed beam ends

The STM design method is based on the lower bound theorem in plasticity, which means it delivers conservative design results. Therefore, if the value of the shear stress calculated using the STM is greater than the $0.18 f'_c$ shear stress limit, the shear stress limit of the beam can be relaxed. However, lowering the shear stress limit when the calculated shear stress is less than the $0.18 f'_c$ shear stress limit may be overly conservative for the beam's actual shear capacity. For these reasons, this study suggests that the shear stress limit can be relaxed only for beams for which the maximum shear stress of the end region exceeds the $0.18 f'_c$ shear stress limit when analyzed by the STM. This research also notes that the $0.18 f'_c$ shear stress limit suggested in the AASHTO LRFD (2020), is still used when the calculated shear stresses based on the analytical method are less than $0.18 f'_c$. Table 8-1 shows the shear stress limits for different types and sizes of all Texas standard prestressed beams evaluated in this project. For the simpler and more conservative shear stress limit, the shear stress limit rounded down to two decimal points is proposed.

Table 8-1. Shear stress limit for each Texas standard prestressed beam

Proposed shear stress limit (f'_c)						
Tx-28	**Tx-34**	**Tx-40**	**Tx-46**	**Tx-54**	**Tx-62**	**Tx-70**
0.22	*0.22*	*0.23*	*0.23*	*0.22*	*0.21*	*0.20*

4B20	**4B28**	**4B34**	**4B40**	**5B20**	**5B28**	**5B34**	**5B40**
0.18	*0.18*	*0.18*	*0.18*	*0.19*	*0.18*	*0.18*	*0.18*
4XB20	**4XB28**	**4XB34**	**4XB40**	**5XB20**	**5XB28**	**5XB34**	**5XB40**
0.18	*0.18*	*0.18*	*0.18*	*0.20*	*0.20*	*0.20*	*0.18*
U-40				**U-54**			
0.18				*0.18*			
6DS20	**6DS23**	**7DS20**	**7DS23**	**8DS20**	**8DS23**		
0.23	*0.22*	*0.23*	*0.23*	*0.23*	*0.24*		
4SB12		**4SB15**		**5SB12**		**5SB15**	
0.18		*0.18*		*0.18*		*0.18*	

According to Table 8-1, it is hard to relax the shear stress limit of all Texas standard prestressed beams. However, relaxing the shear stress limits for specific types and sizes of Texas standard prestressed beam ends will not create structural safety and serviceability issues and is, therefore, acceptable. Especially the shear stress of every size of the Tx-girder and decked-slab beam end regions, for which the $0.18 f'_c$ shear stress limit can be relaxed as shown in the research. In addition, it is also suitable to relax the $0.18 f'_c$ shear stress limit for one size of box beam and for three sizes of X-beam. By relaxing the shear stress limit of Texas standard prestressed beam ends, bridge design and construction can be more economical. In addition, applying the analytical method proposed in this study, the possibility of relaxing the $0.18 f'_c$ shear stress limit for the prestressed beam other than Texas standard prestressed beams can be confirmed.

References

AASHTO(American Association of State Highway and Transportation Officials). (2007). *Bridge Design Specifications*. American Association of State Highway and Transportation Officials, Washington, DC.

AASHTO(American Association of State Highway and Transportation Officials). (2020). *Bridge Design Specifications*. American Association of State Highway and Transportation Officials, Washington, DC.

ACI Committee 318. (2008). *Building Code Requirements for Structural Concrete ACI (318-08)*. American Concrete Institute, Farmington Hills, MI.

ACI Committee 318. (2019). *Building Code Requirements for Structural Concrete ACI (318-19)*. American Concrete Institute, Farmington Hills, MI.

Alshegeir, A., and Ramirez, J. A. (1992). "Strut-and-Tie Approach in Pretensioned Deep Beams." *ACI Structural Journal*, 89(3), 296–304.

Avendano, A., Hovell, C., Moore, A., Dunkman, D., Nakamura, E., Bayrak, O., and Jirsa, J. (2013). *Pretensioned Box Beams: Prestress Transfer and Shear Behavior*. The University of Texas at Austin, Austin, TX, 278.

Avendaño, A. R., and Bayrak, O. (2008). *Shear Strength and Behavior of Prestressed Concrete Beams*. The University of Texas at Austin, Austin, TX, 180.

Avendaño Valderrama, A. R. (2011). "Pretensioned Box Beams: Prestress Transfer and Shear Behavior." Ph.D. Dissertation, The University of Texas at Austin, Austin, TX.

Barton, D. L., Anderson, R. B., Bouadi, A., Jirsa, J. O., and Breen, J. E. (1991). *An Investigation of Strut-and-Tie Models for Dapped Beam Details*. The University of Texas at Austin, Austin, TX, 214.

Bergmeister, K., Breen, J. E., Jirsa, J. O., and Kreger, M. E. (1993). *Detailing for structural concrete*. The University of Texas at Austin, Austin, TX.

Botros, A. W., Klein, G. J., Lucier, G. W., Rizkalla, S. H., and Zia, P. (2017). "Dapped Ends of Prestressed Concrete Thin-Stemmed Members: Part 1, Experimental Testing and Behavior." *PCI Journal*, 62(2), 61–82.

Brice, R. (2020). *Precast, Prestressed Girder Design Example-PGSuper Training*. WSDOT Bridge and Structures Office.

Buckner, C. D. (1995). "A Review of Strand Development Length for Pretensioned Concrete Members." *PCI Journal*, 40(2), 84–105.

Chehab, A. I., Eamon, C. D., Parra-montesinos, G. J., and Dam, T. X. (2018). "Shear Testing and Modeling of AASHTO Type Prestressed Concrete Bridge Girders." *ACI Structural Journal*, 115(3), 801–812.

Cook, W. D., and Mitchell, D. (1988). "Studies of Disturbed Regions Near Discontinuities in Reinforced Concrete Members." *ACI Structural Journal*, 85(2), 206–216.

De Wilder, K., Lava, P., Debruyne, D., Wang, Y., De Roeck, G., and Vandewalle, L. (2015). "Experimental Investigation on The Shear Capacity of

Prestressed Concrete Beams Using Digital Image Correlation." *Engineering Structures*, 82(1), 82–92.
FIB Special Activity Group 5. (2013). *FIB Model Code for Concrete Structures 2010*. Wilhelm Ernst & Sohn, Berlin, Germany.
FIP Commission 3. (1999). *Practical Design of Structural Concrete*. Silhelm Ernst & Sohn, London, U.K.
Floyd, R. W., Pei, J., Murray, C. D., Cranor, B., and Tang, P. F. (2016). *Understanding the Behavior of Prestressed Girders after Years of Service*. The University of Oklahoma, Norman, OK, 189.
Garber, D. B. (2014). "Effect of New Prestress Loss Estimation Procedure on Precast, Pretensioned Bridge Girders." Ph.D. Dissertation, The University of Texas at Austin, Austin, TX.
Garber, D. B., Gallardo, J. M., Deschenes, D. J., and Bayrak, O. (2016). "Nontraditional Shear Failures in Bulb-T Prestressed Concrete Bridge Girders." *Journal of Bridge Engineering*, 21(7), 1–10.
Hamoudi, A. A., and Phang, M. K. S. (1975). "Diagonal Shear in Prestressed Concrete Dapped-Beams." *ACI Journal*, 72(7), 347–350.
Hanson, J. M., and Hulsbos, C. L. (1964). "Ultimate Shear Tests of Prestressed Concrete I-Beams Under Concentrated and Uniform Loadings." *PCI Journal*, 9(3), 15–28.
Hawkins, N. M., and Kuchma, D. A. (2007). *Application of LRFD Bridge Design Specifications to High-Strength Structural Concrete: Shear Provision*. The National Academic Press, Washington, DC, 197.
Higgs, A., Barr, P. J., and Halling, M. W. (2015). "Comparison of Measured and AASHTO LRFD-Predicted Residual Prestress Forces, Shear and Flexural Capacities of High-Strength Prestressed-Concrete Bridge Girders." *Journal of Bridge Engineering*, 20(1), 05014009.
Hovell, C., Avendaño, A., Moore, A., Dunkman, D., Bayrak, O., and Jirsa, J. (2013). *Structural Performance of Texas U-Beams at Prestress Transfer and Under Shear-Critical Loads*. The University of Texas at Austin, Austin, TX, 355.
Katz, A., Yousefpour, H., Kim, H. su, Abyaneh, R. A., Salazar, J., Hrynyk, T., and Bayrak, O. (2017). "Shear Performance of Pretensioned Concrete I-Girders Employing 0.7 in. (17.8 mm) Strands." *ACI Structural Journal*, 114(5), 1273–1284.
Kaufman, M. K., and Ramirez, J. A. (1988). "Re-evaluation of the Ultimate Shear Behavior of High-Strength Concrete Prestressed I-beams." *ACI Structural Journal*, 85(3), 295–303.
Kim, H., Bonetti, R., Longshaw, A., Yousefpour, H., Hrynyk, T., and Bayrak, O. (2018). "End-Region Cracking in Pretensioned Concrete Girders Employing 0.7-in. Strands: Time-Dependent and Service-Load Effects." PCI/NBC, Chicago, IL.
Klein, G., Botros, A., Andrews, B., and Holloway, K. (2017). "Dapped Ends of Prestressed Concrete Thin-Stemmed Members: Part 2, Design." *PCI Journal*, 62(2), 83–100.

Langefeld, D. P. (2012). “Anchorage-Controlled Shear Capacity of Prestressed Concrete Bridge Girders.” Master’s Thesis, The University of Texas at Austin, Austin, TX.

Larson, N. (2010). “Structural Performance of ASR/DEF Damaged Prestressed Concrete Trapezoidal Box Beams with Dapped Ends.” Master’s Thesis, The University of Texas at Austin, Austin, TX.

Laskar, A., Wang, J., Hsu, T. T. C., and Mo, Y. L. (2007). *Rational Shear Provisions for AASHTO LRFD Specifications: Technical Report*. Cullen College of Engineering, Houston, TX, 216.

Llanos, G., Ross, B. E., and Hamilton, H. R. (2009). *Shear Performance of Existing Prestressed Concrete Bridge Girders*. University of Florida, Gainesville, FL, 160.

Martin, B. T., and Sanders, D. H. (2007). *Verification and implementation of strut-and-tie model in LRFD bridge design specification*. American Association of State Highway and Transportation Officials, Washington, DC.

Mattock, A. H. (2012). “Strut-and-Tie Models of Dapped-End Beams.” *Concrete International*, 34(2), 35–40.

Mattock, A. H., and Chan, T. C. (1979). “Design and Behavior of Dapped-End Beams.” *PCI Journal*, 24(6), 28–45.

Murray, C. D., Cranor, B. N., Floyd, R. W., and Pei, J. (2019). “Experimental Testing of Older AASHTO Type II Bridge Girders with Corrosion Damage at The Ends.” *PCI Journal*, 64(1), 49–64.

Nakamura, E. (2011). “Shear Database for Prestressed Concrete Members.” Master’s Thesis, The University of Texas at Austin, Austin, TX.

Osborn, G. P., Barr, P. J., Petty, D. A., Halling, M. W., and Brackus, T. R. (2012). “Residual Prestress Forces and Shear Capacity of Salvaged Prestressed Concrete Bridge Girders.” *Journal of Bridge Engineering*, 17(2), 302–309.

Ramirez, J., and Aguilar, G. (2005). *Shear Reinforcement Requirements for High-Strength Concrete Bridge Girders*. Purdue University, West Lafayette, IN, FHWA/IN/JTRP-2005/19, 2654.

Ramirez, J., Olek, J., Rolle, E., and Malone, B. (2000). *Performance of Bridge Decks and Girders with Lightweight Aggregate Concrete, v. 2 of 2*. Purdue University, West Lafayette, IN, FHWA/IN/JTRP-98/17-2, 2131.

Reineck, K.-H. (Ed.). (2002). *Examples for the Design of Structural Concrete with Strut-and-Tie Models*. ACI international SP, American Concrete Institute, Farmington Hills, MI.

Ross, B., Hamilton, H., and Consolazio, G. (2013). “Design Model for Confinement Reinforcement in Pretensioned Concrete I-Girders.” *Journal of the Transportation Research Board*, 2331(1), 59–67.

Schlaich, J., Schafer, K., and Jennewein, M. (1987). “Toward a Consistent Design of Structural Concrete.” *PCI Journal*, 32(3), 74–150.

Shahawy, M. A., and Batchelor, B. deV. (1996). “Shear Behavior of Full-Scale Prestressed Concrete Girders: Comparison Between AASHTO Specifications and LRFD Code.” *PCI Journal*, 41(3), 48–62.

Shahrooz, B. M., Miller, R. A., Harries, K. A., Yu, Q., and Russell, H. G. (2017). *Strand Debonding for Pretensioned Girders*. The National Academies Press, Washington, DC.

Tan, S., Luu, C. H., Mo, Y. L., Hsu, T. T. C., and Belarbi, A. (2016). "Structural Behavior of Thin Prestressed Slab beams in Bridges." *ACI Structural Journal*, 113(2), 287–299.

Tawfiq, K. (1995). *Cracking and Shear Capacity of High Strength Concrete Girders*. FAMU/FSU College of Engineering, Tallahassee, FL, 145.

TxDOT. (2020a). *Bridge Design Manual-LRFD*. Texas Department of Transportation, Austin, TX.

TxDOT. (2020b). *BridgeLink-PGSuper Design Guide*. Texas Department of Transportation, Austin, TX.

Vecchio, F. J., and Collins, M. P. (1986). "The Modified Compression-Field Theory for Reinforced Concrete Elements Subjected to Shear." *ACI Journal Proceedings*, 83(2), 219–231.

Villamizar, S., Ramirez, J. A., and Aguilar, G. (2017). "Shear Strength and Behavior of High-Strength Concrete Prestressed Beams." *ACI Structural Journal*, 114(1), 277–289.

Wight, J. K., and Parra-montesinos, G. J. (2003). "Strut-and-Tie Model for Deep Beam Design - A practical exercise using Appendix A of the 2002 ACI Building Code." *Concrete International*, 63–70.

Williams, C. S., Deschenes, D. J., and Bayrak, O. (2012). *Strut-and-Tie Model Design Examples for Bridges*. The University of Texas at Austin, Austin, TX, 258.

Yousefpour, H., Kim, H. S., Bonetti, R., Abyaneh, R. A., Katz, A., Longshaw, A., Salazar, J., Hrynyk, T., and Bayrak, O. (2017). *End-Region Behavior and Shear Strength of Pretensioned Concrete Girders Employing 0.7-in. Diameter Strands*. The University of Texas at Austin, Austin, TX, 194.

Appendix A. Strand Layout and Design Concrete Strength

A.1. Tx-girder

Tx-28

		Prestressing Strands			Harped Strand Pattern		Concrete	
Span length (ft)	**Total number (ea)**	**Size (in.)**	**Strength (f_{pu})**	**Eccentricity (in.)**	**Number (ea)**	**Height (in.)**	**Release strength (ksi)**	**28-day strength (ksi)**
40	10	0.6	270	10.48	0	0	4.0	5
45	12	0.6	270	10.48	0	0	4.5	5
50	12	0.6	270	10.48	0	0	4.2	5
55	14	0.6	270	10.48	2	8.5	4.0	5
60	18	0.6	270	10.04	4	14.5	4.0	5.6
65	22	0.6	270	9.75	4	24.5	4.3	5.9
70	26	0.6	270	9.56	4	24.5	5.2	6.3
75	28	0.6	270	9.48	4	24.5	5.6	7.8

Tx-34

		Prestressing Strands			Harped Strand Pattern		Concrete	
Span length (ft)	**Total number (ea)**	**Size (in.)**	**Strength (f_{pu})**	**Eccentricity (in.)**	**Number (ea)**	**Height (in.)**	**Release strength (ksi)**	**28-day strength (ksi)**
40	10	0.6	270	13.01	0	0	4.0	5.0
45	10	0.6	270	13.01	0	0	4.5	5.0
50	12	0.6	270	13.01	0	0	4.0	5.0
55	12	0.6	270	13.01	0	0	4.0	5.0
60	14	0.6	270	13.01	2	6.5	4.0	5.0
65	16	0.6	270	12.76	4	8.5	4.0	5.0
70	20	0.6	270	12.41	4	18.5	4.0	5.1
75	24	0.6	270	12.18	4	30.5	4.3	5.4
80	26	0.6	270	12.09	4	30.5	4.7	5.7
85	30	0.6	270	11.81	6	26.5	5.4	6.1

Tx-40

		Prestressing Strands			Harped Strand Pattern		Concrete	
Span length (ft)	**Total number (ea)**	**Size (in.)**	**Strength (f_{pu})**	**Eccentricity (in.)**	**Number (ea)**	**Height (in.)**	**Release strength (ksi)**	**28-day strength (ksi)**
40	10	0.6	270	15.60	0	0	4.0	5.0
45	10	0.6	270	15.60	0	0	4.5	5.0
50	12	0.6	270	15.60	0	0	4.0	5.0
55	12	0.6	270	15.60	0	0	4.0	5.0
60	14	0.6	270	15.60	0	0	4.0	5.0
65	14	0.6	270	15.60	0	0	4.0	5.0
70	16	0.6	270	15.35	4	6.5	4.0	5.0
75	18	0.6	270	15.16	4	8.5	4.0	5.0
80	22	0.6	270	14.87	4	24.5	4.0	5.0
85	26	0.6	270	14.68	4	36.5	4.4	5.1
90	28	0.6	270	14.60	4	36.5	4.8	5.5
95	32	0.6	270	14.23	6	36.5	5.1	5.8
100	36	0.6	270	13.93	6	36.5	5.8	6.6

Tx-46

		Prestressing Strands			Harped Strand Pattern		Concrete	
Span length (ft)	**Total number (ea)**	**Size (in.)**	**Strength (f_{pu})**	**Eccentricity (in.)**	**Number (ea)**	**Height (in.)**	**Release strength (ksi)**	**28-day strength (ksi)**
40	10	0.6	270	17.60	0	0	4.0	5.0
45	10	0.6	270	17.60	0	0	4.5	5.0
50	12	0.6	270	17.60	0	0	4.0	5.0
55	12	0.6	270	17.60	0	0	4.0	5.0
60	14	0.6	270	17.60	0	0	4.0	5.0
65	14	0.6	270	15.60	0	0	4.0	5.0
70	14	0.6	270	17.60	0	0	4.0	5.0
75	16	0.6	270	17.35	4	6.5	4.0	5.0
80	18	0.6	270	17.16	4	8.5	4.0	5.0
85	22	0.6	270	16.88	4	14.5	4.0	5.0
90	24	0.6	270	16.77	4	20.5	4.0	5.0
95	28	0.6	270	16.60	4	40.5	4.2	5.0
100	32	0.6	270	16.23	6	42.5	4.4	5.0
105	36	0.6	270	15.94	6	42.5	5.0	5.8
110	38	0.6	270	15.81	6	40.5	5.4	6.3
115	42	0.6	270	15.60	6	40.5	6.0	7.0

Tx-54

		Prestressing Strands			Harped Strand Pattern		Concrete	
Span length (ft)	**Total number (ea)**	**Size (in.)**	**Strength (f_{pu})**	**Eccentricity (in.)**	**Number (ea)**	**Height (in.)**	**Release strength (ksi)**	**28-day strength (ksi)**
45	10	0.6	270	21.01	0	0	4.0	5.0
50	12	0.6	270	21.01	0	0	4.0	5.0
55	12	0.6	270	21.01	0	0	4.0	5.0
60	12	0.6	270	21.01	0	0	4.0	5.0
65	14	0.6	270	21.01	0	0	4.0	5.0
70	14	0.6	270	21.01	0	0	4.0	5.0
75	16	0.6	270	20.76	4	6.5	4.0	5.0
80	16	0.6	270	20.76	0	0	4.0	5.0
85	18	0.6	270	20.56	4	8.5	4.0	5.0
90	20	0.6	270	20.41	4	10.5	4.0	5.0
95	22	0.6	270	20.28	4	14.5	4.0	5.0
100	26	0.6	270	20.08	6	28.5	4.0	5.0
105	30	0.6	270	19.81	6	44.5	4.0	5.0
110	32	0.6	270	19.63	6	50.5	4.1	5.0
115	36	0.6	270	19.34	6	50.5	4.7	5.5
120	38	0.6	270	19.22	6	44.5	5.2	6.1
125	42	0.6	270	19.01	6	50.5	5.6	6.6

Tx-62

		Prestressing Strands			Harped Strand Pattern		Concrete	
Span length (ft)	**Total number (ea)**	**Size (in.)**	**Strength (f_{pu})**	**Eccentricity (in.)**	**Number (ea)**	**Height (in.)**	**Release strength (ksi)**	**28-day strength (ksi)**
60	12	0.6	270	25.75	0	0	4.0	5.0
65	12	0.6	270	25.78	0	0	4.0	5.0
70	14	0.6	270	25.78	0	0	4.0	5.0
75	14	0.6	270	25.78	0	0	4.0	5.0
80	16	0.6	270	25.53	0	0	4.0	5.0
85	16	0.6	270	25.53	0	0	4.0	5.0
90	16	0.6	270	25.53	0	0	4.0	5.0
95	20	0.6	270	25.18	4	6.5	4.0	5.0
100	22	0.6	270	25.05	4	10.5	4.0	5.0
105	24	0.6	270	24.94	4	14.5	4.0	5.0
110	26	0.6	270	24.85	4	18.5	4.0	5.0
115	30	0.6	270	24.58	6	40.5	4.0	5.0
120	34	0.6	270	24.25	6	58.5	4.2	5.0
125	36	0.6	270	24.11	6	48.5	4.7	5.6
130	40	0.6	270	23.88	6	54.5	5.1	6.1
135	42	0.6	270	23.78	6	58.5	5.3	6.3

Tx-70

		Prestressing Strands			Harped Strand Pattern		Concrete	
Span length (ft)	**Total number (ea)**	**Size (in.)**	**Strength (f_{pu})**	**Eccentricity (in.)**	**Number (ea)**	**Height (in.)**	**Release strength (ksi)**	**28-day strength (ksi)**
60	10	0.6	270	29.42	0	0	4.0	5.0
65	12	0.6	270	29.42	0	0	4.0	5.0
70	14	0.6	270	29.42	0	0	4.0	5.0
75	14	0.6	270	29.42	0	0	4.0	5.0
80	14	0.6	270	29.42	0	0	4.0	5.0
85	14	0.6	270	29.42	0	0	4.0	5.0
90	14	0.6	270	29.42	0	0	4.0	5.0
95	16	0.6	270	29.17	0	0	4.0	5.0
100	18	0.6	270	28.97	0	0	4.0	5.0
105	20	0.6	270	28.82	4	6.5	4.0	5.0
110	22	0.6	270	28.69	4	10.5	4.0	5.0
115	24	0.6	270	28.58	4	14.5	4.0	5.0
120	28	0.6	270	28.42	4	26.5	4.0	5.0
125	30	0.6	270	28.22	6	36.5	4.0	5.0
130	34	0.6	270	27.89	6	64.5	4.0	5.0
135	36	0.6	270	27.75	6	64.5	4.3	5.1
140	38	0.6	270	27.63	6	52.5	4.8	5.8
145	42	0.6	270	27.42	6	64.5	5.1	6.1
150	46	0.6	270	27.07	8	64.5	5.3	6.3

A.2. Box beam

4B20

	Prestressing Strands				Debonded	Concrete	
Span length (ft)	**Total number (ea)**	**Size (in.)**	**Strength (f_{pu})**	**Eccentricity (in.)**	**Total number (ea)**	**Release strength (ksi)**	**28-day strength (ksi)**
30	6	0.6	270	7.31	0	4.0	5.0
35	6	0.6	270	7.31	0	4.0	5.0
40	8	0.6	270	7.31	0	4.0	5.0
45	10	0.6	270	7.31	0	4.0	5.0
50	12	0.6	270	7.31	0	4.0	5.0
55	14	0.6	270	7.31	0	4.0	5.0
60	18	0.6	270	7.31	2	4.0	5.0
65	20	0.6	270	7.31	4	4.0	5.8

4B28

	Prestressing Strands				Debonded	Concrete	
Span length (ft)	**Total number (ea)**	**Size (in.)**	**Strength (f_{pu})**	**Eccentricity (in.)**	**Total number (ea)**	**Release strength (ksi)**	**28-day strength (ksi)**
30	6	0.6	270	11.12	0	4.0	5.0
35	8	0.6	270	11.12	0	4.0	5.0
40	8	0.6	270	11.12	0	4.0	5.0
45	8	0.6	270	11.12	0	4.0	5.0
50	8	0.6	270	11.12	0	4.0	5.0
55	10	0.6	270	11.12	0	4.0	5.0
60	12	0.6	270	11.12	0	4.0	5.0
65	14	0.6	270	11.12	0	4.0	5.0
70	16	0.6	270	11.12	0	4.0	5.0
75	20	0.6	270	11.12	2	4.0	5.0

4B34

	Prestressing Strands				Debonded	Concrete	
Span length (ft)	**Total number (ea)**	**Size (in.)**	**Strength (f_{pu})**	**Eccentricity (in.)**	**Total number (ea)**	**Release strength (ksi)**	**28-day strength (ksi)**
30	6	0.6	270	13.58	0	4.0	5.0
35	8	0.6	270	13.58	0	4.0	5.0
40	8	0.6	270	13.58	0	4.0	5.0
45	8	0.6	270	13.58	0	4.0	5.0
50	10	0.6	270	13.58	0	4.0	5.0
55	10	0.6	270	13.58	0	4.0	5.0
60	10	0.6	270	13.58	0	4.0	5.0
65	12	0.6	270	13.58	0	4.0	5.0
70	14	0.6	270	13.58	0	4.0	5.0
75	16	0.6	270	13.58	0	4.0	5.0
80	18	0.6	270	13.58	0	4.0	5.0
85	22	0.6	270	13.58	4	4.0	5.0
90	24	0.6	270	13.58	6	4.0	5.4
95	28	0.6	270	13.58	6	4.2	5.0

4B40

	Prestressing Strands				Debonded	Concrete	
Span length (ft)	Total number (ea)	Size (in.)	Strength (f_{pu})	Eccentricity (in.)	Total number (ea)	Release strength (ksi)	28-day strength (ksi)
30	8	0.6	270	15.87	0	4.0	5.0
35	10	0.6	270	15.87	0	4.0	5.0
40	10	0.6	270	15.87	0	4.0	5.0
45	12	0.6	270	15.87	0	4.0	5.0
50	12	0.6	270	15.87	0	4.0	5.0
55	14	0.6	270	15.87	0	4.0	5.0
60	14	0.6	270	15.87	0	4.0	5.0
65	14	0.6	270	15.87	0	4.0	5.0
70	16	0.6	270	15.87	0	4.0	5.0
75	16	0.6	270	15.87	0	4.0	5.0
80	16	0.6	270	15.87	0	4.0	5.0
85	18	0.6	270	15.87	0	4.0	5.0
90	22	0.6	270	15.87	4	4.0	5.0
95	24	0.6	270	15.7	4	4.0	5.0
100	28	0.6	270	15.44	8	4.0	5.0
105	32	0.6	270	15.24	10	4.0	5.0
110	36	0.6	270	14.87	10	4.2	5.3

5B20

	Prestressing Strands				Debonded	Concrete	
Span length (ft)	**Total number (ea)**	**Size (in.)**	**Strength (f_{pu})**	**Eccentricity (in.)**	**Total number (ea)**	**Release strength (ksi)**	**28-day strength (ksi)**
30	8	0.6	270	7.38	0	4.0	5.0
35	8	0.6	270	7.38	0	4.0	5.0
40	10	0.6	270	7.38	0	4.0	5.0
45	10	0.6	270	7.38	0	4.0	5.0
50	12	0.6	270	7.38	0	4.0	5.0
55	16	0.6	270	7.38	0	4.0	5.0
60	18	0.6	270	7.38	0	4.0	5.0
65	24	0.6	270	7.38	6	4.0	5.0

5B28

	Prestressing Strands				Debonded	Concrete	
Span length (ft)	**Total number (ea)**	**Size (in.)**	**Strength (f_{pu})**	**Eccentricity (in.)**	**Total number (ea)**	**Release strength (ksi)**	**28-day strength (ksi)**
30	8	0.6	270	11.24	0	4.0	5.0
35	8	0.6	270	11.24	0	4.0	5.0
40	10	0.6	270	11.24	0	4.0	5.0
45	10	0.6	270	11.24	0	4.0	5.0
50	10	0.6	270	11.24	0	4.0	5.0
55	12	0.6	270	11.24	0	4.0	5.0
60	12	0.6	270	11.24	0	4.0	5.0
65	14	0.6	270	11.24	0	4.0	5.0
70	18	0.6	270	11.24	0	4.0	5.0
75	20	0.6	270	11.24	0	4.0	5.0

5B34

	Prestressing Strands				Debonded	Concrete	
Span length (ft)	**Total number (ea)**	**Size (in.)**	**Strength (f_{pu})**	**Eccentricity (in.)**	**Total number (ea)**	**Release strength (ksi)**	**28-day strength (ksi)**
30	8	0.6	270	13.78	0	4.0	5.0
35	8	0.6	270	13.78	0	4.0	5.0
40	10	0.6	270	13.78	0	4.0	5.0
45	10	0.6	270	13.78	0	4.0	5.0
50	10	0.6	270	13.78	0	4.0	5.0
55	12	0.6	270	13.78	0	4.0	5.0
60	12	0.6	270	13.78	0	4.0	5.0
65	12	0.6	270	13.78	0	4.0	5.0
70	14	0.6	270	13.78	0	4.0	5.0
75	16	0.6	270	13.78	0	4.0	5.0
80	18	0.6	270	13.78	0	4.0	5.0
85	22	0.6	270	13.78	0	4.0	5.0
90	24	0.6	270	13.78	0	4.0	5.0
95	28	0.6	270	13.78	4	4.0	5.0

5B40

	Prestressing Strands				Debonded	Concrete	
Span length (ft)	**Total number (ea)**	**Size (in.)**	**Strength (f_{pu})**	**Eccentricity (in.)**	**Total number (ea)**	**Release strength (ksi)**	**28-day strength (ksi)**
30	10	0.6	270	16.14	0	4.0	5.0
35	12	0.6	270	16.14	0	4.0	5.0
40	14	0.6	270	16.14	0	4.0	5.0
45	14	0.6	270	16.14	0	4.0	5.0
50	16	0.6	270	16.14	0	4.0	5.0
55	16	0.6	270	16.14	0	4.0	5.0
60	18	0.6	270	16.14	0	4.0	5.0
65	18	0.6	270	16.14	0	4.0	5.0
70	18	0.6	270	16.14	0	4.0	5.0
75	20	0.6	270	16.14	0	4.0	5.0
80	20	0.6	270	16.14	0	4.0	5.0
85	20	0.6	270	16.14	0	4.0	5.0
90	22	0.6	270	16.14	0	4.0	5.0
95	24	0.6	270	16.14	0	4.0	5.0
100	28	0.6	270	16.14	4	4.0	5.0
105	32	0.6	270	15.89	6	4.0	5.0
110	36	0.6	270	15.70	8	4.0	5.0

A.3. X-beam

4XB20

Span length (ft)	Prestressing Strands				Debonded	Concrete	
	Total number (ea)	Size (in.)	Strength (f_{pu})	Eccentricity (in.)	Total number (ea)	Release strength (ksi)	28-day strength (ksi)
40	12	0.6	270	7.03	0	4.0	5.0
45	16	0.6	270	7.03	2	4.0	5.0
50	20	0.6	270	7.03	4	4.0	5.0
55	24	0.6	270	6.86	6	4.7	5.0

4XB28

Span length (ft)	Prestressing Strands				Debonded	Concrete	
	Total number (ea)	Size (in.)	Strength (f_{pu})	Eccentricity (in.)	Total number (ea)	Release strength (ksi)	28-day strength (ksi)
45	12	0.6	270	10.64	0	4.0	5.0
50	12	0.6	270	10.64	0	4.0	5.0
55	16	0.6	270	10.64	0	4.0	5.0
60	20	0.6	270	10.64	4	4.0	5.0
65	24	0.6	270	10.48	6	4.0	5.0
70	28	0.6	270	10.21	6	4.3	5.0
75	32	0.6	270	10.02	6	5.1	5.3

4XB34

	Prestressing Strands				Debonded	Concrete	
Span length (ft)	**Total number (ea)**	**Size (in.)**	**Strength (f_{pu})**	**Eccentricity (in.)**	**Total number (ea)**	**Release strength (ksi)**	**28-day strength (ksi)**
45	12	0.6	270	13.09	0	4.0	5.0
50	12	0.6	270	13.09	0	4.0	5.0
55	14	0.6	270	13.09	0	4.0	5.0
60	16	0.6	270	13.09	0	4.0	5.0
65	18	0.6	270	13.09	2	4.0	5.0
70	22	0.6	270	13.09	4	4.0	5.0
75	26	0.6	270	12.78	6	4.0	5.0
85	36	0.6	270	12.31	10	4.6	5.0
90	40	0.6	270	12.19	12	5.0	5.4
95	46	0.6	270	11.96	14	5.8	6.1

4XB40

	Prestressing Strands				Debonded	Concrete	
Span length (ft)	**Total number (ea)**	**Size (in.)**	**Strength (f_{pu})**	**Eccentricity (in.)**	**Total number (ea)**	**Release strength (ksi)**	**28-day strength (ksi)**
45	12	0.6	270	15.68	0	4.0	5.0
50	12	0.6	270	15.68	0	4.0	5.0
55	14	0.6	270	15.68	0	4.0	5.0
60	14	0.6	270	15.68	0	4.0	5.0
65	16	0.6	270	15.68	0	4.0	5.0
70	20	0.6	270	15.68	2	4.0	5.0
75	22	0.6	270	15.68	4	4.0	5.0
80	26	0.6	270	15.38	6	4.0	5.0
85	30	0.6	270	15.15	10	4.0	5.0
90	34	0.6	270	14.98	12	4.0	5.0
95	40	0.6	270	14.78	16	4.5	5.0
100	44	0.6	270	14.68	18	4.9	5.3
105	48	0.6	270	14.43	20	5.3	6.0

5XB20

Span length (ft)	Prestressing Strands				Debonded	Concrete	
	Total number (ea)	Size (in.)	Strength (f_{pu})	Eccentricity (in.)	Total number (ea)	Release strength (ksi)	28-day strength (ksi)
40	12	0.6	270	7.03	0	4.0	5.0
45	14	0.6	270	7.03	0	4.0	5.0
50	20	0.6	270	7.03	0	4.0	5.0
55	24	0.6	270	7.03	4	4.0	5.0
60	30	0.6	270	6.90	6	4.4	5.0
65	36	0.6	270	6.59	8	4.9	5.2

5XB28

Span length (ft)	Prestressing Strands				Debonded	Concrete	
	Total number (ea)	Size (in.)	Strength (f_{pu})	Eccentricity (in.)	Total number (ea)	Release strength (ksi)	28-day strength (ksi)
40	12	0.6	270	10.63	0	4.0	5.0
45	12	0.6	270	10.63	0	4.0	5.0
50	12	0.6	270	10.63	0	4.0	5.0
55	14	0.6	270	10.63	0	4.0	5.0
60	18	0.6	270	10.63	0	4.0	5.0
65	22	0.6	270	10.63	0	4.0	5.0
70	26	0.6	270	10.63	2	4.0	5.0
75	32	0.6	270	10.38	6	4.0	5.0
80	36	0.6	270	10.19	6	4.6	5.0

5XB34

Span length (ft)	Prestressing Strands				Debonded	Concrete	
	Total number (ea)	Size (in.)	Strength (f_{pu})	Eccentricity (in.)	Total number (ea)	Release strength (ksi)	28-day strength (ksi)
40	10	0.6	270	13.11	0	4.0	5.0
45	12	0.6	270	13.11	0	4.0	5.0
50	14	0.6	270	13.11	0	4.0	5.0
55	14	0.6	270	13.11	0	4.0	5.0
60	16	0.6	270	13.11	0	4.0	5.0
65	18	0.6	270	13.11	0	4.0	5.0
70	22	0.6	270	13.11	0	4.0	5.0
75	24	0.6	270	13.11	0	4.0	5.0
80	28	0.6	270	13.11	4	4.0	5.0
85	34	0.6	270	12.75	8	4.0	5.0
90	40	0.6	270	12.51	10	4.2	5.0
95	44	0.6	270	12.38	10	4.6	5.2

5XB40

Span length (ft)	Prestressing Strands				Debonded	Concrete	
	Total number (ea)	Size (in.)	Strength (f_{pu})	Eccentricity (in.)	Total number (ea)	Release strength (ksi)	28-day strength (ksi)
40	10	0.6	270	15.70	0	4.0	5.0
45	12	0.6	270	15.70	0	4.0	5.0
50	14	0.6	270	15.70	0	4.0	5.0
55	14	0.6	270	15.70	0	4.0	5.0
60	14	0.6	270	15.70	0	4.0	5.0
65	16	0.6	270	15.70	0	4.0	5.0
70	18	0.6	270	15.70	0	4.0	5.0
75	20	0.6	270	15.70	0	4.0	5.0
80	24	0.6	270	15.70	2	4.0	5.0
85	28	0.6	270	15.70	4	4.0	5.0
90	32	0.6	270	15.45	6	4.0	5.0
95	36	0.6	270	15.26	10	4.0	5.0
100	42	0.6	270	15.04	12	4.0	5.0
105	48	0.6	270	14.87	16	4.5	5.1

A.4. U-beam

U-40

	Prestressing Strands				Debonded	Concrete	
Span length (ft)	**Total number (ea)**	**Size (in.)**	**Strength (f_{pu})**	**Eccentricity (in.)**	**Total number (ea)**	**Release strength (ksi)**	**28-day strength (ksi)**
40	10	0.6	270	14.18	0	4.0	5.0
45	12	0.6	270	14.18	0	4.0	5.0
50	12	0.6	270	14.18	0	4.0	5.0
55	14	0.6	270	14.18	0	4.0	5.0
60	14	0.6	270	14.18	0	4.0	5.0
65	14	0.6	270	14.18	0	4.0	5.0
70	18	0.6	270	14.18	0	4.0	5.0
75	20	0.6	270	14.18	2	4.0	5.0
80	24	0.6	270	14.18	4	4.0	5.0
85	29	0.6	270	14.045	8	4.0	5.0
90	33	0.6	270	13.822	10	4.0	5.1
95	37	0.6	270	13.648	12	4.0	5.8
100	41	0.6	270	13.508	15	4.0	6.5
105	45	0.6	270	13.392	17	4.8	7.2
110	49	0.6	270	13.296	19	5.4	8.0

U-54

	Prestressing Strands				Debonded	Concrete	
Span length (ft)	**Total number (ea)**	**Size (in.)**	**Strength (f_{pu})**	**Eccentricity (in.)**	**Total number (ea)**	**Release strength (ksi)**	**28-day strength (ksi)**
45	10	0.6	270	20.287	0	4.0	5.0
50	12	0.6	270	20.287	0	4.0	5.0
55	14	0.6	270	20.287	0	4.0	5.0
60	14	0.6	270	20.287	0	4.0	5.0
65	16	0.6	270	20.287	0	4.0	5.0
70	16	0.6	270	20.287	0	4.0	5.0
80	18	0.6	270	20.287	0	4.0	5.0
85	20	0.6	270	20.287	0	4.0	5.0
90	24	0.6	270	20.287	2	4.0	5.0
95	26	0.6	270	20.287	4	4.0	5.0
100	31	0.6	270	20.032	8	4.0	5.0
110	37	0.6	270	19.754	12	4.0	5.4
115	41	0.6	270	19.614	15	4.2	5.9
120	45	0.6	270	19.499	17	4.4	6.4
125	49	0.6	270	19.402	19	5.0	7.0
130	53	0.6	270	19.32	21	5.2	7.7
135	58	0.6	270	19.098	23	5.8	8.3

A.5. Decked-slab beam

6DS20

Span length (ft)	Prestressing Strands				Debonded	Concrete	
	Total number (ea)	Size (in.)	Strength (f_{pu})	Eccentricity (in.)	Total number (ea)	Release strength (ksi)	28-day strength (ksi)
30	10	0.6	270	8.31	0	4.0	5.0
35	12	0.6	270	8.31	0	4.0	5.0
40	14	0.6	270	8.31	0	4.0	5.0
45	18	0.6	270	8.31	0	4.0	5.0
50	22	0.6	270	8.31	2	4.0	5.0

6DS23

Span length (ft)	Prestressing Strands				Debonded	Concrete	
	Total number (ea)	Size (in.)	Strength (f_{pu})	Eccentricity (in.)	Total number (ea)	Release strength (ksi)	28-day strength (ksi)
30	10	0.6	270	10.02	0	4.0	5.0
35	10	0.6	270	10.02	0	4.0	5.0
40	12	0.6	270	10.02	0	4.0	5.0
45	16	0.6	270	10.02	0	4.0	5.0
50	18	0.6	270	10.02	0	4.0	5.0
55	22	0.6	270	10.02	2	4.0	5.0
60	26	0.6	270	10.02	4	4.0	5.0

7DS20

Span length (ft)	Prestressing Strands				Debonded	Concrete	
	Total number (ea)	Size (in.)	Strength (f_{pu})	Eccentricity (in.)	Total number (ea)	Release strength (ksi)	28-day strength (ksi)
30	10	0.6	270	8.73	0	4.0	5.0
35	14	0.6	270	8.73	0	4.0	5.0
40	16	0.6	270	8.73	0	4.0	5.0
45	20	0.6	270	8.73	2	4.0	5.0
50	26	0.6	270	8.73	6	4.0	5.0

7DS23

Span length (ft)	Prestressing Strands				Debonded	Concrete	
	Total number (ea)	Size (in.)	Strength (f_{pu})	Eccentricity (in.)	Total number (ea)	Release strength (ksi)	28-day strength (ksi)
30	10	0.6	270	10.53	0	4.0	5.0
35	12	0.6	270	10.53	0	4.0	5.0
40	14	0.6	270	10.53	0	4.0	5.0
45	16	0.6	270	10.53	0	4.0	5.0
50	20	0.6	270	10.53	0	4.0	5.0
55	24	0.6	270	10.53	2	4.0	5.0
60	30	0.6	270	10.40	6	4.0	5.0

8DS20

Span length (ft)	Prestressing Strands				Debonded	Concrete	
	Total number (ea)	Size (in.)	Strength (f_{pu})	Eccentricity (in.)	Total number (ea)	Release strength (ksi)	28-day strength (ksi)
30	12	0.6	270	8.92	0	4.0	5.0
35	14	0.6	270	8.92	0	4.0	5.0
40	18	0.6	270	8.92	0	4.0	5.0
45	22	0.6	270	8.92	2	4.0	5.0
50	28	0.6	270	8.92	8	4.0	5.3

8DS23

Span length (ft)	Prestressing Strands				Debonded	Concrete	
	Total number (ea)	Size (in.)	Strength (f_{pu})	Eccentricity (in.)	Total number (ea)	Release strength (ksi)	28-day strength (ksi)
30	10	0.6	270	10.76	0	4.0	5.0
35	12	0.6	270	10.76	0	4.0	5.0
40	14	0.6	270	10.76	0	4.0	5.0
45	18	0.6	270	10.76	0	4.0	5.0
50	22	0.6	270	10.76	0	4.0	5.0
55	26	0.6	270	10.76	4	4.0	5.0
60	32	0.6	270	10.51	6	4.2	5.2

A.6. Slab beam

4SB12

Span length (ft)	Prestressing Strands				Debonded	Concrete	
	Total number (ea)	Size (in.)	Strength (f_{pu})	Eccentricity (in.)	Total number (ea)	Release strength (ksi)	28-day strength (ksi)
25	6	0.6	270	3.50	0	4.0	5.0
30	8	0.6	270	3.50	0	4.0	5.0
35	10	0.6	270	3.50	0	4.0	5.0
40	14	0.6	270	3.50	0	4.0	5.0

4SB15

Span length (ft)	Prestressing Strands				Debonded	Concrete	
	Total number (ea)	Size (in.)	Strength (f_{pu})	Eccentricity (in.)	Total number (ea)	Release strength (ksi)	28-day strength (ksi)
25	6	0.6	270	5.00	0	4.0	5.0
30	6	0.6	270	5.00	0	4.0	5.0
35	8	0.6	270	5.00	0	4.0	5.0
40	12	0.6	270	5.00	0	4.0	5.0
45	14	0.6	270	5.00	2	4.0	5.0
50	18	0.6	270	5.00	4	4.0	5.0

5SB12

Span length (ft)	Prestressing Strands				Debonded	Concrete	
	Total number (ea)	Size (in.)	Strength (f_{pu})	Eccentricity (in.)	Total number (ea)	Release strength (ksi)	28-day strength (ksi)
25	8	0.6	270	3.50	0	4.0	5.0
30	10	0.6	270	3.50	0	4.0	5.0
35	14	0.6	270	3.50	0	4.0	5.0
40	18	0.6	270	3.50	0	4.0	5.0

5SB15

Span length (ft)	Prestressing Strands				Debonded	Concrete	
	Total number (ea)	Size (in.)	Strength (f_{pu})	Eccentricity (in.)	Total number (ea)	Release strength (ksi)	28-day strength (ksi)
25	8	0.6	270	5.00	0	4.0	5.0
30	8	0.6	270	5.00	0	4.0	5.0
35	10	0.6	270	5.00	0	4.0	5.0
40	14	0.6	270	5.00	0	4.0	5.0
45	18	0.6	270	5.00	2	4.0	5.0
50	24	0.6	270	5.00	8	4.0	5.0

Appendix B. Parameters for Shear Failure Evaluation Database

Author	Specimen	a/d_v	V_u	V_p	f'_c	v_u/f'_c	b_f/b_w	No. of strands at the bottom flange
Alshegeir & Ramirez	Type 1-4A	2.3	161.5	0	8.8	0.131	2.7	8
	Type 2-1A	2.2	222.0	0	9.0	0.138	3.0	12
	Type 3-1A	2.4	113.0	0	8.8	0.093	2.7	8
Kaufman & Ramirez	1-2	2.2	145.0	0	8.3	0.126	2.7	8
	1-3	2.2	10.0	0	8.4	0.087	2.7	8
	1-4	2.2	110.0	0	8.4	0.095	2.7	8
	2-1	2.4	140.0	0	9.1	0.086	3.0	13
Shahawy & Batchelor	A0-00-R-N	2.1	313.0	0	6.0	0.240	3.0	16
	A0-00-R-S	2.1	276.0	0	6.0	0.212	3.0	16
	A1-00-M-N	2.5	141.0	0	6.0	0.108	3.0	16
	A1-00-M-S	3.1	168.0	0	6.0	0.129	3.0	16
	A1-00-R/2-N	2.5	166.0	0	6.0	0.127	3.0	16
	A1-00-R/2-S	3.1	173.0	0	6.0	0.133	3.0	16
	A1-00-R-N	2.5	210.0	0	6.0	0.161	3.0	16
	A1-00-3R/2-N	2.5	207.0	0	6.0	0.159	3.0	16
	A4-00-0R1-N	2.2	93.9	0	6.0	0.072	3.0	16
	A4-00-0R1-S	2.2	97.6	0	6.0	0.075	3.0	16
	A4-00-0R2-N	1.8	100.5	0	6.0	0.077	3.0	16
	A4-00-0R2-S	1.8	105.7	0	6.0	0.081	3.0	16

Author	Specimen	a/d_v	V_u	V_p	f'_c	v_u/f'_c	b_f/b_w	No. of strands at the bottom flange
Shahawy & Batchelor	B0-00-R-N	2.5	220.0	0	6.0	0.168	3.0	16
	B0-00-R-S	3.1	206.0	0	6.0	0.157	3.0	16
	B1-00-0R-N	1.5	166.0	0	6.0	0.126	3.0	16
	B1-00-0R-S	1.3	155.0	0	6.0	0.118	3.0	16
	B1-00-R-N	1.5	245.0	0	6.0	0.187	3.0	16
	B1-00-R-S	1.3	232.0	0	6.0	0.177	3.0	16
	B1-00-2R-N	1.5	264.0	0	6.0	0.201	3.0	16
	B1-00-2R-S	1.3	247.0	0	6.0	0.188	3.0	16
	B1-00-3R-N	1.5	264.0	0	6.0	0.201	3.0	16
	B1-00-3R-S	1.3	263.0	0	6.0	0.200	3.0	16
	B1-00-2R2-N	1.5	268.0	0	6.0	0.204	3.0	16
	B1-00-2R2-S	1.3	255.0	0	6.0	0.194	3.0	16
Avendaño & Bayrak	TX28-I-L	3.0	400.1	0	13.8	0.164	4.6	36
	TX28-I-D	3.0	416.8	0	13.8	0.171	4.6	36
	TX28-II-L	3.9	370.5	0	11.4	0.184	4.6	36
	TX28-II-D	3.9	375.4	0	11.4	0.187	4.6	36
Laskar et al.	B1-N	1.6	188.9	0	10.5	0.149	2.7	12
	B1-S	1.6	173.5	0	10.5	0.137	2.7	12
	B2-N	1.6	201.1	0	10.8	0.154	2.7	12
	B2-S	1.6	234.0	0	10.8	0.180	2.7	12
	B4-S	4.6	96.8	0	10.3	0.078	2.7	12

Author	Specimen	a/d_v	V_u	V_p	f'_c	v_u/f'_c	b_f/b_w	No. of strands at the bottom flange
Llanos et al.	A2U1	2.0	296.0	0	7.2	0.142	3.3	22
	A2S1	2.0	324.0	0	7.2	0.155	3.3	22
	A1U3	4.3	256.0	0	7.2	0.123	3.3	22
	A1S3	4.3	310.0	0	7.2	0.149	3.3	22
	B1U1	0.9	344.0	17.90681	5.6	0.165	3.1	20
	B2U2	1.7	255.0	17.90681	5.6	0.120	3.1	24
	B4S2	1.7	242.0	17.90681	5.6	0.113	3.1	24
	B2U3	2.6	207.0	17.90681	5.6	0.095	3.1	24
	B1U4	3.5	180.0	17.90681	5.6	0.082	3.1	24
	B4U4	3.5	198.0	17.90681	5.6	0.091	3.1	24
Hanson & Hulsbos	G2-1	3.3	110.0	0	6.7	0.094	3.0	6
	G4-2	2.8	114.0	0	7.6	0.085	3.0	6
	G4-3	2.8	136.0	0	7.6	0.102	3.0	6
Labonte & Hamilton	S1-SCCS	2.3	147.0	0	10.0	0.085	3.0	10
	S2-SCCS	1.9	164.5	0	10.0	0.095	3.0	10
	S1-STDS	2.3	191.2	0	7.5	0.148	3.0	10
	S2-SRDS	1.9	195.1	0	7.5	0.151	3.0	10
	SS2-STDF1	1.6	260.2	0	10.6	0.103	3.0	10
Ramirez & Aguilar	13.3-5.1	3.6	179.9	0	13.3	0.098	2.7	10
	16.2-5.1	3.7	214.9	0	16.2	0.097	2.7	10

Author	Specimen	a/d_v	V_u	V_p	f'_c	v_u/f'_c	b_f/b_w	No. of strands at the bottom flange
Tawfiq	R8N	2.7	275.0	0	8.2	0.155	3.0	16
	R10N	2.7	281.0	0	10.1	0.128	3.0	16
	R12N	2.7	277.0	0	11.0	0.115	3.0	16
	2R8N	2.7	233.0	0	8.1	0.132	3.0	16
	2R10N	2.7	238.0	0	9.9	0.110	3.0	16
	2R12N	2.7	277.0	0	11.0	0.115	3.0	16
	R8S	2.3	300.0	0	8.2	0.169	3.0	16
	R10S	2.3	297.0	0	10.1	0.135	3.0	16
	R12S	2.3	274.0	0	11.0	0.114	3.0	16
	2R8S	2.3	254.0	0	8.1	0.144	3.0	16
	2R10S	2.3	243.0	0	9.9	0.113	3.0	16
	2R12S	2.3	285.0	0	11.0	0.119	3.0	16
Ramirez et al.	PC6N	3.3	79.4	0	7.0	0.073	2.7	8
	PC10N	3.4	116.9	0	6.5	0.117	2.7	8
	PC6S	3.3	104.8	0	10.1	0.067	2.7	8
	PC10S	3.4	120.0	0	10.1	0.077	2.7	8

Author	Specimen	a/d_v	V_u	V_p	f'_c	v_u/f'_c	b_f/b_w	No. of strands at the bottom flange
Garber et al.	Q-8	3.0	543.0	17.18669	11.8	0.179	4.6	52
	Q-10	3.0	570.0	17.29829	11.8	0.188	4.6	52
	Q-20A	3.0	566.0	17.18669	11.8	0.186	4.6	52
	Q-20B	3.0	555.0	17.29829	11.8	0.183	4.6	52
	Q-46	3.0	549.0	17.07509	11.8	0.181	4.6	52
Katz et al.	Tx46-1	3.3	542.0	0	7.6	0.248	4.6	24
	Tx46-2	3.3	465.0	0	6.9	0.272	4.6	30
	Tx70-1	2.5	750.0	0	10.7	0.166	4.6	28
	Tx70-2	2.6	839.0	0	12.7	0.158	4.6	42
Murray et al.	1244A-1	2.2	160.0	20.79638	6.6	0.097	3.0	10
	1244C-1	2.7	204.0	19.80932	7.2	0.118	3.0	16
	1244C-2	3.4	179.0	4.584777	7.2	0.112	3.0	16
Chehab et al.	G1T1	2.5	215.0	0	7.5	0.165	3.0	16
	G1T2	3.0	177.0	0	7.8	0.130	3.0	16
	G1T3	3.0	172.0	0	8.6	0.115	3.0	16
	G2T1	1.8	234.0	0	9.2	0.146	3.0	16
	G2T2	2.5	200.0	0	9.2	0.125	3.0	16
	G2T3	3.2	132.0	0	9.2	0.082	3.0	16

Author	Specimen	a/d_v	V_u	V_p	f'_c	v_u/f'_c	b_f/b_w	No. of strands at the bottom flange
Villamizar et al.	13.3-5.1	3.6	179.9	0	13.3	0.098	3.0	10
	16.2-5.1	3.6	214.9	0	16.2	0.096	3.0	10
	17.0-5.1	3.6	257.3	0	17.0	0.109	3.0	10
Osborn et al.	Girder6	1.5	163.6	0	7.1	0.129	3.0	12
	Girder7	1.4	261.5	0	9.3	0.151	3.0	14
Higgs et al.	1H	1.3	386.0	0	11.3	0.219	2.7	12
	2H	2.5	214.0	0	11.3	0.121	2.7	12
	4H	5.0	110.0	0	11.3	0.062	2.7	12
Langefeld	1-0.6-N	2.8	569.0	0	5.8	0.359	4.6	22
	1-0.6-S	2.6	535.0	0	5.8	0.337	4.6	22
	2-0.5-N	2.6	624.0	0	11.2	0.204	4.6	32
	2-0.5-S	2.6	400.0	0	11.2	0.131	4.6	32

Appendix C. Result for Analysis

C.1. Tx-girder

C.1.1. Tx-28

The span length of Tx-28 ranges from 40 ft to 75 ft. The total number of strands for Tx-28 proposed by TxDOT's standard design is at least ten and at most 28, of which the number of the harped strands is zero to four. The design concrete strength, f'_c, increases from 5.0 ksi to 7.8 ksi depending on the number of strands and span length. When more than 12 strands are used, v_u/f'_c is governed by the shear strength calculated using anchorage capacity. The calculated v_u/f'_c for Tx-28 exceeds the *0.18* shear stress limit ratio when the total number of strands is 12 or more, and the maximum v_u/f'_c is 0.239.

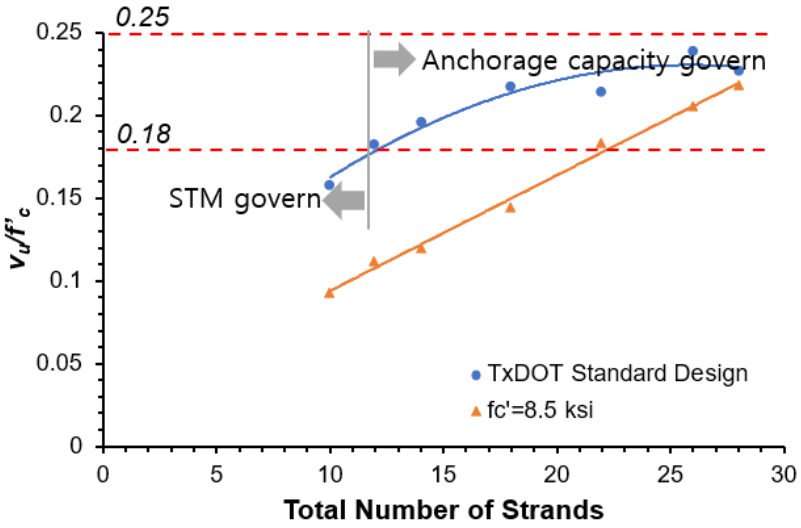

When the nodal failure and horizontal shear failure are checked, Tx-28 does not reach failure at every level of strand quantity. Tx-28 shows that the capacity for nodes and horizontal shear in all strands is always greater than the demand.

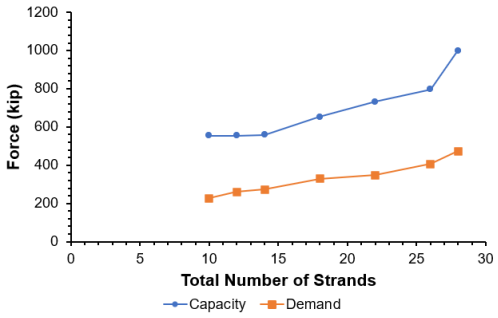

Strut-to-node interface

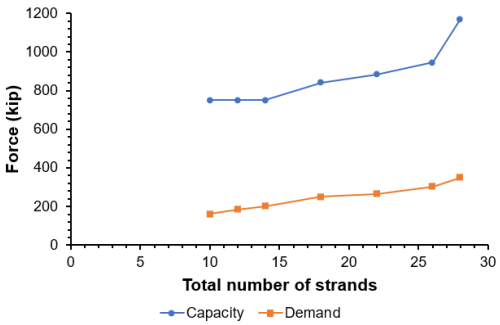

Bearing

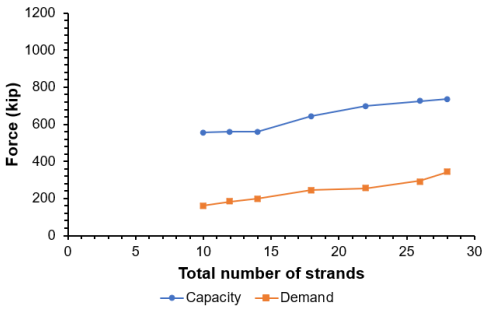

Horizontal shear

For Tx-28 with 28 strands (maximum number of strands), the tie force in the cross-section STM is 227.17 kips. The quantity of confinement required at the calculated applied load, A_{cr}, is 2.1 in^2. Still, the actual quantity of confinement is 3 in^2, so Tx-28 does not experience lateral splitting failure.

C.1.2. Tx-34

The span length of Tx-34 ranges from 40 ft to 85 ft. The total number of strands for Tx-34 proposed by TxDOT's standard design is at least ten and at most 30, of which the number of the harped strands is zero to six. The design concrete strength, f'_c, increases from 5.0 ksi to 6.1 ksi depending on the number of strands and span length. When more than 20 strands are used, v_u/f'_c is governed by the shear strength calculated using anchorage capacity. The calculated v_u/f'_c for Tx-34 exceeds the *0.18* shear stress limit ratio when the total number of strands is 16 or more, and the maximum v_u/f'_c is 0.230.

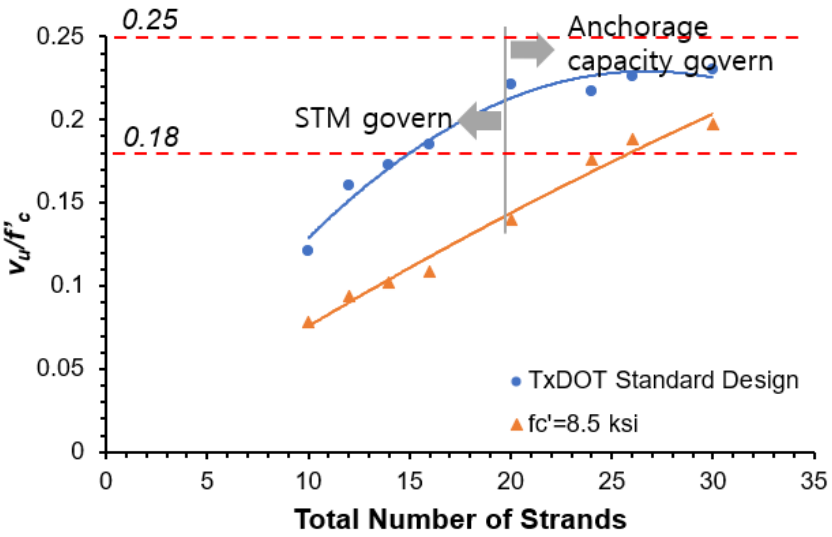

When the nodal failure and horizontal shear failure are checked, Tx-34 does not reach failure at every level of strand quantity. Tx-34 shows that the capacity for nodes and horizontal shear in all strands is always greater than the demand.

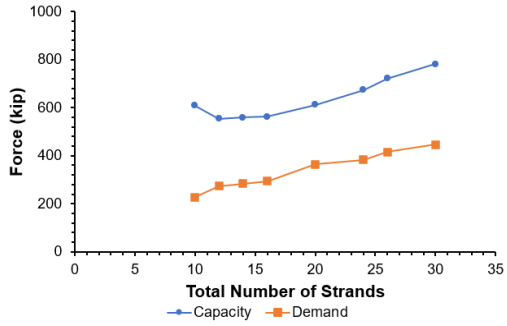

Strut-to-node interface

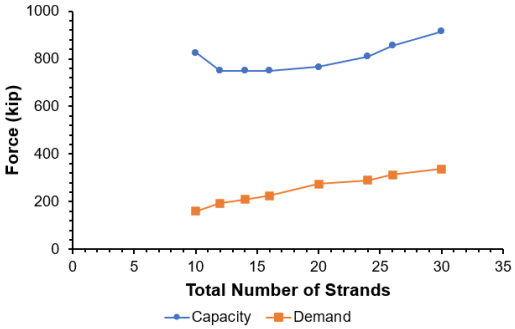

Bearing

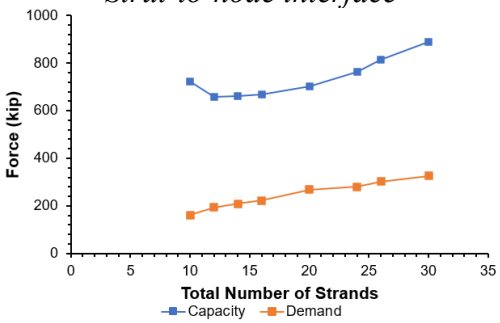

Horizontal shear

For Tx-34 with 30 strands (maximum number of strands), the tie force in the cross-section STM is 204.25 kips. The quantity of confinement required at the calculated applied load, A_{cr}, is 1.89 in^2. Still, the actual quantity of confinement is 3.0 in^2, so Tx-34 does not experience lateral splitting failure.

C.1.3. Tx-40

The span length of Tx-40 ranges from 40 ft to 100 ft. The total number of strands for Tx-40 proposed by TxDOT's standard design is at least ten and at most 36, of which the number of the harped strands is zero to six. The design concrete strength, f'_c, increases from 5.0 ksi to 6.6 ksi depending on the number of strands and span length. When more than 22 strands are used, v_u/f'_c is governed by the shear strength calculated using anchorage capacity. The calculated v_u/f'_c for Tx-40 exceeds the *0.18* shear stress limit ratio when the total number of strands is 18 or more, and the maximum v_u/f'_c is 0.241.

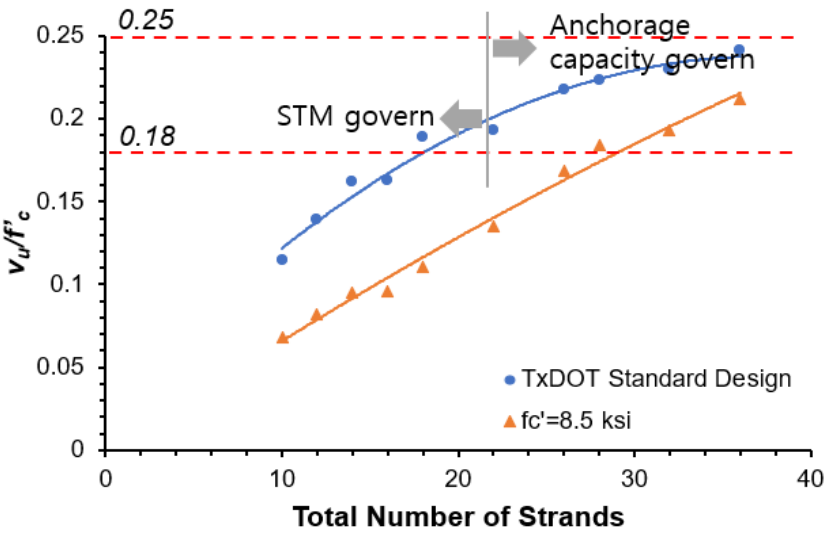

When the nodal failure and horizontal shear failure are checked, Tx-40 does not reach failure at every level of strand quantity. Tx-40 shows that the capacity for nodes and horizontal shear in all strands is always greater than the demand.

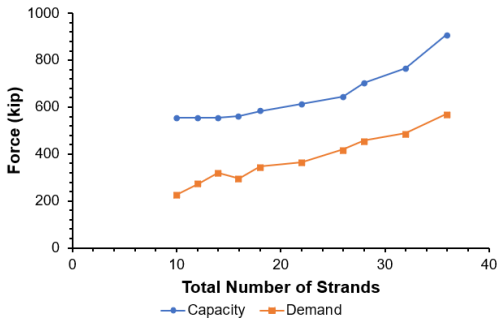

Strut-to-node interface

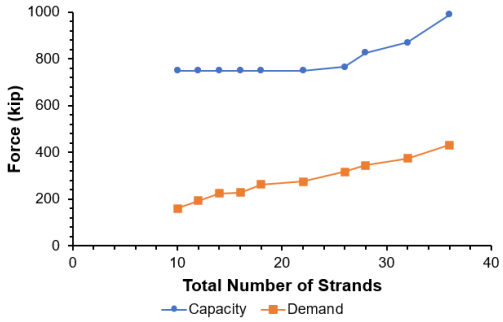

Bearing

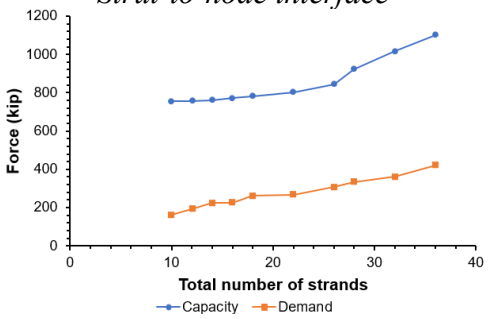

Horizontal shear

For Tx-40 with 36 strands (maximum number of strands), the tie force in the cross-section STM is 220.73 kips. The quantity of confinement required at the calculated applied load, A_{cr}, is 2.04 in^2. Still, the actual quantity of confinement is 3.6 in^2, so Tx-40 does not experience lateral splitting failure.

C.1.4. Tx-54

The span length of Tx-54 ranges from 40 ft to 125 ft. The total number of strands for Tx-54 proposed by TxDOT's standard design is at least ten and at most 42, of which the number of the harped strands is zero to six. The design concrete strength, f'_c, increases from 5.0 ksi to 6.6 ksi depending on the number of strands and span length. When more than 26 strands are used, v_u/f'_c is governed by the shear strength calculated using anchorage capacity. The calculated v_u/f'_c for Tx-54 exceeds the *0.18* shear stress limit ratio when the total number of strands is 22 or more, and the maximum v_u/f'_c is 0.232.

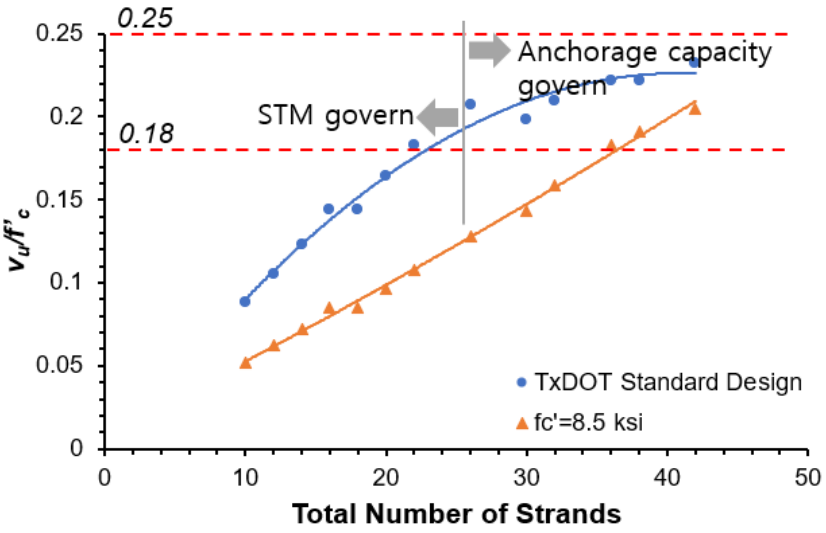

When the nodal failure and horizontal shear failure are checked, Tx-54 does not reach failure at every level of strand quantity. Tx-54 shows that the capacity for nodes and horizontal shear in all strands is always greater than the demand.

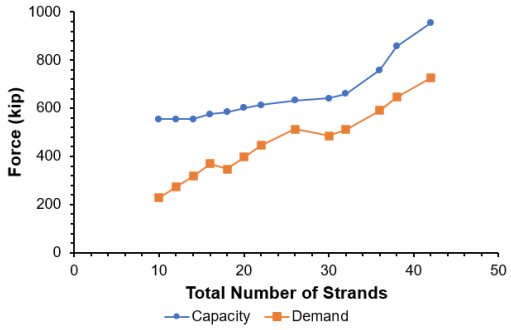

Strut-to-node interface

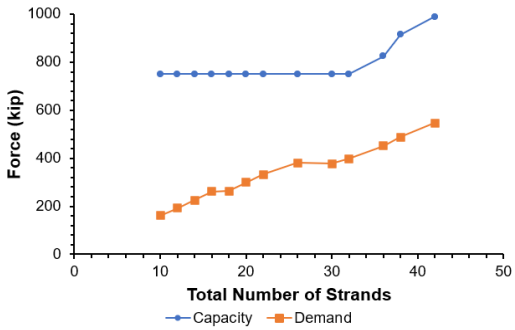

Bearing

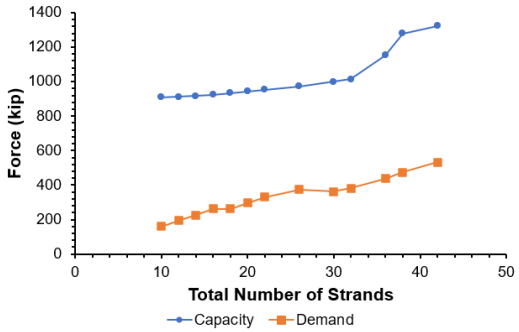

Horizontal shear

For Tx-54 with 42 strands (maximum number of strands), the tie force in the cross-section STM is 303.42 kips. The quantity of confinement required at the calculated applied load, A_{cr}, is 2.81 in^2. Still, the actual quantity of confinement is 4.8 in^2, so Tx-54 does not experience lateral splitting failure.

C.1.5. Tx-62

The span length of Tx-62 ranges from 60 ft to 135 ft. The total number of strands for Tx-62 proposed by TxDOT's standard design is at least 12 and at most 42, of which the number of the harped strands is zero to six. The design concrete strength, f'_c, increases from 5.0 ksi to 6.3 ksi depending on the number of strands and span length. When more than 26 strands are used, v_u/f'_c is governed by the shear strength calculated using anchorage capacity. The calculated v_u/f'_c for Tx-62 exceeds the *0.18* shear stress limit ratio when the total number of strands is 24 or more, and the maximum v_u/f'_c is 0.224.

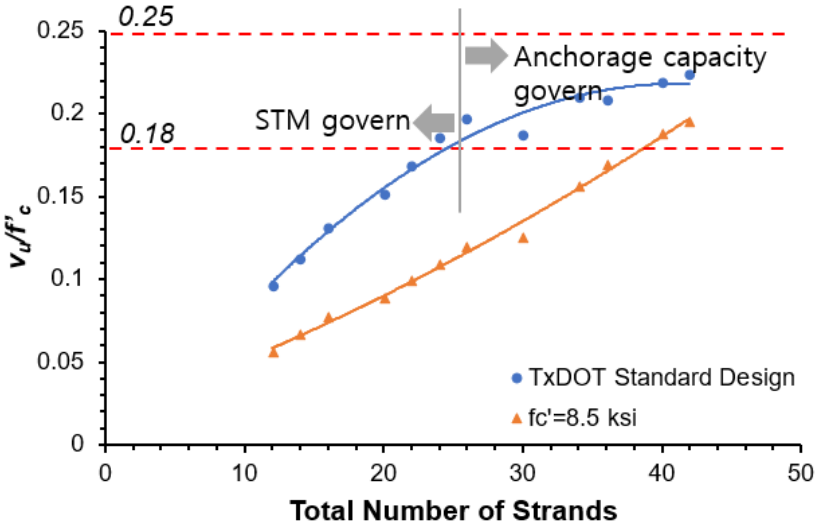

When the nodal failure and horizontal shear failure are checked, Tx-62 does not reach failure at every level of strand quantity. Tx-62 shows that the capacity for nodes and horizontal shear in all strands is always greater than the demand.

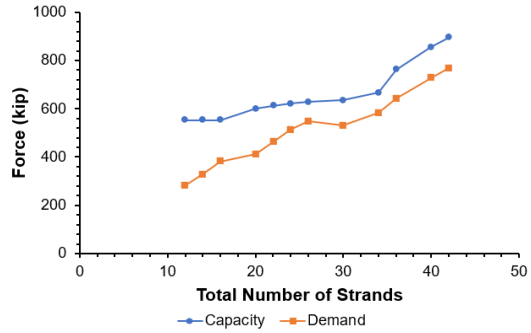

Strut-to-node interface

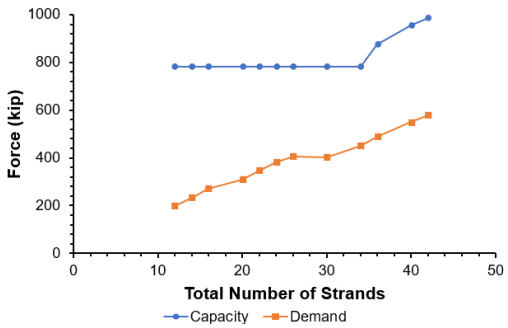

Bearing

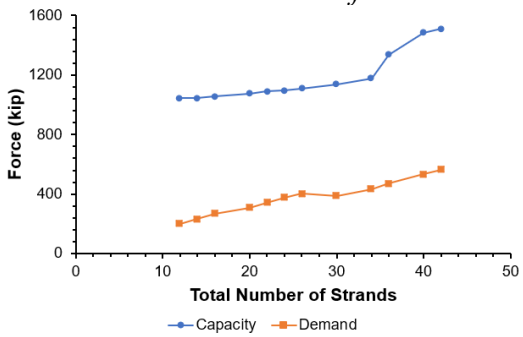

Horizontal shear

For Tx-62 with 42 strands (maximum number of strands), the tie force in the cross-section STM is 321.10 kips. The quantity of confinement required at the calculated applied load, A_{cr}, is 2.97 in^2, but the actual quantity of confinement is 6.0 in^2, so Tx-62 does not experience lateral splitting failure.

C.1.6. Tx-70

The span length of Tx-70 ranges from 60 ft to 150 ft. The total number of strands for Tx-70 proposed by TxDOT's standard design is at least 12 and at most 46, of which the number of the harped strands is zero to eight. The design concrete strength, f'_c, increases from 5.0 ksi to 6.3 ksi depending on the number of strands and span length. When more than 28 strands are used, v_u/f'_c is governed by the shear strength calculated using anchorage capacity. The calculated v_u/f'_c for Tx-70 exceeds the *0.18* shear stress limit ratio when the total number of strands is 28 or more, and the maximum v_u/f'_c is 0.217.

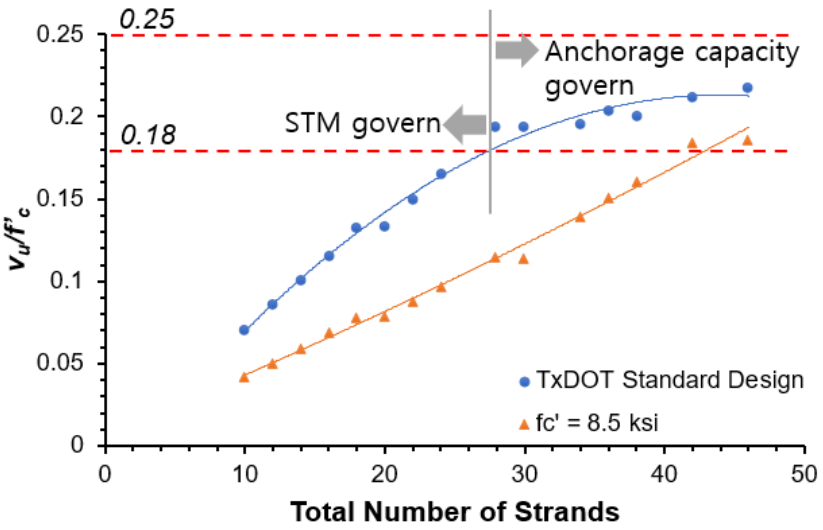

When the nodal failure and horizontal shear failure are checked, Tx-70 does not reach failure at every level of strand quantity. Tx-70 shows that the capacity for nodes and horizontal shear in all strands is always greater than the demand.

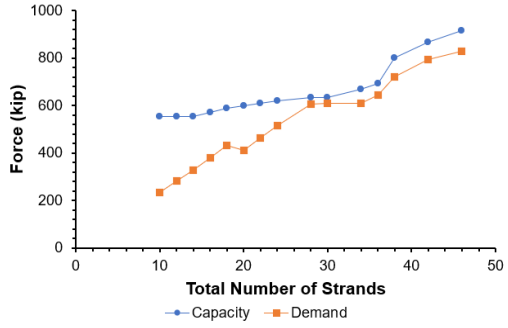

Strut-to-node interface

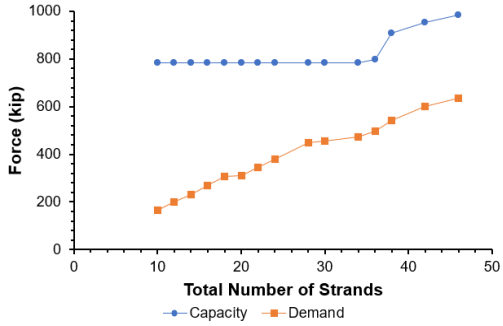

Bearing

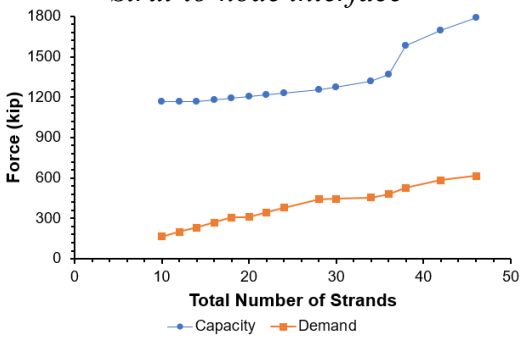

Horizontal shear

For Tx-70 with 46 strands (maximum number of strands), the tie force in the cross-section STM is 314.23 kips. The quantity of confinement required at the calculated applied load, A_{cr}, is 2.91 in^2, but the actual quantity of confinement is 6.6 in^2, so Tx-70 does not experience lateral splitting failure.

C.2. Box beam

C.2.1. 4B20

The span length of 4B20 ranges from 30 ft to 65 ft. The total number of strands for 4B20 proposed by TxDOT's standard design is at least six and at most 20, of which the number of the debonded strands is zero to four. The design concrete strength, f'_c, increases from 5.0 ksi to 5.8 ksi depending on the number of strands and span length. When more than 14 strands are used, v_u/f'_c is governed by the shear strength calculated using anchorage capacity. The calculated v_u/f'_c for 4B20 using STM and anchorage capacity cannot exceed the *0.18* shear stress limit ratio, and the maximum v_u/f'_c is 0.180.

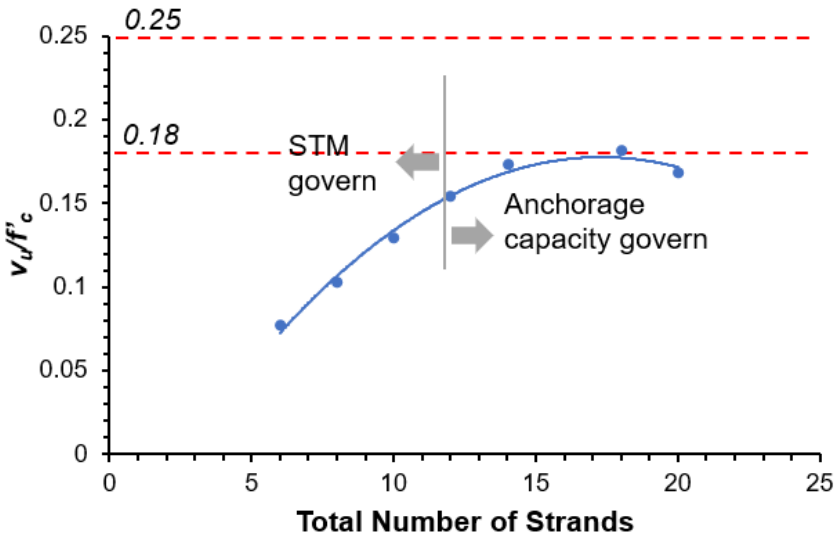

When the nodal failure and horizontal shear failure are checked, 4B20 does not reach failure at every level of strand quantity. 4B20 shows that the capacity for nodes and horizontal shear in all strands is always greater than the demand.

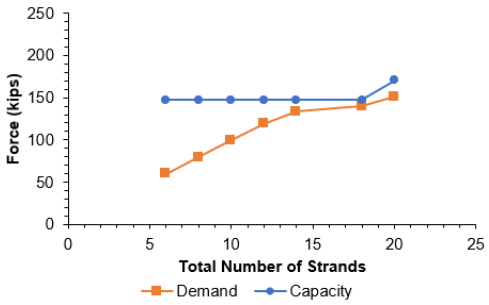

Strut-to-node interface (two plates, 30° skewed)

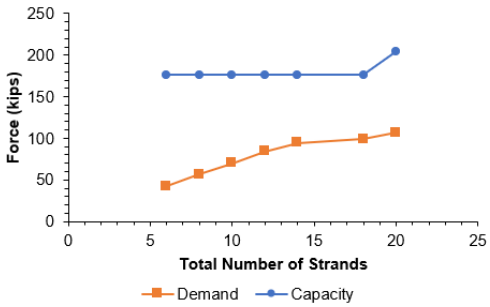

Bearing (two plates, 30° skewed)

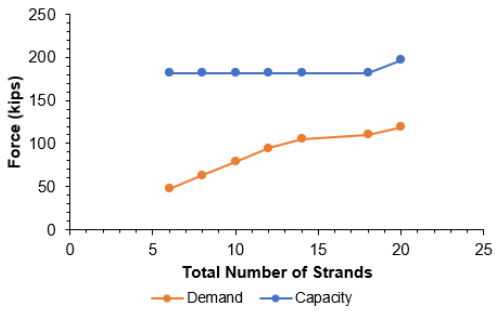

Strut-to-node interface (one plate)

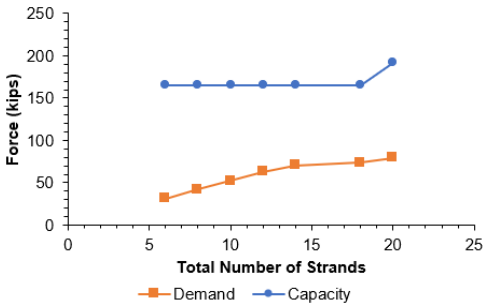

Back face (one plate)

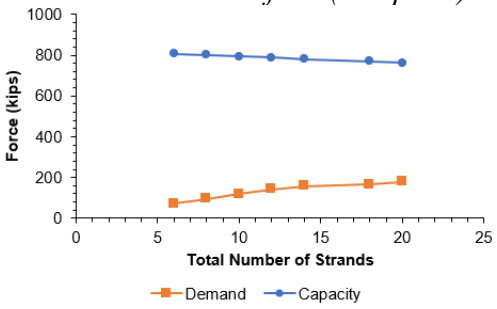

Horizontal shear

C.2.2. 4B28

The span length of 4B28 ranges from 30 ft to 75 ft. The total number of strands for 4B28 proposed by TxDOT's standard design is at least six and at most 20, of which no debonded strand. The design concrete strength, f'_c, is 5.0 ksi for overall span length. When more than 20 strands are used, v_u/f'_c is governed by the shear strength calculated using anchorage capacity. The calculated v_u/f'_c for 4B28 using STM and anchorage capacity cannot exceed the *0.18* shear stress limit ratio, and the maximum v_u/f'_c is 0.164.

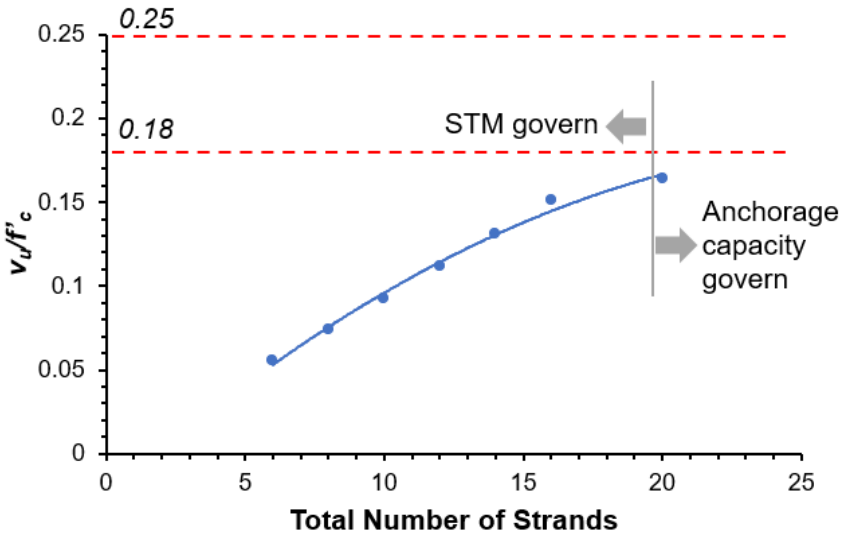

When maximum shear strength calculated by STM or anchorage capacity acts on the end of the 4B28, the strut-to-node interface for the beam end using two bearing

plates with a skewed end fails. Therefore, nodal strength governs the shear capacity for the end of the 4B28, and the maximum v_u/f'_c for the beam is decreased as 0.163.

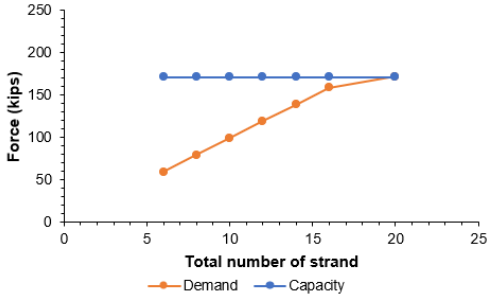

Strut-to-node interface (two plates, 30° skewed)

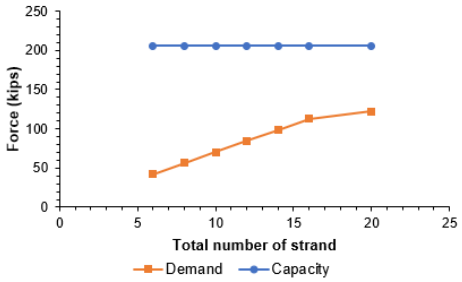

Bearing (two plates, 30° skewed)

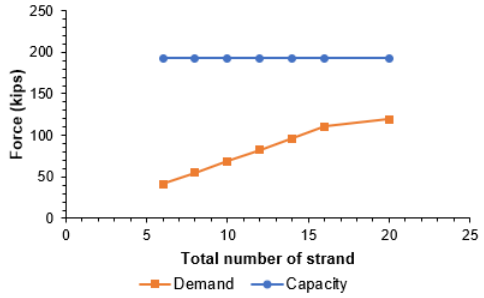

Strut-to-node interface (one plate)

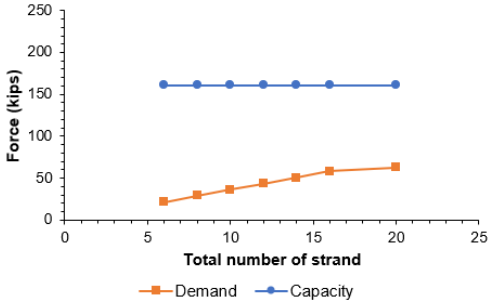

Back face (one plate)

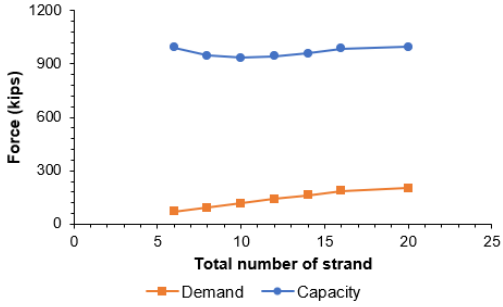

Horizontal shear

C.2.3. 5B28

The span length of 5B28 ranges from 30 ft to 75 ft. The total number of strands for 5B28 proposed by TxDOT's standard design is at least six and at most 20, of which no debonded strand. The design concrete strength, f'_c, is 5.0 ksi for overall span length. When more than 20 strands are used, v_u/f'_c is governed by the shear strength calculated using anchorage capacity. The calculated v_u/f'_c for 5B28 using STM and anchorage capacity cannot exceed the *0.18* shear stress limit ratio, and the maximum v_u/f'_c is 0.176.

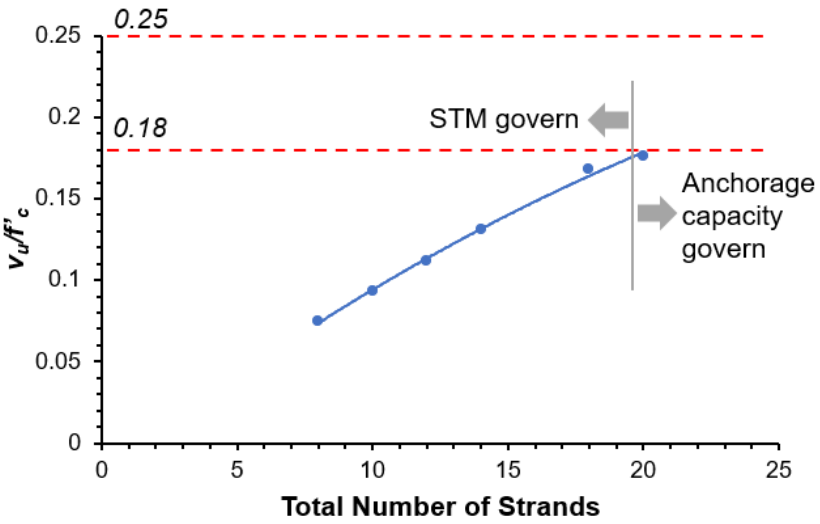

When maximum shear strength calculated by STM or anchorage capacity acts on the end of the 5B28, the strut-to-node interface for the beam end using two bearing plates with a skewed end fails. Therefore, nodal strength governs the shear capacity for the end of the 5B28, and the maximum v_u/f'_c for the beam is decreased as 0.163.

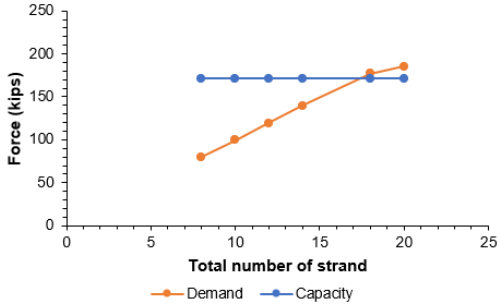

Strut-to-node interface (two plates, 30° skewed)

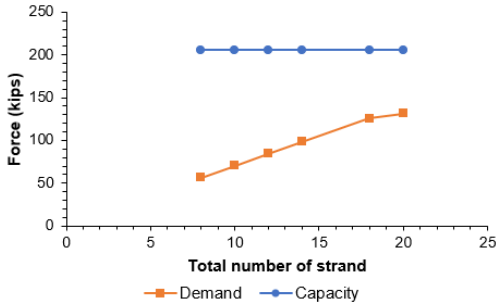

Bearing (two plates, 30° skewed)

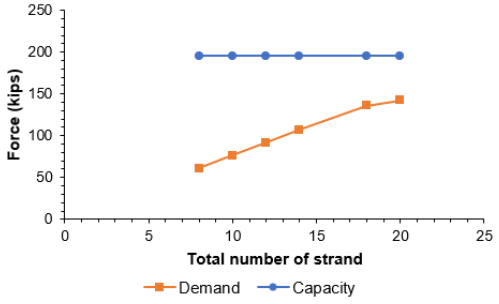

Strut-to-node interface (one plate)

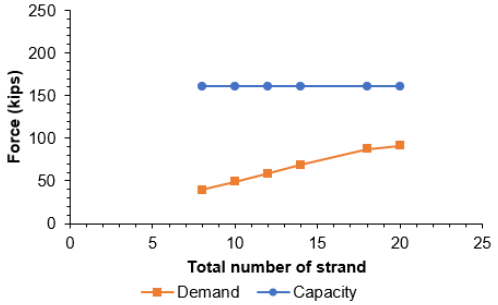

Back face (one plate)

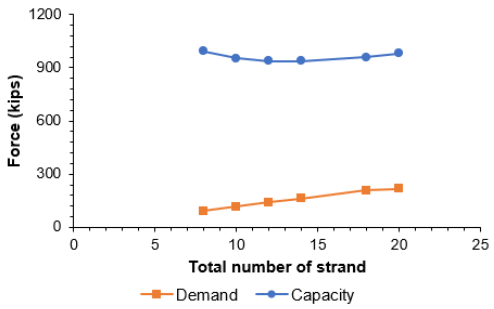

Horizontal shear

C.2.4. 4B34

The span length of 4B34 ranges from 30 ft to 95 ft. The total number of strands for 4B34 proposed by TxDOT's standard design is at least six and at most 22, of which the number of the debonded strands is zero to six. The design concrete strength, f'_c, is 5.0 ksi for overall span length. According to TxDOT's standard design, the v_u/f'_c for 4B34's end region is always governed by the shear strength calculated through STM. The calculated v_u/f'_c for 4B34 using STM and anchorage capacity cannot exceed the *0.18* shear stress limit ratio, and the maximum v_u/f'_c is 0.166.

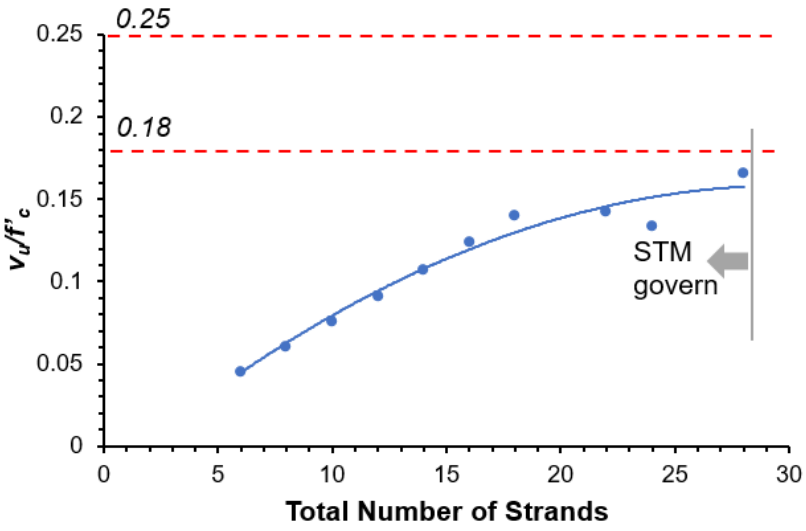

When the nodal failure and horizontal shear failure are checked, 4B34 does not reach failure at every level of strand quantity. 4B34 shows that the capacity for nodes and horizontal shear in all strands is always greater than the demand.

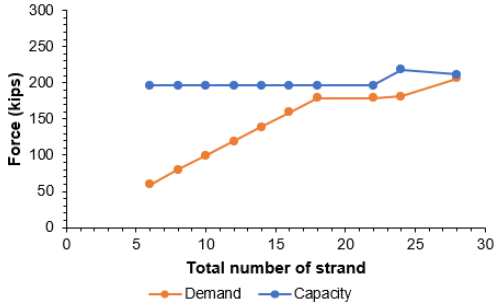

Strut-to-node interface (two plates, 30° skewed)

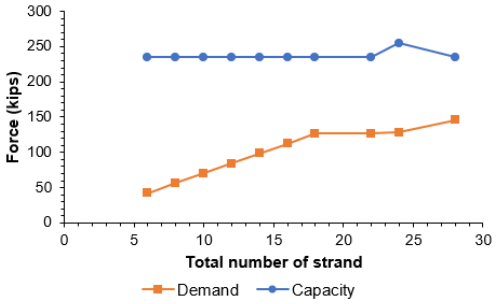

Bearing (two plates, 30° skewed)

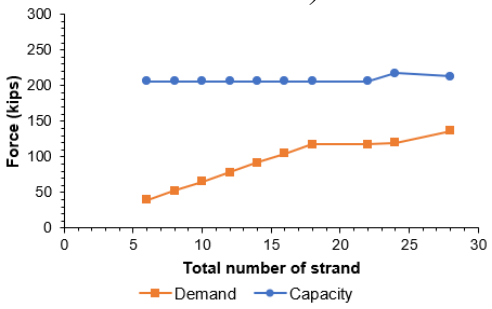

Strut-to-node interface (one plate)

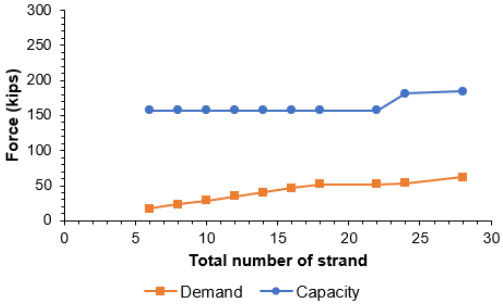

Back face (one plate)

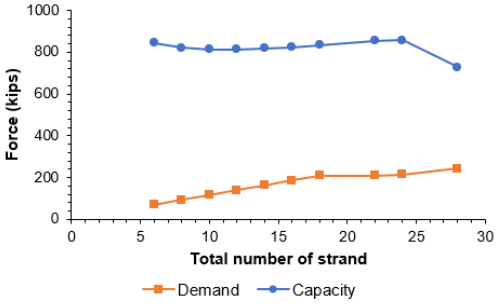

Horizontal shear

C.2.5. 5B34

The span length of 5B34 ranges from 30 ft to 95 ft. The total number of strands for 5B34 proposed by TxDOT's standard design is at least six and at most 28, of which the number of the debonded strands is zero to four. The design concrete strength, f'_c, is 5.0 ksi for overall span length. When more than 22 strands are used, v_u/f'_c is governed by the shear strength calculated using anchorage capacity. The calculated v_u/f'_c for 5B34 using STM and anchorage capacity cannot exceed the *0.18* shear stress limit ratio, and the maximum v_u/f'_c is 0.176.

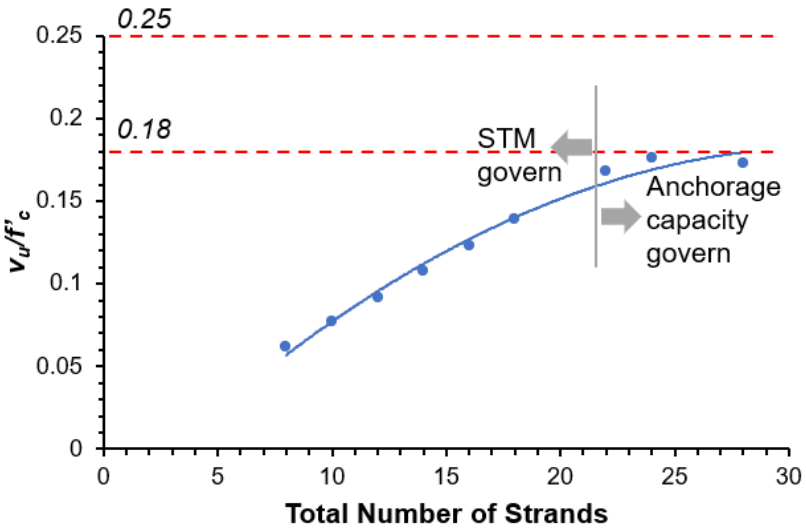

When maximum shear strength calculated by STM or anchorage capacity acts on the end of the 5B34, the strut-to-node interface for the beam end using two bearing plates with a skewed end fails. Therefore, nodal strength governs the shear capacity for the end of the 5B34, and the maximum v_u/f'_c for the beam is decreased as 0.155.

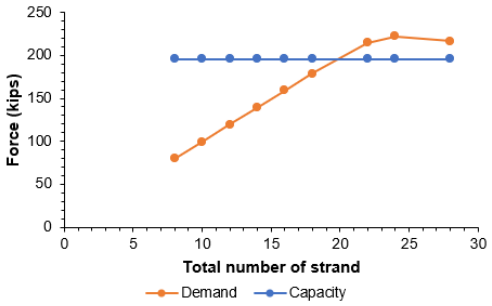

Strut-to-node interface (two plates, 30° skewed)

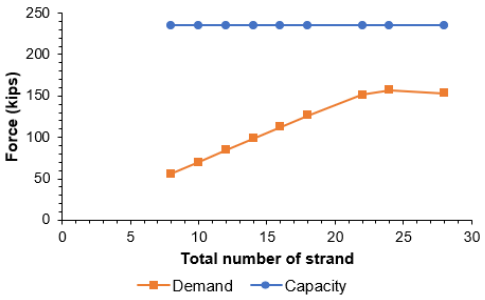

Bearing (two plates, 30° skewed)

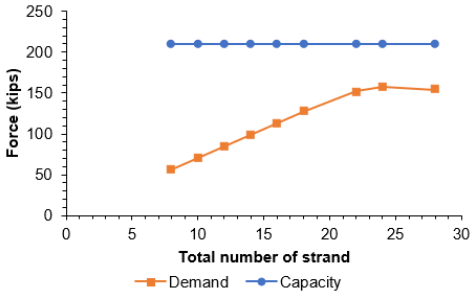

Strut-to-node interface (one plate)

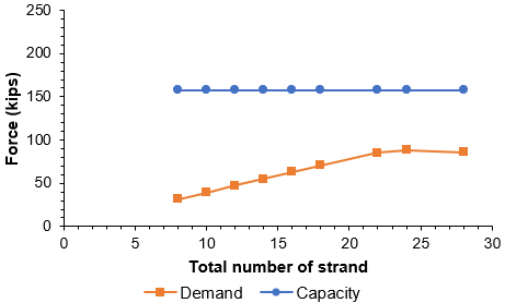

Back face (one plate)

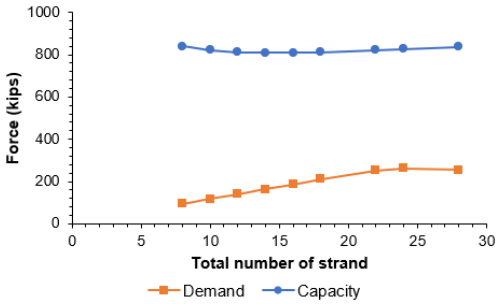

Horizontal shear

C.2.6. 4B40

The span length of 4B40 ranges from 30 ft to 110 ft. The total number of strands for 4B40 calculated by TxDOT's standard design is at least eight and at most 36, of which the number of the debonded strands is zero to 10. The design concrete strength, f'_c, increases from 5.0 ksi to 5.3 ksi depending on the number of strands and span length. When more than 32 strands are used, v_u/f'_c is governed by the shear strength calculated using anchorage capacity. The calculated v_u/f'_c for 4B40 using STM and anchorage capacity cannot exceed the *0.18* shear stress limit ratio, and the maximum v_u/f'_c is 0.170.

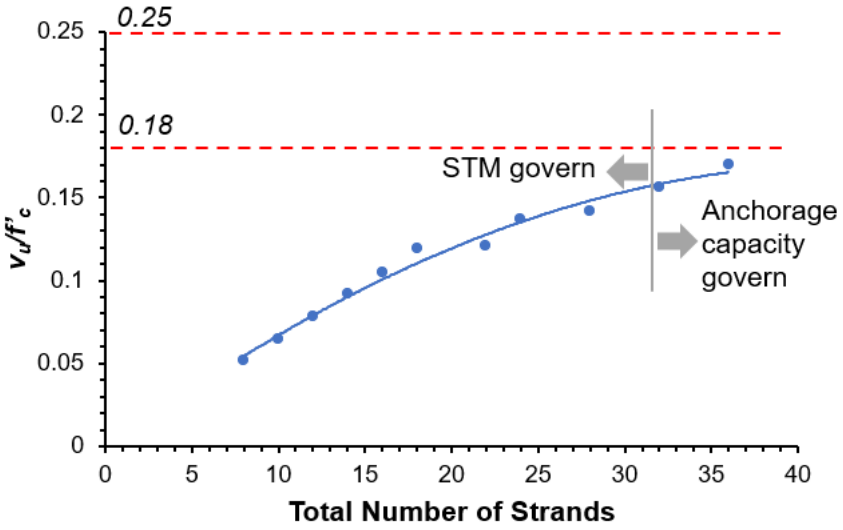

When the nodal failure and horizontal shear failure are checked, 4B40 does not reach failure at every level of strand quantity. 4B40 shows that the capacity for nodes and horizontal shear in all strands is always greater than the demand.

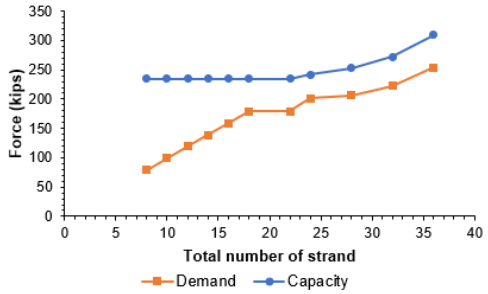

Strut-to-node interface (two plates, 30° skewed)

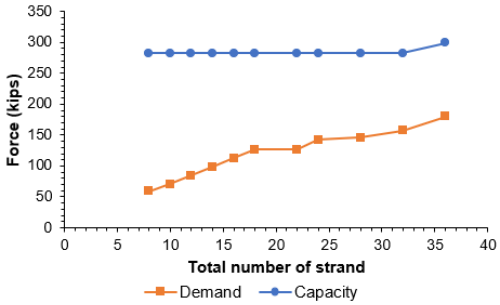

Bearing (two plates, 30° skewed)

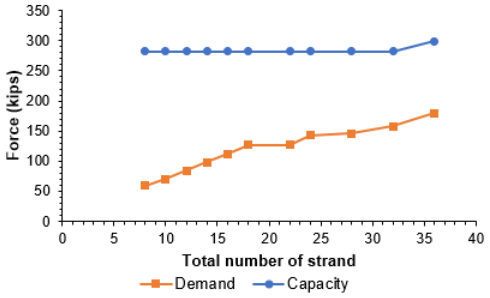

Strut-to-node interface (one plate)

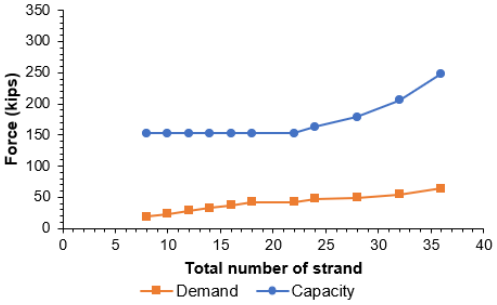

Back face (one plate)

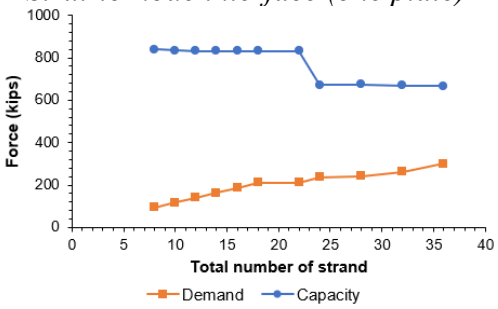

Horizontal shear

C.2.7. 5B40

The span length of 5B40 ranges from 30 ft to 110 ft. The total number of strands for 5B40 calculated by TxDOT's standard design is at least ten and at most 36, of which the number of the debonded strands is zero to eight. The design concrete strength, f'_c, is 5.0 ksi for overall span length. When more than 28 strands are used, v_u/f'_c is governed by the shear strength calculated using anchorage capacity. The calculated v_u/f'_c for 5B40 using STM and anchorage capacity cannot exceed the *0.18* shear stress limit ratio, and the maximum v_u/f'_c is 0.174.

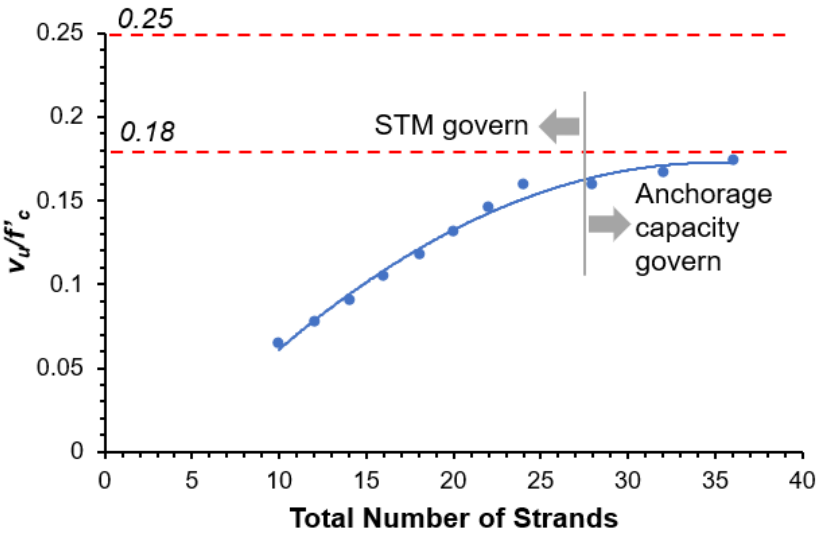

When the nodal failure and horizontal shear failure are checked, 5B40 does not reach failure at every level of strand quantity. 5B40 shows that the capacity for nodes and horizontal shear in all strands is always greater than the demand.

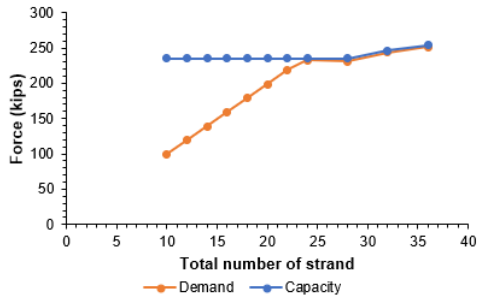

Strut-to-node interface (two plates, 30° skewed)

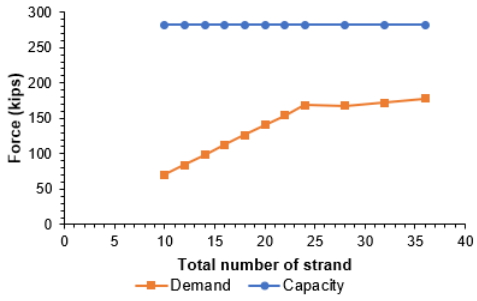

Bearing (two plates, 30° skewed)

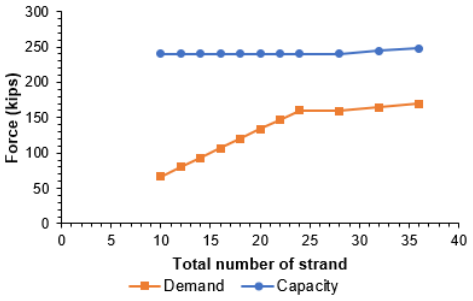

Strut-to-node interface (one plate)

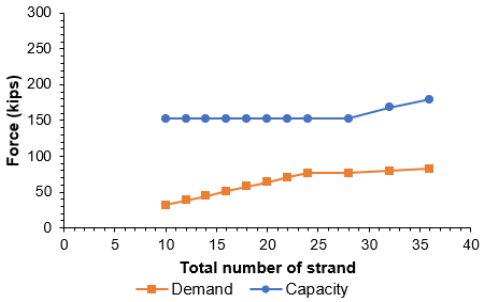

Back face (one plate)

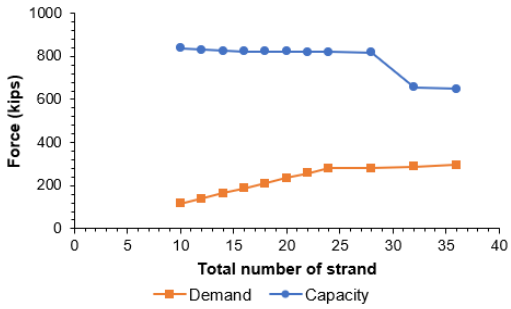

Horizontal shear

C.3. X-beam

C.3.1. 4XB20

The span length of 4XB20 ranges from 30 ft to 65 ft. The total number of strands for 4XB20 calculated by PG Super is at least 12 and at most 30, of which the number of the debonded strands is zero to six. The design concrete strength, f'_c, increases from 5.0 ksi to 5.4 ksi depending on the number of strands and span length. When more than 24 strands are used, v_u/f'_c is governed by the shear strength calculated using anchorage capacity. The calculated v_u/f'_c for 4XB20 using STM and anchorage capacity cannot exceed the *0.18* shear stress limit ratio, and the maximum v_u/f'_c is 0.178.

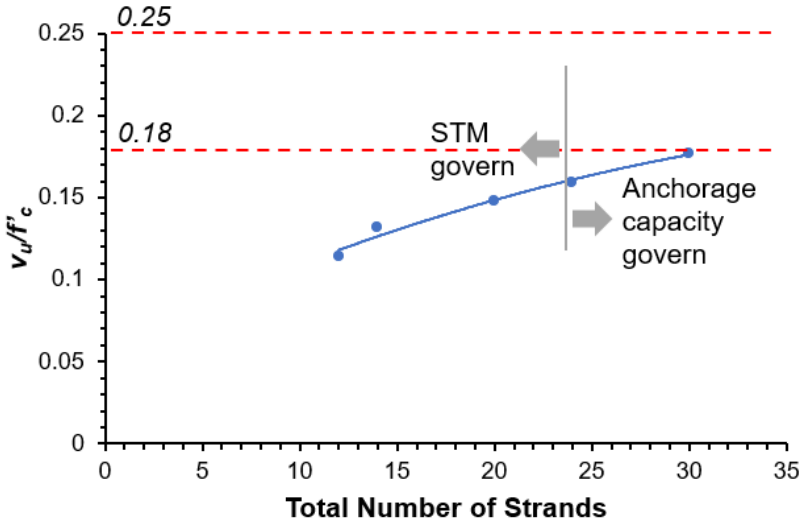

When the nodal failure and horizontal shear failure are checked, 4XB20 does not reach failure at every level of strand quantity. 4XB20 shows that the capacity for nodes and horizontal shear in all strands is always greater than the demand.

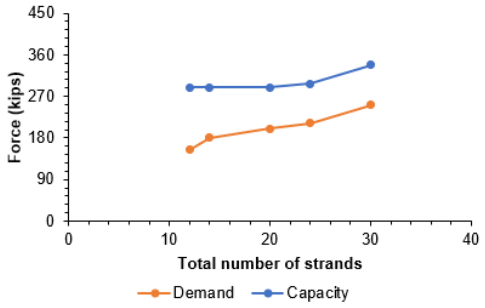

Strut-to-node interface (two plates, 30° skewed)

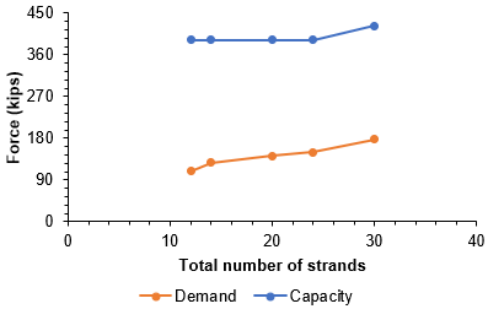

Bearing (two plates, 30° skewed)

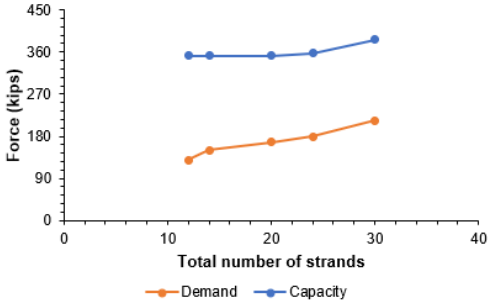

Strut-to-node interface (one plate)

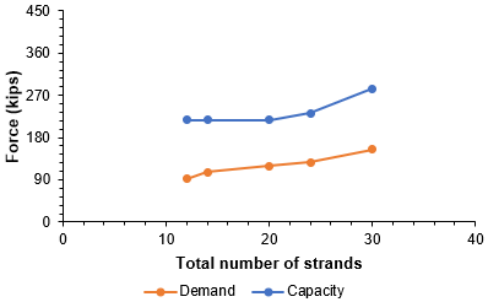

Back face (one plate)

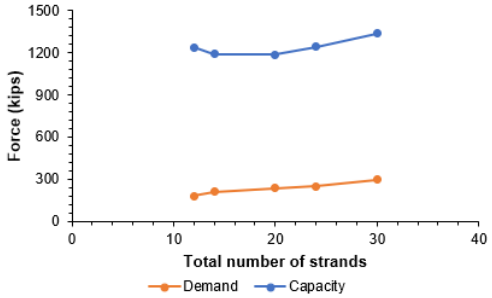

Horizontal shear

C.3.2. 5XB20

The span length of 5XB20 ranges from 30 ft to 65 ft. The total number of strands for 5XB20 proposed by TxDOT's standard design is at least 12 and at most 36, of which the number of the debonded strands is zero to eight. The design concrete strength, f'_c, increases from 5.0 ksi to 5.2 ksi depending on the number of strands and span length. When more than 20 strands are used, v_u/f'_c is governed by the shear strength calculated using anchorage capacity. The calculated v_u/f'_c for 5XB20 exceeds the *0.18* shear stress limit ratio when the total number of strands is 30 or more, and the maximum v_u/f'_c is 0.201.

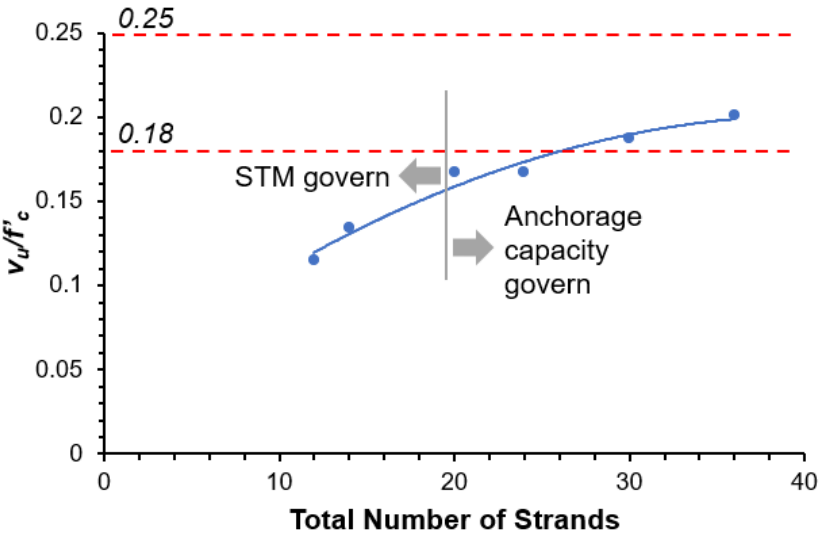

When the nodal failure and horizontal shear failure are checked, 5XB20 does not reach failure at every level of strand quantity. 5XB20 shows that the capacity for nodes and horizontal shear in all strands is always greater than the demand.

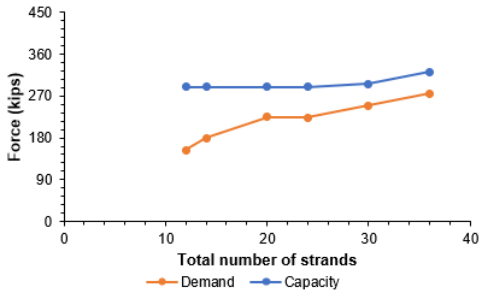

Strut-to-node interface (two plates, 30° skewed)

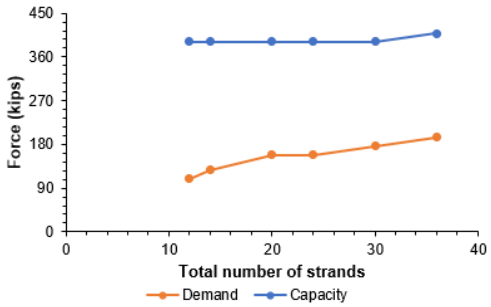

Bearing (two plates, 30° skewed)

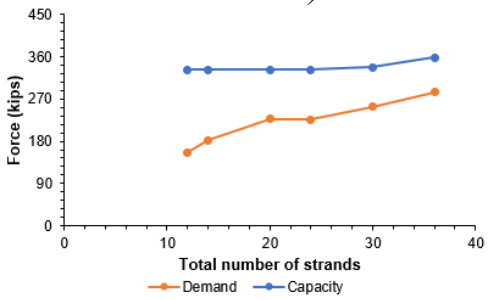

Strut-to-node interface (one plate)

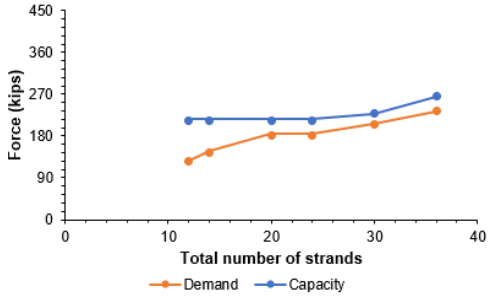

Back face (one plate)

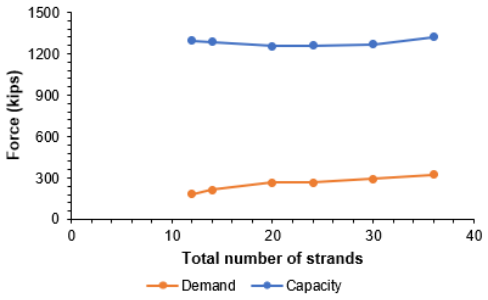

Horizontal shear

C.3.3. 4XB28

The span length of 4XB28 ranges from 45 ft to 75 ft. The total number of strands for 4XB28 calculated by PG Super is at least 12 and at most 32, of which the number of the debonded strands is zero to six. The design concrete strength, f'_c, increases from 5.0 ksi to 5.3 ksi depending on the number of strands and span length. When more than 28 strands are used, v_u/f'_c is governed by the shear strength calculated using anchorage capacity. The calculated v_u/f'_c for 4XB28 exceeds the *0.18* shear stress limit ratio when the total number of strands is 32 or more, and the maximum v_u/f'_c is 0.186.

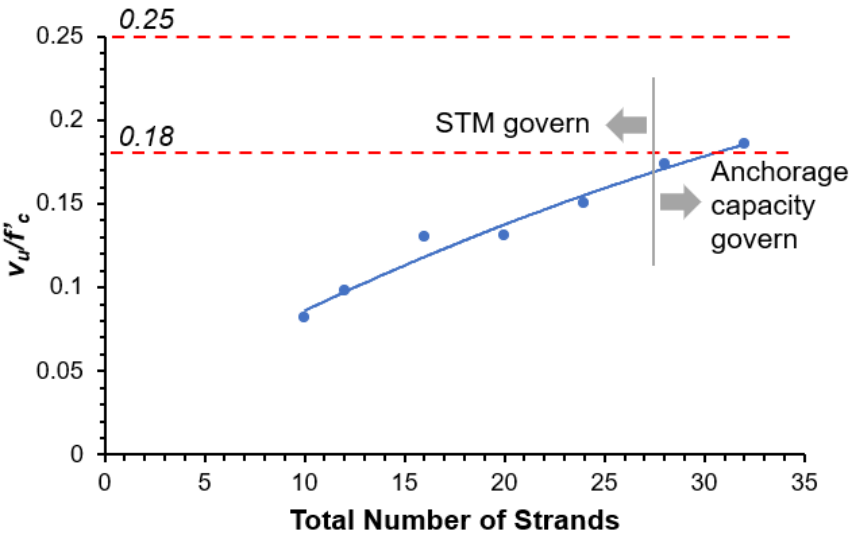

When the nodal failure and horizontal shear failure are checked, 4XB28 does not reach failure at every level of strand quantity. 4XB28 shows that the capacity for nodes and horizontal shear in all strands is always greater than the demand.

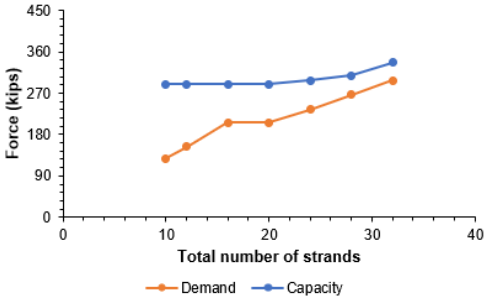

Strut-to-node interface (two plates, 30° skewed)

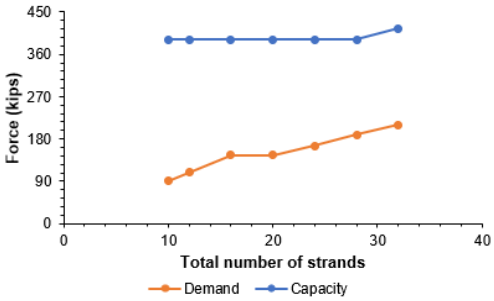

Bearing (two plates, 30° skewed)

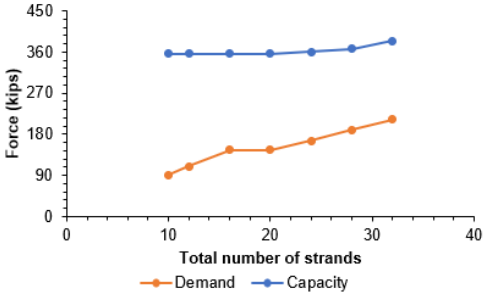

Strut-to-node interface (one plate)

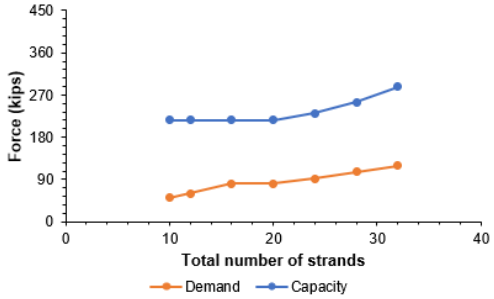

Back face (one plate)

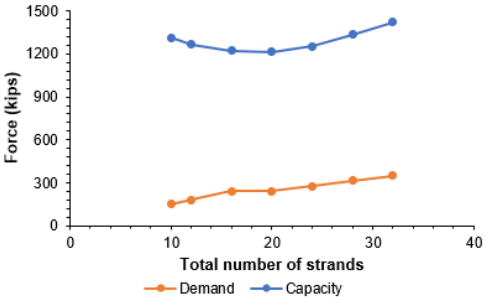

Horizontal shear

C.3.4. 4XB34

The span length of 4XB34 ranges from 45 ft to 95 ft. The total number of strands for 4XB34 calculated by PG Super is at least 12 and at most 46, of which the number of the debonded strands is zero to 14. The design concrete strength, f'_c, increases from 5.0 ksi to 6.1 ksi depending on the number of strands and span length. When more than 36 strands are used, v_u/f'_c is governed by the shear strength calculated using anchorage capacity. The calculated v_u/f'_c for 4XB34 using STM and anchorage capacity cannot exceed the *0.18* shear stress limit ratio, and the maximum v_u/f'_c is 0.176.

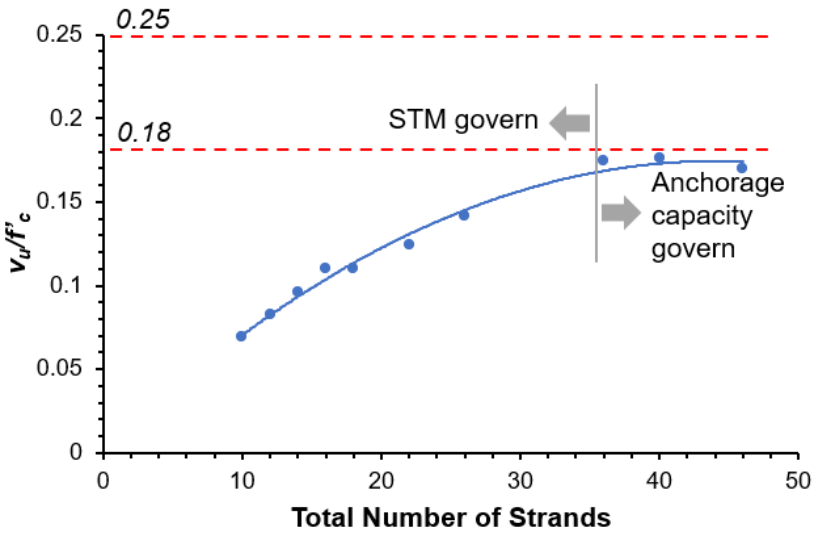

When the nodal failure and horizontal shear failure are checked, 4XB34 does not reach failure at every level of strand quantity. 4XB34 shows that the capacity for nodes and horizontal shear in all strands is always greater than the demand.

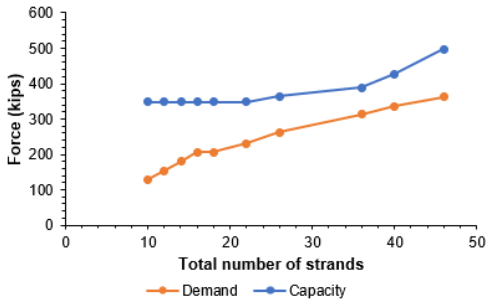

Strut-to-node interface (two plates, 30° skewed)

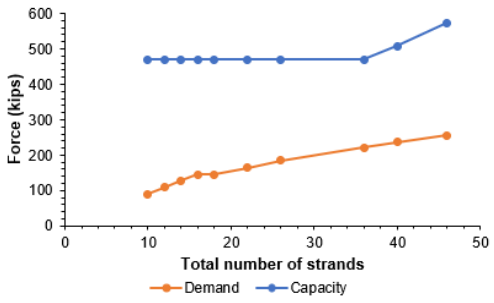

Bearing (two plates, 30° skewed)

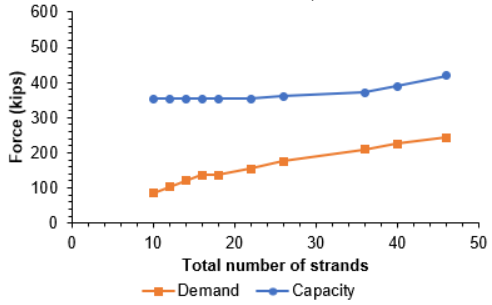

Strut-to-node interface (one plate)

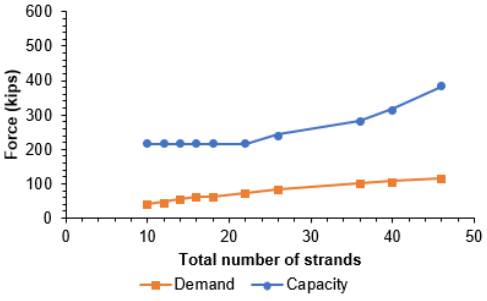

Back face (one plate)

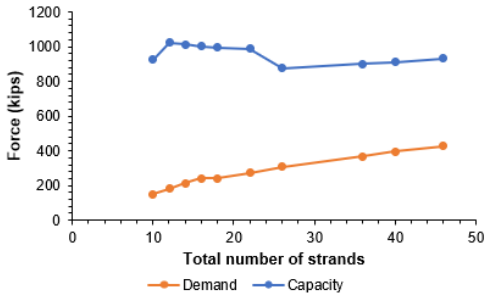

Horizontal shear

C.3.5. 5XB34

The span length of 5XB34 ranges from 40 ft to 95 ft. The total number of strands for 5XB34 proposed by TxDOT's standard design is at least ten and at most 44, of which the number of the debonded strands is zero to eight. The design concrete strength, f'_c, increases from 5.0 ksi to 5.2 ksi depending on the number of strands and span length. When more than 28 strands are used, v_u/f'_c is governed by the shear strength calculated using anchorage capacity. The calculated v_u/f'_c for 5XB34 exceeds the *0.18* shear stress limit ratio when the total number of strands is 40 or more, and the maximum v_u/f'_c is 0.201.

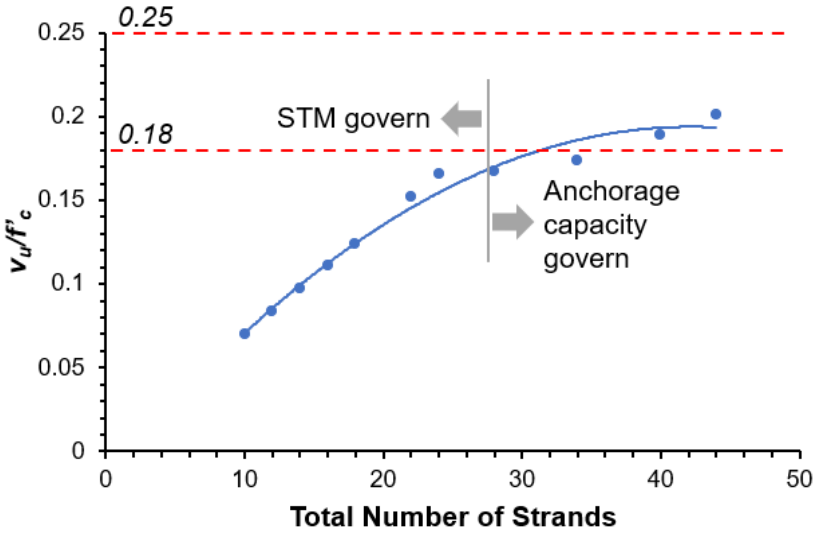

When the nodal failure and horizontal shear failure are checked, 5XB34 does not reach failure at every level of strand quantity. 5XB34 shows that the capacity for nodes and horizontal shear in all strands is always greater than the demand.

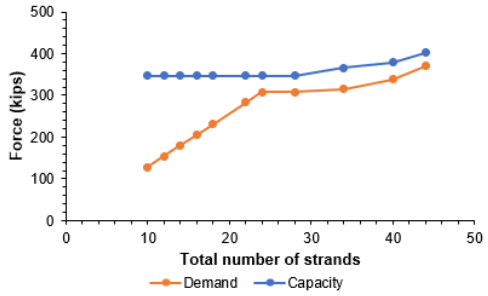

Strut-to-node interface (two plates, 30° skewed)

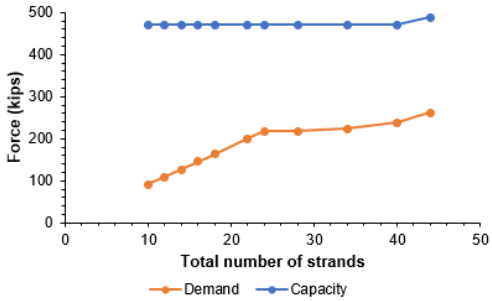

Bearing (two plates, 30° skewed)

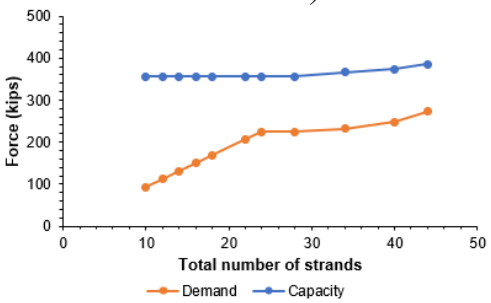

Strut-to-node interface (one plate)

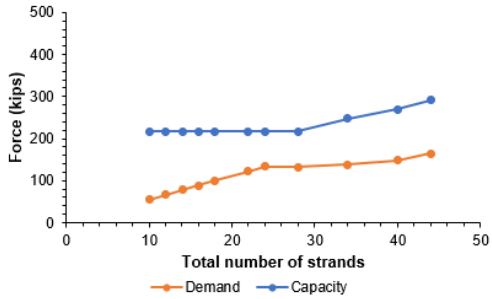

Back face (one plate)

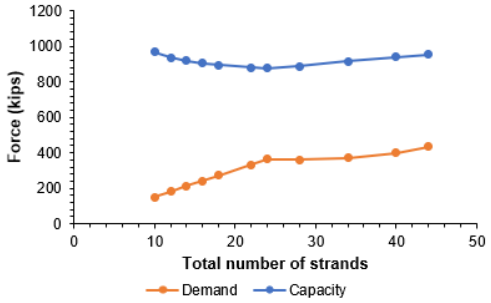

Horizontal shear

C.3.6. 4XB40

The span length of 4XB40 ranges from 45 ft to 105 ft. The total number of strands for 4XB40 calculated by PG Super is at least 12 and at most 48, of which the number of the debonded strands is zero to 20. The design concrete strength, f'_c, increases from 5.0 ksi to 6.0 ksi depending on the number of strands and span length. When more than 40 strands are used, v_u/f'_c is governed by the shear strength calculated using anchorage capacity. The calculated v_u/f'_c for 4XB40 using STM and anchorage capacity cannot exceed the *0.18* shear stress limit ratio, and the maximum v_u/f'_c is 0.157.

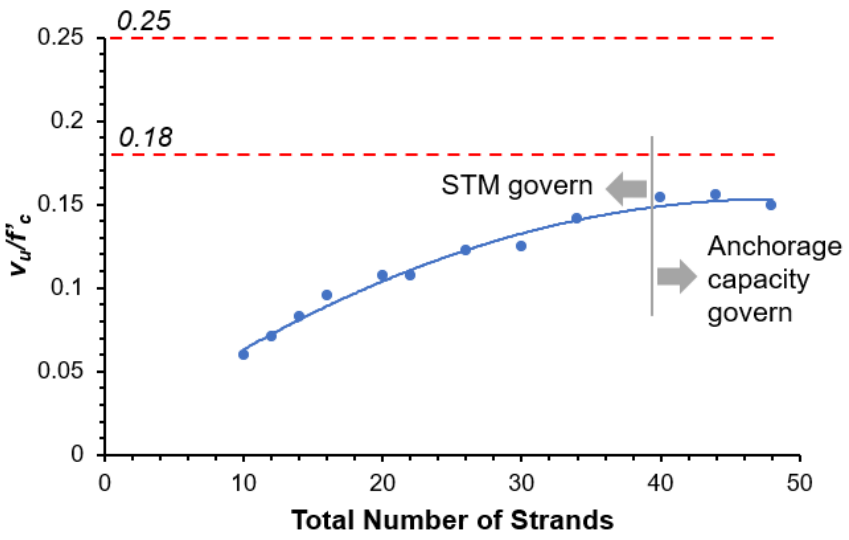

When the nodal failure and horizontal shear failure are checked, 4XB40 does not reach failure at every level of strand quantity. 4XB40 shows that the capacity for nodes and horizontal shear in all strands is always greater than the demand.

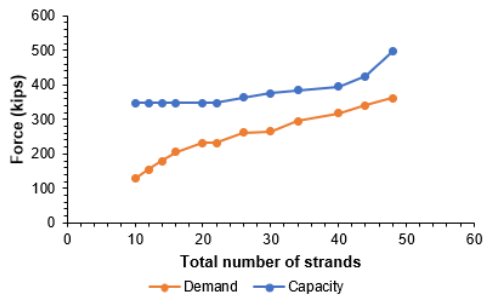

Strut-to-node interface (two plates, 30° skewed)

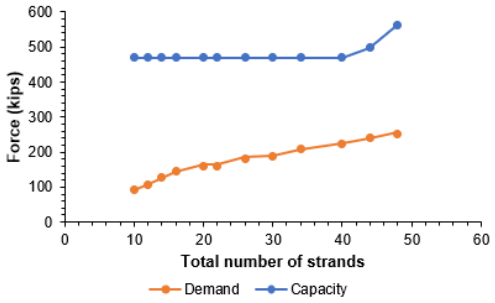

Bearing (two plates, 30° skewed)

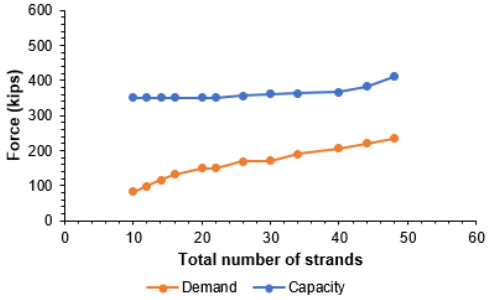

Strut-to-node interface (one plate)

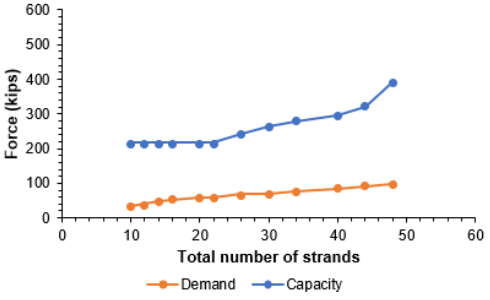

Back face (one plate)

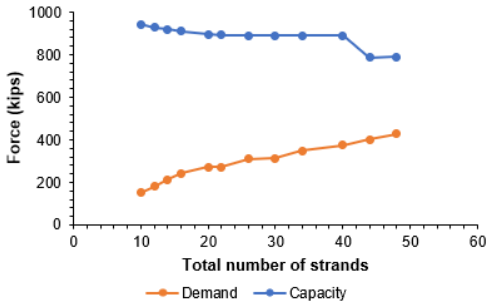

Horizontal shear

C.3.7. 5XB40

The span length of 5XB40 ranges from 40 ft to 105 ft. The total number of strands for 5XB40 proposed by TxDOT's standard design is at least ten and at most 48, of which the number of the debonded strands is zero to 16. The design concrete strength, f'_c, increases from 5.0 ksi to 5.1 ksi depending on the number of strands and span length. When more than 36 strands are used, v_u/f'_c is governed by the shear strength calculated using anchorage capacity. The calculated v_u/f'_c for 5XB40 using STM and anchorage capacity cannot exceed the *0.18* shear stress limit ratio, and the maximum v_u/f'_c is 0.179.

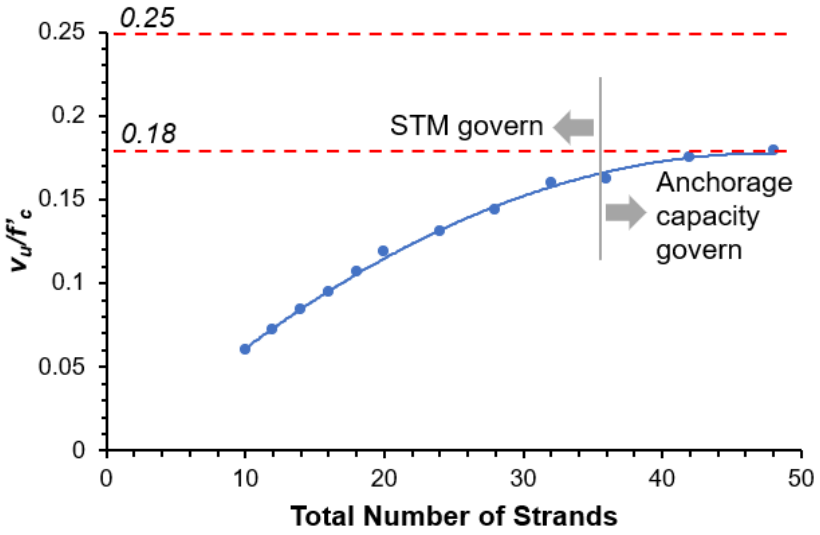

When the nodal failure and horizontal shear failure are checked, 5XB40 does not reach failure at every level of strand quantity. 5XB40 shows that the capacity for nodes and horizontal shear in all strands is always greater than the demand.

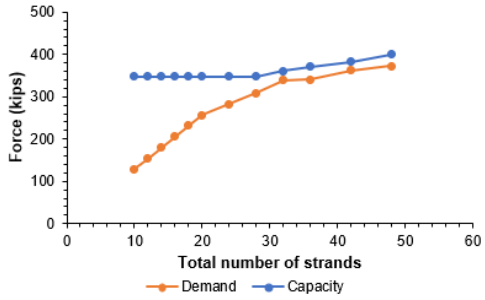

Strut-to-node interface (two plates, 30° skewed)

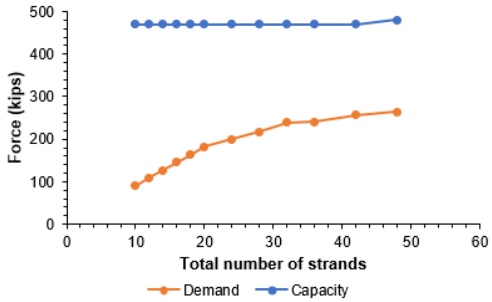

Bearing (two plates, 30° skewed)

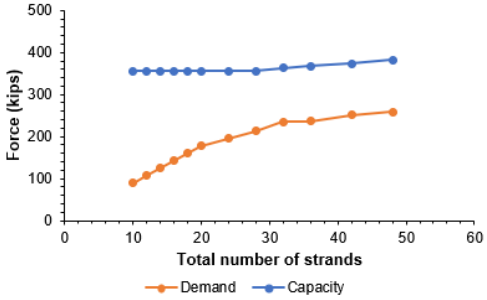

Strut-to-node interface (one plate)

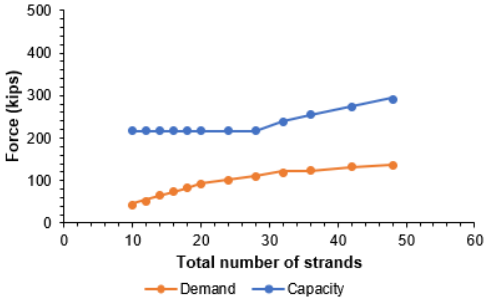

Back face (one plate)

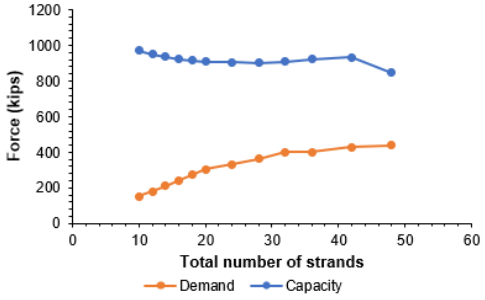

Horizontal shear

C.4. U-beam

C.4.1. U-54

The span length of U-54 ranges from 45 ft to 135 ft. The total number of strands for U-54 calculated by PG Super is at least ten and at most 58, of which the number of the debonded strands is zero to 23. The design concrete strength, f'_c, increases from 5.0 ksi to 8.3 ksi depending on the number of strands and span length. The v_u/f'_c for U-54's end region, per TxDOT's standard design, is governed by the shear strength calculated through STM for every number of strands are used. The calculated v_u/f'_c for U-54 using STM and anchorage capacity cannot exceed the *0.18* shear stress limit ratio, and the maximum v_u/f'_c is 0.143.

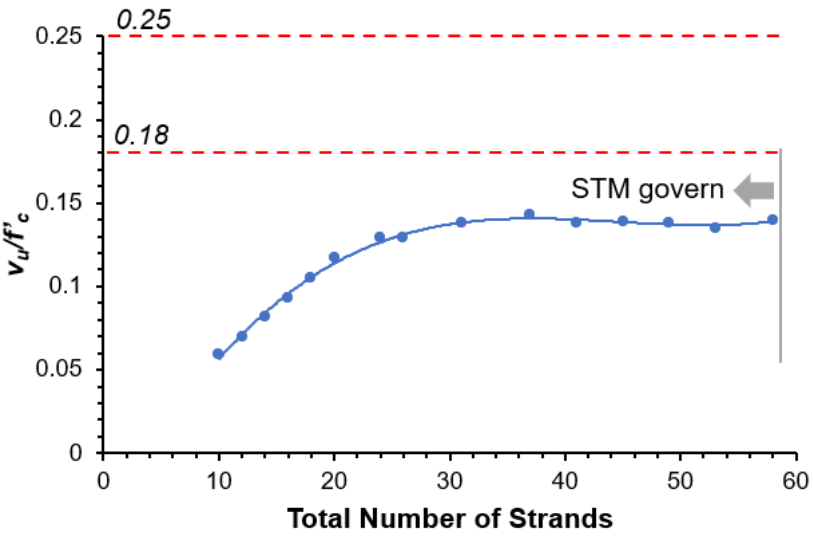

When the nodal failure and horizontal shear failure are checked, U-54 does not reach failure at every level of strand quantity. U-54 shows that the capacity for nodes and horizontal shear in all strands is always greater than the demand.

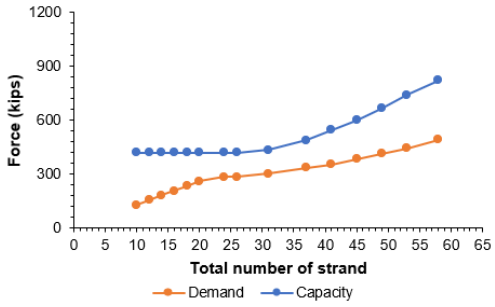

Strut-to-node interface (two plates, 60° skewed)

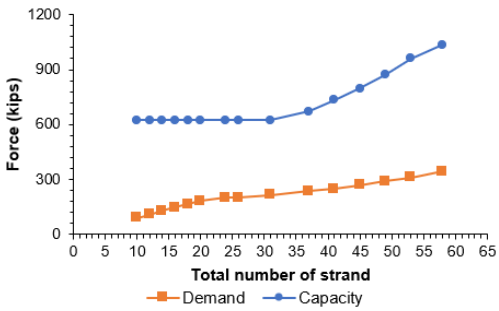

Bearing (two plates, 60° skewed)

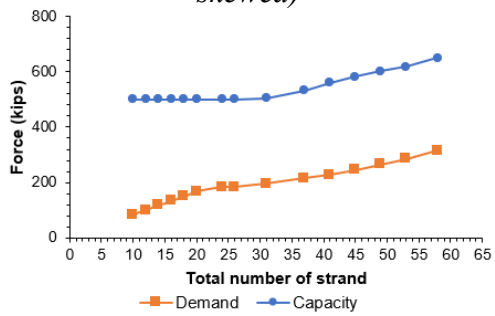

Strut-to-node interface (one plate)

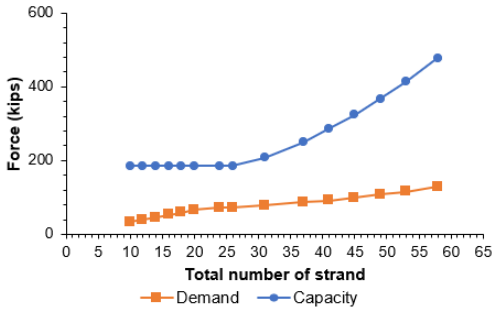

Back face (one plate)

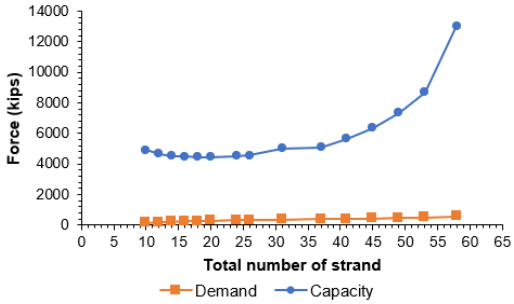

Horizontal shear

C.5. Decked-slab beam

C.5.1. 6DS20

The span length of 6DS20 ranges from 30 ft to 50 ft. The total number of strands for 6DS20 proposed by TxDOT's standard design is at least ten and at most 22, of which the number of the debonded strands is zero to two. The design concrete strength is 5.0 ksi for overall span length. When more than 12 strands are used, v_u/f'_c is governed by the shear strength calculated using anchorage capacity. The calculated v_u/f'_c for 6DS20 exceeds the *0.18* shear stress limit ratio when the total number of strands is 14 or more, and the maximum v_u/f'_c is 0.232.

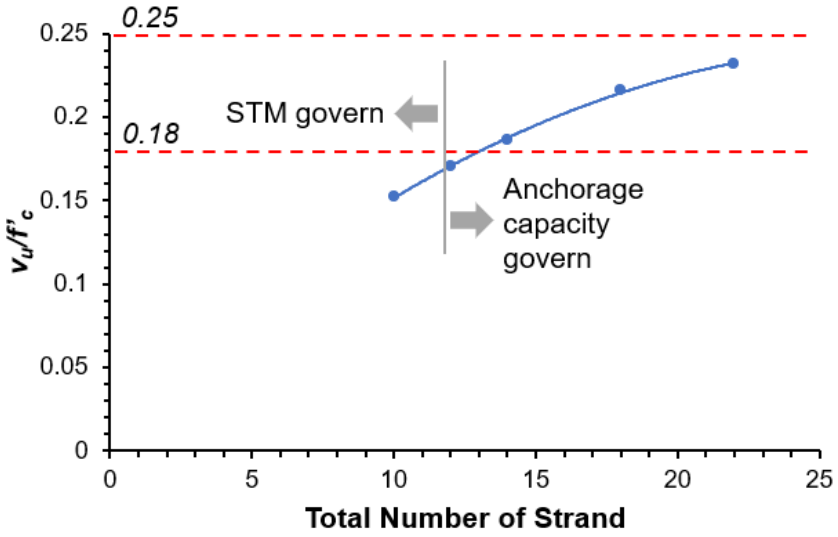

When the nodal failure and horizontal shear failure are checked, 6DS20 does not reach failure at every level of strand quantity. 6DS20 shows that the capacity for nodes and horizontal shear in all strands is always greater than the demand.

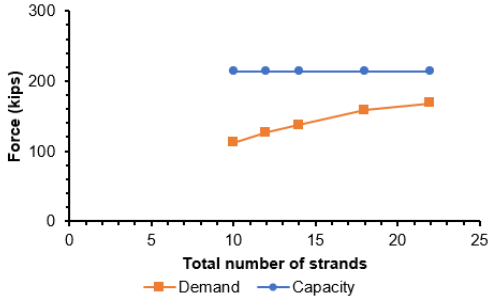

Strut-to-node interface (two plates, 30° skewed)

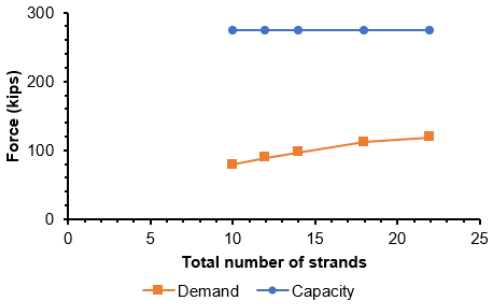

Bearing (two plates, 30° skewed)

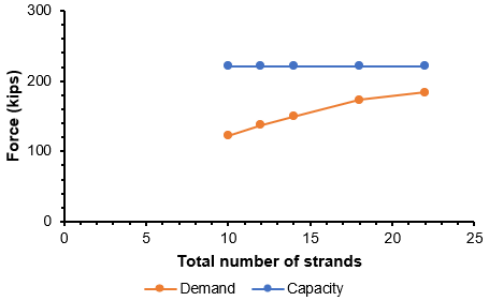

Strut-to-node interface (one plate)

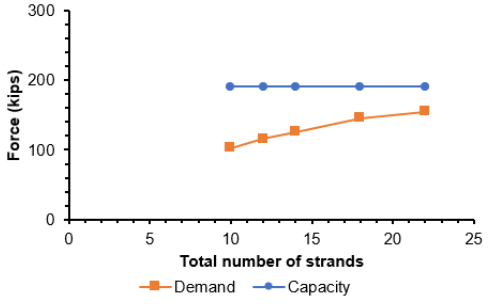

Back face (one plate)

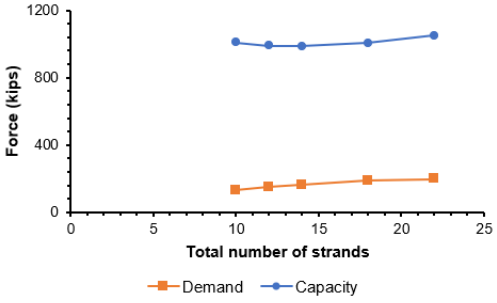

Horizontal shear

C.5.2. 6DS23

The span length of 6DS23 ranges from 30 ft to 60 ft. The total number of strands for 6DS23 proposed by TxDOT's standard design is at least ten and at most 26, of which the number of the debonded strands is zero to four. The design concrete strength is 5.0 ksi for overall span length. When more than 16 strands are used, v_u/f'_c is governed by the shear strength calculated using anchorage capacity. The calculated v_u/f'_c for 6DS23 exceeds the *0.18* shear stress limit ratio when the total number of strands is 16 or more, and the maximum v_u/f'_c is 0.222.

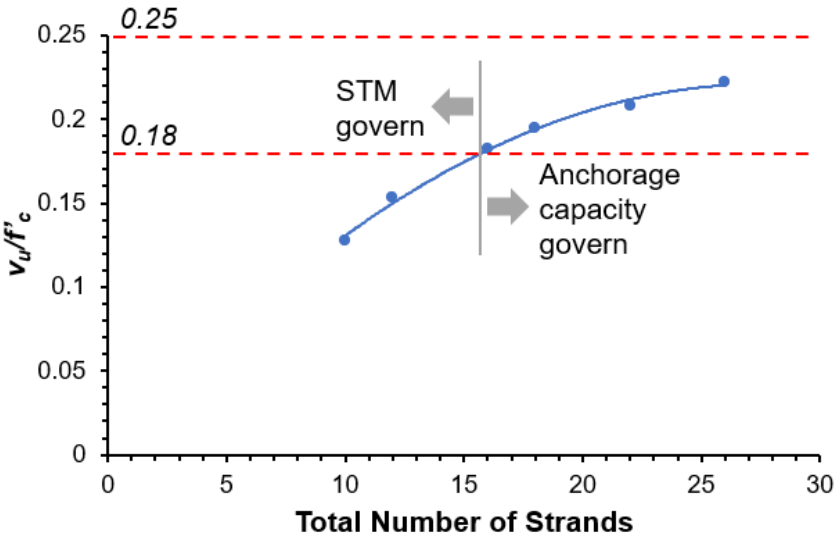

When the nodal failure and horizontal shear failure are checked, 6DS23 does not reach failure at every level of strand quantity. 6DS23 shows that the capacity for nodes and horizontal shear in all strands is always greater than the demand.

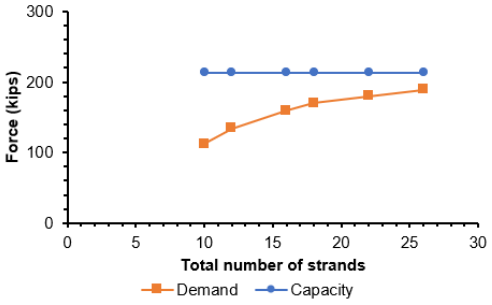

Strut-to-node interface (two plates, 30° skewed)

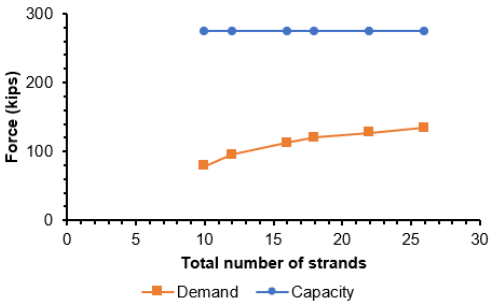

Bearing (two plates, 30° skewed)

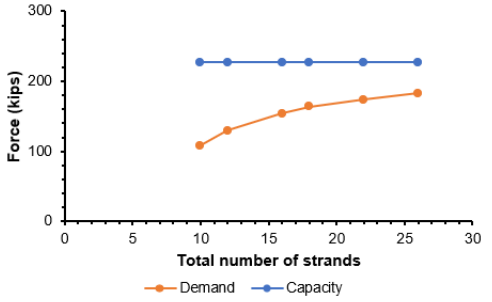

Strut-to-node interface (one plate)

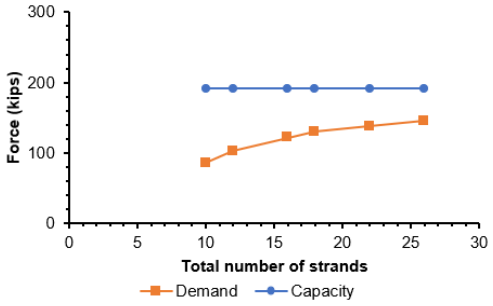

Back face (one plate)

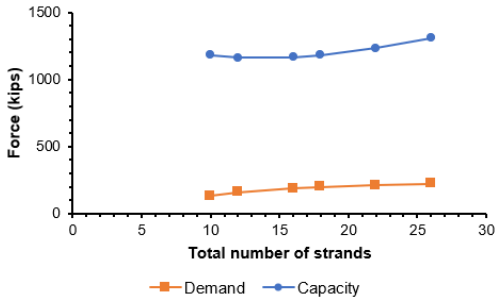

Horizontal shear

C.5.3. 7DS20

The span length of 7DS20 ranges from 30 ft to 50 ft. The total number of strands for 7DS20 proposed by TxDOT's standard design is at least ten and at most 26, of which the number of the debonded strands is zero to four. The design concrete strength is 5.0 ksi for overall span length. When more than 14 strands are used, v_u/f'_c is governed by the shear strength calculated using anchorage capacity. The calculated v_u/f'_c for 7DS20 exceeds the *0.18* shear stress limit ratio when the total number of strands is 14 or more, and the maximum v_u/f'_c is 0.232.

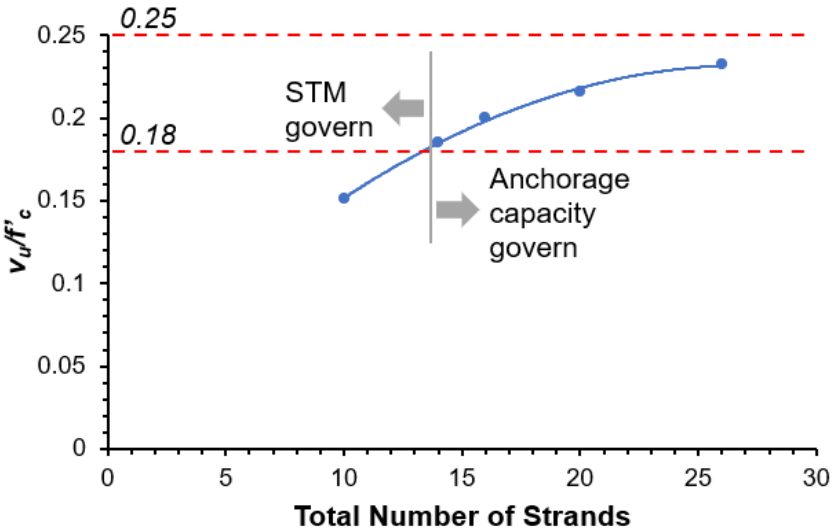

When the nodal failure and horizontal shear failure are checked, 7DS20 does not reach failure at every level of strand quantity. 7DS20 shows that the capacity for nodes and horizontal shear in all strands is always greater than the demand.

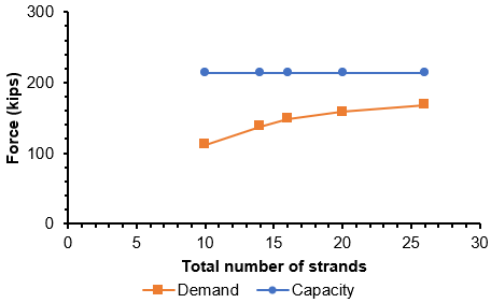

Strut-to-node interface (two plates, 30° skewed)

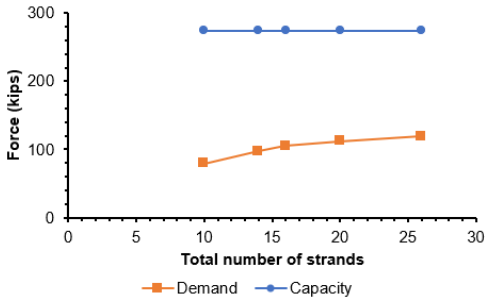

Bearing (two plates, 30° skewed)

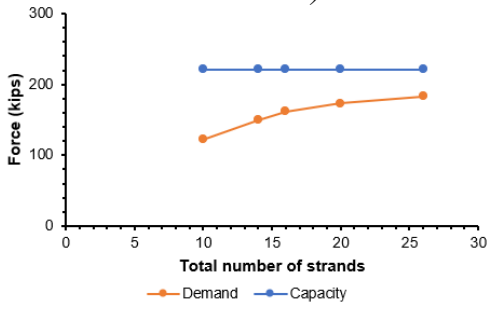

Strut-to-node interface (one plate)

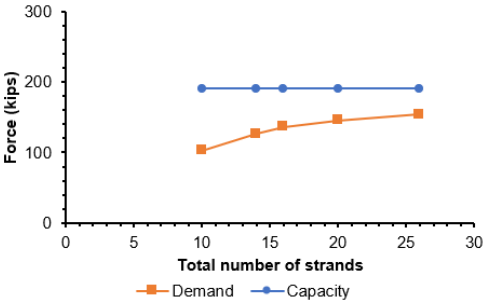

Back face (one plate)

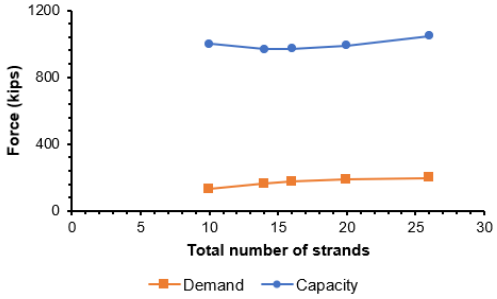

Horizontal shear

C.5.4. 8DS20

The span length of 8DS20 ranges from 30 ft to 50 ft. The total number of strands for 8DS20 proposed by TxDOT's standard design is at least 12 and at most 28, of which the number of the debonded strands is zero to six. The design concrete strength increases from 5.0 ksi to 5.3 ksi depending on the number of strands and span length. When more than 14 strands are used, v_u/f'_c is governed by the shear strength calculated using anchorage capacity. The calculated v_u/f'_c for 8DS20 exceeds the *0.18* shear stress limit ratio when the total number of strands is 14 or more, and the maximum v_u/f'_c is 0.230.

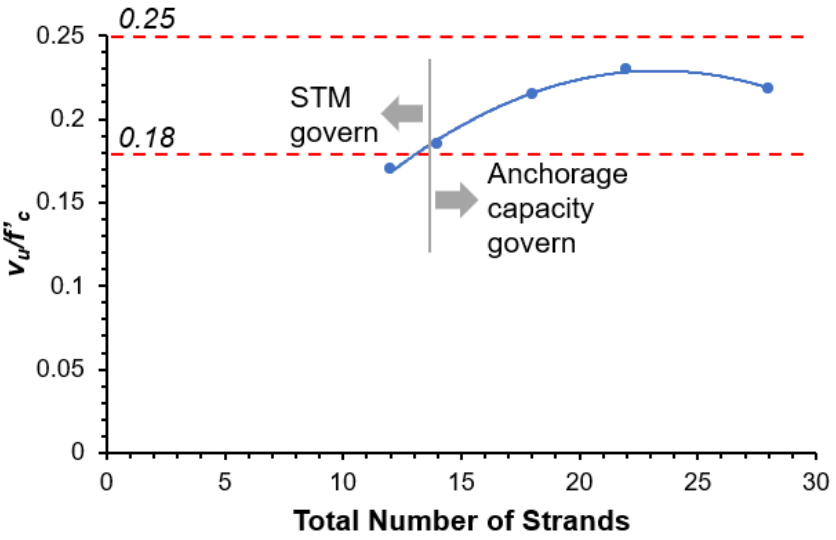

When the nodal failure and horizontal shear failure are checked, 8DS20 does not reach failure at every level of strand quantity. 8DS20 shows that the capacity for nodes and horizontal shear in all strands is always greater than the demand.

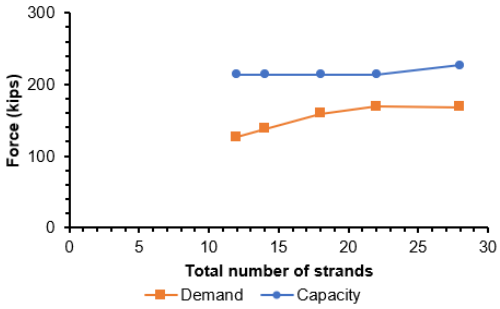

Strut-to-node interface (two plates, 30° skewed)

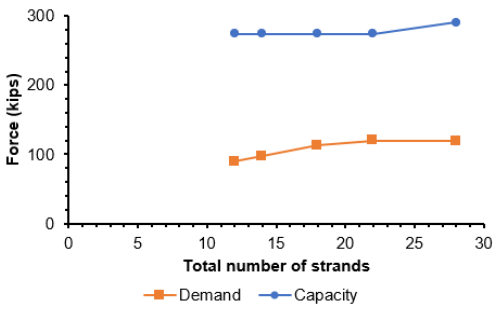

Bearing (two plates, 30° skewed)

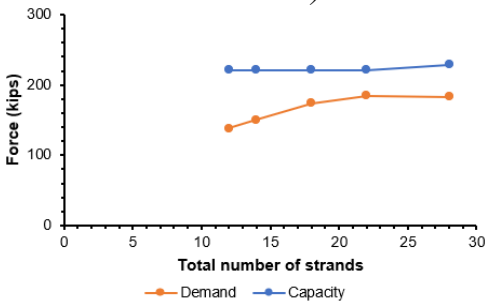

Strut-to-node interface (one plate)

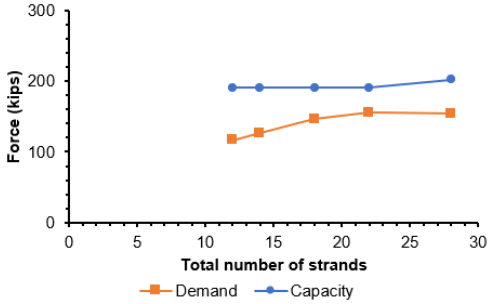

Back face (one plate)

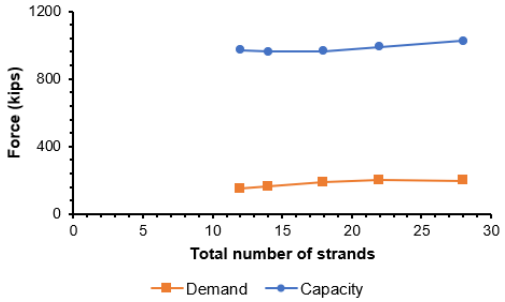

Horizontal shear

C.5.5. 8DS23

The span length of 8DS23 ranges from 30 ft to 60 ft. The total number of strands for 8DS23 proposed by TxDOT's standard design is at least ten and at most 32, of which the number of the debonded strands is zero to six. The design concrete strength increases from 5.0 ksi to 5.2 ksi depending on the number of strands and span length. When more than 14 strands are used, v_u/f'_c is governed by the shear strength calculated using anchorage capacity. The calculated v_u/f'_c for 8DS23 exceeds the *0.18* shear stress limit ratio when the total number of strands is 18 or more, and the maximum v_u/f'_c is 0.243.

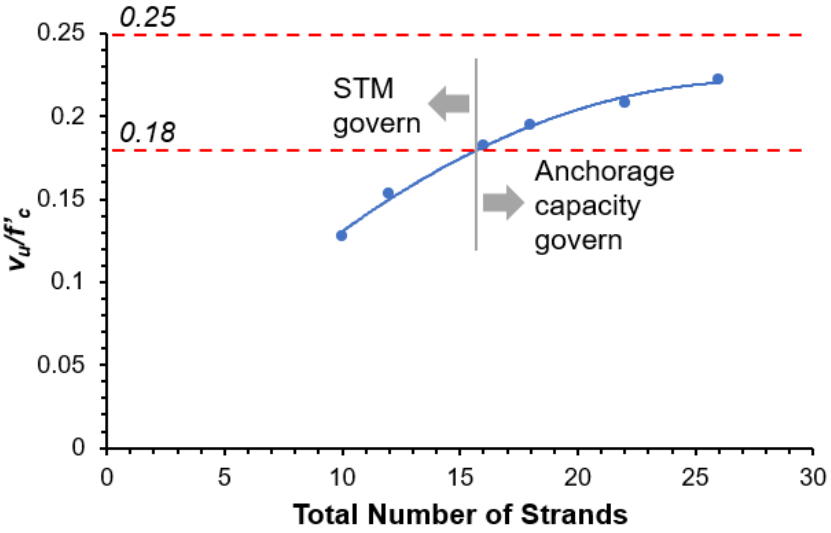

When the nodal failure and horizontal shear failure are checked, 8DS23 does not reach failure at every level of strand quantity. 8DS23 shows that the capacity for nodes and horizontal shear in all strands is always greater than the demand.

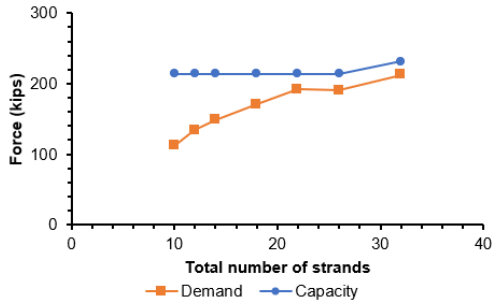

Strut-to-node interface (two plates, 30° skewed)

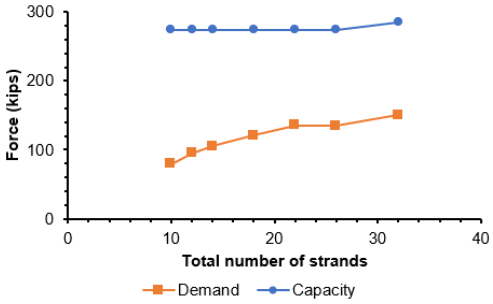

Bearing (two plates, 30° skewed)

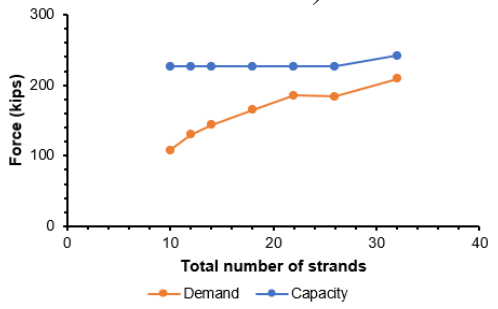

Strut-to-node interface (one plate)

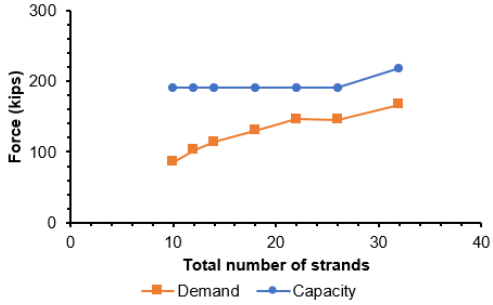

Back face (one plate)

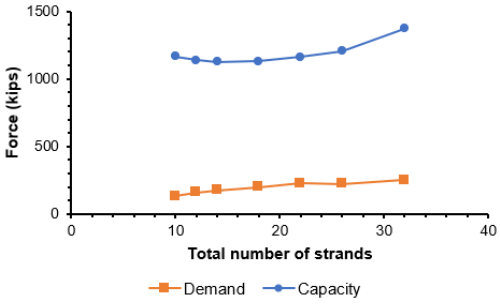

Horizontal shear

C.6. Slab beam

C.6.1. 5SB12

The span length of 5SB12 ranges from 25 ft to 40 ft. The total number of strands for 5SB12 proposed by TxDOT's standard design is at least eight and at most 18, of which the number of the debonded strands is zero for all span lengths. The design concrete strength is 5.0 ksi for overall span length. When more than eight strands are used, v_u/f'_c is governed by the shear strength calculated using anchorage capacity. The calculated v_u/f'_c for 5SB12 using STM and anchorage capacity cannot exceed the *0.18* shear stress limit ratio, and the maximum v_u/f'_c is 0.054.

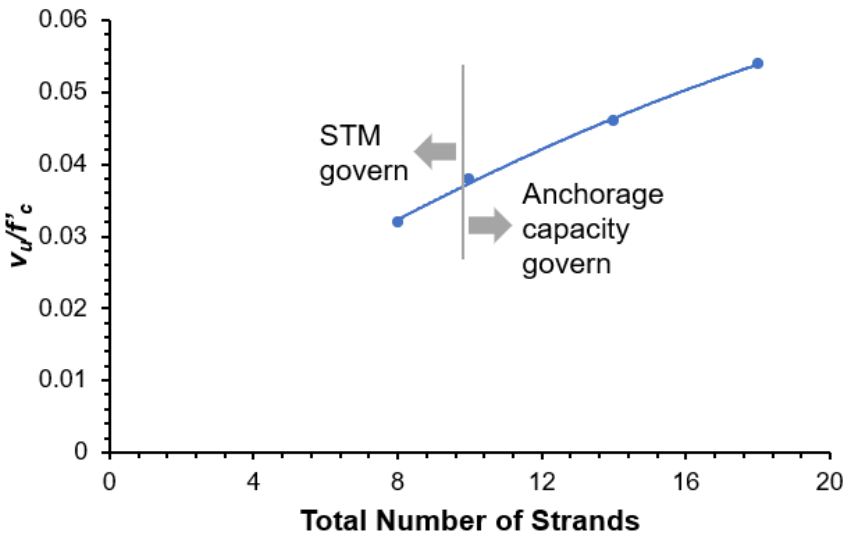

When the nodal failure and horizontal shear failure are checked, 5SB12 does not reach failure at every level of strand quantity. 5SB12 shows that the capacity for nodes and horizontal shear in all strands is always greater than the demand.

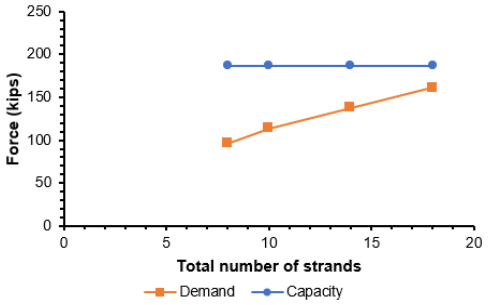

Strut-to-node interface

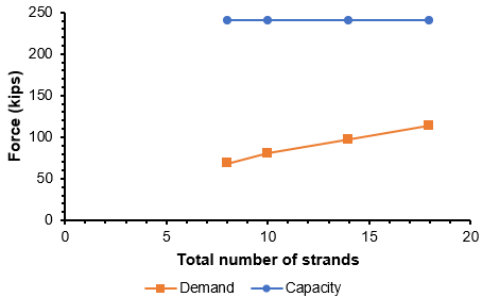

Bearing

C.6.2. 4SB15

The span length of 4SB15 ranges from 25 ft to 50 ft. The total number of strands for 4SB15 proposed by TxDOT's standard design is at least six and at most 18, of which the number of the debonded strands is zero to four. The design concrete strength is 5.0 ksi for overall span length. When more than 12 strands are used, v_u/f'_c is governed by the shear strength calculated using anchorage capacity. The calculated v_u/f'_c for 4SB15 using STM and anchorage capacity cannot exceed the *0.18* shear stress limit ratio, and the maximum v_u/f'_c is 0.052.

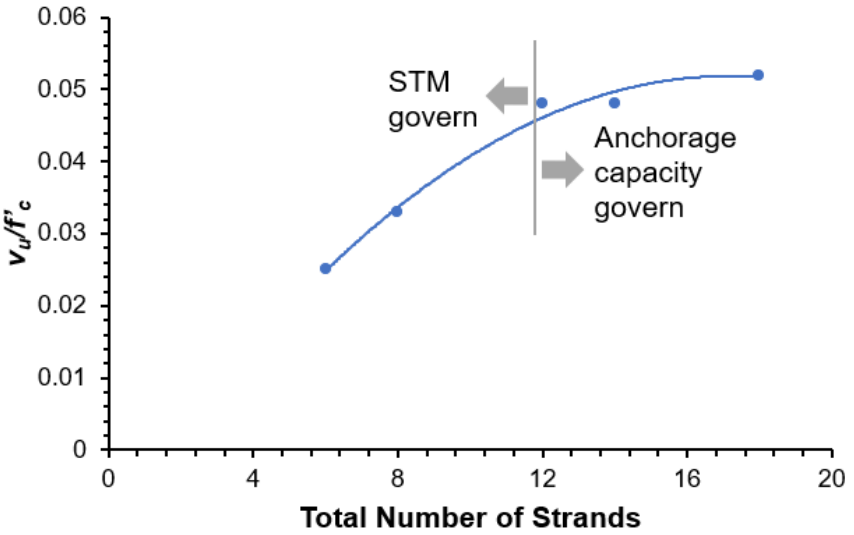

When the nodal failure and horizontal shear failure are checked, 4SB15 does not reach failure at every level of strand quantity. 4SB15 shows that the capacity for nodes and horizontal shear in all strands is always greater than the demand.

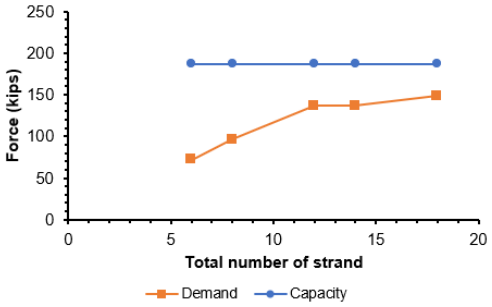

Strut-to-node interface

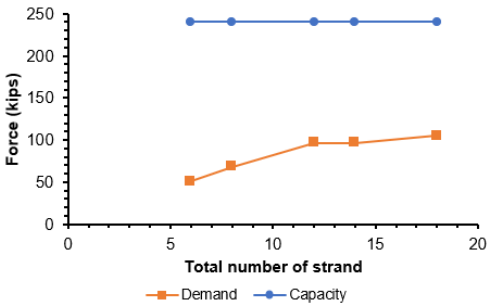

Bearing

C.6.2. 5SB15

The span length of 5SB15 ranges from 25 ft to 50 ft. The total number of strands for 5SB15 proposed by TxDOT's standard design is at least eight and at most 24, of which the number of the debonded strands is zero to eight. The design concrete strength is 5.0 ksi for overall span length. When more than 14 strands are used, v_u/f'_c is governed by the shear strength calculated using anchorage capacity. The calculated v_u/f'_c for 5SB15 using STM and anchorage capacity cannot exceed the *0.18* shear stress limit ratio, and the maximum v_u/f'_c is 0.045.

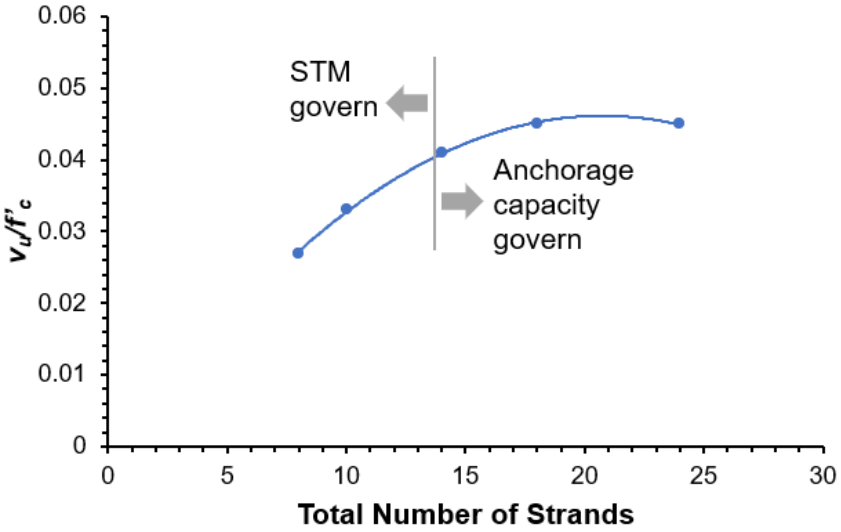

When the nodal failure and horizontal shear failure are checked, 5SB15 does not reach failure at every level of strand quantity. 5SB15 shows that the capacity for nodes and horizontal shear in all strands is always greater than the demand.

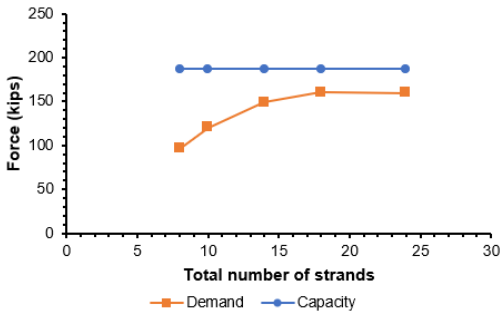

Strut-to-node interface

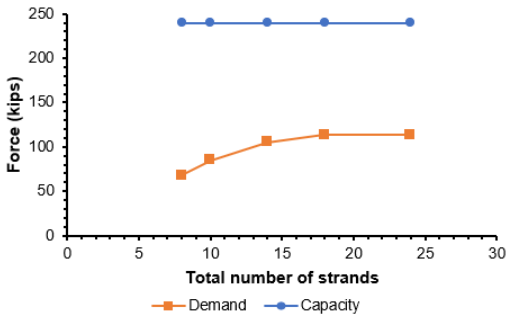

Bearing

Appendix D. Calculated Shear Capacity Based on AASHTO & ACI

D.1. Notation

A_v: area of a transverse reinforcement within distance S

b_w: web width

d_v: effective shear depth

d_p: distance from extreme compression fiber to centroid of prestressed reinforcement

f'_c: compressive strength of concrete

f_y: specified minimum yield strength of reinforcement

M_{cre}: moment causing flexural cracking at section due to externally applied load

M_d: moment due to unfactored dead load

S: spacing of transverse reinforcement

S_{xe}: crack spacing parameter as influenced by aggregate size

V_c: nominal shear resistance of the concrete

V_{ci}: nominal shear strength provided by concrete where diagonal cracking results from combined shear and moment

V_{cw}: nominal shear strength provided by concrete where diagonal cracking results from high principal tensile stress in web

V_d: shear force at section due to unfactored dead load

V_n: nominal shear resistance

V_s: shear resistance provided by transverse reinforcement

β : factor indicating the ability of diagonally cracked concrete to transmit tension and shear

ε_s : net longitudinal tensile strain in the section at the centroid of the tension reinforcement

θ : angle of inclination of diagonal compressive stresses

D.2. AASHTO LRFD bridge design specification 9th edition

	f'_c [ksi]	b_w [in.]	d_v [in.]	A_v [in^2]	S [in.]	f_y [ksi]	ε_s	β	θ [°]	S_{xe} [in.]	V_c [kip]	V_s [kip]	V_n [kip]
Avendaño and Bayrak (2008)													
Tx28-1-L	13.825	7	25.92	0.4	5.6	60	-0.00015	5.41	28.5	31.7	115.3	204.8	320
Tx28-1-D	13.825	7	25.92	0.4	5.6	60	-0.00015	5.41	28.5	31.7	115.3	204.8	320
Tx28-2-L	11.375	7	26.36	0.394	6.35	75	-8.9E-05	5.14	28.7	32.2	101.1	224.2	325
Tx28-2-D	11.375	7	26.36	0.394	6.35	75	-8.9E-05	5.14	28.7	32.2	101.1	224.2	325
Garber, Gallardo, Deschenes, and Bayrak (2016)													
Q-8	11.8	7	35.61	0.4	4	60	0.000377	3.74	30.3	43.5	101.2	365.3	484
Q-10	11.8	7	35.61	0.4	4	60	0.000377	3.74	30.3	43.5	101.2	365.3	484
Q-20A	11.8	7	35.61	0.4	4	60	0.000377	3.74	30.3	43.5	101.2	365.3	484
Q-20B	11.8	7	35.61	0.4	4	60	0.000377	3.74	30.3	43.5	101.2	365.3	484
Q-46	11.8	7	35.60	0.4	4	60	0.000379	3.74	30.3	43.5	101.1	365.2	484

Avendaño, Hovell, Moore, Dunkman, Nakamura, Bayrak, and Jirsa (2013)													
BB-01 (Square)	11.3	10	22.78	0.8	20	60	-7.1E-05	5.07	28.8	22.8	122.7	99.6	222
BB-01 (Skewed)	11.3	10	22.78	0.8	20	60	-1.2E-05	4.84	28.9	22.8	117.2	98.8	216
BB-02 (Square)	11.3	10	22.78	0.8	20	60	-7.1E-05	5.07	28.8	22.8	122.7	99.6	222
BB-02 (Skewed)	11.3	10	22.78	0.8	20	60	-1.2E-05	4.84	28.9	22.8	117.2	98.8	216
BB-03 (Square)	11.16	10	22.75	0.8	20	60	-7.4E-05	5.08	28.7	22.8	122.0	99.6	222
BB-03 (Skewed)	11.16	10	22.75	0.8	20	60	-1.5E-05	4.85	28.9	22.8	116.6	98.7	215
BB-04 (Square)	10.672	10	22.67	0.8	20	60	-8E-05	5.11	28.7	22.7	119.5	99.3	219
BB-04 (Skewed)	10.672	10	22.67	0.8	20	60	-2E-05	4.87	28.9	22.7	114.1	98.4	213
BB-05 (Square)	10.9	10	22.71	0.8	20	60	-7.7E-05	5.09	28.7	22.7	120.7	99.4	220
BB-05 (Skewed)	10.9	10	22.71	0.8	20	60	-1.7E-05	4.86	28.9	22.7	115.2	98.6	214
BB-06 (Square)	9.53	10	22.45	0.8	20	60	-1.0E-04	5.19	28.7	22.5	113.6	98.6	212
BB-06 (Skewed)	9.53	10	22.45	0.8	20	60	-3.6E-05	4.94	28.9	22.5	108.3	97.7	206

BB-07 (Square)	9.575	10	22.46	0.8	20	60	-1.0E-04	5.19	28.7	22.5	113.9	98.7	213
BB-07 (Skewed)	9.575	10	22.46	0.8	20	60	-3.9E-05	4.94	28.9	22.5	108.6	97.8	206
BB-08 (Square)	8.73	10	22.35	0.8	20	60	-0.00012	5.25	28.6	22.4	109.6	98.4	208
BB-08 (Skewed)	8.73	10	22.35	0.8	20	60	-5.4E-05	5.00	28.8	22.4	104.4	97.5	202
BB-09 (Square)	8.9	10	22.35	0.8	20	60	-0.00011	5.23	28.6	22.4	110.3	98.3	209
BB-09 (Skewed)	8.9	10	22.35	0.8	20	60	-4.9E-05	4.98	28.8	22.4	105.0	97.5	202
BB-10 (Square)	9.73	10	22.49	0.8	20	60	-3.6E-05	4.93	28.9	22.5	109.3	97.9	207
BB-10 (Skewed)	9.73	10	22.49	0.8	20	60	-3.6E-05	4.93	28.9	22.5	109.3	97.9	207
5B40-1 (Square)	11.8	10	28.8	0.8	20	65	-2.9E-05	4.91	28.9	35.2	153.4	452.2	606
5B40-1 (Skewed)	11.8	10	28.8	0.8	20	65	-2.9E-05	4.91	28.9	35.2	153.4	452.2	606
5B40-2 (Square)	9.4	10	28.8	0.8	20	65	-4.7E-05	4.98	28.8	35.2	138.8	453.4	592
5B40-3 (Square)	11.2	10	28.8	0.8	20	65	-3.2E-05	4.92	28.9	35.2	149.8	452.4	602
5B40-3 (Skewed)	11.2	10	28.8	0.8	20	65	-3.2E-05	4.95	28.9	35.2	149.8	452.4	602

5B40-4 (Square)	10	10	28.8	0.8	20	65	-4.1E-05	4.95	28.9	35.2	142.5	453.0	595
5B40-4 (Skewed)	10	10	28.8	0.8	20	65	-4.1E-05	4.95	28.9	35.2	142.5	453.0	595
5XB40 (One plate)	10.5	13	42.42	0.4	20	66	-3.8E-05	4.94	28.9	51.8	278.9	338.6	617
5XB40 (Two plate)	10.5	13	42.42	0.4	20	66	-3.8E-05	4.94	28.9	51.8	278.9	338.6	617
Hovell, Avendaño, Moore, Dunkman, Bayrak, and Jirsa (2013)													
U54-1-N	11.96	10	52.2	0.4	4	65.8	0.000688	3.17	31.4	52.2	180.6	562.5	743
U54-1-S	11.96	10	52.2	0.4	4	65.8	0.000688	3.17	31.4	52.2	180.6	562.5	743
U54-2-N	11.48	10	52.2	0.4	4	85.2	0.001315	2.42	33.6	52.2	135.1	669.3	804
U54-3-N	11.31	10	54.53	0.4	4	65.3	0.002855	1.53	38.9	66.6	88.6	439.8	528
U54-3-S	12.1	10	54.53	0.4	4	65.3	0.002876	1.52	.9.1	66.6	91.1	438.7	530
U54-4-N	11.44	10	52.2	0.4	3.5	63	0.00066	3.21	31.3	63.7	179.2	617.9	797
U54-4-S	11.44	10	52.2	1.86	6	60.6	0.003906	1.22	42.7	63.7	68.2	1063.8	1132
U54-5-N	13.23	10	54.26	1.28	6	65	0.003791	1.25	42.3	54.3	77.9	827.8	906

U54-6-S	12.02	10	53.88	1.1	6	85	0.004397	1.12	44.4	45.6	65.9	857.7	924
U54-7-N	12.45	10	52.97	1.02	6	62.5	0.002269	1.78	36.9	52.9	104.9	748.5	853
Tan, Luu, Mo, Hsu, and Belarbi (2016)													
5SB12-1	10.7	59.75	13.05	0.4	4	60	0.002978	1.38	39.4	15.9	111.1	95.2	206
5SB12-2	10.7	59.75	13.05	0.4	4	60	0.004112	1.09	43.4	15.9	87.9	82.8	171
5SB12-3	9.6	59.75	8.64	0.4	4	60	0.00177	2.06	35.2	10.6	104.2	73.5	178
5SB12-4	9.6	59.75	8.64	0.4	4	60	0.002205	1.81	36.7	10.6	91.4	69.5	161
5SB12-5	9.6	59.75	13.05	0.4	4	60	0.001928	1.96	35.7	15.9	149.8	108.8	259
5SB12-6	9.6	59.75	13.05	0.4	4	60	0.002923	1.50	39.2	15.9	114.8	95.9	211
5SB15-1	9.7	59.75	15.8	0.4	4	60	0.004497	1.10	44.7	19.3	102.0	95.7	198
5SB15-2	8.5	59.75	11.49	0.4	4	60	0.003217	1.41	40.3	14.0	89.0	81.4	170
5SB15-3	8.5	59.75	11.49	0.4	4	60	0.004536	1.09	44.9	14.0	69.0	69.2	138
5SB15-4	9.1	59.75	15.75	0.4	4	60	0.002457	1.69	37.6	19.2	151.5	122.7	274

D.3. ACI building code 318-19

	f'_c [ksi]	b_w [in.]	d_p [in.]	A_v [in^2]	S [in.]	f_y [ksi]	M_{cre} [kip-in]	V_d	M_d	V_{ci} [kip]	V_{cw} [kip]	V_s [kip]	V_n [kip]
Avendaño and Bayrak (2008)													
Tx28-1-L	13.825	7	28.78	0.4	5.6	60	11257.7	4.270	0.613	150.17	158.45	176.15	326
Tx28-1-D	13.825	7	28.78	0.4	5.6	60	11257.7	4.270	0.613	150.17	158.45	176.15	326
Tx28-2-L	11.375	7	28.78	0.394	6.35	75	11356.3	5.490	1.014	121.07	157.40	191.27	312
Tx28-2-D	11.375	7	28.78	0.394	6.35	75	11356.3	5.490	1.014	121.07	157.40	191.27	312
Garber, Gallardo, Deschenes, and Bayrak (2016)													
Q-8	11.8	7	36.80	0.4	4	60	20253.6	8.190	1.291	190.12	253.53	315.34	505
Q-10	11.8	7	36.80	0.4	4	60	20253.6	8.190	1.291	190.12	255.08	315.34	505
Q-20A	11.8	7	36.80	0.4	4	60	20253.6	8.190	1.291	190.12	253.53	315.34	505
Q-20B	11.8	7	36.80	0.4	4	60	20253.6	8.190	1.291	190.12	255.08	315.34	505
Q-46	11.8	7	36.80	0.4	4	60	20253.6	8.190	1.291	190.12	252.76	315.34	505

Avendaño, Hovell, Moore, Dunkman, Nakamura, Bayrak, and Jirsa (2013)													
BB-01 (Square)	11.3	10	22.40	0.8	20	60	12611.5	4.242	0.806	189.09	138.44	76.78	215
BB-01 (Skewed)	11.3	10	22.40	0.8	20	60	12602.6	4.949	1.097	164.67	138.44	76.78	215
BB-02 (Square)	11.3	10	22.40	0.8	20	60	12611.5	4.242	0.806	189.09	138.44	76.78	215
BB-02 (Skewed)	11.3	10	22.40	0.8	20	60	12602.6	4.949	1.097	164.67	138.44	76.78	215
BB-03 (Square)	11.16	10	22.40	0.8	20	60	12592.6	4.242	0.806	188.74	137.93	76.78	215
BB-03 (Skewed)	11.16	10	22.40	0.8	20	60	12583.7	4.949	1.097	164.36	137.93	76.78	215
BB-04 (Square)	10.672	10	22.40	0.8	20	60	12525.6	4.242	0.806	187.49	136.10	76.78	213
BB-04 (Skewed)	10.672	10	22.40	0.8	20	60	12516.7	4.949	1.097	163.24	136.10	76.78	213
BB-05 (Square)	10.9	10	22.40	0.8	20	60	12557.1	4.242	0.806	188.07	136.96	76.78	214
BB-05 (Skewed)	10.9	10	22.40	0.8	20	60	12548.2	4.949	1.097	163.75	136.96	76.78	214
BB-06 (Square)	9.53	10	22.40	0.8	20	60	12362.6	4.242	0.806	184.41	131.64	76.78	208
BB-06 (Skewed)	9.53	10	22.40	0.8	20	60	12353.7	4.949	1.097	160.48	131.64	76.78	208

BB-07 (Square)	9.575	10	22.40	0.8	20	60	12369.2	4.242	0.806	184.53	131.82	76.78	209
BB-07 (Skewed)	9.575	10	22.40	0.8	20	60	12360.3	4.949	1.097	160.59	131.82	76.78	209
BB-08 (Square)	8.73	10	22.40	0.8	20	60	12242.5	4.242	0.806	182.16	128.36	76.78	205
BB-08 (Skewed)	8.73	10	22.40	0.8	20	60	12233.5	4.949	1.097	158.48	128.36	76.78	205
BB-09 (Square)	8.9	10	22.40	0.8	20	60	12268.4	4.242	0.806	182.63	129.07	76.78	206
BB-09 (Skewed)	8.9	10	22.40	0.8	20	60	12259.5	4.949	1.097	158.90	129.07	76.78	206
BB-10 (Square)	9.73	10	22.40	0.8	20	60	12382.9	4.949	1.097	160.99	132.44	76.78	209
BB-10 (Skewed)	9.73	10	22.40	0.8	20	60	12382.9	4.949	1.097	160.99	132.44	76.78	209
5B40-1 (Square)	11.8	10	32.00	0.8	20	65	25174.0	8.160	0.703	303.67	205.18	396.07	601
5B40-1 (Skewed)	11.8	10	32.00	0.8	20	65	25174.0	8.160	0.703	303.67	205.18	396.07	601
5B40-2 (Square)	9.4	10	32.00	0.8	20	65	24458.3	8.160	0.703	293.51	192.11	396.07	588
5B40-3 (Square)	11.2	10	32.00	0.8	20	65	25002.5	8.160	0.703	301.24	202.05	396.07	598
5B40-3 (Skewed)	11.2	10	32.00	0.8	20	65	25002.5	8.160	0.703	301.24	202.05	396.07	598

5B40-4 (Square)	10	10	32.00	0.8	20	65	24645.0	8.160	0.703	296.17	195.52	396.07	592
5B40-4 (Skewed)	10	10	32.00	0.8	20	65	24645.0	8.160	0.703	296.17	195.52	396.07	592
5XB40 (One plate)	10.5	13	46.00	0.4	20	66	23328.3	12.570	1.250	237.56	370.55	289.06	527
5XB40 (Two plate)	10.5	13	46.00	0.4	20	66	23328.3	12.570	1.250	237.56	370.55	289.06	527
Hovell, Avendaño, Moore, Dunkman, Bayrak, and Jirsa (2013)													
U54-1-N	11.96	10	49.60	0.4	4	65.8	30938.5	17.068	2.347	244.09	267.23	466.10	710
U54-1-S	11.96	10	49.60	0.4	4	65.8	30938.5	17.068	2.347	244.09	267.23	466.10	710
U54-2-N	11.48	10	49.60	0.4	4	85.2	30733.1	20.234	2.782	245.35	272.31	603.52	849
U54-3-N	11.31	10	49.60	0.4	4	65.3	20179.9	18.566	2.553	176.18	227.77	462.56	639
U54-3-S	12.1	10	49.60	0.4	4	65.3	20458.9	18.566	2.553	179.03	231.14	462.56	642
U54-4-N	11.44	10	49.60	0.4	3.5	63	29408.4	21.688	2.419	237.09	315.13	510.02	747
U54-4-S	11.44	10	49.60	1.86	6	60.6	27865.4	21.688	2.419	231.11	315.13	1330.73	1562
U54-5-N	13.23	10	49.60	1.28	6	65	27850.3	18.566	2.553	229.95	239.85	982.26	1212

U54-6-S	12.02	10	49.60	1.1	6	85	26820.6	21.560	2.965	224.58	230.50	1103.86	1328
U54-7-N	12.45	10	49.60	1.02	6	62.5	29700.2	23.062	3.171	243.12	233.88	752.63	987
Tan, Luu, Mo, Hsu, and Belarbi (2016)													
5SB12-1	10.7	59.75	13.60	0.4	4	60	1383.5	1.108	0.028	128.83	374.64	116.54	259
5SB12-2	10.7	59.75	13.60	0.4	4	60	1382.2	1.751	0.069	100.88	374.64	116.54	259
5SB12-3	9.6	59.75	9.50	0.4	4	60	1337.2	0.747	0.013	145.06	250.85	81.40	226
5SB12-4	9.6	59.75	9.50	0.4	4	60	1336.8	0.968	0.021	119.75	250.85	81.40	201
5SB12-5	9.6	59.75	13.60	0.4	4	60	1534.8	1.110	0.028	134.43	390.80	116.54	252
5SB12-6	9.6	59.75	13.60	0.4	4	60	1533.4	1.805	0.073	101.95	390.80	116.54	252
5SB15-1	9.7	59.75	16.00	0.4	4	60	1815.9	1.566	0.035	147.66	389.77	137.10	297
5SB15-2	8.5	59.75	12.00	0.4	4	60	1732.2	1.197	0.021	152.82	276.54	102.83	256
5SB15-3	8.5	59.75	12.00	0.4	4	60	1730.3	1.965	0.055	109.32	276.54	102.83	215
5SB15-4	9.1	59.75	16.00	0.4	4	60	2145.9	1.648	0.039	156.95	425.30	137.10	294

Appendix E. Calculation Example

E.1. Shear Stress at Tx-46's End Region without Harped Strands

Strand Layout													
Layer	ybot(in)	Max No. of	Max Ratio of	No. of Straight Strands									No. of Harped strand
				Total	DR	0.00	3.00	6.00	9.00	12.00	15.00	27.40	34.25	34.25
Total			25%	14	0.0%	14	14	14	14	14	14	14	14	0
1	2.5	14	40%	14	0.0%	14	14	14	14	14	14	14	14	0
2	4.5	14	40%	0	#DIV/0!	0	0	0	0	0	0	0	0	0
3	6.5	14	0%	0	#DIV/0!	0	0	0	0	0	0	0	0	0
4	8.5	12	0%	0	#DIV/0!	0	0	0	0	0	0	0	0	0
5	10.5	8	0%	0	#DIV/0!	0	0	0	0	0	0	0	0	0
6	12.5	4	0%	0	#DIV/0!	0	0	0	0	0	0	0	0	0
7	14.5	2	0%	0	#DIV/0!	0	0	0	0	0	0	0	0	0
8	16.5	2	0%	0	#DIV/0!	0	0	0	0	0	0	0	0	0
Top Strands	42.5	2		0		0	0	0	0	0	0	0	0	

Reinforcing Steel

Bottom Reinforcement

A_s	0	in2
f_s	60	ksi
d_s	0	in.

Top Reinforcement

A_s'	0.8	in2
f_s'	60	ksi
d_s'	10.00	in.

Deck Reinforcement

A_s''	1.6	in2
f_s''	60	ksi
d_s''	2.5	in.

Input Data

Geometry

D	46	in.	Girder Depth
L	70	ft	Girder Length
L_s	68.5	ft	Span Length
b_w	7.0	in.	Web Thickness
h_{tf}	3.5	in.	Top Flange Height
b_{tf}	36.0	in.	Top Flange Width
b_{deck}	80.0	in.	Girder spacing
h_{deck}	8.5	in.	Deck Height
h_{web}	22.0	in.	Web Height
A_g	761	in2	Girder Area
I_x	198089	in4	Moment of Inertia(x-axis)
I_y	46478		Moment of Inertia(y-axis)
y_{top}	25.9	in.	
y_{bot}	20.1	in.	
$S_{g,top}$	7648	in3	
$S_{g,bot}$	9855	in3	
w	819	lb/ft	Girder Weight
oh	9	in.	Distance from Girder End to CL of Support
e (at CL)	17.6	in	

Concrete

f'_c	5.0	ksi
f'_{ci}	4.0	ksi
$f'_{c,deck}$	4.0	ksi
E_c	4291.2	ksi
E_{ci}	3931.8	ksi
Alpha1	0.85	
Beta1	0.8	
$Beta1_{,deck}$	0.85	

Load location

L_p	50.988	in.	concentrate load point from support
a/d_v	1		shear span-depth ratio

Harped strand location

T_h	0	in.	top harped strand to bottom

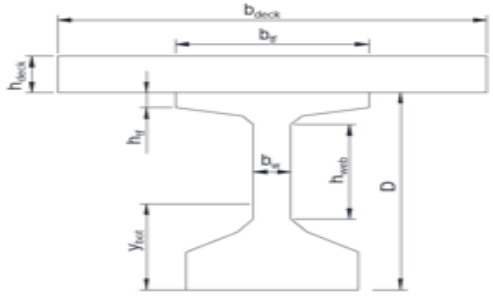

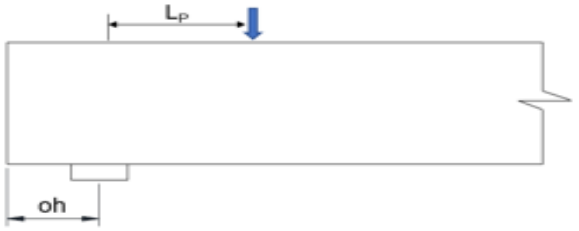

Prestressing Steel

INPUT

f_{pu}	270	ksi	
E_p	28500	ksi	
d_{ps}	0.6	in.	Diameter for strand
N_{ps}	14	ea	Total number of straight strand
N_{ph}	0	ea	Total number of harped strand
A_{ps}'	0.217	in2	Area for one strand

Calculated Data

$A_{ps,s}$	3.038	in2	Total area of straight strand
$A_{ps,h}$	0	in2	Total area of harped strand
A_{ps}	3.038	in2	Total area of total strand
L_t	36	in.	Transfer length = 60dps
Strand	Low relaxation str		Choose strand type
$\gamma 1$	0.9		fpy/fpu
$\gamma 2$	0.75		

verage stress in prestressing steel (fps

$$f_{ps} = f_{pu}\left(1 - k\frac{c}{d_p}\right)$$ AASHTO 5.6.3.1.1-1

= 265.24 ksi

In which

$$k = 2\left(1.04 - \frac{f_{py}}{f_{pu}}\right)$$ AASHTO 5.6.3.1.1-2

= 0.28

For T section behavior

$$c = \frac{A_{ps}f_{pu} + A_s f_s - A_s' f_s' - A_s'' f_s'' - \alpha_1 f'_{c,deck}(b_{deck} - b_w)h_{deck}}{\alpha_1 f'_{c,deck}\beta_1 b_{deck} + kA_{ps}\frac{f_{pu}}{d_{ps}}}$$ AASHTO 5.6.3.1.1-3

For rectangular section behavior

$$c = \frac{A_{ps}f_{pu} + A_s f_s - A_s' f_s' - A_s'' f_s''}{\alpha_1 f'_{c,deck}\beta_1 b_{deck} + kA_{ps}\frac{f_{pu}}{d_{ps}}}$$ AASHTO 5.6.3.1.1-4

c = 3.28 in.

Effective prestress (fpe)

$f_{py} = \gamma 1 \times fpu$ AASHTO Table C5.6.3.1.1-1

= 243 ksi

$f_{po} = \gamma 2 \times fpu$ AASHTO Table 5.9.2.2-1

= 202.5 ksi

Assume final prestressing loss is 20%

f_{pe} = 162.00 ksi

Calculate dv

Other factor

h_t	54.5	in.	total height
y_b'	2.5	in.	bottom to center of strand at CL
d_p	52.0	in.	top to center of strand at CL
a	2.78	in.	

Strand location

y_{bh}	0	in.	bottom to center of harped strand at CL
y_b	2.5	in.	bottom to center of straight strand at CL

Calculate nominal flexure resistance

For T section behavior

$$M_n = A_{ps}f_{ps}\left(d_p-\frac{a}{2}\right)+A_sf_s\left(d_s-\frac{a}{2}\right)+A_s'f_s'\left(d_s'-\frac{a}{2}\right)-A_s'f_s'\left(d_s'-\frac{a}{2}\right)+\alpha_1 f_{c.deck}\left(b_{deck}-b_w\right)h_{deck}\left(\frac{a}{2}-\frac{h_{deck}}{2}\right)$$ AASHTO 5.6.3.2.2-1

For rectangular section behavior

$$M_n = A_{ps}f_{ps}\left(d_p-\frac{a}{2}\right)+A_sf_s\left(d_s-\frac{a}{2}\right)+A_s'f_s'\left(d_s'-\frac{a}{2}\right)-A_s'f_s'\left(d_s'-\frac{a}{2}\right)$$

M_n = 41086 kip-in

Calculate dv

$$d_v = Max\left(\frac{M_n}{A_sf_y+A_{ps}f_{ps}}, 0.9\times d_p, 0.72\times h\right)$$

d_v = 50.988 in.

Calculate Vu Without Harped Strand (STM)

h_{stm} 50.988 in.

Node geometry

b_p	8	in.	bearing size
w_p	21	in.	bearing width
θ	45	degree	
h_t	5	in.	back face height

$w_s = h_t \times \cos(\theta) + b_p \times \sin(\theta)$

= 9.1924 in.

$l_a = \frac{w_s / 2}{\sin(\theta)} + offset$

= 15.5 in.

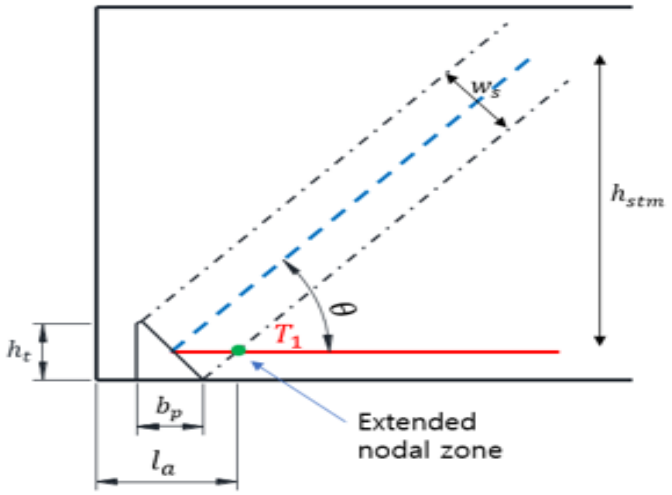

Calculate tie force

$f_1 = \frac{l_a}{l_t} \times f_{pe}$

= 69.75 ksi

$T_1 = f_1 \times A_{bp}$ Abp is total area of bonded strand at the extended nodal zone

= 211.9 kip

Calculate Vu

$R_u = T_1 \times \tan\theta$

= 211.9 kip

$V_{u,s}$ 211.9 kip

Anchorage Longitudinal Check Without Harped Strand

$$A_s f_y + A_{ps} f_{ps} \geq \left(\frac{V_{u,a}}{\phi_v} - 0.5 V_s \right) \cot\theta_1$$ AASHTO 5.7.3.5-2

fpx : Prestress at extended nodal zone

From the above equation

$$A_s f_y + A_{ps} f_{ps} = \left(\frac{V_{u,a}}{\phi_v} - 0.5 V_s \right) \cot\theta_1$$

Equation for Vu'

$$V_{u,a} = \phi_v \left(\frac{A_s f_y + A_{ps} f_{ps}}{\cot\theta_1} + 0.5 V_s \right)$$

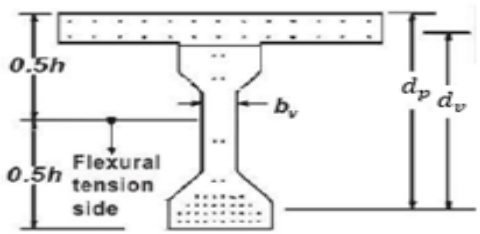

Where

$$V_s = \frac{A_v \times f_y \times d_v \times \cot\theta_1}{S}$$ AASHTO 5.7.3.3-4

$$V_{s,max} = 0.25 f'_c b_v d_v - V_c$$ AASHTO 5.7.3.3-2

V_s = 315.39 kip

$$\varepsilon_s = \frac{\left(\frac{|M_u|}{d_v} + 0.5 N_u + |V_u - V_p| - A_{ps} f_{po} \right)}{E_s A_s + E_p A_{ps}} > 0$$

$$\varepsilon_s = \frac{\left(\frac{|M_u|}{d_v} + 0.5 N_u + |V_u - V_p| - A_{ps} f_{po} \right)}{E_s A_s + E_p A_{ps} + E_c A_{st}} < 0$$

= -9.9E-05

$\theta_1 = 29 + 3500\varepsilon_s$

= 28.654 degree

ϕ_v = 0.9

A*f = 211.9 kip

$V_{u,a}$ = 246.14 kip OK

Calculate vu/fc'

V_u = 211.901 kip

$$v_u = \frac{V_u}{\phi b_v d_v}$$ AASHTO 5.7.2.8-1

= 0.6597

v_u/f'_c = 0.132

When anchorage fail, $V_u = V_{u,a}$

E.2. Shear Stress at Tx-46's End Region with Harped Strands

Strand Layout

Layer	ybot(in)	Max No. of	Max Ratio of	No. of Straight Strands									No. of Harped strand
				Total	DR	0.00	3.00	6.00	9.00	12.00	15.00	45.40	56.75
Total			25%	36	0.0%	36	36	36	36	36	36	36	36	6
1	2.5	12	40%	12	0.0%	12	12	12	12	12	12	12	12	2
2	4.5	12	40%	12	0.0%	12	12	12	12	12	12	12	12	2
3	6.5	12	0%	12	0.0%	12	12	12	12	12	12	12	12	2
4	8.5	10	0%	0	#DIV/0!	0	0	0	0	0	0	0	0	0
5	10.5	6	0%	0	#DIV/0!	0	0	0	0	0	0	0	0	0
6	12.5	2	0%	0	#DIV/0!	0	0	0	0	0	0	0	0	0
7	14.5	2	0%	0	#DIV/0!	0	0	0	0	0	0	0	0	0
8	16.5	2	0%	0	#DIV/0!	0	0	0	0	0	0	0	0	0
Top Strands	42.5	2		0		0	0	0	0	0	0	0	0	

Reinforcing Steel

Bottom Reinforcement

A_s	0	in2
f_s	60	ksi
d_s	0	in.

Top Reinforcement

A_s'	0.8	in2
f_s'	60	ksi
d_s'	10.00	in.

Deck Reinforcement

A_s''	1.6	in2
f_s''	60	ksi
d_s''	2.5	in.

Input Data

Geometry

D	46	in.	Girder Depth
L	115	ft	Girder Length
L_s	113.5	ft	Span Length
b_w	7.0	in.	Web Thickness
h_{tf}	3.5	in.	Top Flange Height
b_{tf}	36.0	in.	Top Flange Width
b_{deck}	80.0	in.	Girder spacing
h_{deck}	8.5	in.	Deck Height
h_{web}	22.0	in.	Web Height
A_g	761	in2	Girder Area
I_x	198089	in4	Moment of Inertia(x-axis)
I_y	46478		Moment of Inertia(y-axis)
y_{top}	25.9	in.	
y_{bot}	20.1	in.	
$S_{g,top}$	7648	in3	
$S_{g,bot}$	9855	in3	
w	819	lb/ft	Girder Weight
oh	9	in.	Distance from Girder End to CL of Support
e (at CL)	15.6	in	

Concrete

f'_c	7.0	ksi
f'_{ci}	6.0	ksi
$f'_{c,deck}$	4.0	ksi
E_c	4928.3	ksi
E_{ci}	4620.4	ksi
Alpha1	0.85	
Beta1	0.7	
$Beta1_{,deck}$	0.85	

Load location

L_p	46.006	in.	concentrate load point from support
a/d_v	1		shear span-depth ratio

Harped strand location

T_h	40.5	in.	top harped strand to bottom

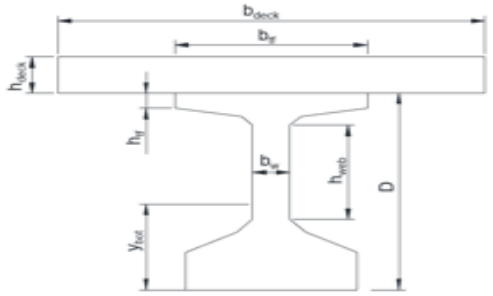

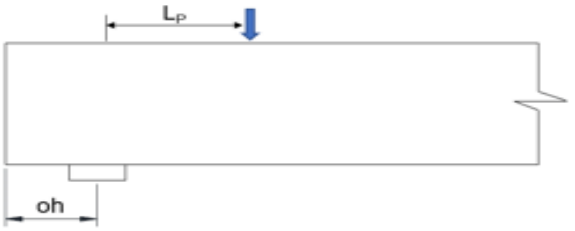

Prestressing Steel

INPUT

f_{pu}	270	ksi	
E_p	28500	ksi	
d_{ps}	0.6	in.	Diameter for strand
N_{ps}	36	ea	Total number of straight strand
N_{ph}	6	ea	Total number of harped strand
A_{ps}'	0.217	in2	Area for one strand

Calculated Data

$A_{ps,s}$	7.812	in2	Total area of straight strand
$A_{ps,h}$	1.302	in2	Total area of harped strand
A_{ps}	9.114	in2	Total area of total strand
L_t	36	in.	Transfer length = 60dps
Strand	Low relaxation str		Choose strand type
$\gamma 1$	0.9		fpy/fpu
$\gamma 2$	0.75		

verage stress in prestressing steel (fps

$$f_{ps} = f_{pu}\left(1 - k\frac{c}{d_p}\right)$$ AASHTO 5.6.3.1.1-1

= 255.12 ksi

In which

$$k = 2\left(1.04 - \frac{f_{py}}{f_{pu}}\right)$$ AASHTO 5.6.3.1.1-2

= 0.28

For T section behavior

$$c = \frac{A_{ps}f_{pu} + A_s f_s + A_s' f_s' - A_s'' f_s'' - \alpha_1 f_{c,deck}'(b_{deck} - b_w)h_{deck}}{\alpha_1 f_{c,deck}'\beta_1 b_{deck} + kA_{ps}\frac{f_{pu}}{d_{ps}}}$$ AASHTO 5.6.3.1.1-3

For rectangular section behavior

$$c = \frac{A_{ps}f_{pu} + A_s f_s + A_s' f_s' - A_s'' f_s''}{\alpha_1 f_{c,deck}'\beta_1 b_{deck} + kA_{ps}\frac{f_{pu}}{d_{ps}}}$$ AASHTO 5.6.3.1.1-4

c = 9.84 in.

Effective prestress (fpe)

$f_{py} = \gamma 1 \times fpu$ AASHTO Table C5.6.3.1.1-1

= 243 ksi

$f_{po} = \gamma 2 \times fpu$ AASHTO Table 5.9.2.2-1

= 202.5 ksi

Assume final prestressing loss is 20%

f_{pe} = 162.00 ksi

Calculate dv

Other factor

h_t	54.5	in.	total height
y_b'	4.5	in.	bottom to center of strand at CL
d_p	50.0	in.	top to center of strand at CL
a	8.37	in.	

Strand location

y_{bh}	4.5	in.	bottom to center of harped strand at CL
y_b	4.5	in.	bottom to center of straight strand at CL

Calculate nominal flexure resistance

For T section behavior

$$M_n = A_{ps}f_{ps}\left(d_p-\frac{a}{2}\right)+A_sf_s\left(d_s-\frac{a}{2}\right)+A_sf_s\left(d_s-\frac{a}{2}\right)-A_sf_s\left(d_s'-\frac{a}{2}\right)+\alpha_1f_{c,deck}\left(b_{deck}-b_w\right)h_{deck}\left(\frac{a}{2}-\frac{h_{deck}}{2}\right)$$ AASHTO 5.6.3.2.2-1

For rectangular section behavior

$$M_n = A_{ps}f_{ps}\left(d_p-\frac{a}{2}\right)+A_sf_s\left(d_s-\frac{a}{2}\right)+A_sf_s\left(d_s-\frac{a}{2}\right)-A_sf_s\left(d_s'-\frac{a}{2}\right)$$

M_n = 106969 kip-in

Calculate dv

$$d_v = Max\left(\frac{M_n}{A_sf_y+A_{ps}f_{ps}}, 0.9\times d_p, 0.72\times h\right)$$

d_v = 46.006 in.

Calculate Vu With Harped Strand (STM)

Variables

L_{hp}	5	ft.	length from hold-down point length to CL
L_h	630	in.	length for harped strand
H_h	34	in.	height forharped strand at end
theta1	3.0892	degree	harped strand angle

Node location for harped strand

X	22.18	in.	Goalseek changing cell
theta 2	25.00	degree	Goalseek to value
theta 2	25.00	degree	Goalseek set cell
X_i	13.181	in.	Minimum Xi = 0
Y_i	32.803	in.	
L_{hi}	22.213	in.	
L_{s1}	35.381	in.	
L_{s2}	35.352	in.	
L_{s3}	65.062	in.	

Node geometry

b_p	8	in.	bearing size
w_p	21	in.	bearing width
θ	45	degree	
h_t	9	in.	back face height
w_s	12.021	in.	
l_s	17.5	in.	

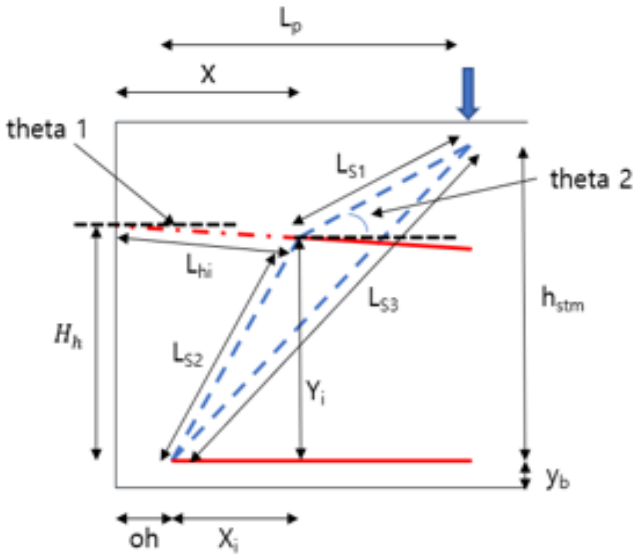

Calculate Strut and Tie force

$$f_1 = \frac{l_a}{L_t} \times f_{pe}$$

$= \boxed{78.75}$ ksi

$$T_1 = f_1 \times A_{bp}$$

$= \boxed{615.2}$ kip

$$f_3 = \frac{L_{hi}}{L_t} \times f_{pe}$$

Maximum f3 is fpe

$= \boxed{99.958}$ ksi

$$T_3 = f_3 \times A_{hbp}$$

Ahbp is total area of bonded harped strand

$= \boxed{130.15}$ kip

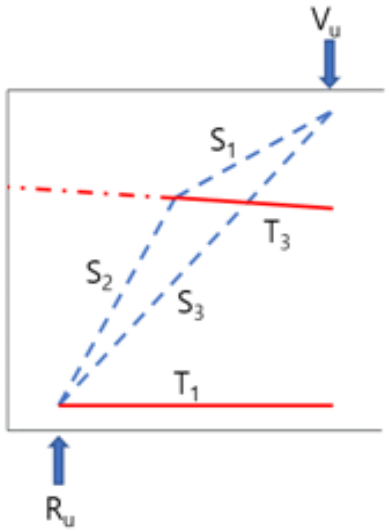

Using equation of equilibrium to calculate strut force

S_1 and S_2 can be calculated from T_3

$$S_1 \frac{L_p - X_i}{L_{s1}} - S_2 \frac{X_i}{L_{s2}} = T_3 \frac{L_h}{\sqrt{L_h^2 + H_h^2}}$$

$$S_1 \frac{h_{zm} - Y_i}{L_{s1}} - S_2 \frac{Y_i}{L_{s2}} = -T_3 \frac{H_h}{\sqrt{L_h^2 + H_h^2}}$$

$S_1 = \boxed{170.7}$ kip

$S_2 = \boxed{76.207}$ kip

S3 can be calculated from T1 and S2

$$S_3 \frac{L_p}{L_{s3}} = T_1 - S_2 \frac{X_i}{L_{s2}}$$

$S_3 = \boxed{829.84}$ kip

Calculate Vu

$V_p = f_{pe} \times A_{ps,h} \times \sin(theta1)$

$= 11.367$ kip

$R_u = S_2 \frac{Y_i}{L_{s2}} + S_3 \frac{h_{stm}}{L_{s3}}$

$= 657.49$ kip

$V_{u,s} = R_u - V_p$

$= 646.13$ kip

Anchorage Longitudinal Check With Harped Strand

$$A_s f_y + A_{ps} f_{px} \geq \left(\frac{V_{u,a}}{\phi_v} - 0.5V_s - V_p \right) \cot\theta_2$$ AASHTO 5.7.3.5-2

From the above equation

$$A_s f_y + A_{ps} f_{px} = \left(\frac{V_{u,a}}{\phi_v} - 0.5V_s - V_p \right) \cot\theta_2$$

Equation for Vu'

$$V_{u,a} = \phi_v \left(\frac{A_s f_y + A_{ps} f_{px}}{\cot\theta_2} + 0.5V_s + V_p \right)$$

f_{px} : Prestress at extended nodal zone

A*f : Consider harped strand if harped strand is in flexural tension side

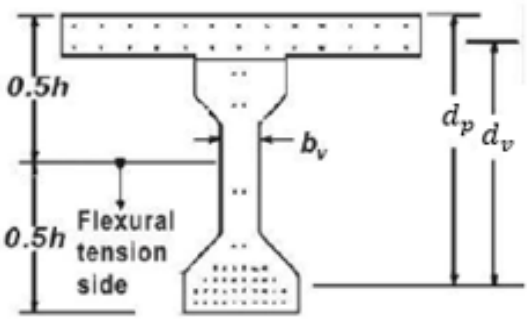

Where

V_s = 406.38 kip

ε_s = -0.00024

$\theta_2 = 29 + 3500\varepsilon_s$

= 28.17 degree

ϕ_v = 0.9

A*f = 615.2 kip

$V_{u,a}$ = 489.61 kip Fail

Calculate v_u/f_c'

Used V_u 489.608

$$v_u = \frac{|V_u - V_p|}{\phi b_v d_v}$$

= 1.65

v_u/f_c' 0.2357

When anchorage fail, $V_u = V_{u,a}$